Absolute Laser Spectrometric Amount Fraction Measurements: Impact to Traceable Breath Gas Analysis

Von der Fakultät für Lebenswissenschaften

der Technischen Universität Carolo-Wilhelmina

zu Braunschweig

zur Erlangung des Grades eines

Doktors der Naturwissenschaften

(Dr. rer. nat.)

genehmigte

D i s s e r t a t i o n

von Javis Anyangwe Nwaboh
aus Etwii-Ngie / Kamerun

1. Referent: Prof. Dr. Karl-Heinz Gericke
2. Referent: Prof. Dr. Peter Jomo Walla
eingereicht am: 05.10.2011
mündliche Prüfung (Disputation) am: 21.11.2011

Druckjahr 2011

Vorveröffentlichungen der Dissertation

Teilergebnisse aus dieser Arbeit wurden mit Genehmigung der Fakultät für Lebenswissenschaften, vertreten durch den Mentor der Arbeit, in folgenden Beiträgen vorab veröffentlicht:

Publikationen

J. A. Nwaboh, D. Schiel, O. Werhahn, "Laser-spectrometric gas analysis: CO_2-TDLAS at 2.0 μm", *Measurement science and technology,* to be submitted.

J. A. Nwaboh, O. Werhahn, and D. Schiel, "Measurement of CO amount fractions using a pulsed quantum-cascade laser operated in the intrapulse mode," *Applied Physics B*, Vol. 103, No. 4, pp. 947-957 (2010).

J. A. Nwaboh, T. Desbois, D. Romanini, D. Schiel, O. Werhahn, "Molecular laser spectroscopy as a tool for gas analysis applications," *International Journal of spectroscopy,* doi: 10.1155/2011/568913 (2011).

J. Nwaboh, S. Persijn, K. Heinrich, M. Sowa, O. Werhahn, "QCLAS and CRDS-based CO quantification as aimed at in breath measurements" *International Journal of Spectroscopy*, submitted 2011-09-07.

Tagungsbeiträge

J. Nwaboh, O. Werhahn, "Calibration free spectrometry for amount fraction measurements", (Talk), *Presented at the iMERA-plus progress meeting/workshop, Lyngby Denmark*, May (2009).

O. Werhahn, J. Nwaboh, "Progress at PTB: experimental and documentary status. T2.J02 (iMERA-plus Breath Analysis)", (Talk), *3rd progress meeting/workshop at LNE-CNAM, Paris, France*, October (2009).

J. Nwaboh, O. Werhahn, D. Schiel, "Amount of substance fraction measurements of gas species using IR-laser spectrometry and its projections for breath analysis", (Poster), *International PhD Symposium, Helmholtz ZI, Braunschweig*, December (2009).

J. Nwaboh, O. Werhahn, "Measurement of amount of CO amount fractions using pulsed quantum cascade lasers", (Talk), *presented at the iMERA-plus progress meeting/workshop, PTB, Braunschweig, Germany*, April (2010).

O. Werhahn, J. Nwaboh, "iMERA-plus Breath Analysis: Work at PTB - experiments and concept documents. iMERA-plus T2.J02", (Talk), *4th progress meeting/workshop, PTB, Braunschweig, Germany,* April (2010).

J. A. Nwaboh, O. Werhahn, D. Schiel, “Reflections on laser spectrometric breath gas analysis: concepts related to metrology”, (Talk), *presented at the Austrian-German conference on breath gas research, Germany*, June (2010).

J. A. Nwaboh, O. Werhahn [ed.], S. Persijn, A. v.d.Veen, J. C. Petersen, J. Hald, “Spectroscopy within the European iMERA-plus Project "Breath Analysis", (Poster), *German-Austrian Workshop on Breath Gas Analysis*, *Greifswald, Germany*, June (2010).

J. A. Nwaboh, T. Desbois, O. Werhahn, D. Schiel, “Application of laser spectrometric techniques to Breath Analysis”, (Poster), *IGSM Summer School of Metrology 2010, Burg Warberg, Elm*, September (2010).

J. A. Nwaboh, T. Desbois, D. Romanini, D. Schiel, O. Werhahn, Traceable infrared laser-spectrometric amount fraction measurement method: A tool to “Breath Analysis”, (Poster), *Breath Analysis workshop, Delft, Netherlands*, April (2011).

J. A. Nwaboh, P. Ortwein, O. Werhahn, V. Ebert, “Towards Traceable Infrared Laser-Spectrometric Amount Fraction Measurements (*TILSAM*): CO_2 and CO quantification results, line data at 2 μm and 4.6 μm”, (Talk), *presented at the FLAIR 2011 conference,* Murnau, Germany, September (2011).

J. Hald, J. A. Nwaboh, O. Werhahn, and J. C. Petersen, “Measurements of CO_2 in a multipass cell and in a hollowcore photonic bandgap fibre at 2 μm”, (Poster), *FLAIR 2011 conference*, Murnau, Germany, September (2011).

List of abbreviations

For the sake of clarity and readability, the description of the abbreviations below are repeated some times in the text.

A/D	Analogue to Digital
AOM	Acousto Optical Modulator
BA	Breath Analysis
BAM	Bundesanstalt für Materialforschung und –prüfung
BO	Born–Oppenheimer
CALOS	Cavity Leak-Out Spectroscopy
CCQM	Comité Consultatif pour la Quantité de Matière – Métrologie en Chimie
CES	Cavity-Enhanced Spectroscopy
CNAM	Conservatoire National des Arts et Métiers
CRD	Cavity Ring Down
CRDS	Cavity Ring Down Spectroscopy
CRV	Comparison Reference Value
DAC	Data Acquisition Card
DFB	Distributed FeedBack
DFM	Danish Fundamental Metrology
DOAS	Differential Optical Absorption Spectroscopy
DOF	Degree Of Freedom
DQO	Data Quality Objective
EU	European Union
EURAMET	European Association of National Metrology Institutes
EMRP	European Metrology Research Programme
FLAIR	Field Laser Applications in Industry and Research
FTIR	Fourier Transform Infrared Spectroscopy

FSR	Free Spectral Range
FWHM	Full Width at Half Maximum
GAW	Global Atmosphere Watch
GAWG	Gas Analysis Working Group
GC	Gas Chromatography
GLR	Generalized Linear Regression
GUM	Guide to the expression of Uncertainty in Measurement
IGSM	International Graduate School of Metrology
ILM	Institut für LaserMedizin
iMERA	Implementing Metrology in the European Research Area
IPQ	Insituto Portugues da Qualidade
JCGM	Joint Committee for Guides in Metrology
LNE	Laboratoire Nationale de Métrologie et d'Essais
MIR	Mid-Infrared
MS	Mass Spectroscopy
MS/s	Mega Sample per second
NICE-OHMS	Noise-Immune Cavity-Enhanced Optical-Heterodyne Molecular Spectroscopy
NIR	Near Infrared
OAP	Off Axis Parabolic mirror
OCO	Orbiting Carbon Observatory
OF	Optical Feedback
OF-CRDS	Optical Feedback - Cavity RingDown Spectroscopy
OF-CEAS	Optical Feedback - Cavity Enhance Absorption Spectroscopy
PAS	Photoacoustic Spectroscopy
PDF	Probability Density Function
POC	Point-Of-Care

PTB	Physikalisch-Technische Bundesanstalt
QCL	Quantum Cascade Laser
QCLAS	Quantum Cascade Laser Absorption Spectroscopy
RP	Rapid Passage
SI	Système International d'unités (International System of Units)
SNR	Signal to Noise Ratio
SP	Sample Points
TCP/IP	Transmission Control Protocol/Internet Protocol
TDL	Tunable Diode Laser
TDLAS	Tunable Diode Laser Absorption Spectroscopy
TE	ThermoElectrically
TEM_{00}	Transverse ElectroMagnetic
TILSAM	Traceable Infrared Laser Spectrometric Amount fraction Measurement
WMO	World Meteorological Organization

Abstract

Laser spectroscopic techniques such as tunable diode laser absorption spectroscopy (TDLAS), quantum cascade laser absorption spectroscopy (QCLAS) and cavity ring down spectroscopy (CDRS) have been shown to be capable of performing absolute amount fraction measurements of gas species such as CO_2 and CO. These techniques have been proven to be very sensitive, selective and have real-time responses.

The aim of this work was to: perform absolute amount fraction measurements of breath gas species using TDLAS, QCLAS and CRDS, reliably quantify breath gas species, address metrological data quality objectives, i.e. uncertainty and traceability issues, as well as define and reduce the uncertainty of amount fraction results from the typical 10 % to levels suitable to fit breath analysis purposes, 5 % and below. Thus, aiming at traceable amount fraction results, measurements have been performed using TDLAS, QCLAS and CRDS based on the absolute method *TILSAM*. GUM compliant uncertainty budgets for spectrometric amount fraction results were developed.

TDLAS in combination with single-pass and multipass gas cells has been used to perform absolute measurements of the CO_2 amount fractions. To check the TDL spectrometer for its feasibility for absolute amount fraction measurements and to be operated on the basis of the *TILSAM* method, gravimetric gas mixtures of CO_2 in the range of 20 to 60 $mmol \cdot mol^{-1}$ were quantified. At the 50 $mmol \cdot mol^{-1}$ level (exhaled breath level) the relative standard uncertainties of the spectrometric CO_2 amount fraction results are in the ±0.7 % range.

The intra-pulse mode QCLAS has been utilized to measure absolute CO amount fractions at the 100 $\mu mol \cdot mol^{-1}$ and 1000 $\mu mol \cdot mol^{-1}$ levels based on the *TILSAM* method. Although, not at the exhaled breath level of 1-3 $\mu mol \cdot mol^{-1}$, the feasibility of intra-pulse mode QCLAS for CO measurements has been shown. The standard uncertainty of the CO amount fraction results, limited by the uncertainties of the line strengths used which were in the range of 2-5 % relative, are in the range of ±2.3 % relative.

A CRDS spectrometer has been used to carry out absolute CO_2 amount fraction measurements referring to the *TILSAM* method. The spectrometric results were in good agreement with the respective gravimetric reference values. The standard uncertainties of the CO_2 amount fraction results, also limited by the uncertainty of the used line strength, were in the range of ±2.1 % relative. In a separate measurement, it has been shown in coperation with other partners that CO amount fractions in the $nmol \cdot mol^{-1}$ levels can be quantified using CRDS.

It has been found that the *TILSAM* method suffers from the unavailability of traceable line data. Thus, line strengths and broadening coefficients of CO_2 in the ro-vibrational band around 2 µm have been measured. The derived line data are in agreement to a high degree with published data. Compared to literature, improved GUM compliant standard uncertainties in the ±0.6 % range for the measured line strengths have been reported.

The validity of the absolute method, *TILSAM*, has been further proven in a measurement campaign. The TDLAS-based quantifications were performed on CO_2 at the 300 and

500 µmol·mol^{-1} level. The spectrometric results from the different laboratories were in good agreement, expressed by a degree of equivalence being in the 1 % range, with the respective comparison reference values (CRVs).

Table of contents

1 Introduction

1.1 Laser spectroscopic techniques and absolute amount fraction measurements

Throughout the last few years laser spectroscopic techniques such as tunable diode laser absorption spectroscopy (TDLAS), quantum cascade laser absorption spectroscopy (QCLAS) and cavity ring down spectroscopy (CRDS) have been used to perform absolute amount fraction (concentration) measurements of molecular species in many gas analysis applications such as environmental monitoring and breath analysis [1-6]. Other very sensitive spectroscopic techniques such as Noise-Immune Cavity-Enhanced Optical-Heterodyne Molecular Spectroscopy (NICE-OHMS) and Photoacoustic spectroscopy (PAS) have also been used to quantify and qualify molecular species [7], [8]. NICE OHMS, PAS and other similar techniques are very important and valuable, however, they have not been used in this work because they can not be used to perform absolute amount fraction measurements. The theoretical background of the above-mentioned techniques are well documented in [1], [9], [10].

The increased success of laser spectroscopic techniques for amount fraction measurements in the past decade has been due to the fast developing availability of new light sources, e.g., distributed feedback (DFB) diodes and quantum cascade lasers (QCL) [11]. By means of these two types of lasers, the near infrared (NIR) and mid-infrared (MIR) were made accessible by compact and easy-to-use spectrometers. Most molecular gas species have absorption bands in the NIR and MIR region of the electromagnetic spectrum. This gives a huge advantage to laser spectroscopic techniques over other techniques such as mass spectrometry [12]. The line width of these lasers is less than the line width of molecular transitions under typical conditions, typically in the range of tens to a few hundreds of megahertz and is, thus, good for gas sensing. The low cost and the mass production of DFB diode lasers combined with the high technological level of optics and detectors in the NIR justify the work in this infrared (IR) spectral region. Near-infrared and MIR laser sources are used to probe molecular overtone transitions and the fundamental transitions, respectively. Molecular overtone transition intensities are obviously weaker than those of fundamental transitions. In this regard, MIR spectroscopy is a more sensitive technique than NIR spectroscopy. However, the availability of multipass gas cells, e.g, the White [13] and Herriot cell [14], providing long effective path lengths (increasing the signal to noise ratio), has made it possible to perform overtone spectroscopy to quantify the amount fraction of molecular species. In addition, the good quality of optics in the NIR compared to that in the MIR is a reason to carry out overtone spectroscopy.

Laser spectroscopic techniques have been reported to be very sensitive, selective and have near real-time response in gas analysis applications [12]. These techniques have their advantages and some disadvantages as discussed in several reviews [15-17]. Regarding other spectroscopic techniques, laser spectroscopy has severe competition with Fourier transform infrared spectroscopy (FTIR). This is because; FTIR spectrometers have a good sensitivity

and cover a wider spectral range. However, FITR spectrometers have a broad and non-directional light source compared to laser light, a large system size, a low resolution, and long measurement times and can not be used to carry out absolute amount fraction measurements. FTIR spectrometers have a longer response time than e.g., tunable diode laser (TDL) absorption spectrometers. Compared to other techniques such as mass spectroscopy (MS) and gas chromatography (GC) [18-20], laser spectroscopic techniques do not require complicated sample preparation methods and are non-invasive.

In gas metrology, laser spectroscopic techniques are used to assign absolute amount fractions to species in gas mixtures of known molecular constituents. The determinataion of the amount fraction of a species without the use of calibrated reference gas mixtures, leads to the so-called "calibration-free" infrared spectrometry. Calibration-free means the amount of substance fraction of a species is measured in terms of the International System of Units (SI) derived unit $mol \cdot mol^{-1}$ without referencing to a standard or a measurement expressed in the same unit [21]. Aiming towards absolute amount fraction results by means of spectroscopy that are directly traceable[1] to the SI, triggered the idea of a traceable infrared laser spectrometric amount fraction measurement (*TILSAM*) method [21].

To apply the *TILSAM* method, a sufficiently, spectrally isolated molecular ro-vibrational transition is desirable. As to what concerns the derivation of the amount fraction of a molecular species, the *TILSAM* method describes the raw data processing, the modeling and influence quantities. The *TILSAM* method aims to represent and document a combination of steps necessary to apply IR spectrometry as an absolute method. Most studies to measure the amount fraction of molecular species, so far, have not referenced to any documented standardized method for the spectrometric measurements, except for the most prominent exception of DOAS [23]. The *TILSAM* method is a first step towards standardization for gas analysis applications e.g. in breath analysis, by means of laser spectroscopy.

An amount fraction result derived from spectrometric measurements based on the *TILSAM* method would be traceable if all input quantities, such as the line strength of the probed transition, the gas pressure, and the gas temperature were traceable to the SI. Unfortunately, traceability is very rarely achieved in amount fraction measurements. Presently, the traceability [22] of an amount fraction result is limited by the availability of line strength values with associated Guide to the expression of uncertainty in measurement (GUM) [24] compliant uncertainties in literature [25] that are traceable. Line strength values could be taken from data bases like HITRAN [26] and GEISA [27]. These data bases provide absolutely valuable information to any spectroscopists. However, none of the line strengths, with comparably large uncertainties, in these data bases are traceable. Uncertainty budgets in accordance with the ISO GUM [24] are generally not provided. The lack of line strength with GUM compliant uncertainty figures in these data bases has also been reported earlier [25].

[1] Traceability "is a property of a measurement result whereby the result can be related to a reference through a documented unbroken chain of calibrations, each contributing to the measurement uncertainty" [22]

Regarding line data, traceable collisional broadening parameters of spectral lines are also necessary for modeling spectrometric measurements in gas analysis applications. Self- and foreign-broadening parameters serve to determine what line profile function is necessary to accurately calculate the absorption spectrum. Apart from modeling spectrometric amount fraction measurements, line data are used as input parameters for climate change and radiation transfer models in atmospheric science. There have been a couple of studies undertaken to report line data values [29] with GUM compliant uncertainty figures [28]. Presently, there is a proposal to establish a new reference line data measurement program [30].

Traceability is an indispensable prerequisite for the comparability of measurement results. A traceable spectrometric result should consist of a value component and its associated GUM compliant uncertainty component. The comparability of measurement results is possible when the results are reported with associated uncertainties. International comparisons, for instance, would establish equivalence between similar laboratories. The comparability of measurement results is crucial in, e.g., medical treatment.

Traceable absolute amount fraction results were benefiting in laser spectrometric breath gas analysis. Laser spectroscopic techniques have a point-of-care function (POC) feasibility [12] which could be very beneficial to breath gas analysis. GC-MS techniques used in breath analysis require complicated (time-consuming) procedures for sample preparation and they have high instrument costs. Laser spectroscopic techniques are seemingly ideal to perform amount fraction measurements of breath gas species because of their robustness from sample preparation to measurement and their comparably low instrument costs.

Healthy human breath contains over a thousand types of molecule including atmospheric molecules such as CO_2, N_2 and O_2. The amount of substance fraction of each of these molecules in breath images the biochemical processes taking place in the human body. Some of these molecules have been established as biomarkers [12]. Carbon dioxide and carbon monoxide, which are studied in this thesis, have been established as biomarkers [12]. Carbon dioxide and ^{13}C-isotopes are biomarkers for oxidation stress, liver malfunction, excessive growth of bacteria in the body, Helicobacter pyroni infections, etc, [31-34]. Carbon monoxide is a biomarker for anemia.

Carbon dioxide and its isotopes are used in breath analysis as discussed. The average CO_2 in exhaled breath of healthy humans is about 50 $mmol \cdot mol^{-1}$. Typically, in breath analysis the target species are quantified and the result is normalizing to e.g. the assumned 50 $mmol \cdot mol^{-1}$ CO_2, present in exhaled breath, to correct for variations in ventilation and room air admixture. A simultaneous absolute measuerement of CO_2 together with the target species using e.g. a laser absorption spectroscopy, would provide in real time the exact CO_2 amount fraction to be used in the normalization process, which would result to a more reliable result. In this situation, a 5 % relative expanded uncertainty for CO_2 measurements is already sufficient. The $^{13}CO_2/^{12}CO_2$ ratio is used in breath analysis. The analysis of the isotopes of carbon can be used for drug administration [12].

The CO amount fraction in healthy humans varies. The average CO in the exhaled breath of non smokers is in the range of 1-3 μmol·mol^{-1} whereas for smokers it could be about 4 times higher. It seems, hence, advisable to achieve an accuracy in the order of ±10 % (k = 2) for the CO amount fraction of a reference measurement procedure. In addition to the information provided in the previous paragraph, clinical measurements are focused on measuring the level of a species before and after treatment to check if there is a change. In order to compare the two measurements, GUM compliant uncertainties of the derived results are necessary.

The relation between a biomarker and a specific disease is often multifold and the large number of biomarkers in exhaled human breath is in low concentration. Thus, a highly sensitive and highly selective instrument is needed in order to identify and quantify these biomarkers. Laser spectrometric techniques are seemingly ideal to perform these measurements as discussed.

Laser spectroscopic techniques have been used to perform non-invasive breath analysis [12], [16], [17]. They have been proven to be able to identify and quantify biomarkers found in exhaled human breath with detection limits in the pmol·mol^{-1} range [12]. Nowadays, single molecule laser absorption spectrometers are commercially available. There is the Ekips Technologies, Inc., exhaled nitric oxide sensor (Breathmeter) and the Pranalytica, Inc. exhaled ammonia sensor (Nephrolux). The availability of widely tunable laser source such as optical parametric oscillators and advances in broadly tunable laser sources using quantum cascade lasers provide the possibility of developing multi-species laser absorption breath analyzers in the future [35], [36].

Regarding the measurement and the derivation of traceable spectrometric amount fractions of biomarkers, the metrological quality of the measured data, the traceability of the measurement results as well as meaningful associated uncertainties of the results have been missing in most reports. Following on from the last sentence, the *TILSAM* method is a potential candidate to address the presented concerns. There have been other groups and other termini dealing with this idea. The *TILSAM* method promotes these ideas, from a metrology point of view, on some standardized basis, providing some descriptive framework and is flexible as possible to different experimental implementations.

As to what concerns the uncertainty of breath gas measurement results, so far, some doctors proposed that a 5 % GUM compliant relative expanded uncertainty is sufficient. In contrast to calculating the uncertainty of the amount fraction results of breath gas species, most reports focusing on large sensitivities, are calculating instead the reproducibility over several measurements. In this latter case, the traceability of the results to the SI is missing in most reports as discussed.

Absolute amount fraction measurements sometimes have specific challenges. Some of the challenges include: matching the line strength to the temperature at which spectrometric measurements were performed, the correction of the abundance of the probed isotopologue and the nonlinearity of detectors in the MIR. Also, for instance, the correction of an effect in intra-pulse mode QCLAS known as rapid passage is indispensable.

This thesis is focused on the investigation of the feasibility of absolute amount fraction measurement, using TDLAS, QCLAS and CRDS, based on the *TILSAM* method. Results on absolute amount fraction measurements of CO_2 and CO are presented. Due to the unavailability of traceable line data in literature, traceable line strengths of CO_2, that could be used as input quantities in the determination of traceable amount fraction results, are measured. The last part of this work focuses on the validation of the *TILSAM* method by means of a measurement campaign. In this work, there is emphasis on data quality, data retrieval, uncertainty assessment and traceability. The importance of the focus points to the intended possible applications are discussed. The lab-based experiments were performed in the framework of the iMERA-plus project on breath analysis [37]. The project aimed to define measurement procedures, perform IR laser spectrometry with defined and where possible reduced uncertainties of input quantities, e.g. line strengths, and as a consequence provide an impact on breath analysis. The iMERA-plus project was a joint research project involving different national metrology institutes in the European Union [37]. The project partners were, the Danish Fundamental Metrology - Denmark (DFM), Insituto Portugues da Qualidade (IPQ) - Portugal, Conservatoire National des Arts et métiers (CNAM) – France and the Physikalisch-Technische Bundesanstalt - (PTB) Germany.

1.2 The goal of this work

The main goals of this work were:

-laboratory investigations on the feasibility of TDLAS, QCLAS and CRDS for absolute amount fraction measurements (based on the *TILSAM* method) of molecular species present in exhaled human breath; gravimetric gas mixtures contained in gas cylinders were used to perform the spectrometric measurements.

-addressing metrological data quality objectives, i.e. uncertainty and traceability issues.

-defining and reducing where possible the uncertainty of the spectrometric amount fraction results to levels suitable to fit breath analysis purposes.

1.3 The structure of this work

The theoretical background and the details of all experimental setups used in this work are presented in chapters 2 and 3. Chapters 4, 5, 6 and 7 consist of submitted and published papers. The papers are on TDLAS, QCLAS and CRDS, respectively. Chapter 8 is devoted to the determination of line strength and collisional broadening parameters using TDLAS. In chapter 9, comparison measurements to validate the *TILSAM* method are presented.

There are four publications presented in this thesis as discussed. These publications were prepared by the author of this thesis as main author because all the experimental work presented in the first three papers was exclusively carried out by the author of this thesis. Also the text of those were drafted by the author of this thesis. The latter one is also true for the fourth paper. In addition, the experimental work on pulsed QCLAS contained in paper four

was carried out by the author of this thesis, whereas the remaining results were achieved at two partner institutes.

2 Theoretical aspects

In this chapter, the theoretical background needed for this work is presented. The first part of this chapter comprises of the theory of gas interaction with light. This work is focused on molecular transitions in the NIR and MIR regions of the electromagnetic spectrum. Therefore, in the second part of this section, the theory of molecular vibrational and rotational transitions is presented. The last part of this section is devoted to the broadening of spectral lines, line profiles and the Beer-Lambert law.

2.1 Gas interaction with light

When light from e.g. a laser interacts with a gas molecule, it can be absorbed, emitted or scattered. Figure 2.1 depicts a simple schematic view of the absorption, emission and scattering of light.

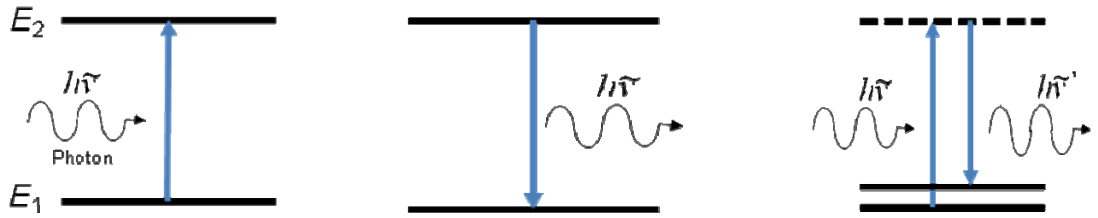

Figure 2.1 a) Absorption b) Emission c) Inelastic scattering

When a molecule absorbes a photon of radiation, it is excited from a lower energy state E_1 to a higher energy state E_2 (Figure 2.1a). The emission of radiation on the other hand occurs when a molecule in the excited state E_2 undergoes a transition to the lower energy state E_1 (Figure 2.1b). The absorbed or emitted photon energy is equal to the energy difference ΔE between the two energy states involved. A measurement of an absorption or emission by a molecule is usually depicted as a function of frequency. Absorption spectra are used to e.g., quantify and qualify molecular parameters.

Inelastic scattering of radiation is depicted in Figure 2.1c as a transition to and from a virtual state (dashed line). There are energy losses when radiation is scattered (the frequency of the scattered light $\tilde{\nu}'$ is smaller than that of the incident light $\tilde{\nu}$). The loss in energy could be due to e.g. molecular vibrations. Therefore, the scattered radiation can also be used to quantify and qualify molecular species as utilized in Raman spectroscopy.

2.2 Molecular transitions

At normal temperature and pressure molecules vibrate, rotate and translate. The quantum states of molecules are described by the solutions to the time independent schrödinger equation,

$$E\Psi = \hat{H}\Psi \tag{2.1}$$

where Ψ is a wave function (quantum state), $\hat{H}$ the Hamiltonian operator and E is the total energy. The Born–Oppenheimer (BO) approximation allows the wavefunction of a molecule to be broken into its electronic and nuclear (vibrational, rotational) components. An in-depth explanation of this is found in literature [39]. Therefore, a molecule can be seen as composing of reservoirs of energy due to e.g. its vibration, rotation and translation. Considering that a molecule consist of reservoirs of energies, its total energy E could be expressed as

$$E = E_{\text{vibration}} + E_{\text{rotation}} + E_{\text{electronic}} \tag{2.2}$$

When a photon of electromagnetic radiation of energy ΔE is absorbed by a molecule, a molecular transition from an energy state E_1 to E_2 could occur as discussed. The energy states E_1 and E_2 could be vibrational, rotational or electronic energy states. Purely rotational transitions are typically in the microwave region of the electromagnetic spectrum. Vibrational transitions on the other hand are typically in the NIR and MIR regions. Electronic transitions are typically in the visible and ultraviolet regions. The absorbed energy ΔE, corresponding to the quantum of energy required for a transition between the two energy states, is usually expressed as

$$\Delta E = h\tilde{\nu} = E_2 - E_1 \tag{2.3}$$

where, E_1 and E_2 are the energies of the original and final states of the molecule. The quantity h is the Planck's constant.

2.2.1 Vibrational and rotational molecular transitions

When a molecule absorbes IR light, the energy state changes. A change in the vibrational state of a molecule, as a result of a change in the inter nuclei distance leading to a change in the moment of inertia, results to a change in the rotational state.

Regarding molecular vibrations, when a quantum of energy is absorbed by a molecule, its fundamental vibration mode is excited. The fundamental mode is typically approximated to a simple harmonic oscillator. Generally, vibrational modes of molecules are anharmonic. Because of anharmonicity of molecular vibrations, higher over tones when excited have progressively lower energy as would be expected, e.g., the first overtone has energy slightly less than twice that of the fundamental mode.

From quantum mechanics, the vibrational energy of a molecule is usually approximated by

$$E_v = E_0\left[\left(v+\frac{1}{2}\right) - x_e\left(v+\frac{1}{2}\right)^2 + \ldots\right] \tag{2.4}$$

where, E_0 is the energy of the vibrational ground state, v the vibrational quantum number ($v = 0, 1, 2, \ldots$); and x_e is the first anharmonicity constant (unitless). The first term in Eqn. (2.4) is the harmonic oscillator term. The selection rule of vibrational transitions is given by

$\Delta v = \pm 1$. Other vibrational transitions, i.e. $\Delta v = \pm 2$, ± 3, …, are only permitted for an anharmonic oscillator.

As to what concerns the rotation of molecules, rotational transitions usually occur when there are vibrational transitions. Purely rotational transitions occur (without changing the vibrational state of a molecule) if the molecule has a permanent electrical dipole moment. From quantum mechanics, rotating molecules posses only discrete quanta of angular momentum. Therefore, the rotational energy of a linear molecule (rigid rotor) can be expressed in terms of the rotational angular momentum quantum number J as

$$E_{\mathrm{r}} = B \cdot J(J+1) - D \cdot J^2 \cdot (J \cdot +1)^2 + \ldots \tag{2.5}$$

where, D is the centrifugal constant and B is the rotational constant expressed as

$$B = \frac{h}{8 \cdot \pi^2 \cdot I_{\mathrm{B}}} \tag{2.6}$$

with I_{B} being the moment of inertia about an axis perpendicular to the inter-nuclear axis, and going through the molecule's center of mass. The selection rule of rotational transitions is given by $\Delta J = \pm 1$. This rule applies to any transition that influences the rotational energy state of a molecule.

Rotational transitions occur with energy usually in the order of 10^{-23} J while vibrational transitions occur with energy of the order of 10^{-20} J. Since the energy associated with rotation is smaller than that from vibration, it means that highly resolved vibrational transitions will contain fine structure of rotational transitions. Thus, for a first approximation, the vibrational-rotational energy is usually expressed as

$$E_{v+r} = E_v + E_{\mathrm{r}} = E_0\left(v + \frac{1}{2}\right) + B \cdot J(J+1) \tag{2.7}$$

If a molecule undergoes a vibrational transition, then $\Delta v = \pm 1$, ± 2, ± 3 …, and $\Delta J = \pm 1$ since the rotational state changes when there is a change in the vibrational state of the molecule. If a molecule undergoes a purely rotational transition, i.e. a transition where the vibrational state does not change, then $\Delta J = \pm 1$ and $\Delta v = 0$.

In laser absorption spectroscopy, the transitions corresponding to a change in J are named. For $\Delta v = 1$, transitions corresponding to $\Delta J = -1$ are referred to the P-branch, those for $\Delta J = 1$ are referred to as the R-branch and those for $\Delta J = 0$ are the Q-branch. Details about vibrational and rotational transition of molecules are found in [1], [38], [39].

2.2.2 Line strength

From the theory of radiation transfer, considering two states of a rotational-vibrational system, the line strength of a molecular transition i at a reference temperature T_{ref}, $S_{\mathrm{i}}(T_{\mathrm{ref}})$, is expressed as

$$S_i(T_{ref}) = \frac{8\cdot\pi^3}{3\cdot h\cdot c}\cdot\tilde{\nu}_{0,i}\,\frac{I_a\cdot g''\cdot\exp(-c_2\cdot E_i''/T_{ref})}{Q_{T_{\mathrm{ref}}}}\cdot\left[1-\exp\left(\frac{-c_2\cdot\tilde{\nu}_{0,i}}{T_{ref}}\right)\right]\cdot\Re_i\cdot 10^{-36} \tag{2.8}$$

where, h is the Planck constant, c is the speed of light in vacuum, $v_{0,i}$ is the spectral transition wave number, I_a is the natural terrestrial isotopic abundance, c_2 is the second radiation constant = $h\cdot c/k_B$, E_i" is the lower state energy for the transition i, $\Re_i$ is the weighted transition-moment squared, g" the state statistical weight in the absorbing state [26] and $Q_{T\mathrm{ref}}$ is the total internal partition function of the molecule at the reference temperature. The total internal partition functions describe how molecules in thermodynamic equilibrium at temperature T_{ref} are distributed among various energy states [26].

By using the ratio of the line strength at the reference temperature T_{ref} (S_{To}), T_o = 296 K, to that at temperature T (S_T), the line strength at temperature T can be expressed as

$$S_T = S_{T_0}\left(\frac{Q_{T_0}}{Q_T}\right)\exp\left\{-hc\,\frac{E_i''}{k_B}\left(\frac{1}{T}-\frac{1}{T_0}\right)\right\}\frac{\left[1-\exp\left\{-hc\,\dfrac{\tilde{\nu}_{0,i}}{k_B T}\right\}\right]}{\left[1-\exp\left\{-hc\,\dfrac{\tilde{\nu}_{0,i}}{k_B T_0}\right\}\right]} \tag{2.9}$$

where, the quantities Q_{To} and Q_T are the internal partition functions of the probed molecule at temperature T_o = 296 K and T, respectively. The total partition function at temperature T can be approximated to

$$Q_T = a + bT + cT^2 + dT^3 \tag{2.10}$$

if energy levels are not known to high enough states to calculate the total partition function [40]. The approximation of Q_T does not work for heavy systems with many vibrational degrees of freedom. The quantities a, b, c and d are constants whose values could be obtained from [40]. Table 2.1 holds the constants for CO_2 and CO.

Table 2.1: Coefficients of Q_T for CO_2 and CO in the temperature range of 70 K < T < 500 K

	Molecule	
Coefficient	CO_2	CO
a	-1.3617	0.27758
b	9.4899×10^{-1}	0.36290
c	-6.9259×10^{-4}	-0.74669×10^{-5}
d	2.5974×10^{-6}	0.14896×10^{-7}

Using Eqn. (2.10), Eqn. (2.9) can be approximated to

$$S_T = S_{T_0}\left(\frac{T_0}{T}\right)^{\mathrm{j}} \exp\left\{-hc\frac{E}{k_{\mathrm{B}}}\left(\frac{1}{T}-\frac{1}{T_0}\right)\right\}\frac{\left[1-\exp\left\{-hc\frac{\tilde{\nu}_0}{k_{\mathrm{B}}T}\right\}\right]}{\left[1-\exp\left\{-hc\frac{\tilde{\nu}_0}{k_{\mathrm{B}}T_0}\right\}\right]} \tag{2.11}$$

Where E_i'' and $\tilde{\nu}_{0,\mathrm{i}}$ are simply written as E and $\tilde{\nu}_0$ and j is a real number.

2.2.3 Vibrational and rotational transitions of CO_2 and CO

The work is focused on CO_2 and CO. Therefore, in this subsection only the vibrational and rotational transitions of CO_2 are discussed. A schematic of the vibrational modes of CO_2 and spectra of CO_2 and CO in the region of interest of this work are presented

A system of N independent particle has 3N degrees of freedom. The degree of freedom is a component of the momentum of the system. Carbon monoxide and carbon dioxide are linear and symmetric molecules and have 6 and 4 degrees of freeedom, recpectively. Linear molecules e.g., CO and CO_2 have 3N-5 normal modes of vibration. This implies that CO has a single normal mode of vibration while CO_2 has four. Figure 2.2 shows the vibrational modes of CO_2, i.e. two bending modes and two stretching modes.

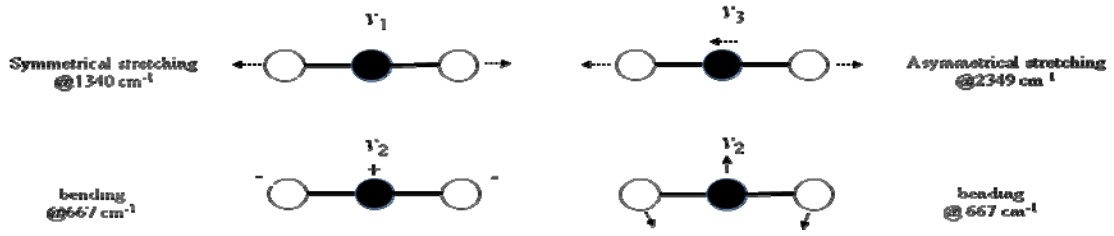

Figure 2.2**:** A schematic view of the vibrational modes of CO_2

When excited, the vibrational and rotational transition energies of CO_2 and CO are expressed as in Eqn. (2.4) and (2.5), respectively. The line strengths of molecular transitions are usually measured or calculated and the values stored in data bases such as HITRAN [26] and the GEISA [27]. Figure 2.3 shows the HITRAN spectra [26] of CO_2 in the 2-10 μm range. The red strip in Figure 2.3 shows the wavelength region utilized for CO_2 measurements in this thesis.

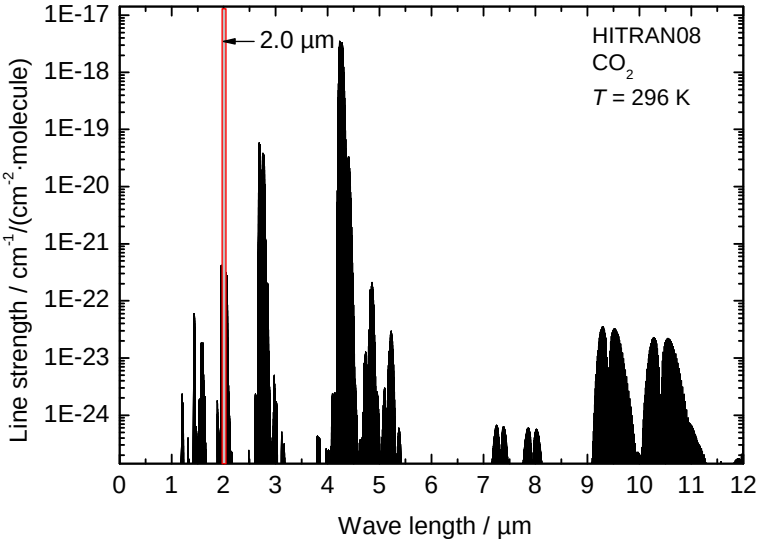

Figure 2.3: Spectra: Plot of the line strength of CO_2 as a function of wavelength in nanometers.

Figure 2.4 below shows a HITRAN spectra [26] of CO. The wave length region used for CO measurements in this thesis is shown in red.

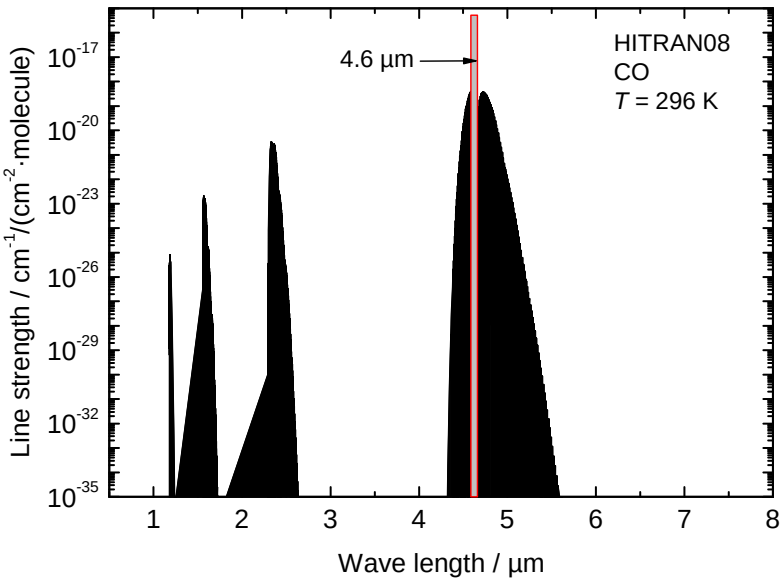

Figure 2.4: Spectra: Plot of the line strength of CO as a function of wavelength in nanometers.

2.3 Broadening mechanisms and line profile functions.

The spectral line widths of probed transitions are usually broadened due to e.g. temperature (Doppler broadening) or pressure (collisional broadening). In order to model spectral lines, normalized line profile functions $g(\tilde{\nu})$ such as a Lorentz, a Gauss and a Voigt are used.

2.3.1 Natural broadening

For a molecule which does not interact with its environment, the life time of the excited state of a transition determines the natural line width of the transition as expressed by the Heisenberg uncertainty principle ($\Delta E \cdot \Delta t = \hbar$, where, Δt is the life time of the excited state) [1]. Hence, absorption processes show a distribution of frequencies with natural line width $\Delta\nu_{\mathrm{Nat}}$ due to the life time of the connected states. The Lorentz function Eqn. (2.14) is used to describe a naturally broadened spectral line. Typical natural line widths of vibrational transitions in the NIR and MIR are $3.18 \cdot 10^{-1}$ MHz and $3.18 \cdot 10^{-4}$ MHz, respectively.

2.3.2 Doppler broadening

The Doppler effect is caused by the thermal motion of molecules. This thermal motion of molecules is described by the Maxwell-Boltzmann distribution. The distribution of the velocities of the moving molecules result in a shift of the absorption frequency when these molecules interact with light. This causes broadening of a spectral line. A Gauss line shape describes a Doppler broadened spectral line,

$$g_{\mathrm{G}} = \frac{2}{\Delta\tilde{\nu}_{\mathrm{D}}} \cdot \left(\frac{\ln 2}{\pi}\right)^{1/2} \cdot \exp\left\{-4 \cdot \ln 2 \cdot \left(\frac{\tilde{\nu} - \tilde{\nu}_0}{\Delta\tilde{\nu}_{\mathrm{D}}}\right)^2\right\} \tag{2.12}$$

where, $\Delta\nu_{\mathrm{D}}$ is the Doppler FWHM, given by

$$\Delta\tilde{\nu}_{\mathrm{D}} = 2 \cdot \tilde{\nu}_0 \cdot \left(\frac{2 \cdot k_{\mathrm{B}} \cdot T \cdot \ln 2}{m \cdot c^2}\right)^{1/2} \tag{2.13}$$

with $\tilde{\nu}_0$ the center frequency of the probed transition, T the temperature of the molecule, m its mass and c the speed of light. The isotopologue mass m has to be identified as being different to the molar mass of the gas species comprising a composition of different isotopologues. Typical Doppler line widths of vibrational transitions in the NIR are greater than a 100 MHz.

2.3.3 Collisional broadening

Collisions between molecules leads to an energy shift of the excited state, resulting to a short life time, and broadening of a spectral line. Collisional broadening depends on the type and strength of molecular interactions and the quantum state of the absorber and the collision partner. Although, presently, there is no exact analytical description of collisional broadening

e.g. at a given pressure, a Lorentz function is used to described a collisional broadened spectral line,

$$g_{\mathrm{L}} = \frac{1}{2\cdot\pi}\cdot\frac{\Delta\tilde{\nu}_{\mathrm{L}}}{(\tilde{\nu}-\tilde{\nu}_0)^2+(\Delta\tilde{\nu}_{\mathrm{L}}/2)^2} \tag{2.14}$$

where, $\tilde{\nu}_0$ is the central frequency of the probed transition and $\Delta\tilde{\nu}_{\mathrm{L}}$ is the Lorentzian width (FWHM) given by

$$\Delta\tilde{\nu}_{\mathrm{L}} = p_{\mathrm{total}}\cdot\sum_{\mathrm{i}} x_{\mathrm{i}}\cdot 2\cdot\gamma_{\mathrm{A\text{-}B}}\cdot\left(\frac{T_0}{T}\right)^n \tag{2.15}$$

with p_{total} being the total pressure of the molecules containing e.g., an analyte A and a collision partner B. The quantity x_{i} is the amount of substance fraction of a molecular species, and $\gamma_{\mathrm{A\text{-}B}}$ is the collision broadening coefficient of the collision partner B. If the molecule B is the same as A then $\gamma_{\mathrm{A\text{-}A}}$ is termed the self broadening parameter (γ_{self}), else it is called the foreign broadening parameter ($\gamma_{\mathrm{foreign}}$). The pressure broadened line width can then be expressed as

$$\Delta\tilde{\nu}_{\mathrm{L}} = 2\cdot p_{\mathrm{self}}\cdot\gamma_{\mathrm{self}}\cdot\left(\frac{T_0}{T}\right)^{\mathrm{n}} + 2\cdot\sum_{\mathrm{i}} p_{\mathrm{i}}\cdot\gamma_{\mathrm{foreign}}\cdot\left(\frac{T_0}{T}\right)^{\mathrm{n}} \tag{2.16}$$

where the total gas pressure p is summed up as

$$p = p_{\mathrm{self}} + \sum_{\mathrm{i}} p_{\mathrm{i}} \tag{2.17}$$

The quantities p_{self} and p_{i} are the partial pressures of the analyte and the collision partner (foreign molecule), respectively. For this work the constant n = 0.5 is used in all calculations as derived from the kinetic gas theory.

2.3.4 Voigt profile

When the two broadening mechanisms described above are present, a Lorentz or a Gauss function is insufficient to describe a spectral line. Typically, in such situation a Voigt profile is used. The Voigt function is a convolution of a Lorentz and a Gauss function, expressed below,

$$g_v(\tilde{\nu}) = \frac{2\cdot\ln 2}{\pi^{3/2}}\cdot\frac{\Delta\tilde{\nu}_{\mathrm{L}}}{\Delta\tilde{\nu}_{\mathrm{D}}^2}\cdot\int_{-\infty}^{+\infty}\frac{e^{-t^2}}{\left(\sqrt{\ln 2}\cdot\frac{\Delta\tilde{\nu}_{\mathrm{L}}}{\Delta\tilde{\nu}_{\mathrm{D}}}\right)^2+\left(\sqrt{4\cdot\ln 2}\cdot\frac{\tilde{\nu}-\tilde{\nu}_0}{\Delta\tilde{\nu}_{\mathrm{D}}}-t\right)}dt \tag{2.18}$$

The quantities, $\Delta\tilde{\nu}_{\mathrm{L}}$ and $\Delta\tilde{\nu}_{\mathrm{D}}$ are the Doppler and Lorentzian widths of the spectral line, respectively, and the quantity t is given by $t = 2\cdot\sqrt{\ln 2}\cdot\tilde{u}/\Delta\tilde{\nu}_{\mathrm{D}}$.

To summarize this subsection and to compare the shapes of the three line profiles discussed above, Figure 2.5 depicts a Voigt, a Lorentz and a Gauss function. The line areas of the three functions are set to unity.

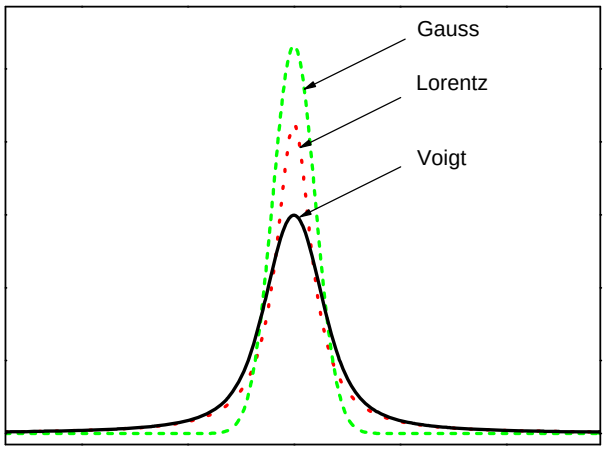

Figure 2.5: The Voigt, Lorentz and Gauss line shape functions. The line area of each of the three profiles is unity.

Futhermore, regarding collisions between molecules discussed above, they may also cause a narrowing of the Gaussian line width (collisional narrowing). This is known as Dicke narrowing [41]. This happens when the life time of the excited state of a molecular is long compared to the mean time between successive collisions. Dicke narrowing is usually described in terms of hard and soft collision models. Line profile functions such as Galatry (soft collision model) and Rautian-Sabelman (hard collsion model) are used to describe spectra data that are affected by the Dicke narrowing effect [42],[43] .

2.4 Beer Lambert law

In absorption spectroscopy, an absorption spectrum can be quantitatively related to the amount of substance fraction of a sample e.g., a gas species, using the Beer Lambert law.

The Beer Lambert law states the relationship between the incident radiation Φ and the transmitted radiant power Φ_0 through a homogenous absorbing medium of thickness z as

$$\Phi(\tilde{\nu}, z) = \Phi_0(\tilde{\nu}) \cdot \exp\{-\alpha(\tilde{\nu}) \cdot z\} \tag{2.19}$$

where the quantity $\alpha(\tilde{\nu})$ is the absorption coefficient at frequency $\tilde{\nu}$. The absorption coefficient is proportional to the density of the absorbing medium n and is expressed as

$$\alpha(\tilde{\nu}) = -\sigma(\tilde{\nu}) \cdot n \tag{2.20}$$

with $\sigma(\tilde{\nu})$ being the absorption cross section. In laser-spectrometric gas analysis, the absorption coefficient is typically expressed as

$$\alpha(\tilde{\nu}) = -S_T \cdot \mathrm{g}(\tilde{\nu} - \tilde{\nu}_0) \cdot n \tag{2.21}$$

where, $\mathrm{g}(\tilde{\nu} - \tilde{\nu}_0)$ is a normalized line profile function centred at $\tilde{\nu}_0$ and S_T is the line strength of a molecular transition at gas temperature T (see Eqn.(2.9). From Eq.(2.21), the line strength of a molecular transition can be derived from experimental data by integrating the absorption coefficient over wave number,

$$S = \int_{-\infty}^{+\infty} \sigma(\tilde{\nu}) d\tilde{\nu} \tag{2.22}$$

For z = L, where L is the optical path length, the Beer Lambert law is expressed as

$$\Phi(\tilde{\nu}, L) = \Phi_0(\tilde{\nu}) \cdot \exp\{-S_T \cdot \mathrm{g}(\tilde{\nu} - \tilde{\nu}_0) \cdot n \cdot L\} \tag{2.23}$$

when Eqn. (2.19) and (2.21) are combined. Relying on the ideal gas law, the molecular density n of the absorbing species can be expressed in terms of the partial pressure p_{partial} of the absorbing molecules and the gas temperature. The partial pressure can be related to the total pressure p_{total} using the amount of substance fraction of the absorbing species, $x_{\mathrm{species}} = p_{\mathrm{partial}} / p_{\mathrm{total}}$. Thus, Eqn. (2.23) becomes

$$\Phi(\tilde{\nu}, L) = \Phi_0(\tilde{\nu}) \cdot \exp\left\{\frac{-S_T \cdot \mathrm{g}(\tilde{\nu} - \tilde{\nu}_0) \cdot L \cdot x_{\mathrm{species}} \cdot p_{\mathrm{total}}}{k_{\mathrm{B}} \cdot T}\right\} \tag{2.24}$$

Introducing the spectral absorbance $\mathrm{A}(\tilde{\nu}) = -\ln(\Phi(\tilde{\nu})/\Phi_0(\tilde{\nu}))$, which in cases[2] can also be called extinction ($\Phi(\tilde{\nu})/\Phi_0(\tilde{\nu})$ = transmission), and making use of the normalization of $\mathrm{g}(\tilde{\nu} - \tilde{\nu}_0)$, Eqn. (2.24) can also be written in its integral form

$$\int_{-\infty}^{\infty} A(\tilde{\nu})\,\mathrm{d}\tilde{\nu} = \frac{S_T \cdot L \cdot x_{\mathrm{species}} \cdot p_{\mathrm{total}}}{k_{\mathrm{B}} \cdot T} \tag{2.25}$$

From Eqn. (2.25) the amount of substance fraction of a molecular species is given by

$$x_{\mathrm{species}} = \frac{k_{\mathrm{B}} \cdot T}{S_T \cdot r_{\mathrm{iso}} \cdot L \cdot p_{\mathrm{total}}} \int_{-\infty}^{\infty} A(\tilde{\nu})\,\mathrm{d}\tilde{\nu} = \frac{k_{\mathrm{B}} \cdot T}{S_T \cdot r_{\mathrm{iso}} \cdot L \cdot p_{\mathrm{total}}} \cdot A_{\mathrm{line}} \tag{2.26}$$

where A_{line} is the line area and r_{iso} is the isotopic composition factor, given e.g. as $r_{\mathrm{iso}} = x_{12\mathrm{C16O}} / x_{12\mathrm{C16OHIT}}$, for a probed $^{12}\mathrm{C}^{16}\mathrm{O}$ excitation, where $x_{12\mathrm{C16O}}$ and $x_{12\mathrm{C16OHIT}}$ are the abundances of $^{12}\mathrm{C}^{16}\mathrm{O}$ in the sample and the conventional value given by HITRAN, respectively.

[2] see e.g. http://goldbook.iupac.org/A00028.html

3 Experimentals

There is a brief description of the TDLAS, QCLAS and CRDS setups in the following chapters. However, in this chapter, there is a detailed description of the setups. The chapter begins with the TDL/QCL setup followed by the CRD spectrometer.

3.1 TDL/QCL spectrometer

3.1.1 Setup

Figure 3.1 below depicts the experimental setup (a two-channel spectrometer) used for TDLAS and QCLAS. The laser could be replaced in order to apply these two techniques. After collimation, the laser beam was split into a reference beam and a second sample beam transmitted through either a 0.82 m single-pass stainless steel absorption cell or a 21 m multipass absorption gas cell. By means of a replaceable mirror (R-OAP) and mirrors (M), laser light could be guided to the multipass gas cell while simultanuously blocking the beam going to the single-pass cell. The reference beam was used for intensity normalization and for fixing the wavelength axis by means of a removable Fabry-Perot etalon (R-FP etalon) with a free spectral range of ≈ 0.05 cm^{-1}.

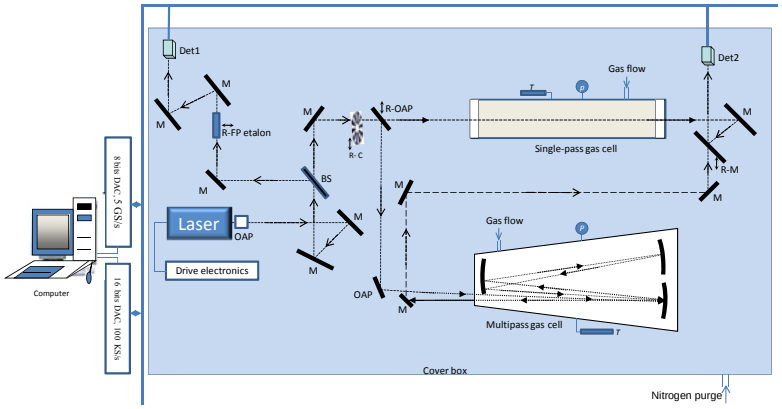

Figure 3.1: Schematic diagram of the setup used for species quantification in a two-channel regime. The single-pass and the multipass absorption cells have path lengths of L = 0.82 m and 21 m, respectively. OAP: Off axis parabolic mirror, R-OAP: Removable off axis parabolic mirror, BS: Beam splitter, M: Mirror, Det: Detector, R-P etalon: Removable Fabry-Perot etalon, R-C: Removable chopper, T: Temperature sensor, p: Pressure sensor, R-M: Removable mirror.

Both channels in Figure 3.1 were terminated into indium-gallium-arsenide (XInGaAs) detectors (laser components, model J18-181-R01M-2.2) for TDLAS or TE-cooled HgCdZnTe detectors (Vigo PDI-2TE-10.6) for QCLAS. The signals from the reference and sample detectors were first preamplified by individual preamplifers and later amplified in some cases (TDLAS) by a home-made two-channel amplifier. The electrical signals were digitized at 100 KS/s by a 16 bit ADLINK A/D converter (PCI-9114DG) or at 5 GS/s by an 8 bit Gage (Compuscope 85G) A/D converter. The acquisition of the data by the ADLINK 9114 DAC

was controlled by a Labview program (Appendix III) whereas that of the Gage DAC was controlled by GasAnalyst [44], which is a software developed in C++.

A turbomolecular pumping system connected, through the gas flow inlet(s), to the gas cell was used for evacuating the gas cell(s). Capacitance detector gauges, MKS model 626AX11TDE and MKS model 626AX13TDE [45], were used to measure gas pressures in the ranges 1-10 hPa and 1-100 hPa, respectively. A Pt-100 temperature sensor connected to a testo 650 with an accuracy specification of 0.1 °C was stocked on the gas cell wall(s) to measure the sample temperature. Gravimetrically prepared gas mixtures in gas cylinders, containing the sample gas, were filled into the gas cell for the spectrometric measurements.

For TDLAS, the light source was a continuous wave distributed feedback tunable GAInSbAs diode laser emitting at 2.004 µm (nanoplus model 057/4-15). The diode laser was cooled thermoelectrically. The laser controller and the thermoelectric cooling system for the laser were home built. The tuning of the laser was measured to be 0.26 nm/°C. For spectroscopic measurements, the laser frequency was tuned by a 5 Hz current ramp from an Agilent model 33120 A function generator. An HMS model 221 variable speed light chopper whose wheel rotation was phase-locked to a TTL output trigger of the function generator was placed along the sample beam path.

For QCLAS a quantum cascade laser emitting at 4.6 µm in an air-cooled laser housing delivered by the Fraunhofer-IPM [46] was used. The QCL was produced and structured with a distributed feedback (DFB) grating by the Fraunhofer-IAF [47]. A µ-processor controlled driver for the QCL with a TCP/IP connection to a master PC generates laser pulses with lengths between 8 and 255 ns at repetition rates between 100 Hz and 7.5 MHz and laser voltages up to 25 V. For spectroscopic measurements, the QCL was operated in the intra-pulse mode. The tuning speed of the QCL was 255 MHz/ns.

3.1.1.1 Used lasers

The distributed feedback (DFB) diode laser

The active region of a diode laser is a semiconductor. The semiconductor is a crystal wafer doped to produce an n-type region on the upper surface and a p-type region on the lower surface (see Figure 3.2). The n-doped side of the semiconductor is populated with electrons as charge carrier and the p-doped side contains excess holes as charge carriers. The physical contact of the n-doped side and the p-doped side of the semiconductor forms a depletion region, between the two, containing no charge carrier, i.e., electrons or holes. This is because of a difference in potential between the n and the p-side of the semiconductor.

Some diode lasers are pumped by electric current as shown in Figure 3.2, while others are pumped optically (i.e. using a flash lamp or another laser). By pumping a diode laser, holes from the p-doped side and electrons from the n-doped side are injected in to the depletion

region. The electrons and holes in the depletion region "annihilate" i.e. recombine resulting to spontaneous emission of electromagnetic photons.

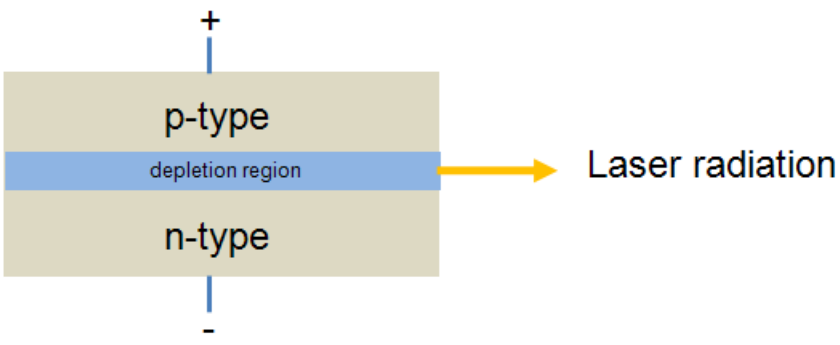

Figure 3.2: A schematic of a p-n junction of a diode laser

The initial emitted photons cause further recombination of electron hole pairs, resulting to the emission of more photons with the same frequency, polarization and phase as the initial and travelling in the same direction (amplification). With a laser resonator formed by coated or uncoated end facets (cleaved edges) of the semiconductor wafer, emitted photons are reflected many times, and resulting to a burst of laser radiation through one of the end facet. This occurs when the amplification of light in the resonator is larger than the losses due to absorption and incomplete reflections.

DFB diode lasers are made with the active region periodically structures as a diffraction grating. The grating, acting a distributed reflector, provides feedback to the laser. In DFB lasers only a narrow band of wavelengths is reflected by the grating (wave length selector), thus producing a single longitudinal mode at which the laser is lasing. A change in the temperature of the active region of the DFB laser leads to a change in its refractive index and thus the pitch of the grating. Hence, by changing the temperature of the active region, the wavelength selection of the grating structure changes, and as a consequence, the wavelength of output radiation changes. Therefore, DFB lasers are tunable. The design configuration theoretically permits them to operate only at a single wave length. Typical laser line widths of DFB diode lasers are in the range of a few megahertz as discussed, enabling them to be used for high resolution laser absorption spectroscopy. DFB diode lasers have typical output powers in the range of tens of miliwatts. For operating temperatures of -10 to 40 C, DFB diode lasers can be tuned over several nanometers.

The DFB quantum cascade laser (QCL)

QCLs are semiconductor lasers. The active region is design such that it contains a periodic series of thin layers of varying material compositions, forming a super lattice. Lasing in QCLs is achieved through intersubband transition in a repeated stack of semiconductor multiquantum well heterostructures as oppose to the recombination of electron hole pairs

described above (see Figure 3.3). Further details of the design and functioning of QCLs is found in [11].

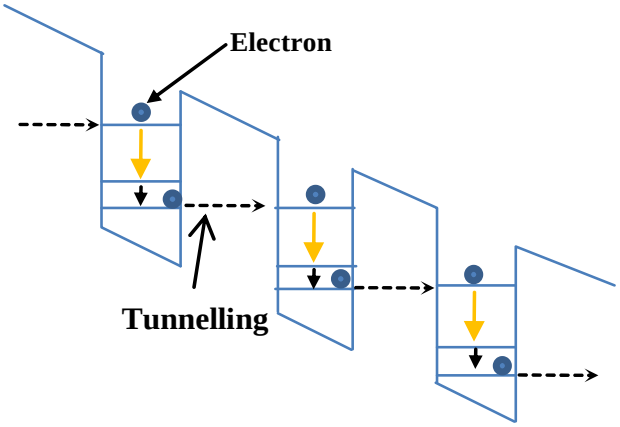

Figure 3.3: A schematic of the active region of a quantum cascade laser.

By applying an electric current to pump a QCL, electrons cascade down an energy staircase, emitting a photon at each step (yellow arrows). There is a second non-radiative transition at each step before the electron tunnels to the next quantum well. Due to a DFB structure, QCLs can be made single mode emitting. Most QCLs emit radiation in the mid infrared (IR) region with output power of hundreds of milliwatts. Typical line widths of such single mode QCLs are in the range of megahertz and below, good for gas sensing. Since the fundamental band of most IR active molecular are found in the mid IR region of the electromagnetic spectrum, QCLs are considered an important light source for high resolution laser absorption spectroscopy in the mid infrared (MIR) region of the electromagnetic spectrum. There are pulse and continuous wave QCLs now available.

The intra-pulse mode operation of QCLs

The intra-pulse chirp operation mode utilizes the intrinsic temperature rise inside the active area of the laser chip when a long current pulse is applied to pump the QCL. Right from the beginning of each pulse the emission wavelength increases within several nanoseconds. Thus, the laser emission spans a certain pulse-length-dependent spectrum within a single pulse. The laser wavelength sweeps from the blue towards the red side of the spectrum. By setting the laser temperature and the laser voltage, chirp-onset wavelength and laser power can be tuned. The sweep width is fixed by the pulse length. The lower panel of Figure 3.4 shows intra-pulse mode QCL pulses measured by QCLAS (Figure 3.1). The signal of the sample channel detector is in black (with CO absorption) and the reference channel detector in red (with the etalon removed). The upper panel of Figure 3.4 shows the signal of the reference detector when a QCL pulse with 255 ns length is transmitted through the FP etalon having a free spectral range (FSR) of about 0.05 cm^{-1}. The intra-pulse chirp for this condition is shown to be 1.85 cm^{-1} as evidenced by the number of 37 fringes. In principle intra-

pulse mode spectroscopy allows us to study the molecular spectrum of interest within one single laser pulse of a few nanoseconds, which might be important, e.g., in fast process studies or for sensing purposes in high dynamic environments.

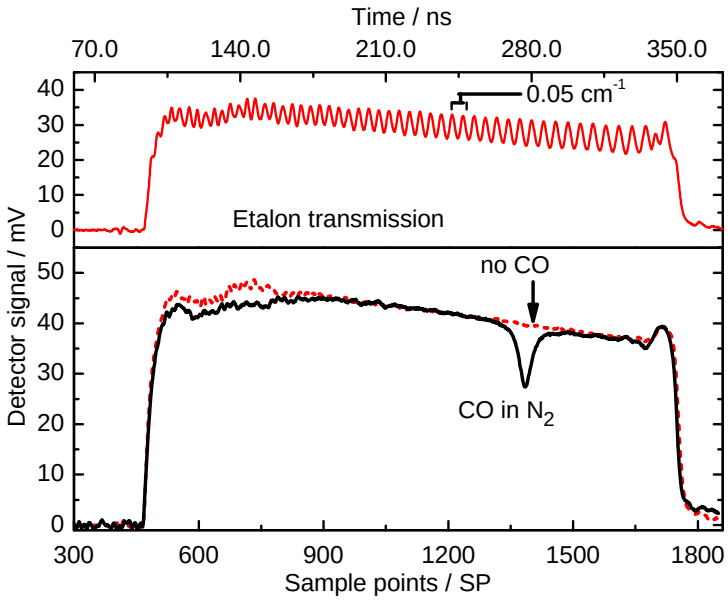

Figure 3.4: Intra-pulse chirp spectroscopy. Lower panel: Raw data from HgCdZnTe detectors (Det. 1 (red) and Det. 2 (black) in Figure 3.1). Data was measured when the QCL beam of light was passed through the 0.82 cm gas cell. Upper panel: Etalon transmission signal seen by the HgCdZnTe detector (Det. 1) with the etalon ($FSR_v \approx 0.05$ cm^{-1}) placed in the reference beam path.

3.1.1.2 Calibration of HgCdZnTe detectors

In order to derive an absolute amount fraction result, the linearity of the detectors used has to be ensured as discussed in the previous section. Detectors in the NIR might be linear in most cases, however, this is not the case when working in the MIR. Therefore, the HgCdZnTe detectors used for the QCLAS are discussed below.

The HgCdZnTe detectors used for the QCLAS (QCL emitting at 4.6 µm) measurements were nonlinear. Nonlinearity is a known concern for such detectors in the MIR [48]. There is presently no predicting model describing the HgCdZnTe detectors in the MIR [49].

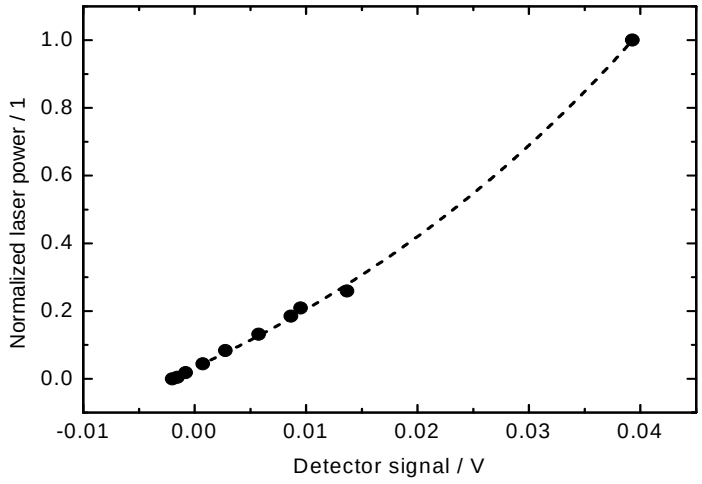

Figure 3.5: Measured dependence of incident laser power and resulting detector signal. The laser power was varied by stepping down the full laser power (no filter) by means of calibrated filters that had well-defined transmissions at 4.6 µm. An exponential growth, $y = 0.68578 \cdot \exp(x/0.04468) - 0.65273$, has been fitted to the measured data points in order to describe the detector's response function.

Figure 3.5 depicts a measured signal of the TE-cooled HgCdZnTe detector as a function of the incident laser power. The laser power was varied by stepping down the full laser power by means of calibrated filters that had well-defined transmissions at 4.6 µm. The result is a nonlinear behavior of the detector. What is displayed in Figure 3.5 is the so-called analytical function with axes flipped to power vs. signal to ease the application of a correction function[3]. Because of the measured nonlinearity of the HgCdZnTe detector, measured QCL signals, e.g., in Figure 3.4, have to be corrected for this nonlinearity to provide a linear signal scale and subsequently a linear transmission scale. This has to be done by means of the measured detector response function $y = 0.68578 \cdot \exp(x/0.04468) - 0.65273$ using a Labview code developed by the author.

Effect of detection nonlinearity

To demonstrate the effect of the nonlinearity of the TE-cooled HgCdZnTe detectors to the final amount of substance fraction, spectrometric CO amount fraction measurements were performed (signals in Figure 3.4). A gravimetric gas mixture containing 936 $\mu mol \cdot mol^{-1}$ CO in N_2 was used to perform the spectrometric measurements. The measurements were performed by probing the P(1) line of CO at 2139.43 cm^{-1}. Amount fraction results were derived when the measured QCL signals (Figure 3.4) were corrected or not corrected for the nonlinearity of the HgCdZnTe detector.

[3] Analytical versus calibration function, see also http://goldbook.iupac.org/A00332.html

Figure 3.6 shows CO amount fraction results evaluated when measured QCL signals were corrected and not corrected for the nonlinearity of the detectors. As shown in Figure 3.6, only the CO amount fraction results (open circles) calculated when the QCL signals were corrected meet the gravimetric target value of 936 µmol·mol^{-1}. The difference between the two (solid and open circles) CO amount fraction results in Figure 3.6 is about 30 %, indicating that the correction of the nonlinearity of the HgCdZnTe detectors used in this work for absolute CO amount fraction measurements was indespensable.

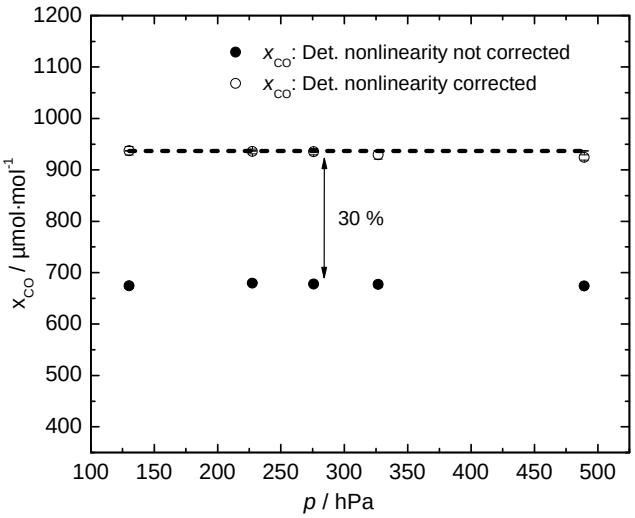

Figure 3.6: Plot of the amount fraction of CO when measured QCL signals are corrected (solid circles) or not corrected (open circles), for the HgCdZnTe detectors' detector nonlinearity, as a function of pressure. Each data point is the mean of 10 consecutive measurements (at the same pressure). The dashed line is the gravimetric reference target value of (936.6 µmol/mol).

3.1.1.3 Path length calibration

The path length of a gas cell should be accurately known (TDLAS and QCLAS, Figure 3.1) for any amount fraction quantification. For single-pass gas cells, the path length can easily be determined using mechanical measurements. For multipass gas cells, it becomes more challenging. In this thesis, for instance, the path length of the multipass 21 m gas cell (cell 2) shown in Figure 3.1 was calibrated by means of a reference gas cell of a known path length of 20 cm (cell 1). In this section, a general view of the calibration method is presented without referring to a specific setup.

Figure 3.7 depicts a schematic diagram of a laser absorption spectrometer, similar to Figure 3.1, used to determine the path length of a 21 m multipass gas cell. Here, a gas mixture, injected into the gas cell(s), was used to perform the calibration measurements [21], [50]. Note: Information of the exact amount fraction of the target species in the gas mixture is not necessary for the calibration process.

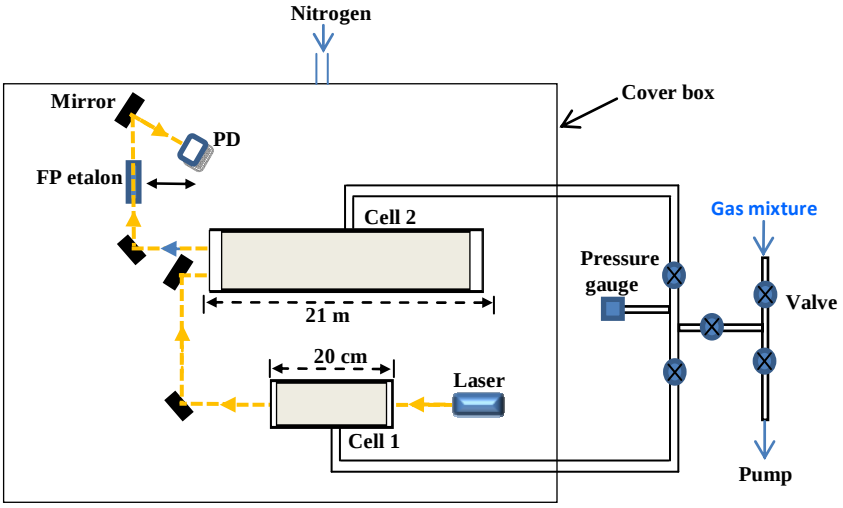

Figure 3.7: Schematic of the setup used to determine the path length of the multipass gas cell used. PD: Photo diode. FP: Fabry-Perot etalon (removable). The cover box is continuously purged with nitrogen.

To determine the path length of the 21 m gas cell, Eqn. (2.26) is used, i.e.,

$$x_{\text{species}} = A_{\text{line}} \cdot \frac{k_B \cdot T}{S_T \cdot r_{\text{iso}} \cdot L \cdot p} \tag{3.1}$$

By filling the 20 cm gas cell with a gas mixture, spectrometric measurements will yield

$$\begin{aligned} x_{\text{species}} &= A_{\text{line}(l_i)} \cdot \frac{k_B \cdot T_{l_i}}{S_{T_{l_i}} \cdot r_{\text{iso}} L_1 \cdot p_{l_i}} \\ &= A_{\text{line}(l_i)} \cdot \chi_i \end{aligned} \tag{3.2}$$

where the subscript 1 represents gas cell 1 and i the measurement number. The quantity $\chi_i = k_B \cdot T_{l_i} / (S_{T_{l_i}} \cdot r_{\text{iso}} \cdot L_1 \cdot p_{l_i})$.

Next, by filling the 21 m gas cell with the same gas mixture, after the 20 cm gas cell has been evacuated and purged with nitrogen, the spectrometric measurements will result to

$$\begin{aligned} x_{\text{species}} &= A_{\text{line}(2_j)} \cdot \frac{k_B \cdot T_{2_j}}{S_{T_{2_j}} \cdot r_{\text{iso}} \cdot L_2 \cdot p_{2_j}} \\ &= A_{\text{line}(2_j)} \cdot \kappa_j \end{aligned} \tag{3.3}$$

where 2 represents the gas cell 2 (21 m gas cell) and j the measurement number. The quantity $\kappa_j = k_B \cdot T_{2j} / (S_{T_{2_j}} \cdot r_{\text{iso}} \cdot L_2 \cdot p_{2_j})$. By combining Eqn. (3.2) and (3.3), the length of the 21 m gas cell L_2 is given by

$$L_2 = \left(\frac{\kappa_j}{\chi_i} \right) \cdot L_1 \tag{3.4}$$

The length of the 21 m gas cell can be evaluated by averaging all the values of L_2 for different combinations of i and j or simply by dividing the mean κ_j values by those of χ_i values (see an example in Table 3.1).

Table 3.1 shows results of the 21 m gas cell calibration. The spectrometric measurements were performed by TDLAS using a gas mixture containing CO_2 in N_2. The R(12) transition of CO_2 at 4987.31 cm^{-1} was probed. Typical absorbance data from the spectrometer in Figure 3.7 is shown in Figure 3.8.

Table 3.1: Results of the 21 m gas cell calibration. The quantities Sd and Se are the standard deviation and standard error, respectively.

p_{1i}	T_{1i}	S_{Ti} x 10^{-21}	$A_{line(1i)}$	χ_i x 10^{18}	Mean χ_i x 10^{18}	Sd χ_i x 10^{15}	Se χ_i x 10^{14}
/ hPa	/ K	/ cm^{-1}/(molec.·cm^{-2})	/ cm^{-1}	cm^{-1}·K/(cm/molec·hPa)			
605.94	295.72	1.25613	0.007214	2.8028	2.8031	1.0121	5.0606
499.13	295.71	1.25617	0.005942	2.8024			
289.01	295.7	1.25622	0.003441	2.8026			
187.43	295.78	1.25589	0.002232	2.8046			
p_{2i}	T_{2i}	S_{T2i} x 10^{-21}	$A_{line(2i)}$	κ_j x 10^{20}	Mean κ_j x 10^{20}	Se κ_j x 10^{18}	Se κ_j x 10^{18}
25.91	296.54	1.25282	0.03334	3.0457	3.0610	2.6576	1.5344
21.94	296.58	1.25266	0.02865	3.0917			
17.78	296.59	1.25262	0.02287	3.0456			
15.07	296.59	1.25262	0.01871	2.9397			
	Length calculation						
L_1	**u(L_1)**	**L_2**	**GUM-u(L_2) / m**				
/ m	**/ m**	**/ m**	**/ m**				
0.2	**2.50 x 10^{-7}**	**21.84**	**1.1 x 10^{-1}**				

The value of L_2 of (21.84 ± 0.11) m at the bottom of Table 3.1 is calculated by means of Eqn. (3.4) using the mean values of κ_j and χ_i in Table 3.1. The standard uncertainty of L_2 of 0.11 m (±0.5 % relative), calculated using the Se values in Table 3.1 as the standard uncertainties of κ_j and χ_i, was calculated by means of the GUM workbench software [51].

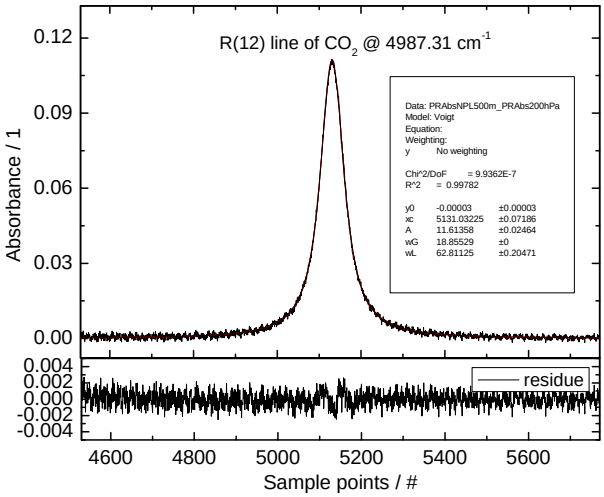

Figure 3.8: 21 m gas cell calibration. Plot of the absorbance data as a function of sample points. A voigt profile is fitted to the absorbance data to derive a value for the line area.

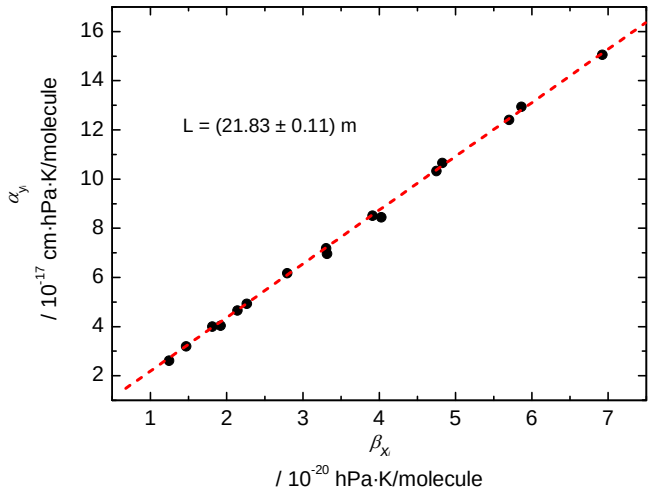

Figure 3.9: Plot of the values of α_{y_i} as a function of values of β_{x_i}. The slope of the linear regression yielded L_2.

Alternatively, by combining Eqn. (3.2) and (3.3),

$$(S_{T_{l_i}} \cdot L_1 \cdot p_{l_i} \cdot A_{line(2_j)} \cdot T_{2_j}) = L_2 \cdot (A_{line(l_i)} \cdot T_{l_i} \cdot S_{T_{2_j}} \cdot P_{2_j}) \quad (3.5)$$

$$\alpha_{y_i} = L_2 \cdot \beta_{x_i} \quad (3.6)$$

where $\alpha_{y_i} = S_{T_{l_i}} \cdot L_1 \cdot p_{l_i} \cdot A_{line(2_j)} \cdot T_{2_j}$ and $\beta_{x_i} = A_{line(l_i)} \cdot T_{l_i} \cdot S_{T_{2_j}} \cdot P_{2_j}$. The slope from a generalized linear regression applied to values of α_{y_i} plotted as a function of β_{x_i} yields the value of L_2. Figure 3.9 depicts a linear regression applied to values of α_{y_i} plotted as a function β_{x_i} for the measurements presented in Table 3.1. The slope value of L_2 of (21.83 ± 0.11) m agrees perfectly with the value of L_2 in Table 3.1. Typical standard uncertainties of path lengths used for amount fraction calculations in this work were in the range of ±0.5 % relative.

3.1.1.4 Correction of offsets

Two offsets, a DAC card offset (Ω_{card}) and an optical zero offset (Ω_{zero}) were identified and later during data processing corrected for. The description of the measurements and correction process is part of an in-house quality ensurance document [52].

Card offset

An example of measured data used to correct for the zero offset (card offset Ω_{card}) of the Gage DAC card is shown in Figure 3.10. A plot of a reference signal as a function of the measured signal from two channels (A-reference and B-sample) is depicted in Figure 3.10.

One expects the slopes in Figure 3.10 to pass through the origin with their values unity. This is, however, not the case. Thus, in order to get a zero intercept value, one has to apply the card offset Ω_{card} (intercept values in Figure 3.10). Applying a card offset to establish a zero signal level and consequently a zero transmittance level (see section 3.1.2) is indispensable in absolute amount fraction measurements. In order to compensate for the slope deviating from unity, the raw data has to be scaled [52].

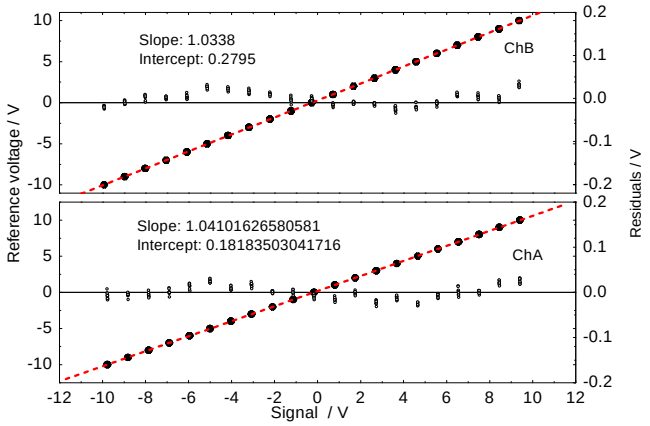

Figure 3.10: Plot of reference voltage (solid circles) as a function of measured voltage for a Gage DAC (Compuscope 85G) 8 bit A/D converter. The lower panel and the upper panels are the reference and sample channels, respectively. A linear function is fitted to the data of each channel. The black data points (open circles) in the vicinity of zero are the residuals from the fit.

Optical zero offset

In Figure 3.11a is an example of a measurement depicting a reference signal (black) with no absorption and a sample signal (with absorption). The measurement was performed using TDLAS. The R(12) line of CO_2 at 4987.31 cm^{-1} was probed. The XInGaAs detectors were linear in the ± 10 V range used.

Here, it is called optical zero if the sample signal is zero caused by molecular absorption (total absorption) in the probed absorption line. The measurement presented in Figure 3.11 was performed using pure CO_2. One expects the detector signal at optical zero (signal zero, Figure 3.11a) to be at the same voltage level as for a blocked beam (chopper zero, Figure 3.11a). Here, this is not the case, as shown in Figure 3.11b, because of possible side mode emissions of the DFB 2.004 µm laser whose emitted photons can not be absorbed by the molecule.

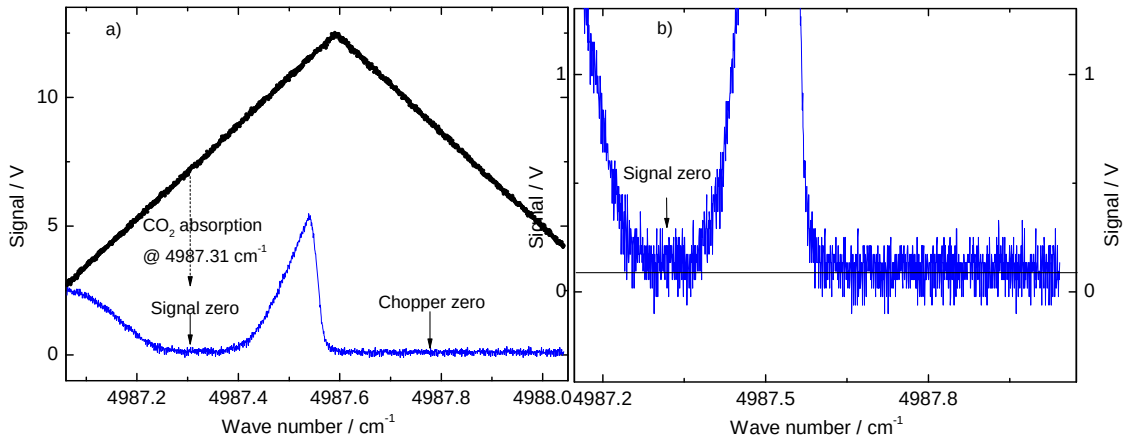

Figure 3.11: a) Signal from the reference detector (black) and the sample detector (blue) as a function of wave number. b) Zoom in of the blue signal in (a) showing the signal zero level.

Because of the side mode emissions of the laser, a non-vanishing detector signal is detected even in the case when all light of the main mode is absorbed by the molecules (Figure 3.11, signal zero). From Figure 3.11, the difference between chopper zero and signal zero yields a value of optical zero offset of $\Omega_{zero} = 0.04242$ V, with a standard deviation of $u(\Omega_{zero}) = 0.006928$ V. This optical zero offset value is subtracted from all measured signals of the sample channel [52].

3.1.2 Data processing

Figure 3.12a depicts typical signals measured by TDLAS (setup in Figure 3.1). The QCL signals in Figure 3.4 could also be used in the description of data processing in this

subsection. The data in Figure 3.12 was measured when the beam of light of the 2 µm DFB laser was passed through the 0.82 m gas cell. (note: R-OAP was removed). The red (without absorption) and the black (with absorption) are the reference and the sample signals (from Det.1 and Det. 2), respectively. The transmission in the bottom panel of Figure 3.12a is derived as the ratio of the sample signal to the reference signal. In the top panel is the signal of Det. 1 when an FP etalon is placed on the beam path to Det. 1. The advantages of using a two-channel spectrometer in Figure 3.1 are as follows. There is effective control of

- baseline changes due to e.g. fluctuations in the laser power
- the drift of detection system during measurements and
- residual gas, e.g. CO_2, that might be present in the optical bench.

These three points are important in absolute amount fraction measurements. In order to derive an absolute amount fraction result, three important tasks had to be done,

- the transmittance levels 0 and 1 (see Figure 3.12a) had to be properly established
- the linearity of the detectors between the transmittance level 0 and 1 had to be ensured
- a linear wave number axis also had to be established.

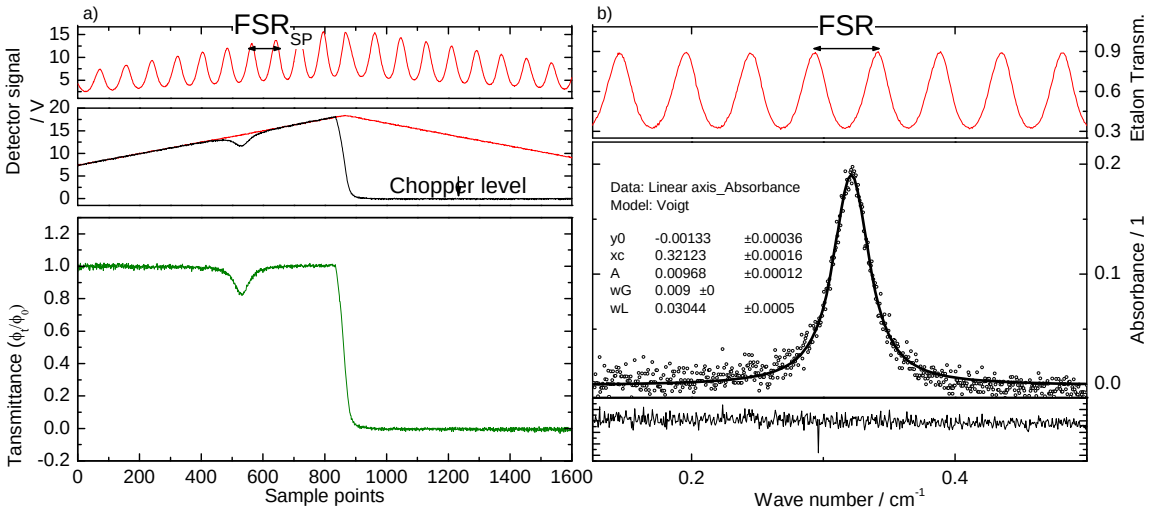

Figure 3.12: Data processing. a): Bottom panel: Transmission as a function of sample points. Middle panel: Reference signal (red, from Det. 1) and sample signal (black, from Det. 2). b) Middle panel: Absorbance plotted as a function of wave number. A Voigt profile is fitted to the absorbance data to obtain a value for the line area.

In this work, the transmittance level 0 was established by means of the chopper level.

The transmittance level 1 was established by properly matching, by adjusting the gain and offset of e.g., an amplifier, the reference signal to the sample signal as shown in Figure 3.12a.

The linearity of the detectors was ensured by performing a separate measurement such as, e.g., the example in section 3.1.5. The XInGaAs detectors used for TDLAS were linear as discussed above.

A linear wave number axis was accomplished by means of the sweep rate $r_{sweep} = FSR_{\nu} / FSR_{SP}$. FSR_{ν} is the known free spectral range of the etalon of 0.05 cm^{-1} and FSR_{SP} is the experimental fringe separation measured in the time domain (SP), derived by fitting a multipeak function to the data, visible in the top panel of Figure 3.12a and b.

The middle panel of Figure 3.12b shows absorbance data derived by means of the detector signals in the middle panel of Figure 3.12a. The absorbance is plotted as a function of the wave number (linear axis). A voigt profile is fitted to the absorbance data by means of a nonlinear least square fit (Levenberg-Marquardt) [50] to derive a value for the line area (A_{line}). The voigt is fitted keeping the Gaussian width fixed due to a constant temperature maintained in the gas cell during the measurements. The Gaussian width is calculated using Eqn. (2.13). By deriving a value of the line area, the amount fraction were calculated using Eqn. (2.26).

The data processing procedure described above was also applied to QCLAS amount fraction measurements presented in the work.

3.2 CRD spectrometer

3.2.1 Setup

The schematic depiction of the optical feedback (OF)-CRDS setup used in this work is shown in Figure 3.13. The OF-CRDS setup is also capable of performing optical feedback cavity enhance absorption spectroscopy (OF-CEAS). A detailed description of the setup in Figure 3.13 is found in [3], [53-55].

The light source is a DFB laser emitting at 1.6 μm mounted in a cylindrical housing and placed on a translation stage. The drive electronics contain an inbuilt driving current ramp to tune the wavelength of the DFB laser. The emitted light from the laser is colliminated by an aspheric lens attached to the laser housing.

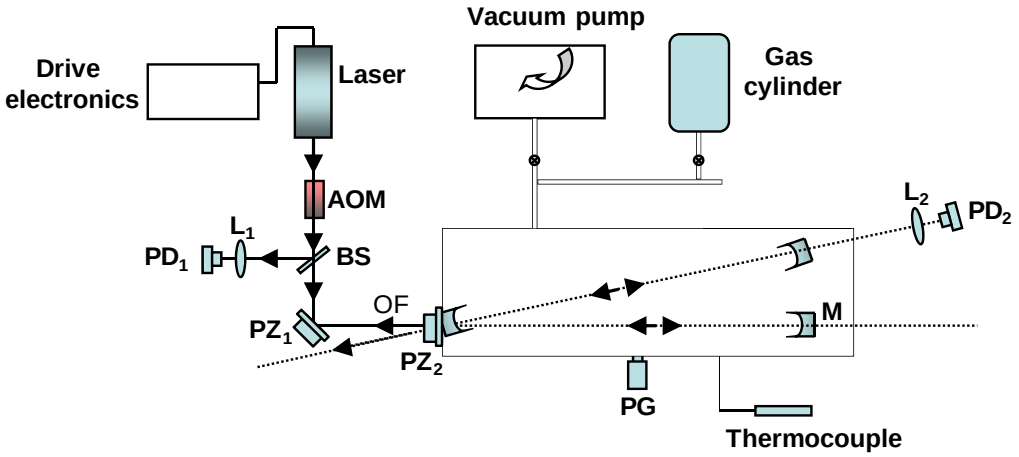

Figure 3.13: Schematic diagram of the experimental OF-CRDS setup. AOM: Acousto optical modulator, PZ: Piezo-controlled mirrors, OF: Optical feedback, PD: Photodiode, M: Mirror, PG: Pressure gauge, BS: Beam splitter, L: Lens.

An acousto optical modulator (AOM) placed along the collimated beam path, acting as an attenuator, controls the returning radiation to the laser for optical feedback (OF) locking. The AOM also functions as a switch for CRDS. A beam splitter splits the output beam from the AOM, the first part being incident on a reference detector to monitor the laser power incident to the cavity, and the second part injected into a V-shaped cavity of length 50 cm (gas cell). A piezo-controlled mirror placed just before the cavity controls the optical feedback phase by adjusting the laser-cavity distance. In some cases a second piezo-element, attached to the input window of the V-cavity, was used to modulate the cavity length, thus, increasing the spectral resolution of the spectrometer. InGaAs photodiodes, PD_1 and PD_2, are used for signal detection. The advantage of a V-shaped cavity in the setup in Figure 3.13, as opposed to multipass gas cells, is the small sample volume that can be reduced to about 10 cm^3 for the 50 cm long V-shaped gas cell. The Pt-100 temperature sensor and the MKS pressure gauges used in the setup in Figure 3.1 were used to measure the temperature and the pressure of an analyte, respectively. Spectrometric amount fraction measurements were performed using gravimetric gas mixtures. Data acquisition was performed by a 16 bit National Instrument DAC at a sampling rate of 1.25 MS/s. The acquisition of the data was controlled by a Labview program.

3.2.2 CRDS data processing

The top panel of Figure 3.14 depicts the transmitted intensity through the V-shaped cavity in Figure 3.13 as a function of mode number when a gas mixture containing CO and CO_2 is present in the cavity. The ring down times with absorption and without absorption are used to derive the absorption coefficient data in the lower panel of Figure 3.14 according to Eqn. (6.10). The detection limit of the OF-CES instrument when operated in the CRDS mode is about $1 \cdot 10^{-9}$ cm^{-1}.

In order to avoid saturation effects and accurately calculate the ring down times, spectrometric measurements are done in the pressure regime where the probe transitions are not affected by saturation effects. Typical ring down times of the OF-CES setup were 20 µs.

The spectrometer in Figure 3.13 is capable of performing OF-CEAS as discussed in the previous section. For OF-CEAS, absorption coefficient data is obtained by recording the transmission maxima of the successive TEM_{00} resonances (modes in the upper panel of Figure 3.14) of the high finesse V-shaped cavity. By fitting an appropriate function to the measured absorption coefficient yields the line area of an absorption peak. The line area is used to determine the amount of substance fraction of the target species, e.g., CO_2, as presented in chapter 6 (Eqn. (6.11)).

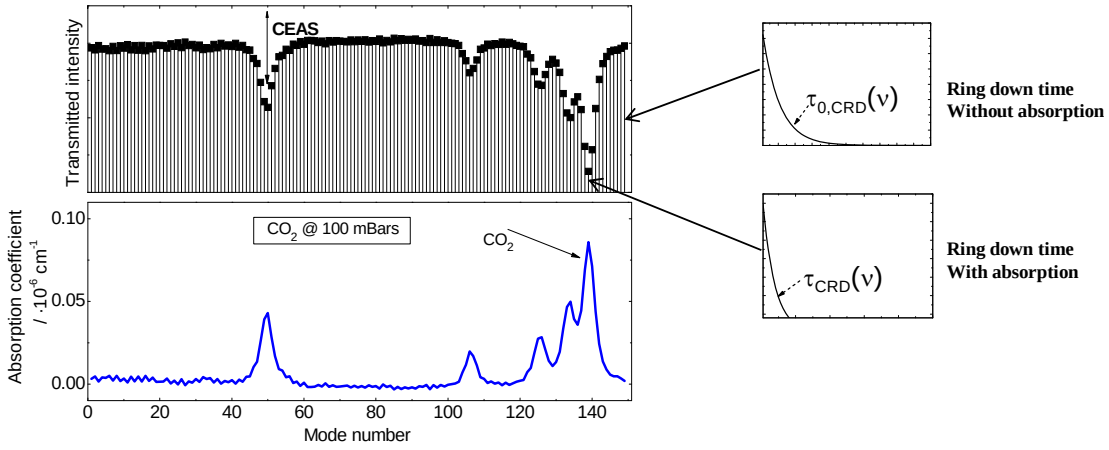

Figure 3.14: Top panel: Transmitted intensity through the V-shaped cavity as a function of mode number. Bottom panel: Absorption coefficient data of CO (100 µmol/mol) and CO_2 (50 mmol/mol) as a function of mode number.

A huge advantage of the OF-CRDS setup over the TDLAS/QCLAS setup in Figure 3.1 is the enhancement of the optical path length to 6000 m (ringdown time of 20 µs). Also, since the spacing of the data (modes) points in Figure 3.14 correspond to a free spectral range (152 MHz), the frequency scale of the absorption coefficient data is linear to a high degree, thus, no calibration of the frequency scale is required.

3.3 Measurement method

This subsection is devoted to the measurement method (*TILSAM*) and the different amount fraction retrieval strategies used in this work. It begins with a decription of the *TILSAM* method, showing the different steps in a flow diagram (schematic) steps necessary to derive a traceable amount fraction result, and ends with the direct and regression-based amount fraction retrieval strategies.

3.3.1 The *TILSAM* method

The spectrometric measurements are all performed based on the *TILSAM* method [21]. The *TILSAM* method in its present form only considers TDLAS. However, an improved version of it, including the implementation of QCLAS and CRDS will soon be available [56]. Figure 3.15 depicts a schematic diagram that summarizes the implementation of the *TILSAM* method to TDLAS, QCLAS and CRDS measurements.

Following the Beer-Lambert law (Eqn. (2.23)), the spectral absorbance is measured in the case of TDLAS and QCLAS and the absorption coefficient in the case of CRDS. The line areas of TDLAS and QCLAS or CRDS are derived by integrating the spectral absorbance data or the absorption coefficient over wave number, respectively. A traceable amount fraction of the gas species present in the gas cell is calculated using the known input parameters path length L of the gas cell (TDLAS and QCLAS), the line strength of a probed transition S of the analyte, the Boltzmann constant k_B, the measured gas temperature T and the total gas pressure p_{total}. The traceability of the final amount fraction results depends on the traceability of all the input quantities. This is the ultimate goal for performing measurements based on the *TILSAM* method [21].

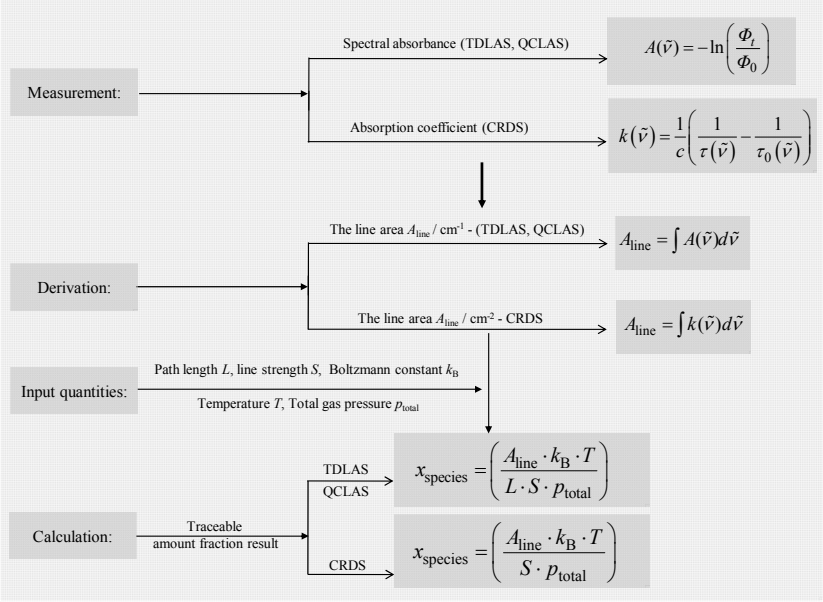

Figure 3.15: A schematic diagram of the *TILSAM* method implemented to TDLAS, QCLAS and CRDS. The line area A_{line} for CRDS is given in units of cm^{-2} as compared to that of TDLAS and QCLAS given in units of cm^{-1}.

As discussed in section 1, for the derivation of an amount fraction, the *TILSAM* method aims to standardize the raw data processing and modelling as well as represent and document a combination of steps necessary to apply IR spectrometric as an absolute method.

3.3.1.1 Measurement sequence

The measurement procedure of the amount fraction measurement for this thesis as described in [57] is as follows. With the spectrometer in operation,

- The optical bench and the gas cell are purged with e.g. nitrogen.
- The gas cell is evacuated.
- A background measurement is performed, i.e., a measurement with no analyte in the gas cell.
- The sweep rate (tuning rate of the laser) for TDLAS and QCLAS is measured.
- The sample measurements are performed.
- A second background measurement is performed at the end of the last sample measurement. This is done after the gas cell has been purged with nitrogen and evacuated.
- The sweep rate of the laser is measured a second time.

Measuring the background and the sweep rate at the beginning and at the end of the measurements is to check the quality of the measurements as well as the stability of the laser during the measurement process as it is also documented in [21], [57]. The establishment of a measurement procedure, briefly described above, was to enable consistency in all spectrometric measurements presented in this thesis.

3.3.1.2 Amount fraction retrieval strategies

In this work, two data retrieval strategies were used to derive the amount fraction of an analyte: direct and regression-based retrievals.

Direct retrieval

The amount fraction of the specific analyte is expressed as (Eqn. (2.26))

$$x_{\text{species}} = A_{\text{line}(\text{l}_\text{i})} \cdot \frac{k_\text{B} \cdot T_{\text{l}_\text{i}}}{S_{T_{\text{l}_\text{i}}} \cdot r_\text{iso} \cdot L_\text{l} \cdot p_{\text{l}_\text{i}}} = A_{\text{line}(\text{l}_\text{i})} \cdot (\Gamma_i)^{-1} \tag{3.7}$$

where $\Gamma_\text{i} = S_{T\text{i}} \cdot r_\text{iso} \cdot L \cdot p_\text{i} / (k_\text{B} \cdot T_\text{i})$. A variation in Γ, in this work, was mostly related to a controlled variation in the total gas pressure and to some extent to the temperature. The mean amount fraction of an analyte, derived by averaging all amount fraction results at different Γ values, was termed “directly retrieved”. The evaluation of a directly retrieved amount fraction result is documented in an in-house protocol [58].

Regression-based retrieval

In this thesis, regression-based retrieval means an amount fraction result is calculated by means of a generalized linear regression (GLR). Eqn. (3.7) can thus be rewritten as

$$A_{\text{line(i)}} = x_{\text{species}} \cdot \left(\frac{S_{T_i} \cdot r_{\text{iso}} \cdot L \cdot p_i}{k_B \cdot T_i} \right) = x_{\text{species}} \cdot \Gamma_i \tag{3.8}$$

From Eqn. (3.8), the slope from a GLR applied to values of $A_{\text{line(i)}}$ plotted as a function of Γ_i yields a "regression-based" amount fraction result. In this thesis, all generalized linear regressions were performed with the B_Least software developed by the BAM [59]. A GLR is recommended by the ISO 6143 [60] for purposes like this. The B_Least software calculates the slope by means of a GLR and outputs the result alongside the associated uncertainty and covariance. The regression-based retrieval strategy described above is documented in a protocol written by the author [58].

3.4 Uncertainty analysis

The uncertainty of a measurement result is defined as a parameter, associated with the result of a measurement that characterizes the dispersion of the values that could reasonably be attributed to the measurand [22]. In the following paragraphs a description of uncertainty calculations for this work, according to the prescriptions of the GUM, is outlined.

The mathematical relation between a measurand Y, e.g. the amount fraction of a gas species (xspecies), and the input quantities X_i, e.g. the line strength (S_T), the pressure (p), the gas temperature (T) and the path length (L), is given by

$$Y = f(X_i) \tag{3.9}$$

The input quantities X_i may be dependent on other input quantities, corrections and correction factors and maybe correlated. The function f may be explicitly written down, e.g Eqn. (2.26) for an amount fraction calculation, or determined experimentally [24].

The estimates of Y are denoted by y. In some cases y is computed as the average of a number of independent determinations of Y. The estimates of X_i are denoted by x_i. Therefore, from Eqn. (3.9), the output estimate of y can be expressed as

$$y = f(x_i) \tag{3.10}$$

The uncertainty associated with the estimated (measurand) y depends on the uncertainties of the input quantities x_i. The uncertainties of the input quantities x_i may be obtained from a single observation, repeated observations, based on experience or taken from external sources such as reference data obtained from handbooks. If the uncertainty of the input quantity is determined from a statistical analysis of a series of observations, it is termed type A uncertainty. If the uncertainty of an input quantity is obtained by means other than statistical analysis, it is termed type B uncertainty. Type B uncertainties are estimated using known or assumed probability density functions (PDF) [24].

The standard uncertainty of y is calculated using the uncertainties of all the input quantities. The combination of the uncertainties of all the input quantities ($u(x_i)$) to an uncertainty of y of $u_c(y)$ (combined uncertainty) is done using the law of propagation of uncertainty. The law of propagation of uncertainty as presented in [24] is expressed by

$$u_c^2(y) = \sum_{i=1}^{N} \left(\frac{\partial f}{\partial x_i} \right)^2 \cdot u^2(x_i) + 2 \sum_{i=1}^{N-1} \sum_{j=i+1}^{N} \frac{\partial f}{\partial x_i} \frac{\partial f}{\partial x_j} u(x_i, x_j) \cdot (x_i, x_j) \tag{3.11}$$

when the input quantities are correlated. The quantity $\partial f / \partial x_i$ is called the sensitivity coefficient. The sensitivity coefficient describes how the output estimate y varies with changes in the values of the input estimates x_i. In cases where correlations can be excluded, only the first term in Eqn. (3.11) is used to calculate the combined uncertainty $u_c(y)$.

It is necessary, e.g., in regulatory applications, that an interval which encompasses a large fraction of the distribution of the values of a measurand be defined. A measure of uncertainty that meets the requirements of an interval is termed the expanded uncertainty U [24]. The expanded uncertainty is calculated by multiplying $u_c(y)$ by a coverage factor k, i.e.,

$$U = k \cdot u_c(y) \tag{3.12}$$

The coverage factor k expresses the probability that the true value of the measurand y is contained within a specified interval of measured values based on the information available. For a situation where the possible values of the measurand are normally distributed, then $k = 2$ produces an interval having a level of confidence of 95 % that the true value is included.

There are several software tools that could be used to calculate the uncertainty of a measurand. In this work the GUM workbench [51] was used. In calculating the uncertainty of a measurand, the GUM workbench follows the principles given in the Joint Committee for Guides in Metrology (JCGM) guidelines on the evaluation of the uncertainty in measurements which are the same as the guidelines of the ISO GUM [24], [61], [62].

The GUM workbench supports a systematic procedure in assessing an uncertainty budget, starting with a mathematical equation which models the physical relationship of quantities involved in the respective measurement and all available information on uncertainties. The result of the analysis is an uncertainty budget [51]. The uncertainty budget holds all used quantities with their symbols, assigned standard uncertainties and actual degrees of freedom [51] (number of observations minus one), the sensitivity coefficients derived from the model equation and the resulting contribution to the standard uncertainty of the final measurement result. Finally, the value component of the measurement result, its expanded uncertainty, and the coverage factor are reported in the budget. Expressing it as a table, it is easy to see which input quantity has the most significant uncertainty contribution, since this is expressed by the index figure in a GUM workbench budget (Appendix IV). This information can be used to predict an improvement in the uncertainty of the measurement result, while optimizing certain or multiple input quantities [51].

3.4.1 Uncertainty assessment for spectrometric amount fraction results

To calculate the uncertainty of the amount fraction results in this work, Eqn. (2.26)

$$x_{\text{species}} = A_{\text{line}} \cdot \frac{k_{\text{B}} \cdot T}{S \cdot r_{\text{iso}} \cdot L \cdot p} \tag{3.13}$$

was used as model funnction for TDLAS and QCLAS and Eqn. (6.11),

$$x_{\text{species}} = A_{\text{line}} \cdot \frac{k_{\text{B}} \cdot T}{S \cdot r_{\text{iso}} \cdot p} \tag{3.14}$$

was used as model function for CRDS. The uncertainties of all the input quantities in Eqn. (3.13) and (3.14) were calculated as follows:

The uncertainty of the line area A_{line}

The uncertainty of the line area was calculated using the uncertainty of the line area fitting [63] and that of the sweep rate $u(r_{\text{sweep}})$. The uncertainty of the sweep rate was evaluated using $r_{\text{sweep}} = \text{FSR}/\text{FSP}_{\text{SP}}$ as model equation (see Table 4.2).

The uncertainty of the Boltzmann constant

The value of the Boltzmann constant of 1.380 6505 x 10-23 J/K and its standard uncertainty of 0.000 0024 x 10-23 J/K was taken from [64].

The uncertainty of the temperature

The gas temperatures were measured with a Pt-100 temperature sensor connected to a testo 650 with an accuracy specification of 0.1 °C as discussed in section 3.1.1. The temperature sensor was calibrated by [65]. Its standard uncertainty at a temperature in the vicinity of 296 K, where most of the measurements in this work were performed, was ±0.2 K. However, a more conservative value of ±0.5 % relative was used in some cases. This was to account for the fact that the gas temperature was measured on the cell walls instead of inside the gas cell.

The uncertainty of the line strength S_T

The uncertainty of the line strength at gas temperature T (S_T) was calculated by means of the GUM workbench. Eqn. (2.11) was used as the model function

$$S_T = S_{T_0} \left(\frac{T_0}{T} \right)^{\text{j}} \exp\left\{ -hc \frac{E}{k_{\text{B}}} \left(\frac{1}{T} - \frac{1}{T_0} \right) \right\} \frac{\left[1\text{-}\exp\left\{ -hc \frac{\tilde{\nu}_0}{k_{\text{B}} T} \right\} \right]}{\left[1\text{-}\exp\left\{ -hc \frac{\tilde{\nu}_0}{k_{\text{B}} T_0} \right\} \right]} \tag{3.15}$$

The uncertainty of S_{To} ($T_0 = 296$ K) was taken from published papers or from a data base, e.g., HITRAN [26]. The estimation of j and its uncertainty is described in section 8.2.3. The uncertainties of k_B and T have been discussed above. The speed of light (c) of 299792458 $m \cdot s^{-1}$ and the Plank constant of 6.626 0693 x 10^{-34} Js and its standard uncertainty of 0.000 0011 x 10^{-34} Js were taken from [64]. The constants E and $\tilde{\nu}_0$ were obtained from [26]. An example of an uncertainty budget of S_T is shown in Appendix V.

The uncertainty of the path length L

Depending on the gas cell, the uncertainty of the path length(s) was (were) calculated as presented in section 3.1.1.3 or taken from a calibration certificate of the gas cell. For instance, here, the calibration certificate of the 20 cm gas cell, used to calibrate the 21 m gas cell in section 3.1.1.3, was provided by working group 5.32, Coordinate Measurements, of PTB.

The uncertainty of the pressure p

The uncertainty of the pressure (p) was calculated by means of the GUM workbench software. The model equation was a correction function derived using data from the calibration certificate of the capacitance detector gauge MKS model 626AX11TDE and MKS model 626AX13TDE [45]. An example of estimating the uncertainty of the gas pressure is shown in Appendix IV.

The uncertainty of directly retrieved amount fraction result

The uncertainty of the directly retrieved amount fraction results was calculated by means of the GUM workbench. Eqn. (3.13) was used as the model equation. An example of an uncertainty budget for a directly retrieved amount fraction (x_{CO2} at the 500 µmol/mol level), at single pressures, is shown in Table 3.2. The budget holds the model equations, input quantities such as the line area A_{line}, the total gas pressure p_{total}, the temperature T, the path length L, the values of input quantities and the associated standard uncertainties, degrees of freedoms, sensitivity coefficients and indices [51].

The combined uncertainty of directly retrieved amount fractions, evaluated from N individual amount fraction uncertainties $u(x_i)$, was calculated as

$$u_c = {}^{1}\!\Big/\!_{\sqrt{N}} \cdot \sqrt{\sum_{i}^{N} u^2(x_i)} \qquad (3.16)$$

Table 3.2: An uncertainty budget, derived by means of GUM workbench, of a directly retrieved CO_2 amount fraction at the 500 µmol/mol level.

Model equation: $x_{CO2} = A_{line} \cdot k_B \cdot T / (S_T \cdot r_{iso} \cdot L \cdot p_{total})$ with $r_{iso} = x_{12CO2} / x_{12CO2HITRAN}$

TILSAM CO_2

x_{CO2}: Result

Uncertainty Budget:

Quantity	Value	Standard Uncertainty	Degrees of Freedom	Sensitivity Coefficient	Uncertainty Contribution	Index
A_{line}	0.010420 cm^{-1}	$104 \cdot 10^{-6}$ cm^{-1}	49	0.048	$5.0 \cdot 10^{-6}$ mol/mol	46.7 %
p_{total}	309.6310 hPa	0.0280 hPa	50	$-1.6 \cdot 10^{-6}$	$-45 \cdot 10^{-9}$ mol/mol	0.0 %
T	295.90 K	1.00 K	50	$3.3 \cdot 10^{-6}$	$3.3 \cdot 10^{-6}$ mol/mol	20.3 %
L	2184.0 cm	11.8 cm	6	$-230 \cdot 10^{-9}$	$-2.7 \cdot 10^{-6}$ mol/mol	13.6 %
S_{To}	$1.25500 \cdot 10^{-21}$ $cm^{-1}/(cm^{-2} \cdot molecule)$	$6.28 \cdot 10^{-24}$ $cm^{-1}/(cm^{-2} \cdot molecule)$	50	$-400 \cdot 10^{15}$	$-2.5 \cdot 10^{-6}$ mol/mol	11.7 %
k_B	$13.8065050 \cdot 10^{-24}$ J/K/molecule	$24.0 \cdot 10^{-30}$ J/K/molecule	50	$36 \cdot 10^{18}$	$870 \cdot 10^{-12}$ mol/mol	0.0 %
E	60.8709 cm^{-1}					
c	$29.9792458 \cdot 10^{9}$ cm/s					
h	$662.606930 \cdot 10^{-36}$ Js	$110 \cdot 10^{-42}$ Js	50	$76 \cdot 10^{24}$	$8.3 \cdot 10^{-15}$ mol/mol	0.0 %
T_0	296.0 K					
v_0	4987.30830 cm^{-1}	$4.00 \cdot 10^{-3}$ cm^{-1}	50	0.0	0.0 mol/mol	0.0 %
j	1.250	0.144	infinity	$-170 \cdot 10^{-9}$	$-24 \cdot 10^{-9}$ mol/mol	0.0 %
S_T	$1.25540 \cdot 10^{-21}$ $cm^{-1}/(cm^{-2} \cdot molecule)$	$7.47 \cdot 10^{-24}$ $cm^{-1}/(cm^{-2} \cdot molecule)$				
x_{12CO2}	0.98420	$4.00 \cdot 10^{-3}$	50	$-510 \cdot 10^{-6}$	$-2.0 \cdot 10^{-6}$ mol/mol	7.7 %
$x_{12CO2HITRAN}$	0.984204					
r_{iso}	1.00000	$4.06 \cdot 10^{-3}$				
x_{CO2}	$501.4 \cdot 10^{-6}$ mol/mol	$7.34 \cdot 10^{-6}$ mol/mol	110			

An example of the combined uncertainty of a directly retrieved amount fraction, evaluated from the uncertainties $u(x_i)$ of N individual amount fraction uncertainties, is shown in Appendix VI.

The uncertainty of a regression-based amount fraction result

The B_Least software was used to calculate the uncertainty of the regression-based amount fraction results. Eqn. (3.8) was used as model function. The slope from a GLR of values of $A_{line(i)}$ plotted as a function of Γ_i yields a "regression-based" amount fraction result and its associated uncertainty. The uncertainties of A_{line} and Γ were evaluated by means of the GUM workbench software [51]. Table 4.3 and Appendix I hold the uncertainty budget for A_{line} and Γ, respectively.

The repeatability

In this work, the standard deviation of the mean of, e.g., N individual amount fraction results, was used to assign a value for the repeatability.

The reproducibility

Here, the standard deviation of, e.g., N individual amount fraction results, was used to assign a value for the reproducibility.

The normalized error

The normalized error E_n of a spectrometric amount fraction results, $x_{species}$, is expressed as

$$E_n = D/U(D)$$

where D is the degree of equivalence and $U(D)$ its expanded uncertainty. The degree of equivalence is given by

$$D = x_{species} - x_{ref}$$

where x_{ref} is the reference amount of substance fraction. The expanded uncertainty of D is

$$U(D) = 2 \cdot u(D) = 2 \cdot \sqrt{(u^2(x_{species}) + u^2(x_{ref}))} ,$$

where $u(D)$ represents the standard uncertainty of D. A coverage factor $k = 2$ is applied additionally.

If $|E_n| < 1$, the spectrometric amount fraction results ($x_{species}$) agree with the reference value (x_{ref}). If on the other hand $|E_n| > 1$, then the spectrometric amount fraction results do not agree with the reference value.

3.5 References for section 1 - 3

[1] W. Demtröder, *Laser spectroscopy - basic principles*, vol. 1. Berlin: Springer, 2008.

[2] K. Wunderle, S. Wagner, I. Pasti, R. Pieruschka, U. Rascher, U. Schurr, and V. Ebert, *Appl. Opt.*, vol. 48, pp. B172-B182, (2009).

[3] J. Morville, S. Kassi, M. Chenevier, and D. Romanini, *Appl. Phys. B*, vol. 80, pp. 1027-1038 (2005).

[4] V. Ebert and J. Wolfrum, "Absorption spectroscopy," in Optical Measurements-Techniques and Applications, 227-265 (Springer, 2001).

[5] S.T. Persijn, F. Harren, and A. van der Veen, *Appl. Phys. B*, vol. 100, pp. 383–390 (2010).

[6] P. Ortwein, W. Woiwode, S. Fleck, M. Eberhard, T. Kolb, S. Wagner, M. Gisi, and V. Ebert, Exp. Fluids online first (2010), DOI: 10.1007/s00348-010-0904-2

[7] A. Foltynowicz, W. Ma, and O. Axner, *Opt. Express*, vol. 16, no. 19, pp. 14689 - 14702, (2008).
[8] J. P. Lima, H. Vargas, A. Miklos, M. Angelmahr, and P. Hess, *Appl. Phys. B*, vol. 85, pp. 279-284, (2006).
[9] R. D. v Zee, *Cavity-enhanced spectroscopies*, vol. 40. Amsterdam: Acad. Press, 2002.
[10] David W. Ball, "*Photoacoustic Spectroscopy Spectroscopy*," vol. 21, no. 9, (2006).
[11] J. Faist, F. Capasso, D. L. Sivco, C. Sirtori, A. L. Hutchinson, and A. Y. Cho, "Quantum cascade laser," *Science*, vol. 264, pp. 553-556, (1994).
[12] C. Wang and P. Sahay, *Sensors*, vol. 9, pp. 8230-8262, (2009).
[13] J. U. White, *J. Opt. Soc. Am. B*, vol. 32, pp. 285-288, (1942).
[14] D. Herriot, H. Kogelnik and R. Kompfner, *Appl. Opt.*, vol. 3, pp. 523, (1964).
[15] R. F. Curl and F. K. Tittel, "*Tunable infrared laser spectroscopy*," *Annu. Rep. Prog. Chem., Sect. C*, vol. 98, pp. 219-272, (2002).
[16] W. Cao and Y. Duan, *Critical Reviews in Analytical Chemistry*, vol. 37, pp. 3-13, (2007).
[17] M. R. McCurdy, Y. Bakhirkin, G. Wysocki, R. Lewicki, and F. K. Tittel, *J. Breath Res.*, vol. 1, pp. 014001, (2007).
[18] C. Grote and J. Pawliszyn, *Anal. Chem.*, vol. 69, pp. 587-596, (1997).
[19] H. Lord, Y. F. Yu, A. Segal, and J. Pawliszyn, *Anal. Chem.*, vol. 74, pp. 5650-5657, (2002).
[20] B. Buszewski, M. Kesy, T. Ligor, and A. Amann, *Biomedic. Chromatography*, vol. 21, pp. 553-566, (2007).
[21] O. Werhahn and J.C. Petersen (eds.), "TILSAM-protocol-V1_2010-09-29," 2010. Available from: http://www.euramet.org/fileadmin/docs/projects/934_METCHEM_Interim_Report.pdf.
[22] JCGM 200:2008, International vocabulary of metrology - Basic and general concepts and associated terms VIM 3rd edition, 2008. Available from: http://www.bipm.org/en/publications/guides/vim.html.
[23] V. Rozanov and A. Rozanov, *Atmospheric Measurement Techniques*, vol. 3, pp. 751-780, (2010).
[24] ISO Guide 98-3, Guide to the Expression of Uncertainty in Measurement, 1. International Organization for Standardization, Geneva 2008, ISBN 9267101889.
[25] L. S. Rothman, N. Jacquinet-Husson, C. Boulet, and A. M. Perrin, *C. R. Physique*, vol. 6, pp. 897-907, (2005).
[26] HITRAN2008, http://www.cfa.harvard.edu/HITRAN/, L. Rothman et al., J. Quant. Spectrosc. Rad. Transf. 110, 533 (2009)
[27] N. Jacquinet-Husson, N. A. Scott, A. Chédin, and e al., "The GEISA spectroscopic database : Current and future archive for Earth and planetary atmosphere studies," *J. Quant. Spectrosc. Rad. Trans.*, vol. doi:10.1016/j.jqsrt.2007.12.015, (2008).
[28] G. Padilla Viquez, J. Koelliker Delgado, O. Werhahn, K. Jousten, and D. Schiel, *IEEE Trans. Instr. Measur. J.*, vol. 56, no. 2, pp. 529-533, (2007).

[29] G. Casa, D. A. Parretta, A. Castrillo, R. Wehr, and L. Gianfrani, " *J. Chem. Phys.*, vol. 127, pp. 084311, (2007).
[30] EURAMET, "EMRP Call 2010 Industry and Environment," 2010. [Online]. Available: http://www.emrponline.eu/call2010/srte.html.
[31] R.H. Eggers, A. Kulp, R. Tegeler, F.E. Ludtke, G. Lepsien, B. Meyer, F.E. Bauer, Eur. J. Gastroenterol. Hepatol. **2**, 437 (1990)
[32] P. D. Klein, H. M. Malaty, R. F. Martin, and K. S. Graham, *Am. J. Gastroenterol.*, vol. 91, pp. 690-694, (1996).
[33] E.G. Giannini, R. Testa, Eur. Rev. Med. Pharmacol. Sci. **8**, 51 (2004).
[34] N. W. Solomons, D. A. Schoeler, J. B. Wagonfeld, D. G. Ott, I. H. Rosenberg, and P. D. Klein, *J. Lab. Clin. Med.*, vol. 90, pp. 431-439, (1977).
[35] G. Wysocki, R. F. Curl, F. K. Tittel, R. Maulini, J. M. Bulliard, and J. Faist, *Appl Phys B*, vol. 81, pp. 769-777 (2005).
[36] E. Andrieux, T. Zanon-Willette, M. Cadoret, A. Rihan, and J.J. Zondy, *Opt. Letters*, vol. 36, no. 7, pp. 1212-1214, (2011).
[37] EMRP, T2.J02–Breath Analysis, Joint Research Projects funded under iMERA-plus, 2010, http://www.euramet.org/index.php?id=imera-plus.
[38] Helmut H. Telle, Robert J. Donovan, *Laser Chemistry, Spectroscopy, Dynamics and Applications*. John Wiley & Sons Ltd, 2007.
[39] P. W. Atkins, *Physical Chemistry*, Second. 1983.
[40] R.R. Gamache, L.S. Rothman, *J.Molec. Structure*, vol. 517–518, p. 407–425, (2000).
[41] R. H. Dicke, *Phys. Rev.* vol. 89, no. 2, pp. 472 (1953).
[42] Lepère M., *Spectrochimica Acta A*, vol. 60, pp. 3249-3258, 2004.
[43] Luque J. M., et al., *J. Quant. Spectrosc. Radiat. Transfer*, vol. 92, pp. 151-161, 2005.
[44] QUANSYS FK7 13N8123, *Techn. Meseen* 72(6), 413-410 (2005)
[45] Calibration certificate for capacitance detector gauge MKS model 626AX13TDE", Calibration mark: 70328 PTB 10.
[46] IPM, Fraunhofer Institut für Physikalische Messtechnik, Freiburg, Germany, http://www.ipm.fraunhofer.de
[47] IAF, Fraunhofer Institut für Angewandte Festkörperforschung, Freiburg, Germany, http://www.iaf.fraunhofer.de
[48] E. Theocharous, J. Ishii, and N. P. Fox, *Appl. Opt.*, vol. 43, no. 21, pp. 4182-4188, (2004).
[49] L. Gianfrani, private e-mail communication.
[50] J. Nwaboh, P. Ortwein, O. Werhahn and V. Ebert, "PTB-3.22-AA-4 - "Path length calibration by means of a reference gas cell".
[51] GUM Workbench, 1.2 Win32, Metrodata GmbH, Grenzach-Wyhlen, Germany 1999, http://www.metrodata.de
[52] J. Nwaboh, O. Werhahn, "PTB-3.22-AA-1 - Correction of offsets for spectrometric measurements".
[53] J. A. Nwaboh, T. Desbois, D. Romanini, D. Schiel, and O. Werhahn, *Int. J. Spectrosc.*, vol. 2011 (2011), doi:10.1155/2011/568913.

[54] D. Romanini, M. Chenevier, S. Kassi, M. Schmidt, C. Valant, M. Ramonet, J. Lopez, H.-J. Jost, *Appl. Phys. B*, vol. 83, pp. 659-667, (2006).

[55] S. Kassi, M. Chenevier, L. Gianfrani, A. Salhi, Y. Rouillard, A. Ouvrard, and D. Romanini, *Optics Express*, vol. 14, No. 23, pp. 11442-11452, (2006).

[56] EMRP, T2.J02–Breath Analysis, Joint Research Projects funded under iMERA-plus, 2010, http://www.euramet.org/index.php?id=imera-plus.

[57] J. Nwaboh, O. Werhahn, "PTB-3.22-AA-2 - Measurement procedure based on IR absorption spectroscopy for amount fraction evaluation".

[58] J. Nwaboh, O. Werhahn, "3.22-AA-3 - Processing procedure for amount fraction derivation from infrared absorption spectra".

[59] BAM, Bundesanstalt für Materialforschung und -prüfung, Berlin, Germany, http://www.bam.de

[60] ISO 6143: 2001 Gas analysis - Comparison methods for determining and checking the composition of calibration gas mixtures. 2001.

[61] JCGM 104:2009, Evaluation of measurement data - An introduction to the "Guide to the expression of uncertainty in measurement" and related documents, 2009. Available from: http://www.bipm.org/en/publications/guides/gum.html.

[62] JCGM 100:2008, Evaluation of measurement data - Guide to the expression of uncertainty in measurement, GUM 1995 with minor corrections, ISO IEC Guide 98-3, 2008. Available from: http://www.bipm.org/en/publications/guides/gum.html.

[63] Origin 7.5 SR6, OriginLab Cooperation, Northampton, MA, USA 2006, http://www.OriginLab.com.

[64] CODATA Internationally recommended values of the Fundamental Physical constants, NIST(2000).

[65] Calibration certificate of temperature sensor PT-100-testo 650, calibration mark: 2551 PTB 09.

4 CO_2 quantification at 2 µm

Editorial note

In this chapter, a manuscript is presented that has to be submitted for publication in Measurement Science and Technology. The coauthorship is being held by J. Nwaboh, D. Schiel and O. Werhahn. The numbering of the manuscript was changed from the original version to match that of this thesis. Due to its independent manuscript nature, some of the experimental and theoretical sections are representing similar issues as given in chapter 2 and 3.

Manuscript

Work described in this manuscript was focused on TDLAS. A TDL-spectrometer was used to check its feasibility for absolute CO_2 amount fraction measurements based on the *TILSAM* method. The R(12) rotational line in the combination band around 2µm was used for CO_2 quantification.

4.1 Laser-spectrometric gas analysis: CO_2–TDLAS at 2µm

Abstract:

A method has been developed to measure absolute amount of substance fractions of molecular species by infrared (IR) laser spectrometry. Employing direct absorption spectroscopy, we probed the R(12) line of carbon dioxide (CO_2) in the combination band around 2 µm as a proof-of-principle laboratory experiment. A gravimetric gas standard containing CO_2 in N_2 was used to perform the spectrometric measurements and to validate the capability of the absolute CO_2 amount fraction measurements method. We describe details on the implementation of the "Guide to the expression of uncertainty in measurements" (GUM) to infrared laser-spectrometric gas analysis. This work is mainly focused on data quality objectives expressed by uncertainty and traceability flags which are essential for the intended use. Uncertainty budgets are presented to show the quality of the results and to demonstrate software-assisted uncertainty assessment. Two different strategies of retrieving CO_2 amount fractions and their associated uncertainties, one based on a purely statistical approach and a second regression-based analysis are discussed. For the current work, the relative expanded uncertainty of the spectrometrically measured CO_2 amount fractions is 1.6 %, $k = 2$. The value component of the amount fraction nicely agrees with the gravimetric reference value, at the 20 $mmol \cdot mol^{-1}$ level within ±0.1 %, the reproducibility of individual results reads ±1.2 %.

4.1.1 Introduction

During the last decade different laser spectroscopic techniques have been extensively used to measure the amount fraction of different molecular gas species [1-13]. Each of these techniques is applied depending on the intended use [10,14]. The spectral fingerprints of molecular species are typically in the mid-infrared spectral region and detection limits of laser spectrometric techniques achieved so far even for biomarkers range from µmol·mol^{-1} to pmol·mol^{-1} [3,15]. New laser sources in the mid-infrared on the one hand side and low cost, mass production distributed feedback diode lasers combined with high technological level optics and detectors in the near-infrared on the other side justify to work in all of the infrared spectral region. Advances in laser spectroscopic techniques generally have triggered an increase in infrared-spectrometric gas detection [16-18]. In breath analysis for example, laser spectroscopic techniques have high sensitivity and high selectivity like the mass spectroscopic-based techniques, near real-time response, and comparably low instrument costs [3].

Carbon dioxide and its ^{13}C-isotopes, for instance, are important molecules in atmospheric monitoring, breath analysis, and car exhaust emission measurements [6,13,19-27]. Carbon dioxide (CO_2) has been measured using different laser spectrometric techniques by several groups [28-33] with detection limits down to the pmol·mol^{-1} level [3]. However, what can been found very rarely in most molecular gas measurement reports, e.g. on CO_2 measurements, is information on the metrological quality of the data, the traceability of the measurement results as well as GUM-compliant associated uncertainties of the results [34]. Accordingly and as a result, this lack is also present in the most prominent databases, e.g. such as those of HITRAN [35] and GEISA [36].

In this paper, we present CO_2 amount fraction results measured with a tunable diode laser spectrometer. The lab-based experiments are performed in the framework of an iMERA-plus project [37], using the Traceable Infrared Laser Spectrometric Amount fraction Measurement (*TILSAM*) method [38], which was developed within the scope of EURAMET project no. 934 [39], addressing metrological concepts as those of traceability and uncertainty. Combining standard TDLAS technique with the *TILSAM* method we focus on data quality, data retrieval strategies, uncertainty assessments and traceability. We proceed to discuss the importance of our focus points to the intended possible applications.

4.1.2 Theory, conceptual background

In tunable diode laser absorption spectroscopy (TDLAS), a sample gas is probed recording the transmitted radiant power with a detector as the laser wavelength is (repetitively) swept across an absorption line of the gas. The interaction of the gas species molecules and the sensing radiation at wave number $\tilde{\nu}$ is modelled by the Beer-Lambert law

$$\Phi(\tilde{\nu}, L) = \Phi_0(\tilde{\nu}) \cdot \exp\{-S_T \cdot \mathrm{g}(\tilde{\nu} - \tilde{\nu}_0) \cdot L \cdot n\} \tag{4.1}$$

where Φ_0 and Φ are the incident and transmitted radiant powers, S_T the molecular transition line strength at gas temperature T, which is assumed to be matched to the actual present isotopic abundance ratio by means of r_{iso} (see end of chapter, Appendix I), g the normalized absorption profile centered at $\tilde{\nu}_0$, and L the absorption path length. Using the ideal gas law, the molecular density n of the absorbing species can be expressed in terms of the partial pressure $p_{partial}$ of the absorbing molecules and the gas temperature. The partial pressure $p_{partial}$ can be related to the total pressure p_{total} using the amount of substance fraction of the absorbing species $x_{species}$, $p_{partial} = x_{species} \cdot p_{total}$. Making use of the normalization of g, Eq (4.1) can also be written in its integral form

$$x_{species} = \frac{k_B \cdot T}{S_T \cdot L \cdot p_{total}} \int_{-\infty}^{\infty} A(\tilde{\nu})\,\mathrm{d}\tilde{\nu} = \frac{k_B \cdot T}{S_T \cdot L \cdot p_{total}} \cdot A_{line} \tag{4.2}$$

where, the quantity $A(\tilde{\nu}) = -\ln(\Phi(\tilde{\nu})/\Phi_0(\tilde{\nu}))$ is the spectral absorbance (Naperian), in cases[4] also called extinction. Direct absorption spectroscopy is described by the Beer-Lambert law as expressed in Eq.(4.1). Thus, using Eq.(4.2) to determine the amount of substance fraction $x_{species}$ of, e.g., a biomarker delivers results that were SI-traceable, if all input quantities are traceable as well. This is the concept underlying the *TILSAM* method [38].

Traceability "is a property of a measurement result whereby the result can be related to a reference through a documented unbroken chain of calibrations, each contributing to the measurement uncertainty" [40]. A traceable measurement result consists of a value and its associated uncertainty. Traceability is an indispensable prerequisite for the comparability of measurement results. Ensuring the comparability of measurement results is crucial in e.g. environmental measurements for decision making procedures or in medical treatment. Typical tasks for the latter are, for instance, comparing a patient's result before and after treatment or results of measurements performed on a patient at different sites.

Respective results would never be identical, thus, the requirement that measurement results are supposed to have a "stated" reference, irrespective of where and when the measurement was performed, is brought up. Referring finally to the SI-units themselves, is called traceability. The comparability of measurement results is assured if the results are traceable. Traceability is also inline with the stated aims of the international quality assurance standard ISO EN 17025 [41].

The uncertainty of any measurement result is supposed to be expressed according to the ISO standard "Guide to the expression of uncertainty in measurement" (GUM) [34,42,43]. In cases where correlations can be excluded, the uncertainty associated to a measurement result y of a measurand Y is given by, $u_y^2 = \sum_i (\partial y / \partial x_i)^2 \cdot u^2(x_i)$, where, u_y is the combined standard

[4] See e.g. http://goldbook.iupac.org/A00028.html.

uncertainty of the measurand, $u(x_i)$ is the standard uncertainty of an input parameter value x_i and $(\partial y / \partial x_i)$ is the sensitivity coefficient [43]. The uncertainty of the input quantity can either be determined from statistical analysis of a series of observations (type A uncertainty) or obtained by means of other than statistical analysis (type B uncertainty). When the uncertainties of all the input parameters are known, an expanded uncertainty of the measurand is calculated as $U = k \cdot u_y$, where k is a coverage factor expressing the probability that the true value of the measurand is contained within a specified interval of measured values based on the information available. If the possible values of the measurand are normally distributed, then $k = 2$ is producing an interval having a level of confidence of 95 % that the true value is included. Knowing the uncertainty of a result, the measurand can be expressed as $Y = y \pm U$.

There are many software tools which can be used to assist a user in order to evaluate the uncertainty of a measurement result in accordance with the ISO GUM as well as to indicate and maybe to optimize the uncertainty contribution of every used input quantity. The GUM workbench software [44] used in this work is an example of available software tools that help to calculate the uncertainty of a measurement result. The calculations follow the principles given in the Joint Committee for Guides in Metrology (JCGM) guidelines on the evaluation of the uncertainty in measurements which are the same as the guidelines of the ISO GUM [34,42,43].

The GUM workbench supports a systematic procedure in assessing an uncertainty budget, starting with a mathematical equation which models the physical relationship of quantities involved in the respective measurement and all available information on uncertainties. The result of the analysis is an uncertainty budget [44]. The uncertainty budget holds all used quantities with their symbols, assigned standard uncertainties and actual degrees of freedom [43], the sensitivity coefficients derived from the model equation and the resulting contribution to the standard uncertainty of the final measurement result. Finally, the value component of the measurement result, its expanded uncertainty, and the coverage factor are reported in the budget. Expressing it as a table, it is easy to see which input quantity has the most significant uncertainty contribution, since this is expressed by the index figure in a GUM workbench budget. This information can be used to predict an improvement in the uncertainty of the measurement result, while optimizing a certain or multiple input quantities [44]. In the following paragraphs, we will report on calculations based on the GUM workbench to present individual uncertainty budgets for most of the input quantities which will finally combine to the final measurement result.

4.1.3 Experimental

The experimental setup similar to the one presented earlier is shown in Figure 4.1. For the measurements presented in this paper, a continuous wave (cw), thermoelectrically cooled, distributed-feedback (DFB) tunable diode laser (TDL) emitting around 4987.3 cm^{-1} was used as the laser source.

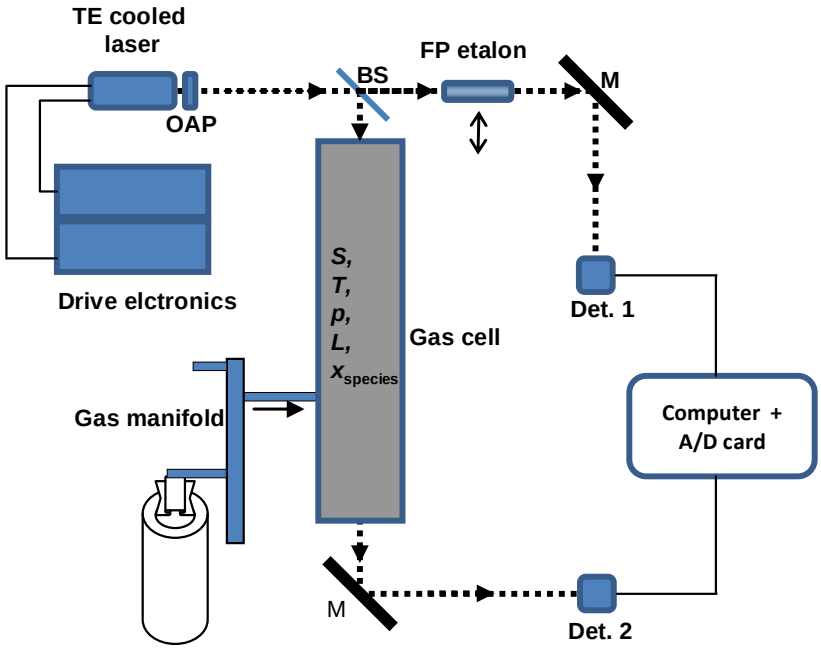

Figure 4.1: Schematic diagram of the setup used for species quantification in a two-channel regime. The single path absorption cell has a length of L = 0.82 m. OAP: off axis parabolic mirror. BS: Beam splitter, M: mirror, Det: detector.

The temperature tunability of the laser of 0.38 cm^{-1}/K was used to reach the line of interest. A triangular-shaped laser current modulation was applied to sweep the diode laser wavelength across the line. Measurements with a FTIR (IFS-120 HR Bruker) confirmed the single mode operation of the laser which is essential for the *TILSAM* method [45]. For the spectroscopic gas analysis, a two-channel scheme was used as shown in Figure 4.1. After collimation, the TDL beam was split into a reference beam and the sample beam transmitted through a 0.82 m stainless steel absorption cell. The reference beam was used for intensity normalization and for fixing the wavelength axis before and after the sample measurements by means of a removable etalon. Both channels were terminated into extended indium-gallium-arsenide (XInGaAs) photo detectors. A low vertical resolution 8 bit A/D converter was used to digitize the electrical signals at 10 kS/s.

Prior to measurements, the optical bench was purged with nitrogen. A reference gas mixture of carbon dioxide in nitrogen, gravimetrically prepared by BAM [46] with a nominal level of 20 mmol·mol^{-1} CO_2 was filled into the gas cell for analysis. Quantitative measurements were performed with p_{total} preset in the range of 100 to 500 hPa with the help of a gas sampling system equipped with a turbo molecular vacuum pump (Ilmvac CD 160). The filling and evacuation of the gas cell was controlled by manual metering bellow valves. The gas pressure was measured by a Baratron capacitance pressure gauge and the temperature T with a Pt100-resistance device stuck on the absorption cell. A measurement procedure according to the *TILSAM* method [38] was applied.

The lower panel of Figure 4.2a represents the signals of the sample channel detector with CO_2 absorption and the reference channel detector without any absorption feature while the etalon was removed, respectively. The upper panel of Figure 4.2a depicts the signal of the reference channel detector when the etalon was placed in the reference beam path. Data were measured in the time domain in units of sample points (SP).

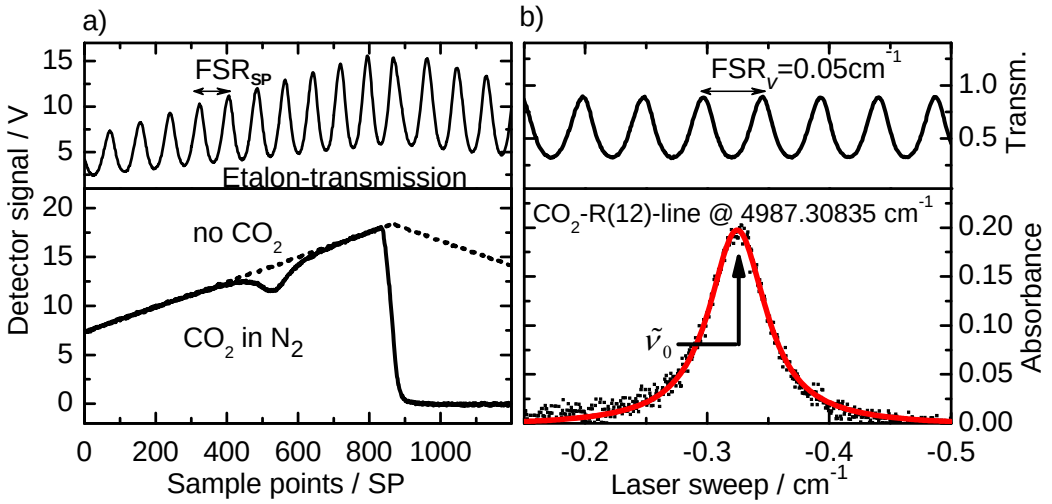

Figure 4.2: a) Lower panel: Data from the reference channel without CO_2 absorption (dashed line) and the sample channel (full line) featuring CO_2 absorption, respectively. The absorption was measured at p_{total} = 350 hPa. Upper panel: Etalon transmission signal seen by detector 1 with the etalon ($FSR_\nu \approx 0.05$ cm^{-1}) placed in the reference beam path. b) Data transferred to the wave number domain. Upper panel: Etalon transmittance curve. Lower panel: Data of the lower panel of a), converted to absorbance values (solid dots). A Voigt profile has been fitted to the data (full line) representing the CO_2-R(12) line at 4987.31 cm^{-1}.

Figure 4.2b, lower panel, depicts the absorbance derived from the detector signals of the two channels as displayed in Figure 4.2a, representing a simultaneous two channel measurement scheme. The noise level, calculated as the standard deviation of the baseline multiplied by a factor of 3, was 0.019 in absorbance units. This means there were a SNR of just 10 for the data presented in Figure 4.2, however, this proves to be sufficient regarding the CO_2 quantification presented below. The observed noise level dominating the present SNR stems mostly from the poor A/D converter resolution. Although, the SNR would be somewhat larger for higher values of p_{total} or simply by an increased CO_2 amount fraction. Accordingly, a SNR of 30 was evaluated for a 60 mmol·mol^{-1} gas mixture presented at the end of this section. The wave number axis in Figure 4.2b was accomplished by means of the sweep rate $r_{sweep} = FSR_\nu / FSR_{SP}$. FSR_ν is the known free spectral range of the etalon in wave numbers and FSR_{SP} is the experimental fringe separation measured in the time domain (SP) visible in the upper panel of Figure 4.2b. FSR_ν was determined using the refractive index of the etalon material and its measured length. Table 4.1 shows the uncertainty budget for FSR_ν evaluated using the GUM workbench [44]. Its estimated standard uncertainty of $\pm 38.7 \cdot 10^{-6}$ cm^{-1} is equivalent to ±0.07 % relative.

Table 4.1: Model equation: $FSR_\nu = 1/(2 \cdot n \cdot d)$, where n is the refractive index of silicon [62] and d is the length of the etalon. $d = z + a + q + r$, *with* z being the reading of a calliper, a is the correction due to the Abbe error of the calliper, q the correction due to parallel reading, and r the correction due to the resolution of the calliper.

Quantity	Value	Standard Uncertainty	DOF	Sensitivity Coefficient	Uncertainty Contribution	Index
z	2.990000000 cm	$100 \cdot 10^{-9}$ cm	50	-0.016	$-1.6 \cdot 10^{-9}$ cm^{-1}	0.0 %
a	0.0 cm	$600 \cdot 10^{-6}$ cm	50	-0.016	$-9.7 \cdot 10^{-6}$ cm^{-1}	6.3 %
q	0.0 cm	$600 \cdot 10^{-6}$ cm	50	-0.016	$-9.7 \cdot 10^{-6}$ cm^{-1}	6.3 %
r	0.0 cm	$1.40 \cdot 10^{-3}$ cm	50	-0.016	$-23 \cdot 10^{-6}$ cm^{-1}	34.5 %
d	2.99000 cm	$1.64 \cdot 10^{-3}$ cm				
n	3.44900	$2.00 \cdot 10^{-3}$	50	-0.014	$-28 \cdot 10^{-6}$ cm^{-1}	52.9 %
FSR_ν	0.048485 cm^{-1}	$38.7 \cdot 10^{-6}$ cm^{-1}	120			

The standard uncertainties of all the quantities in Table 4.1 are expressed assuming normal distributions. The standard uncertainties of all the quantities are type B except that of z which is type A. The values of a, q, and r are zero because they are corrections to the measurement of d. DOF is the degree of freedom. The DOF of a single measurement estimated by the arithmetic mean of n independent observations is given by n-1 (type A) [44]. For type B, the DOF is set to 50 assuming a normal distribution. Assuming a rectangular distribution instead the DOF is set to infinity [44].

The GUM workbench evaluates the uncertainty of a measurand in accordance with the guidelines of the GUM [43]. The GUM requires a model that can be linearized in the vicinity of all actual values of the input quantities for a particular measurement. As a consequence, the GUM workbench software linearizes the model equation when calculating the uncertainty of the measurand. For this work, the GUM workbench was used with the option activated to perform a linearity test [44]. However, if the model were not to be linearized, the guidelines of the GUM supplement 1 [47] would have to be followed. The GUM supplement 1 implements the Monte Carlo method to evaluate the uncertainty of a measurand. Software tools that assist the uncertainty evaluation according to this guideline are available [48,49].

The FSR_{SP} was evaluated by fitting the measured etalon transmission spectrum with a multi-peak function. For simplicity, the fringe separation at the absorption peak position was used as FSR_{SP} to determine r_{sweep}. Typical standard uncertainties of FSR_{SP} evaluated as the standard deviation of the mean of FSR_{SP} values derived from 10 consecutive measurements were 0.02 % relative. Table 4.2 summarizes the determination of the uncertainty of the sweep rate using [44]. Typical standard uncertainties of r_{sweep} were in the range of ±0.08 % relative. However, the long-run reproducibility of the sweep rate measured as the standard deviation was ±1 % relative, indicating that the sweep rate of this particular laser changes with time. This reproducibility figure confirmed our applied approach that, r_{sweep} had to be measured for each data set individually as recommended by the *TILSAM* method.

Table 4.2: The model equation is $r_{sweep} = FSR_v / FSR_{SP}$.

Quantity	Value	Standard Uncertainty	DOF	Sensitivity Coefficient	Uncertainty Contribution	Index
FSR_v	0.0484850 cm^{-1}	$38.7 \cdot 10^{-6}$ cm^{-1}	50	0.013	$490 \cdot 10^{-9}$ cm^{-1}/SP	95.9 %
FSR_{SP}	78.8192 SP	0.0130 SP	50	$-7.8.0 \cdot 10^{-6}$	$-100 \cdot 10^{-9}$ cm^{-1}/SP	4.1 %
r_{sweep}	$615.14 \cdot 10^{-6} cm^{-1}$/SP	$501 \cdot 10^{-9} cm^{-1}$/SP	54			

The standard uncertainties of the quantities are expressed assuming normal distributions. $u(FSR_v)$ is type B and $u(FSR_{SP})$ is type A.

Fitting a Voigt profile to the measured absorbance data in Figure 4.2 by means of a nonlinear least square fit (Levenberg-Marquardt) [50] delivered the absorption peak area A_{line}.

Amount fractions of CO_2 were directly calculated using Eqn.(4.2). This is referred to as "direct retrieval". Results of CO_2 amount fraction measurements are depicted in the middle panel of Figure 4.3 as a function of the experimental parameter $\Gamma = S_T \cdot L \cdot p_{total} / (k_B \cdot T)$. Γ is typically given in units of cm^{-1}. A variation in Γ is mostly related to the controlled variation in the total pressure and to some extend to the measured gas temperature T. Each data point of the middle panel in Figure 4.3 is shown as the mean of 10 consecutive individual measurements at the same pressure (same Γ) under repeatability conditions. The expanded uncertainty of each of the x_{CO2}, calculated as the standard deviation of the mean, and, by that, yielding a repeatability figure, is in the range of ±0.9 % relative, $k = 2$. The dashed line is the gravimetric reference target value $x_{ref} = (20.0078 \pm 0.0040)$ mmol·mol^{-1} [51].

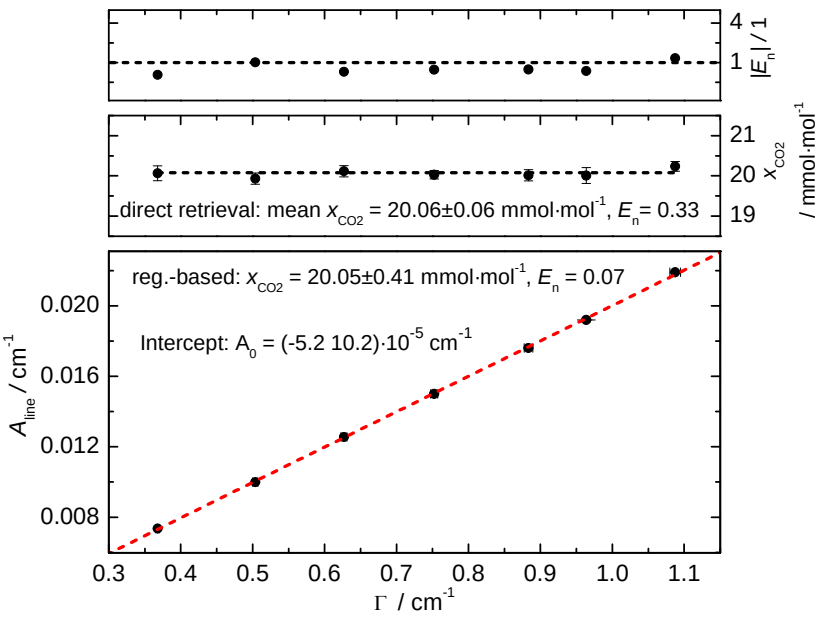

Figure 4.3: Spectrometric amount fraction determination of CO_2 in a gas mixture with N_2, pressures in the range 100 to 500 hPa. Bottom panel: Generalized linear regression (dashed line) of values of A_{line} as a function of Γ, the slope yielding the CO_2 amount fraction x_{CO2}. The uncertainty bars are partially smaller than the data points and are therefore not visible. Middle panel: Direct retrieval. Mean of 10 consecutive measurements (at the same pressure); gravimetric reference value as dashed line. Top panel: Direct retrieval. Normalized error E_n of each data point depicted in the middle panel.

The normalized error $E_n = D/U(D)$, depicted in the top panel of Figure 4.3, is used to grade the results. The quantity D is the degree of equivalence and $U(D)$ its expanded uncertainty. The degree of equivalence is given by $D = x_{CO2} - x_{ref}$ and $U(D) = 2 \cdot u(D) = 2 \cdot \sqrt{(u^2(x_{CO2}) + u^2(x_{ref}))}$, where $u(D)$ is representing the standard uncertainty of D. A coverage factor $k = 2$ is applied additionally.

As given in Figure 4.3, most of the directly retrieved CO_2 amount fractions agree with the gravimetric reference value, yielding $|E_n| < 1$. Two of the results do not agree with the reference value, $|E_n| > 1$. Looking for a reproducibility figure by averaging all the x_{CO2} results at the different Γ values (direct retrieval), the standard deviation was found to be ±1.2 % relative. A mean CO_2 amount fraction of (20.06±0.06) mmol·mol^{-1}, $k = 2$, and a normalized error of $E_n = 0.33$ was derived from this averaging.

The x_{CO2} results presented in the previous paragraphs agree with the gravimetric reference value, however, the uncertainties are based only on simple statistical parameters. This could be problematic because the uncertainties of the input quantities were not used. An alternative method to evaluate x_{CO2} would be to rewrite Eqn. (4.2) as

$$A_{line} = x_{CO2} \cdot \left(\frac{S_T \cdot L \cdot p_{total}}{k_B \cdot T} \right) = x_{CO2} \cdot \Gamma \qquad (4.3)$$

From Eq. (4.3), the CO_2 amount fraction can be identified as the slope of a linear regression of A_{line} versus Γ. Consequently, applying a generalized linear regression (GLR) to the values of A_{line} versus Γ for the data presented in the bottom panel of Figure 4.3 is referred to as "regression-based" retrieval which yields also a CO_2 amount fraction result. A GLR is recommended by the ISO 6143 [52] for purposes like that, and, as also mentioned in ISO 6143, we applied the B_Least software to perform the GLR [52]. The result using this alternative approach is depicted in the bottom panel of Figure 4.3.

The line area uncertainties in the bottom panel of Figure 4.3 (vertical bars smaller than symbol size) are based on the uncertainty of the line area fitting [53] and $u(r_{sweep})$. Table 4.3 below shows an example uncertainty budget of A_{line} for the first data point in Figure 4.3 evaluated using [44]. Typical relative uncertainties of A_{line} were in the ±0.4 % range, $k = 1$.

Table 4.3: Model equation, $A_{line} = A \cdot r_{sweep}$, where A is the line fitting parameter of the area.

Quantity	Value	Standard Uncertainty	DOF	Sensitivity Coefficient	Uncertainty Contribution	Index

r_{sweep}	$615.142 \cdot 10^{-6}$ cm^{-1}/SP	$101 \cdot 10^{-9}$ cm^{-1}/SP	50	12	$1.2 \cdot 10^{-6}$ cm^{-1}	0.1 %
A	11.9545 SP	0.0546 SP	50	$620 \cdot 10^{-6}$	$34 \cdot 10^{-6}$ cm^{-1}	99.9 %
A_{line}	$7.354 \cdot 10^{-3}$ cm^{-1}	$33.6 \cdot 10^{-6}$ cm^{-1}	50			

The standard uncertainties are expressed assuming a normal distribution. $u(r_{sweep})$ and $u(A)$ are type A.

The uncertainty of the Γ values (horizontal bars) are based on respective uncertainties of S_T, p_{total}, T and L. An uncertainty budget of Γ for the first data point in Figure 4.3 is shown in Appendix I. Typical relative uncertainties of Γ were in the ±0.7 % range, $k = 1$.

The regression-based retrieval yielded an amount fraction of (20.05±0.33) mmol·mol^{-1}, $k = 2$, $|E_n| = 0.07$. This x_{CO2} result agrees with the value of (20.06±0.06) mmol·mol^{-1}, $k = 2$, $E_n = 0.33$, originating from the direct retrieval. However, the ±0.33 mmol·mol^{-1} (±1.6 % relative), $k = 2$, uncertainty of the regression-based CO_2 amount fraction was evaluated based on the uncertainty of all the input parameters (T, L, p_{total}, S_T, etc.), whereas that of the directly retrieved x_{CO2} calculated as ±0.06 mmol·mol^{-1}, $k = 2$, was based only on simple statistical parameters. The comparably larger uncertainty of the regression-based x_{CO2} indicates that the uncertainty evaluated by the direct retrieval was underestimated.

To check this, in the following, we would like to compare the uncertainty of x_{CO2} for an individual single measurement based exclusively on statistical parameters to that provided by the GUM Workbench budget referring to the GUM. Table 4.4 presents the budget for a measured x_{CO2} result, first data point in Figure 4.3, based on input quantities A_{line} and Γ.

Table 4.4: Model equation, $x_{CO2} = A_{line} / \Gamma$.

Quantity	Value	Standard Uncertainty	DOF	Sensitivity Coefficient	Uncertainty Contribution	Index
A_{line}	$7.354 \cdot 10^{-3}$ cm^{-1}	$33.6 \cdot 10^{-6}$ cm^{-1}	50	2.7	$92 \cdot 10^{-6}$ mol·mol^{-1}	31.0 %
Γ	0.36650 cm^{-1}	$2.50 \cdot 10^{-3}$ cm^{-1}	50	-0.055	$-140 \cdot 10^{-6}$ mol·mol^{-1}	69.0 %
x_{CO2}	0.02007 mol·mol^{-1}	$165 \cdot 10^{-6}$ mol·mol^{-1}	87			

The standard uncertainties of the quantities are expressed assuming a normal distribution.

The resulting x_{CO2} standard uncertainty of $\pm 165.0 \cdot 10^{-6}$ mol·mol^{-1} (±0.8 % relative, $k = 1$) in Table 4.4 is larger than the uncertainty figure of $\pm 91.5 \cdot 10^{-6}$ mol·mol^{-1} (±0.4 % relative), $k = 1$, assigned to the first data point in Figure 4.3, middle panel, as vertical bar, but compares well with the standard uncertainty of $165.3 \cdot 10^{-6}$ mol·mol^{-1} (±0.8 % relative, $k = 1$) originating from the regression-based retrieval. The latter was reported above as an expanded uncertainty of 0.33 mmol·mol^{-1} (±1.6 % relative, $k = 2$). This, in turn, confirms that the regression-based retrieval is yielding a complete uncertainty figure. Thus, applying the regression-based retrieval is preferable to the direct retrieval because the evaluation of the uncertainty of x_{CO2}

considers all input quantities whereas a simple statistics-based view on repeatabilities does not.

The regression-based analysis has an additional advantage over the direct retrieval in determining the CO_2 amount fractions. The intercept of a free regression can be viewed as a measurand. The linear model in Eq. (4.3) does not predict any intercept. This means that applying a generalized linear regression should yield an insignificant intercept parameter. If the resulting intercept were significant, i.e. its uncertainty were smaller than its numerical value, then the model would not be appropriate to the experiment. The resulting intercept, $A_0 = (-5.2 \pm 10.2) \cdot 10^{-5}$ cm^{-1} of the generalized linear regression, visible in the bottom panel of Figure 4.3, indicates that the experimental conditions of the TDL spectrometer to perform x_{CO2} measurements were appropriately described.

To check our spectrometer for its feasibility to be operated on basis of the *TILSAM* method, additional CO_2 quantifications were performed, expanding the range of amount fractions. Figure 4.4 depicts the results of spectrometrically derived CO_2 amount fractions in the range of 20 mmol·mol^{-1} to 60 mmol·mol^{-1} versus their gravimetric reference values. The x_{CO2} values were derived using the regression-based retrieval.

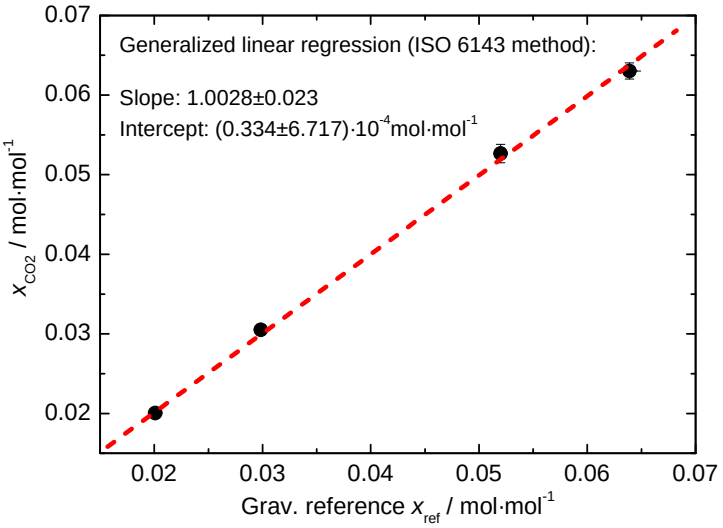

Figure 4.4: Spectrometrically derived CO_2 amount fractions x_{CO2} as a function of their gravimetric reference values x_{ref}.

Typical expanded uncertainties of the spectrometric CO_2 amount fractions were in the range of ±1.6 % relative, $k = 2$, which is in line with the uncertainty of the 20 mmol·mol^{-1} result already presented in the bottom panel of Figure 4.3. As shown in Figure 4.4, we applied a regression analysis to the values of the spectrometrically derived x_{CO2} versus their gravimetric reference values in order to compare them on a quantitative basis. The regression yields a slope of 1.003±0.023 and an intercept of $(0.334 \pm 6.717) \cdot 10^{-4}$ mol·mol^{-1}. From a slope equal to 1 it is concluded that the spectrometrically derived x_{CO2} nicely agree with the respective reference values. Furthermore, from an intercept parameter of $(0.334 \pm 6.717) \cdot 10^{-4}$ mol·mol^{-1}, which is insignificant, it is proved that the spectrometrically derived CO_2 amount fraction

results were not biased. Based on extrapolation of data in Figure 4.4, the intercept value and its uncertainty can be used to estimate a limit of detection for the used spectrometer. By adding the uncertainty of the intercept to its value, the limit of detection of the spectrometer were thus estimated to be 705.1 µmol·mol^{-1}. However, this value would be in contradiction to the presented noise level which, by itself, is limiting the minimum detectable absorbance for the present implementation of the spectrometer to an equivalent limit of detection of well above 2000 µmol·mol^{-1} (a factor of 10 below the data presented in Figure 4.2).

4.1.4 Discussions

The spectrometrically derived CO_2 amount fractions agree with the gravimetric reference values. The relative expanded uncertainties of the amount fractions evaluated using a regression-based retrieval were in the ±1.6 % range, $k = 2$. This uncertainty covers the tiny deviation from the gravimetric reference values, which was 0.1 % relative at the 20 mmol·mol^{-1} level. The uncertainty of the different input parameters, e.g., the line area and Γ, was calculated by means of the GUM workbench software, demonstrating software-assisted uncertainty assessment. Software-assisted uncertainty assessment is beneficial to spectroscopists in many applications since this makes the implementation of the GUM principle to certain applications easier and more transparent to spectroscopy's operators and customers. The evaluation of the uncertainty of an amount fraction based exclusively on simple statistical parameters suffers from the danger of delivering an incomplete uncertainty figure. The regression-based retrieval is the preferred method for evaluating amount fractions because the uncertainties of all the input quantities were considered.

Table 4.5 below provides the evolution of the most significant uncertainty contribution to the final uncertainty of the spectrometric CO_2 amount fraction for the range 20 to 60 mmol·mol^{-1} (sum of the index values is not delivering 100 %, since some input quantities are omitted in Table 4.5). The relative x_{CO2} uncertainty decreases towards higher amount fractions. The line strength S delivers the most significant uncertainty contribution. Although, at lower x_{CO2}, finally the main uncertainty source will be the line area A_{line} as its relative contribution to the uncertainty of x_{CO2} grows towards lower CO_2 amount fractions.

Table 4.5: Most significant uncertainty sources for x_{CO2} in the range of 20 to 60 mmol·mol^{-1}.

Quantity*	**x_{CO2} / mmol·mol^{-1}:**	**20**	**30**	**50**	**60**
	standard uncertainty	**index (contribution to the combined uncertainty)**			
L	constant	8.8 %	10.6 %	11.8 %	12.2 %
T	constant	2.6 %	3.1 %	3.5 %	3.6 %
p	constant	0.7 %	0.8 %	2.0 %	2.2 %
S	constant	48.3 %	58.0 %	64.8 %	66.7 %
FSR_{SP}	constant	0.0 %	0.0 %	0.0 %	0.1 %

Quantity*	**x_{CO2} / mmol·mol^{-1}:**	**20**	**30**	**50**	**60**
FSR_v	constant	0.9 %	1.1 %	1.3 %	1.3 %
A_{line}	relative growth with decrease of x_{CO2}	30.6 %	16.0 %	4.7 %	2.0 %
Relative expanded uncertainty $U(x_{CO2})$, k=2		**1.6 %**	**1.5 %**	**1.4 %**	**1.4 %**

To improve the uncertainties of the CO_2 amount fraction results, more efforts were to be invested in the determination of a traceable line strength figure with a smaller uncertainty. The carbon dioxide level in vehicle exhaust emissions, for instance, is in the range of 150 mmol·mol^{-1}. This means that the line strength and its uncertainty would be crucial in a *TILSAM*-referring determination of CO_2 amount fractions based on a TDL spectrometer like the presented while probing the R(12) line at 2 µm. Vehicle CO_2 exhaust emission measurements might be of increased commercial interest regarding CO_2 emission regulations for cars [26]. The same holds for regulations of power and biogas plant emissions [27]. The carbondioxide level in exhaled human breath is in the 50 mmol·mol^{-1} level. This means that the determination of CO_2 amount fraction in exhaled breath using the TDL spectrometer will be restricted to an expanded uncertainty of ±1.4 % relative, $k = 2$. This might not be sufficient, thus some improvements are necessary, e.g. on the part of the line strength uncertainty as is visible in Table 4.5.

The line strength of the CO_2 R(12) line used in this work was also measured by G. Casa et al. [54]. G. Casa's et al. line strength figure has a standard uncertainty of ±0.1 % relative which is considerably smaller than the value reported in [55] and that which was used in this work. Taking the line strength of $(1.2344\pm0.0014)\cdot10^{-21}$ cm^{-1}/(molecules·cm^{-2}) from Ref. [54], instead of $(1.255\pm0.00725)\cdot10^{-21}$ cm^{-1}/(molecules·cm^{-2}) used in the uncertainty budgets presented in Appendix I and Table 4.4, corresponds to a CO_2 amount fraction of 20.40 mmol·mol^{-1}. Then, accordingly, the calculated relative expanded uncertainty would read 1.2 %, $k = 2$, which is smaller than the 1.6 % reported using the line strength value from [55]. However, the x_{CO2} value evaluated with the line strength figure of G. Casa et al. does not agree with the reference value, as it reveals a normalized error of $|E_n| = 1.3$. At 50 mm·mol^{-1} level the expanded uncertainty of the amount fraction evaluated with the line strength of 54] is in the subpercentage level although the amount fraction results do not agree with the reference value. It should be noted here, that the unresolved discrepancy between R(12) line strength figures from Refs. [54] and [55] shall be object of a joint investigation of both author groups [56], even though the value from Ref. [54] is very close to the recently updated value reported in the HITRAN 2008 edition [35], whereas the value from [55] has been transferred to a new revalidation step [57].

According to the message of the previous paragraphs and its original idea, the *TILSAM* methodology could also be applied to other molecular species, assuming premises are

kept [38]. For a *TILSAM*-based quantification of most molecular species, however, a limitation would be the unavailability of traceable line strength data and their associated uncertainties. Traceable line strength values are rarely found in literature [58]. Nevertheless, there might also be a concern on the line strength temperature dependences which have to be handled appropriately. Line strength values are usually reported for some reference temperature as, e.g., that of 296 K by HITRAN's convention [35]. Consequently these S_0 data first of all have to be matched to the actual gas temperature T at which the measurement is performed using an appropriate transfer function [35]. The transfer of the uncertainty of the line strength reported at 296 K to a new value at T has to be done in accordance with the GUM [34,42,43].

Nowadays, as a quality measure, the requirement of the uncertainty of a measurement result in combination with its traceability is indispensable. This is often necessary in, e.g., medical diagnosis or atmospheric measurements as outlined in section 2. Thus, an instrumentation that is able to perform *TILSAM* could be optimized to measure molecular gas species for different possible gas analysis applications. For such purposes, the predicted quality of respective amount fraction results on a certain molecular gas species based on the *TILSAM* method and their associated GUM-compliant uncertainty figures could be compared to existing data quality objectives (DQOs), e.g. such as those established by the WMO within the Global Atmosphere Watch (GAW) program [59]. An example is the GAW DQO for CO in field measurements specified to be 1 %, relative [60]. The CO_2 amount fraction uncertainty figure of 1.6 % reported in the present work would be close to this accuracy level already, however, not validated for field measurements yet. Otherwise, our repeatability figure of ~0.9 % relative, is apparently calling for an improvement in order to match, e.g., the desired precision of ~0.3 % required by the Orbiting Carbon Observatory (OCO) for space-based x_{CO2} measurements [61]. However, our repeatability is reported with a multiplicative factor (coverage factor) of $k = 2$ included. In contrast, our reproducibility reached so far, needs definitely some further optimization, when aiming at the OCO DQO level. Concerning the fact that the line area uncertainty grows larger at lower CO_2 amount fractions, see Table 4.5, an improvement to the presented setup would be to use larger optical path lengths, leading to higher absorption signals, and to use a better vertical resolution A/D conversion, thus improving the signal to noise ratio.

4.1.5 Conclusions

Data presented in this work have been used to demonstrate the feasibility of the *TILSAM* method to perform absolute amount fraction measurements with a simple TDL spectrometer. A reference gas mixture of CO_2 in N_2 was used to perform spectrometric measurements. Results of CO_2 amount fractions were compared to their gravimetric reference values. At the 20 $mmol \cdot mol^{-1}$ level, we showed that the regression-based CO_2 amount fraction retrieval provides reliable uncertainty figures, which were, in the presented spectrometer design, estimated to be in the range of ±1.6 % relative, $k = 2$. This spectrometric CO_2 amount fraction result agrees with its respective gravimetric reference value to within ±0.1 % relative. The

reproducibility of individual measurements were found to be in the ±1.2 % range. At the 50 mmol·mol^{-1} level (exhaled breath CO_2 level), the relative expanded uncertainty of the spectrometric CO_2 amount fraction results were ±1.4 %, $k = 2$. From the comparison of spectrometric results with gravimetric reference values in the range of 20 to 60 mmol·mol^{-1} a resulting slope of 1 shows that all results were in nice agreement. This encourages the application of the *TILSAM* analysis idea also to other gas analysis applications. However, improvements on the uncertainty figure are still possible working on the spectrometer's noise level and the line strength uncertainty.

4.1.6 Acknowledgements

Parts of this work were financially supported by ERA-NET Plus, under the iMERA-plus Project - Grant Agreement No. 217257, by the Braunschweig International Graduate School of Metrology, the TU Braunschweig, and by the BMBF projects MEX07/004, and QUANSYS/QUANKAS, FKZ 13N8123. The authors acknowledge the continuous collaboration of Prof. Dr. Karl-Heinz Gericke (TU Braunschweig), Hans-Joachim Heine (BAM), and Jorge Koelliker Delgado (CENAM).

4.1.7 References and Notes

[1] J. Manne, W. Jäger, and J. Tulip, Appl. Phys. B 94, 337-344 (2009).
[2] D. Halmer, G. von Basum, P. Hering, and M. Mürtz, Opt. Lett. 30, 2314-2316 (2005).
[3] C. Wang and P. Sahay, Sensors 9, 8230-8262 (2009).
[4] G. Wysocki, M. McCurdy, S. So, D. Weidmann, C. Roller, R. F. Curl, and F. K. Tittel, Appl. Opt. 43, 6040-6046 (2004).
[5] S. Welzel, G. Lombardi, P. B. Davies, R. Engeln, D. C. Schram, and J. Röpcke, J. Appl. Phys. 104, 093115 (2008).
[6] V. Ebert and J. Wolfrum, "Absorption spectroscopy," in Optical Measurements-Techniques and Applications, 227-265 (Springer, 2001).
[7] T. Fritsch, P. Hering, and M. Mürtz, J. Breath Res. **1**, 014002 (2007).
[8] C. Mitscherling, J. Lauenstein, C. Maul, A. A. Veselov, O. S. Vasyutinskii, and K. -H. Gericke, J. Breath Res. **1**, 026003 (2007).
[9] F. M. Schmidt, O. Vaittinen, M. Metsälä, P. Kraus, and L. Halonen, Appl. Phys. B online first (2010), DOI: 10.1007/s00340-010-4027-5.
[10] I. Ventrillard-Courtillot, and D. Romanini, J. Biomed. Opt. 14, 064026 (2009).
[11] P. Ortwein, W. Woiwode, S. Fleck, M. Eberhard, T. Kolb, S. Wagner, M. Gisi, and V. Ebert, Exp. Fluids online first (2010), DOI: 10.1007/s00348-010-0904-2.
[12] J. A. Nwaboh, O. Werhahn, and D. Schiel, Appl. Phys. B online first (2010), DOI: 10.1007/s00340-010-4322-1.
[13] C. Schulz, A. Dreizler, V. Ebert, and J. Wolfrum, "Combustion Diagnostics," in Springer Handbook of Experimental Fluid Mechanics, 1241-1315 (Springer Verlag, Heidelberg, München, 2007).
[14] G. Wysocki, A. A. Kosterev, and F. K. Tittel, Appl. Phys. B 80, 617-625 (2005).

[15] E. Schlosser, J. Wolfrum, L. Hildebrandt, H. Seifert and B. Oser, and V. Ebert, Appl. Phys B 75, 237-247 (2002).
[16] J. Faist, F. Capasso, D. L. Sivco, C. Sirtori, A. L. Hutchinson, and A. Y. Cho, Science 264, 553-556 (1994).
[17] M. R. McCurdy, Y. Bakhirkin, G. Wysocki, R. Lewicki, and F. K. Tittel, J. Breath Res. **1**, 014001 (2007).
[18] E. Kerstel and L. Gianfrani, Appl. Phys. B 92, 439-449 (2008).
[19] J. Koelliker Delgado, O. Werhahn, and D. Schiel, VDI-Berichte 1959, 303-313, VDI-Verlag, Düsseldorf 2006, ISBN-3-18-091959-0.
[20] D. E. Cooper, R. U. Martinelli, C. B. Carlisle, H. Riris, D. B. Bour, and R. J. Menna, Appl. Opt. 3, 6727-6731 (1993).
[21] T. Le Barbu, B. Parvitte, V. Zeninari, I. Vinogradov, O. Korablev, and G. Durry, Appl. Phys. B 82, 133-140 (2006).
[22] J. Wolfrum, T. Dreier, V. Ebert, and C. Schulz, Laser-based combustion diagnostics, in Encyclopedia of Analytical Chemistry, 2118-2148 (J. Wiley & Sons Ltd.: Chichester, 2000).
[23] I. Pouchet, V. Zéninari, B. Parvitte, and G. Durry, J. Quant. Spectrosc. Rad. Trans. 83, 619-628 (2004).
[24] D. Weidmann, G. Wysocki, C. Oppenheimer, and F. K. Tittel, Appl. Phys. B 80, 255-260 (2005).
[25] E. R. Crosson, Appl. Phys. B 92, 403-408 (2008).
[26] DIRECTIVE 1999/94/EC OF THE EUROPEAN PARLIAMENT AND OF THE COUNCIL of 13 December 1999 relating to the availability of consumer information on fuel economy and CO2 emissions in respect of the marketing of new passenger cars. Available from: http://eur-lex.europa.eu/LexUriServ/LexUriServ.do?uri=OJ:L:2000:012:0016:0023:EN:PDF
[27] V. Ebert, T. Fernholz, C. Giesemann, H. Pitz, H. Teichert, J. Wolfrum, H. Jaritz, Proc. Comb. Inst. 28, 423-430 (2000).
[28] A. Castrillo, E. De Tommasi, and L. Gianfrani, Opt. Lett. 31, 3040 (2006).
[29] V. Weldon, J. O'Gorman, P. Phelan, J. Hegarty, and T. Tanbun-Ek, Sens. Actuat. B **29**, 101-107 (1995).
[30] R. M. Mihalcea, M. E. Webber, D. S. Baer, R. K. Hanson, G. S. Feller, and W. B. Chapman, Appl. Phys. B 67, 283-288 (1998).
[31] E. R. Crosson, K. N. Ricci, B. A. Richmann, F. C. Chilese, T. G. Owano, R. A. Provencal, M. W. Todd, J. Glasser, A. A. Kachanov, B. A. Paldus, T. G. Spence, and R. N. Zare, Anal. Chem. 74, 2003-2007 (2002).
[32] L. Croizé, M. Schmidt, Appl. Phys. B 101, 411-421 (2010).
[33] G. B. Rieker, R. K. Hanson, Appl. Phys. B 94, 51-63 (2009).
[34] JCGM 104:2009, Evaluation of measurement data - An introduction to the "Guide to the expression of uncertainty in measurement" and related documents, 2009. Available from: http://www.bipm.org/en/publications/guides/gum.html.

[35] HITRAN2008, http://www.cfa.harvard.edu/HITRAN/, L. Rothman et al., J. Quant. Spectrosc. Rad. Transf. 110, 533 (2009).

[36] N. Jacquinet-Husson et al., "The GEISA spectroscopic database: Current and future archive for Earth and planetary atmosphere studies," J. Quant. Spectrosc. Rad. Transf. (2008),
DOI: 10.1016/j.jqsrt.2007.12.015.

[37] EMRP, T2.J02–Breath Analysis, Joint Research Projects funded under iMERA-plus, 2010, http://www.euramet.org/index.php?id=1011.

[38] O. Werhahn, J. C. Petersen (eds.), *TILSAM* technical protocol V1_2010-09-29. Available from:
http://www.euramet.org/fileadmin/docs/projects/934_METCHEM_Interim_Report.pdf.

[39] EUROMET project no. 934, *TILSAM*–Traceable Infrared Laser Spectrometric Amount fraction Measurement, 2008, http://www.euramet.org.

[40] JCGM 200:2008, International vocabulary of metrology - Basic and general concepts and associated terms VIM 3rd edition, 2008. Available from: http://www.bipm.org/en/publications/guides/vim.html.

[41] ISO/IEC 17025:2005, General requirements for the competence of testing and calibration laboratories. Available from:
http://www.iso.org/iso/catalogue_detail.htm?csnumber=39883.

[42] ISO Guide 98-3, Guide to the Expression of Uncertainty in Measurement, 1. International Organization for Standardization, Geneva 2008, ISBN 9267101889.

[43] JCGM 100:2008, Evaluation of measurement data - Guide to the expression of uncertainty in measurement, GUM 1995 with minor corrections, ISO IEC Guide 98-3, 2008. Available from: http://www.bipm.org/en/publications/guides/gum.html.

[44] GUM Workbench 1.2 Win32 and GUM workbench manual, Metrodata GmbH, Grenzach-Wyhlen, Germany 1999, http://www.metrodata.de.

[45] J. Koelliker Delgado, Amount of carbon dioxide fraction determination by TDLAS: Evidences for a potential primary method directly applied in gas analysis, dissertation, Technische Universität Carolo-Wilhelmina, Braunschweig, 2006.

[46] BAM, Bundesanstalt für Materialforschung und -prüfung, Berlin, Germany, http://www.bam.de.

[47] JCGM 101:2008, Evaluation of measurement data — Supplement 1 to the "Guide to the expression of uncertainty in measurement" — Propagation of distributions using a Monte Carlo method. Available from:
http://www.bipm.org/en/publications/guides/gum.html.

[48] GUM Workbench professional version 2.4 and GUM workbench manual for version 2.4, Metrodata GmbH, Grenzach-Wyhlen, Germany, http://www.metrodata.de.

[49] NPLUnc. Available from: http://www.npl.co.uk/mathematics-scientific-computing/software-support-for-metrology/software-downloads-(ssfm).

[50] Levenberg-Marquardt, Numerical Recipes, 2005,
http://www.library.cornell.edu/nr/bookcpdf/c15-5.pdf.

[51] BAM, PRM certificate CO_2 in N_2, 2003, BAM-G050, Fl.-Nr. BAM-076-030403.
[52] ISO 6143: 2001 Gas analysis - Comparison methods for determining and checking the composition of calibration gas mixtures, 2001.
[53] Origin 7.5 SR6, OriginLab Cooperation, Northampton, MA, USA 2006, http://www.OriginLab.com.
[54] G. Casa, R. Wehr, A. Castrillo, E. Fasci, and L. Gianfrani, J. Chem. Phys. 130, 184306 (2009).
[55] G. J. Padilla-Viquez, J. Koelliker-Delgado, O. Werhahn, K. Jousten, and D. Schiel, IEEE Trans. Instr. Measur. J. 56, 529-533 (2007).
[56] L. Gianfrani, private e-mail communication.
[57] G. Wübbeler, G. J. Padilla Viquez, K. Jousten, O. Werhahn and C. Elster, to be published, 2011.
[58] L. S. Rothman, N. Jacquinet-Husson, C. Boulet, and A. M. Perrin, C. R. Physique 6, 897-907 (2005).
[59] Global Atmosphere Watch (GAW), http://www.wmo.int/pages/prog/arep/gaw/gaw_home_en.html.
[60] GAW Report No. 186 (2009), T. Laurila [ed.], 14th WMO/IAEA Meeting of Experts on Carbon Dioxide, Other Greenhouse Gases and Related Tracers Measurement Techniques. Available from: http://www.wmo.int/pages/prog/arep/gaw/documents/GAW_186_TD_No_1487_web.pdf
[61] D. Crisp, R. M. Atlas, F.-M. Breon, et al., Adv. Space Res. 34, 700-709 (2004).
[62] D. F. Edwards, Silicon (Si), in: Handbook of Optical Constants of Solids, Academic Press, Boston 1985, p. 547, ISBN 0-12-544420-6.

4.1.8 Appendix I

The uncertainty budget of Γ.

Model equation, $\Gamma = S_T \cdot r_{iso} \cdot L \cdot p_{total} / (k_B \cdot T)$,

where

$$S_T = S_0 \left(\frac{T_0}{T}\right)^j \exp\left\{-\mathrm{hc}\frac{\mathrm{E}}{k_\mathrm{B}}\left(\frac{1}{T}-\frac{1}{T_0}\right)\right\}\frac{\left[1-\exp\left\{-\mathrm{hc}\frac{v_0}{k_\mathrm{B}T}\right\}\right]}{\left[1-\exp\left\{-\mathrm{hc}\frac{v_0}{k_\mathrm{B}T_0}\right\}\right]}, \text{ and } r_{iso} = x_{12CO2} / x_{12CO2HITRAN} \cdot$$

Quantity	Value	Standard Uncertainty	DOF	Sensitivity Coefficient	Uncertainty Contribution	Index
p	145.910 hPa	0.100 hPa	50	$2.5 \cdot 10^{-3}$	$250 \cdot 10^{-6}$ cm^{-1}	1.0 %

T	295.750 K	0.200 K	50	$-2.4\cdot10^{-3}$	$-480\cdot10^{-3}$ cm^{-1}	3.8 %
L	81.652 cm	0.200 cm	50	$4.5\cdot10^{-3}$	$900\cdot10^{-6}$ cm^{-1}	12.9 %
T_0	296.0 K					
v_0	4987.308350 cm^{-1}	$577\cdot10^{-6}$ cm^{-1}	inf.	0.0	0.0 cm^{-1}	0.0 %
x_{12CO2}	0.98420	$2.31\cdot10^{-3}$	inf.	0.37	$860\cdot10^{-6}$ cm^{-1}	11.8%
$x_{12CO2HITRAN}$	0.9842					
S_{To}	$1.25500\cdot10^{-21}$ cm^{-1}/(molecules·cm^{-2})	$7.20\cdot10^{-24}$ cm^{-1}/(molecules·cm^{-2})	50	$290\cdot10^{18}$	$2.1\cdot10^{-3}$ cm^{-1}	70. %
j	1.250	0.144	inf.	$310\cdot10^{-6}$	$45\cdot10^{-6}$ cm^{-1}	0.0 %
h	$662.606930\cdot10^{-36}$ Js	$110\cdot10^{-42}$ Js	50	$-140\cdot10^{27}$	$-15\cdot10^{-12}$ cm^{-1}	0.0 %
c	$29.9792458\cdot10^{9}$ cm/s					
E	60.8709 cm^{-1}					
k_B	$13.8065050\cdot10^{-24}$ J/K/molec	$24.0\cdot10^{-30}$ J/K/molec	50	$-27\cdot10^{21}$	$-640\cdot10^{-9}$ cm^{-1}	0.0 %
r_{iso}	1.00000	$2.35\cdot10^{-3}$				
S_T	$1.25613\cdot10^{-2}$ cm^{-1}/(molecules·cm^{-2})	$7.25\cdot10^{-24}$ cm^{-1}/(molecules·cm^{-2})				
Γ	0.3665 cm^{-1}	$2.50\cdot10^{-3}$ cm^{-1}	96			

The quantity h is the Planck constant, c the speed of light, E the ground state energy[12], k_B the Boltzmann constant, x_{12CO2} is the abundance of $^{12}CO_2$ in the sample, $x_{12CO2HITRAN}$ is the conventional $^{12}CO_2$ abundance set by HITRAN [35]and j is the exponent of the partition sum approximation used. The standard uncertainties of all the quantities are expressed assuming a normal distribution except those of v_0, x_{12CO2} and j which are expressed assuming a rectangular distribution.

5 CO quantification at 4.6 µm

Editorial note

In this chapter, a manuscript is presented that has been published in Appl. Phys. B, vol. 103, No. 4, pp. 947-957 (2011). The coauthorship is being held by J. Nwaboh, D. Schiel and O. Werhahn. Similar to chapter 4, the numbering of the manuscript was changed from the original version to match that of this thesis. The experimental and theoretical sections are representing similar issues as given in chapter 2 and 3.

Manuscript

Work described in this manuscript was focused on the measurement of CO amount fractions using intra-pulse mode QCLAS. A QCL-spectrometer was used to check its feasibility for absolute CO amount fraction measurements based on the *TILSAM* method. The P(1) line of CO at 4.6 µm was used for CO quantification.

5.1 Measurement of CO amount fractions using a pulsed quantum cascade laser operated in the intra-pulse mode

Abstract

Carbon monoxide (CO) is an important molecule for environmental monitoring, industrial process control, and a biomarker in exhaled human breath. The need for obtaining reliable and traceable data is indispensable. We employed direct absorption spectroscopy-based absolute amount fraction measurements of CO in a gravimetrically prepared gas mixture. A quantum cascade laser operated in the intra-pulse mode was used to probe the P(1) line of CO at 2139.4 cm^{-1}. The spectrometrically determined CO amount fraction agrees perfectly with the gravimetric reference value. We focused on the method, the uncertainty analysis of the spectrometry-based data retrieval and the respective traceability of input parameters to the SI. An uncertainty budget is presented. Our reproducibility is better than 1 %. The relative deviation of the spectrometric CO amount fractions from the gravimetric reference value reads minus 1.8 %, which is covered by a 4 % relative expanded uncertainty of single measurements ($k = 2$).

5.1.1 Introduction

The development of quantum cascade lasers (QCLs) [1] for the mid-infrared (MIR) wavelength range from 4 to 10 µm where most of the molecules' fundamental vibration lines are located has been of great interest to spectroscopists during the last few years. Its capability to work at room temperature, its possible single mode operation and its comparably large

output power provide the possibility to keep most of the favorable parameters of near infrared (NIR)-diode laser systems, e.g. tunability, system size, output power, simply taking them over to the MIR.

The physical and technological aspects of QCLs and their underlying theory are reported in several reviews and publications [1-8]. Room temperature QCLs in pulsed and continuous wave (cw) operation have been demonstrated and commercialized [2-4, 9-12]. Two methods for operating pulsed QCLs had been applied, the inter-pulse [13, 14] and the intra-pulse mode [10, 15, 16]. A comparison of these two modes is published in [17, 18].

QCL-based trace gas detection applies to environmental monitoring, industrial process control, and to medical diagnostics [19-25]. It is selective, non-invasive and can be used for the fast monitoring of biomarkers such as CO or NO [26], e.g. for medical breath analysis [27]. For absolute measurements using pulsed QCLs, the spectrometric technique of choice is most likely to be direct absorption spectroscopy. Using Beer-Lambert's law, a QCL-based system would offer the possibility of direct-traceable quantitative measurements without the need for routine calibration with certified gas mixtures. Systems working on this principle, generally utilize the tunability of the laser, probing a rovibrational molecular absorption line [28-32]. Thus, the method of "traceable infrared laser spectrometric amount fraction measurements" (*TILSAM*) [33] developed within the scope of the EURAMET project [34] can also be used in a QCL intra-pulse mode spectrometer.

In order to perform the *TILSAM* method, the absorption peak area is evaluated, and relying on known spectroscopic and molecular parameters, it is directly converted into a species concentration. From a metrological point of view, the species concentration would be directly traceable to the international system of units (SI), i.e. the *T* in *TILSAM*. Different studies of the feasibility to perform absolute measurements have been published, applying NIR-laser spectroscopy [30, 35]. Recently, some groups have also applied pulsed QCLs for absolute measurements based on direct absorption spectroscopy [18, 36] or cavity enhanced spectroscopy [19, 37].

In this paper, in contrast to most published studies typically aiming towards improved sensitivities or challenging environments [12, 22, 38-43], we focus on the feasibility and accuracy of the intra-pulse mode of operation of a QCL spectrometer in combination with an absolute method for measuring the amount of substance fractions in gas mixtures. The emphasis is shifted on realized data quality objectives (DQO) expressed by uncertainty budgets. DQO typically refer to the accuracy, precision, completeness, representativeness, or comparability of desired measurement results. DQOs are frequently defined for specific applications, such as e.g. that of the World Metrological Organization (WMO)-Global Atmospheric Watch (GAW) programme [44]. We present results on absolute amount fraction measurements of CO. All but one of the input parameters are traceable to the international system of units (SI). So far not published on QCL spectroscopy to the best of our knowledge, an uncertainty budget presented in Appendix II is used to report complete measurement results, comprising both the value and the uncertainty component.

5.1.2 Theory

Concerning only absorption processes, the interaction of the gas species molecules and the sensing radiation at wave number $\tilde{\nu}$ is modeled by the Beer-Lambert law

$$\Phi(\tilde{\nu}, L) = \Phi_0(\tilde{\nu}) \cdot \exp\{-S_T \cdot \mathrm{g}(\tilde{\nu} - \tilde{\nu}_0) \cdot L \cdot n\} \tag{5.1}$$

with Φ_0 and Φ being the incident and transmitted radiant powers, respectively, of which the SI unit is W. The absorption is governed by the molecular transition line strength S_T at gas temperature T, the respective normalized absorption profile g centered at $\tilde{\nu}_0$, and the absorption path length L. The line strength S_T is specific for the probed molecular transition. Relying on the ideal gas law, the molecular density n of the absorbing species can be expressed in terms of the partial pressure p_{partial} of the absorbing molecules and the gas temperature. The partial pressure can be related to the total pressure p_{total} using the amount of substance fraction of the absorbing species, $x_{\mathrm{species}} = p_{\mathrm{partial}} / p_{\mathrm{total}}$. Thus, Eq. (5.1) becomes

$$\Phi(\tilde{\nu}, L) = \Phi_0(\tilde{\nu}) \cdot \exp\left\{\frac{-S_T \cdot \mathrm{g}(\tilde{\nu} - \tilde{\nu}_0) \cdot L \cdot x_{\mathrm{species}} \cdot p_{\mathrm{total}}}{k_{\mathrm{B}} \cdot T}\right\} \tag{5.2}$$

Measuring Φ and Φ_0 for a known path length, measuring p_{total} and T, and probing a certain molecular transition leads to the amount of substance fraction of the species

$$x_{\mathrm{species}} = -\ln\left(\frac{\Phi(\tilde{\nu})}{\Phi_0(\tilde{\nu})}\right) \frac{k_{\mathrm{B}} \cdot T}{S_T \cdot \mathrm{g}(\tilde{\nu} - \tilde{\nu}_0) \cdot L \cdot p_{\mathrm{total}}} \tag{5.3}$$

Introducing the spectral absorbance $\mathrm{A}(\tilde{\nu}) = -\ln(\Phi(\tilde{\nu})/\Phi_0(\tilde{\nu}))$, which in cases[5] can also be called extinction, and making use of the normalization of g, Eq. (5.2) can also be written in its integral form

$$x_{\mathrm{species}} = \frac{k_{\mathrm{B}} \cdot T}{S_T \cdot L \cdot p_{\mathrm{total}}} \int_{-\infty}^{\infty} A(\tilde{\nu})\,\mathrm{d}\tilde{\nu} = \frac{k_{\mathrm{B}} \cdot T}{S_T \cdot L \cdot p_{\mathrm{total}}} \cdot A_{\mathrm{line}} \tag{5.4}$$

where A_{line} is the line area obtained by integration of the measured absorbance data over wave number. Direct absorption spectroscopy is described by the Beer-Lambert law, as expressed in Eq. (5.2). All input quantities are SI-traceable. In turn, using Eq. (5.4) to determine the amount of substance fraction, x_{species}, in a given gas mixture would deliver results that are SI-traceable. An uncertainty budget for the measurement according to the ISO Guide to the expression of uncertainty in measurement (GUM) [45] can be evaluated with Eq. (5.4) as model function.

[5] see e.g. http://goldbook.iupac.org/A00028.html

Regarding the accompanied uncertainty, the feasibility of absolute spectrometric amount of substance fraction measurements relies on two crucial input quantities, the experimental determination of the absorption peak area A_{line} and the knowledge of the transition line strength S_T. Line strength values can be obtained, e.g. from data bases like HITRAN [46]. Line strength uncertainties given in HITRAN are sometimes large and imprecise. An uncertainty budget in accordance with the ISO GUM [45] has unfortunately not been provided up to now. This prevents claiming that a spectrometrically measured amount fraction based on HITRAN is traceable. Therefore, additional effort would be necessary to improve the lack of more precise and reliable data on individual molecular line strengths. Consequently a couple of laser-based studies were undertaken [31, 47-53]. However, only few of them were also to improve the quality of uncertainty statements [31, 52, 54]. The uncertainty of the line strength of the P(1) CO transition (fundamental band around 4.6 µm) probed in this work is specified by HITRAN to be in the range of 2 to 5 % [46]. However, this is not GUM compliant and traceable.

5.1.3 Experimental

We used a QCL controller setup based on a driving circuit inside an air-cooled laser housing delivered by the Fraunhofer-IPM [55]. The µ-processor controlled setup with a TCP/IP connection to a master PC generates laser pulses with lengths between 8 and 255 ns at repetition rates between 100 Hz and 7.5 MHz and laser voltages up to 25 V. Inside the air-cooled laser housing the QCL chip temperature is kept constant between 245 and 320 K to within ±30 mK by a TE-cooler. The QCL was produced and structured with a distributed feedback (DFB) grating by the Fraunhofer-IAF [56].

Figure 5.1 sketches the bread board where the QCL was incorporated. For the spectroscopic gas analysis, a two-channel scheme was used. After collimation, the QCL beam was split into a reference beam and a second sample beam transmitted through a 0.82 m stainless steel absorption cell. The reference beam was used for intensity normalization and for fixing the wavelength axis by means of a removable etalon. Both channels were terminated into TE-cooled HgCdZnTe detectors (Vigo PDI-2TE-10.6). The electrical signals were digitized at 5 GS/s by an 8 bit A/D-converter (Compuscope 85G).

The gas pressure in the cell, p_{total}, could be adjusted by means of a gas sampling system equipped with a turbo molecular vacuum pump and measured by a capacitance pressure gauge. The gas temperature T was measured with a Pt100-resistance device stuck on the absorption cell. The measured data were processed according to the *TILSAM* method based on Eq. (5.4).

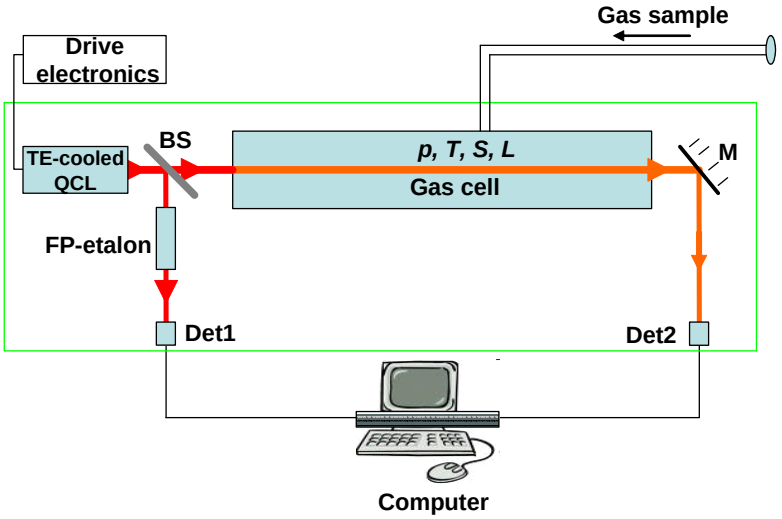

Figure 5.1: Schematic diagram of the setup used for species quantification in a two-channel regime. The single path absorption cell has a length of $L = 0.82$ m. BS: beam splitter, M: mirror, Det: detector, FP: Fabry Perot. Operation conditions: laser voltage 10.5 V, laser substrate temperature 292 K, pulse length 255 ns, repetition rate 2 kHz.

5.1.4 Quantitative CO detection

The pulsed quantum cascade laser was operated in the intra-pulse mode to probe the P(1) line of CO at 2139.4261 cm^{-1}. The choice of the intense P(1) line ($S_{T=296K} = 9.072 \cdot 10^{-20}$ cm/molecule) was only to demonstrate the feasibility. Nevertheless, for a certain application, appropriate line selection would be a problem of its own [35]. The spectrometric measurements were performed varying the total gas pressure in the cell within the range of 100 hPa to 450 hPa. A reference gas mixture of carbon monoxide in nitrogen, gravimetrically prepared by the BAM (Bundesanstalt für Materialforschung und –prüfung) [57] with a nominal level of 1000 µmol/mol CO was analyzed. The uncertainty of the exact value x_{ref} is certified to be ±0.051 % relative [58].

As known from published studies on QCL spectroscopy, some aspects have to be considered in order to perform spectrometric measurements using a pulsed QCL.

Firstly, the experimental conditions should be such that the effect known as “rapid passaging” [59] does not affect the measured signal. Rapid passaging occurs when the laser frequency sweep through an absorption line is faster than the collisionally induced relaxation. This results in an asymmetric or even inverted or oscillating absorption signal [60]. For the present work, this is evidenced by measurements on pure CO. An example is shown in Figure 5.2 where the CO line measured at 2.1 hPa exhibits a large inverted feature instead of the second part of a normal absorption line. However, increasing the pressure transfers the inverted signal to a symmetric line as depicted in the inset of Figure 5.2. This latter measurement was performed at 28 hPa.

Secondly, because of the fast spectral sweeping within a QCL pulse, neither the chirp rate nor the instantaneous line width of the QCL is constant on a pulse duration time scale [15, 37]. It

was shown that for longer pulses, e.g. up to µ-second duration, the chirp rate change gets smaller towards the end of the pulse as does the instantaneous line width [60]. Thus, longer pulses, as well as placing the spectrum at the end of the pulse are recommended.

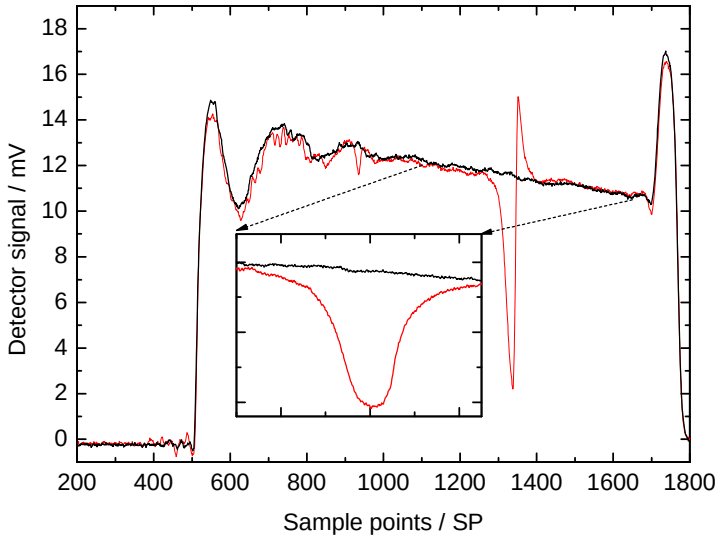

Figure 5.2: Reference beam with no CO absorption (blank). Samples with CO (pure) absorption (red line) at a total pressure of 2.1 hPa affected by the rapid passing effect. Inset: Absorption at 28 hPa with no rapid passaging effect observable. The chirp rate expressed in units of the sample point axis was 0.0017 cm^{-1}/SP, which is equivalten to $8.50 \cdot 10^{-3} cm^{-1}$/ns or 255 MHz/ns**.**

Figure 5.3b shows a QCL pulse (around 4.6 µm) with a 255 ns pulse length. The pulses are transmitted through an etalon having a free spectral range (FSR) of about 0.05 cm^{-1}. The intra-pulse chirp for this condition is shown to be 1.85 cm^{-1} as evidenced by the number of 37 fringes. Figure 5.3a represents the signal of the sample channel detector with CO absorption and the reference channel detector with the etalon removed, respectively. One hundred QCL pulses were averaged and data were measured in the time domain in units of sample points (SP). The spectral feature is placed at the end of the pulse by tuning the onset wavelength. We assume that the measured signals in Figure 5.3a are not affected by the rapid passaging effect. Firstly, because measurements were performed at 100 hPa, a pressure definitely higher than 28 hPa, and secondly, because the relaxation rate is furthermore increased due to the presence of additional collision partners in the gas mixture. This effect was not observable in a series of measurements performed in the pressure range 50 to 100 hPa.

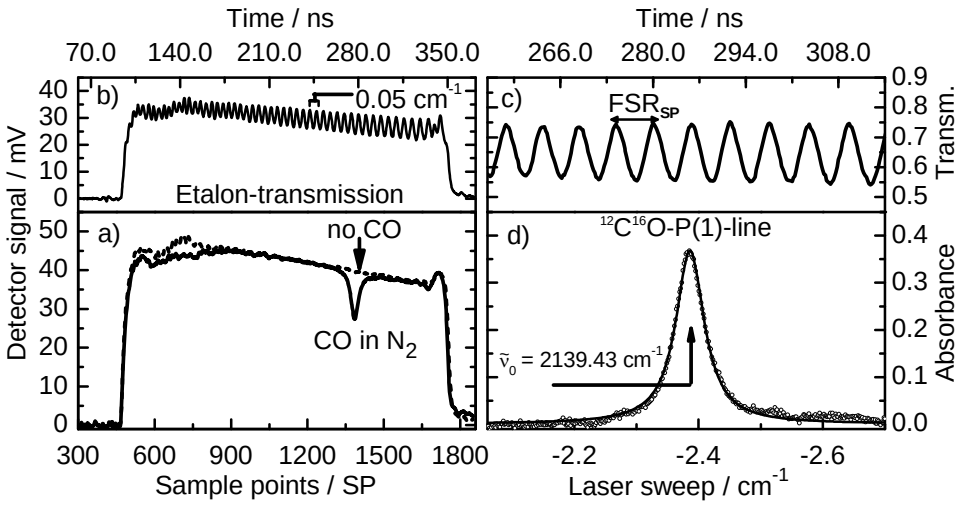

Figure 5.3: Intra-pulse chirp spectroscopy. a) Data from the reference channel, without CO absorption (dashed line) and the sample channel (full line) featuring CO absorption, respectively. b) Etalon transmission signal seen by detector 1 with the etalon ($FSR_\nu \approx 0.05$ cm^{-1}) placed in the reference beam path. c and d) Data transferred to the wave number domain. c) Etalon transmittance curve. d) Data of the of a), converted to absorbance values (open circles). A Voigt profile has been fitted to the data (full line) representing the CO-P(1) line at 2139.4261 cm^{-1}. QCL operating parameters: substrate temperature 292 K, pulse length 255 ns, laser voltage 10.5 V, repetition rate 2 kHz, chip: Fraunhofer-IAF [56].

The data in Figure 5.3a were converted to absorbances as depicted in Figure 5.3d using the detector signals of the two channels, representing a simultaneous two channel measurement scheme. The wave number axis in Figure 5.3d was accomplished by means of the chirp rate $r_{sweep} = FSR_\nu / FSR_{SP}$. FSR_ν is the known free spectral range of the etalon in wave numbers and FSR_{SP} is the experimental fringe separation measured in the time domain (SP) visible in the upper panel of Figure 5.3c. FSR_ν was determined by calculation, using the refractive index of the etalon material and its length; FSR_{SP} by fitting the measured etalon transmission spectrum with a multi-peak function.

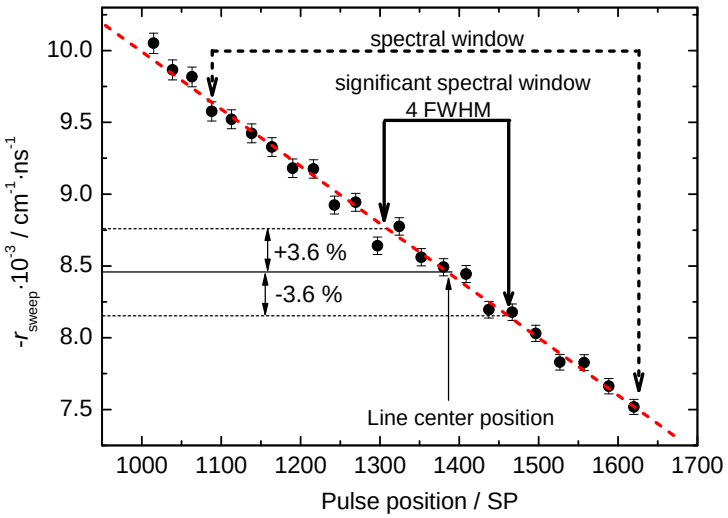

Figure 5.4: Plot of the sweep rate r_{sweep} as a function of position within the QCL pulse. The derived regression is displayed as a dashed line.

For a careful evaluation of the sweep rate, an appropriate function $r_{sweep}(SP)$ developed in the time domain should be applied. In Figure 5.4 the determined chirp rates r_{sweep} are plotted as a function of their positions within the QCL pulse. Based on the measured chirp rates, (see Figure 5.4), a linear regression was used to predict the sweep rate at any given temporal position within the QCL pulse. For simplicity, we utilized the sweep rate at the absorption peak position to realize the wave number axis. The uncertainty of r_{sweep} was determined in accordance with the GUM. Typical expanded uncertainties were ±0.7 % relative.

The measured signal of the TE-cooled HgCdZnTe detector as a function of the incident laser power is shown in Figure 5.5. Displayed is the so-called analytical function with axes flipped to power vs. signal to ease the application of a correction function[6]. One just has to take the detected signal as the independent variable to the analytical function in order to derive the corrected laser power. It was deduced that a nonlinear response of the detector was responsible for a large bias in the resulting amount fractions.

[6] analytical versus calibration function, see also http://goldbook.iupac.org/A00332.html

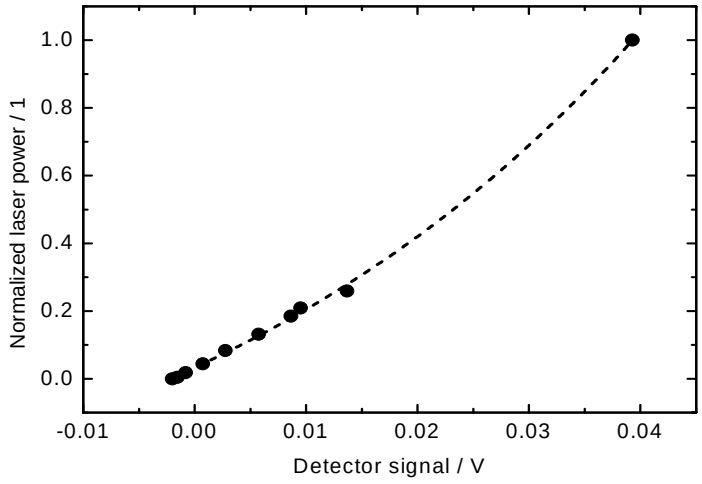

Figure 5.5: Measured dependence of incident laser power and resulting detector signals. The laser power was varied by stepping down the full laser power (no filter) by means of calibrated filters that had well defined transmissions at 4.6 µm. An exponential growth, $y = 0.68578 \cdot \exp(x/0.04468) - 0.65273$, has been fitted to the measured data points in order to describe the detector's response function.

As a consequence, all the signals, e.g. those of Figure 5.3a, were to be reprocessed to correct for this nonlinearity. This was realized by means of their measured detector response function shown in Figure 5.5, providing a linear signal scale and subsequently a linear transmission scale. Nonlinearity is a known concern for HgCdZnTe detectors which are very often used in MIR spectroscopy [61] although there is presently no predicting model available [62]. In fact, assuring a linear transmission scale is mandatory for any absolute spectrometric method like *TILSAM*.

Fitting a Voigt profile to the measured absorbance data by means of a nonlinear least square fit [63] (Levenberg-Marquardt [64]) delivered the absorption peak area. The uncertainties in the absorption peak area from fitting ranged from 0.5 to 1 % relative.

Amount fractions of CO were directly calculated using Eqn. (5.4). This is referred to as "direct retrieval". Results measured under reproducibility conditions for six sets of measurements are presented in Figure 5.6 as a function of the experimental parameter $\Gamma = S_T \cdot L \cdot p_{\text{total}} / (k_B \cdot T)$. Γ is typically given in units of cm^{-1}. A variation in Γ is mostly related to the variation of the total gas pressure. The dashed line is the gravimetric reference target value of 936.6 µmol/mol. Each data point in Figure 5.6 is shown as the mean of 10 consecutive individual measurements at the same pressure (same Γ) under repeatability conditions. Each measurement consists of 100 averaged laser pulses to improve the signal to noise ratio.

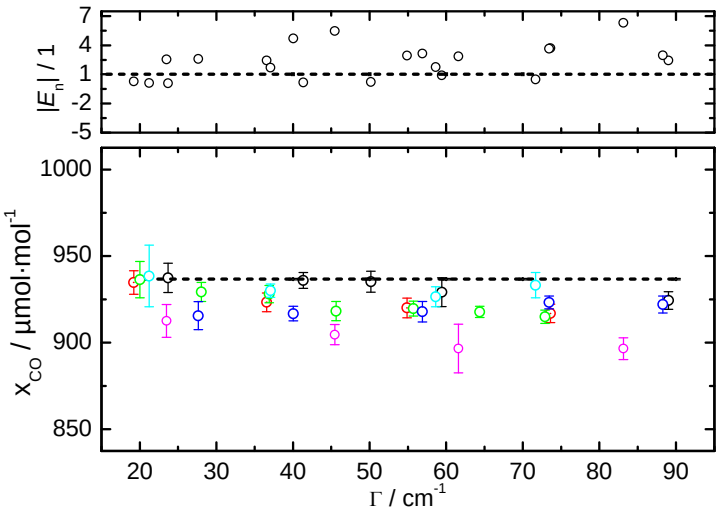

Figure 5.6: Spectrometric amount fraction determination of CO in a gas mixture with N_2, pressures in the range 100 hPa to 450 hPa, for six sets of measurements. Bottom panel: Direct retrieval. Mean of 10 consecutive measurements (at the same pressure); gravimetric reference value as a dashed line. Top panel: Direct retrieval. Normalized error E_n of each data point depicted in the bottom panel.

The normalized error $E_n = D/U(D)$, depicted in the upper panel of Figure 5.6, is used to grade these results [65-67]. It is given by the degree of equivalence D between the spectrometry-based amount fraction value x_{CO} and the gravimetric reference value x_{ref} and their uncertainties u,

$$D = x_{co} - x_{ref},$$

$$U(D) = 2 \cdot u(\mathrm{D}) = 2 \cdot \sqrt{(u^2(x_{CO}) + u^2(x_{ref}))},$$

where, $u(D)$ is the standard uncertainty of D. A coverage factor $k = 2$ is applied additionally. As featured in the top panel of Figure 5.6, only some of the spectrometric results, derived from the direct retrieval agree with the reference target value, i.e. yielding $|E_n| < 1$. The relative deviations from the reference, $D_{rel} = D/x_{ref}$, are in the range of -1.2 %. Nevertheless, the majority of the results in the top panel of Figure 5.6 yield normalized errors $|E_n| > 1$, indicating that they do not agree with the gravimetric reference value. This means that the uncertainties were probably underestimated. These uncertainties were simply based on the repeatability of ±0.8 % within the 10 consecutive measurements at the same pressure, given by the standard deviation of the mean multiplied by a coverage factor $k = 2$. This has to be compared to the expanded uncertainty of an individual measurement (single point) given in Appendix II as being in the range of ±4 % relative, evidencing that the repeatability figure does not represent an appropriate uncertainty.

Looking for the reproducibility by averaging all the individual spectrometric results, i.e. at different realized Γ, for the six sets, a mean amount of substance fraction for each set was calculated. This mean amount fraction is depicted in the bottom panel of Figure 5.7. The mean CO amount fraction for measurement number 1 is (932±3) µmol/mol.

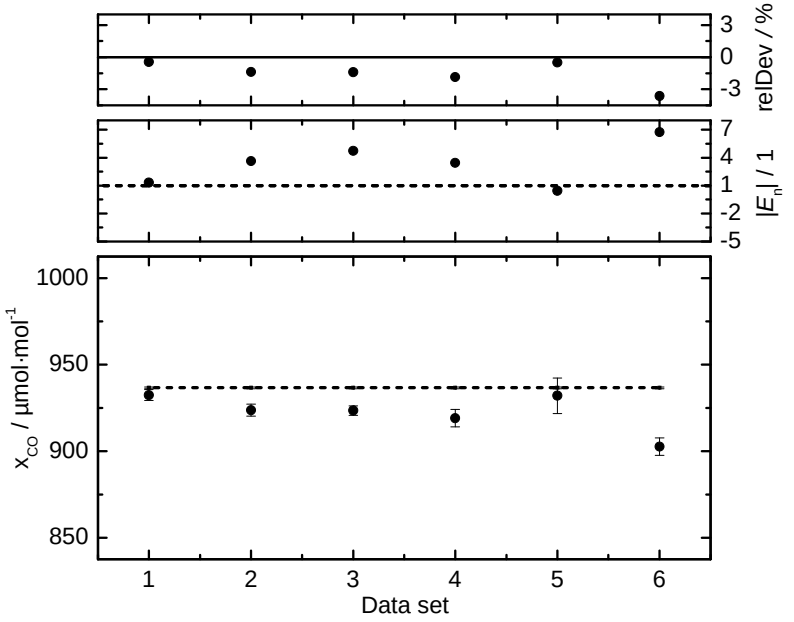

Figure 5.7: Direct retrieval analysis. Bottom panel: Results of the mean of x_{CO}, for five sets of measurements performed on the mixture with x_{ref} = (936.66 ± 0.5) µmol/mol. Dashed line: gravimetric reference value. Middle panel: The respective normalized errors. Top panel: Relative deviation of spectrometric x_{CO} from gravimetric reference value.

The normalized errors and the respective relative deviation from the gravimetric reference value of 936.6 µmol/mol are depicted in the middle and upper panels of Figure 5.7. All but one of the normalized errors are larger than one, confirming that most of the results based on the described statistics do not agree with the gravimetric reference value. The relative deviation is in the range of -0.4 to -1.8 %. The reproducibility measured as the standard deviation within all sets of data is 1 % relative.

However, apart from the direct retrieval described above, there is another option to retrieve amount fraction results from the spectrometric data. Alternatively Eqn (5.4) can be rewritten as

$$A_{\text{line}} = x_{\text{CO}} \cdot \left(\frac{S_T \cdot L \cdot p_{\text{total}}}{k_{\text{B}} \cdot T} \right) = x_{\text{CO}} \cdot \Gamma \tag{5.5}$$

giving rise to a linear model of the line area versus Γ with the slope being identified as x_{CO}. The linear generalized regression for measurement number 1 of Figure 5.7 is depicted in

Figure 5.8. Applying a generalized linear regression to the data is in accordance with ISO 6143 [68]. The line area uncertainties (vertical bars smaller than symbol size) are based on the uncertainty of the line area fitting parameters [63] and $u(r_{sweep})$, whereas those of the Γ values (horizontal bars) are based on respective uncertainties of S_T, p_{total}, T and L given in Appendix II. For the line strength, a smallest standard uncertainty of 2 % was taken from HITRAN [46]. The generalized regression yields an amount fraction of 929±41 µmol/mol. This is slightly smaller than the value resulting from the direct retrieval, giving rise to a slightly increased relative deviation.

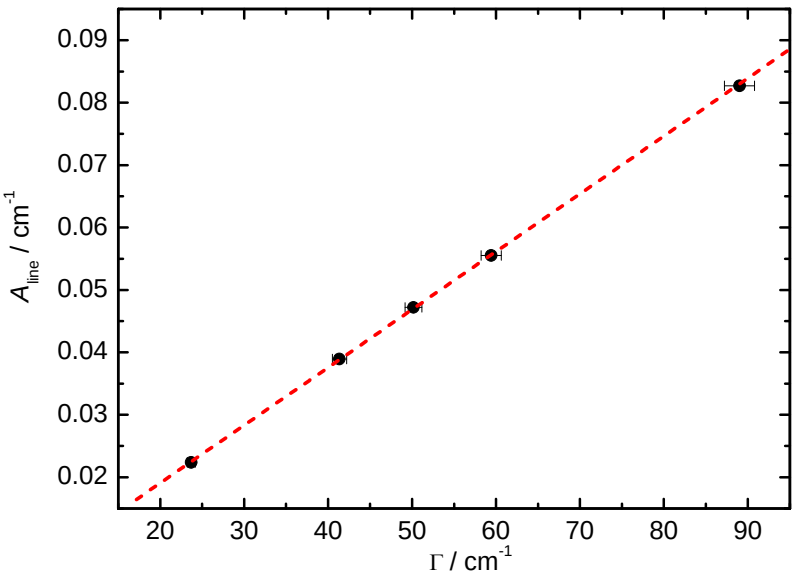

Figure 5.8: Generalized linear regression (dashed line) of values of A_{line} as a function of Γ for measurement number 1 in Fig. 8.

However, because of the larger expanded uncertainty figure of ±41 µmol/mol (±4.4 %), the normalized error $|E_n|$ of the regression-based x_{CO} is much smaller than unity ($|E_n|$ = 0.2), expressing that this spectrometric result agrees now with the gravimetric reference value.

Applying this regression-based retrieval to the other five sets of measurements presented in Figure 5.7, yields the results depicted in Figure 5.9. A slightly increased relative deviation for the regression-based x_{CO} with respect to the direct retrieval is observed. However, the normalized errors are much smaller than unity, expressing that these spectrometric results agree with the gravimetric reference value. The respective relative deviations are in the range -0.8 to -3 % and the reproducibility is 1 % relative, given as the standard deviation within the six sets of data.

The resulting expanded uncertainties from the regression-based analysis are observed to be larger than those of the direct retrieval. The reason for the larger expanded uncertainties of the

regression-based analysis is that uncertainties of all influence quantities were considered, whereas for the direct retrieval just statistical parameters have been used. Referring back to the previous paragraphs, the uncertainty of an individual measurement for which a budget is given in Appendix II compares well with the uncertainty resulting from the generalized linear regression analysis, both being in the four percentage range.

The regression-based retrieval has some further benefit regarding the measurement quality for which the intercept parameter of a free regression can be viewed as a measurand. The linear model does not predict any intercept. Applying a generalized linear regression with a free intercept parameter yields a figure which is either insignificant as predicted by the model or not. If the resulting intercept were significant, i.e. its uncertainty were smaller than its numerical value, the model would not describe the experimental condition appropriately. The intercept parameter given by the generalized linear regression in Figure 5.8 is $a_0 = (4.2 \pm 8.2) \cdot 10^{-4}$, indicating that the experimental conditions were appropriate. The same holds for the other five sets of measurements.

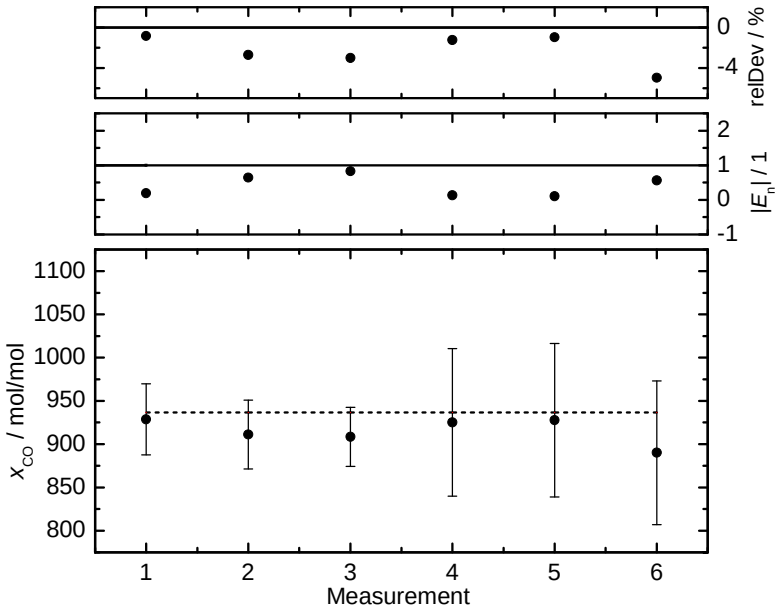

Figure 5.9: Regression-based analysis. Bottom panel: Results of x_{CO} for six sets of measurements performed on the mixture with x_{ref} = (936.66 ± 0.5) µmol/mol. Dashed line: gravimetric reference value. Middle panel: The respective normalized errors. Top panel: Relative deviation of spectrometric x_{CO} from gravimetric reference value.

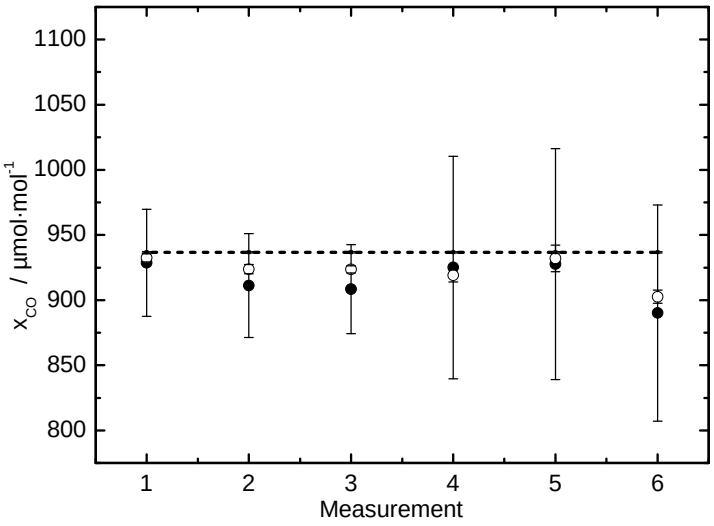

Figure 5.10: Comparison of amount fractions obtained by the direct and the regression-based retrieval. Open circles are the directly retrieved and solid circles are the regression-based CO amount fractions.

A comparison of the amount fraction results from both types of evaluation with the gravimetric reference is summarized in Figure 5.10. All the regression-based retrievals agree with the directly retrieved amount fractions and the gravimetric reference value.

5.1.5 Discussions

Data have been processed according to two retrieval strategies. The results derived by the direct retrieval presented in the bottom panel of Figure 5.7 are based on a statistical analysis while not containing complete uncertainties. Only the repeatabilities were considered in order to express the uncertainties of the spectrometric CO amount fractions. However, the repeatability alone does not represent the complete uncertainty figure of a measurement result, therefore, Figure 5.7 reveals an apparent bias of the spectrometric CO amount fractions, which, in turn, is due to underestimated uncertainties. Instead, a complete uncertainty budget accounted for by the regression-based retrieval (see Figure 5.9) removes this apparent bias. The spectrometric CO amount fraction results with the full uncertainty figures calculated in accordance with the ISO GUM [45] are shown in the bottom panel of Figure 5.9, demonstrating a good agreement with the gravimetric reference value. Here, it is worthwhile noting that statistics alone do not replace a complete uncertainty consideration. In contrast to some other approaches, we would like to emphasize that they neither provide the full nor sufficient information on the quality of a measurement result.

The relative expanded uncertainty (k = 2) of the spectrometric CO amount fraction is in the range of 4 %. The uncertainty of the gravimetric reference value used in this work is less than ±0.5 % [58]. However, the spectrometric amount fraction agrees with the gravimetric reference. The DQO for CO established within the GAW is expressed by the WMO as 1.0 %

relative expanded uncertainty, $k = 2$ [44]. The uncertainty of the spectrometric CO amount fraction is larger than the one established within the GAW. Compared to the 15 % relative uncertainty established in the EU directive 2000/69/EC [69] for field measurements to guide air quality assurance, our uncertainty would already be within this scope, although it is not yet validated for field measurements. Nevertheless, the QCL-based gas analysis has to be improved considerably in terms of the accompanied uncertainty to be comparable to the needs of the WMO or to become a standard in gas metrology. One of the main input quantities that contributes the most to the final uncertainty of the amount fraction result is the line strength as reported in Appendix II. Its uncertainty is specified to be within a range of 2 to 5 % for the CO-P(1) line [46]. If the line strength uncertainty were less than a percent, then the relative expanded uncertainty of the spectrometric amount of substance fraction would be much smaller. In that case, the spectrometric uncertainty would match that of the GAW DQO. Thus, with an uncertainty figure of less than one percent, the QCL-based measurements presented in this paper, not being calibrated with any reference gas, could be applicable to environmental measurements. The repeatability and reproducibility is in the one or even sub-percentage range.

Regarding the uncertainty of the line strength, an additional concern has to be addressed based on the fact that the line strength figure taken from HITRAN is not GUM-compliant, i.e. neither $S_{T=296\mathrm{K}}$ nor S_T. The latter makes the T in *TILSAM* not feasible while relying on HITRAN.

The nonlinearity of the MIR detectors used was an important influencing factor. The data processing described in section 5.4 comprised a nonlinear relation between the IR-radiant powers and the electrical output signals of the detectors, transferred by an exponential growth function. For example, assuming instead a linear relation between the IR-radiant powers and the electrical output signals leads to an amount fraction of CO of about 30 % less.

As observed in the detector response curves in Figure 5.5, no data point is present in the range of normalized laser powers between 0.4 to 1. Nevertheless, a check of the validity of applying these response functions was achieved by stepping down the laser power to the range between 0 and 0.4. By doing this, the spectrometric results of the CO amount fractions using the full laser power and the stepped down laser power, respectively, agree perfectly with each other, confirming that our preliminary measure to correct the measured signals for the detector nonlinearity has been valid so far.

5.1.6 Conclusion

Applying intra pulse QCL spectroscopy as an absolute method, we quantified the amount of substance fraction of CO in a gravimetrically prepared gas mixture. Data have been measured in a two-channel-regime and fitted by a Voigt profile in order to determine the area of the CO-P(1) line. We have identified an issue with detector nonlinearity which made the results not comparable at all to the gravimetric reference value before correction. Comparing the spectrometric amount fraction derived from a regression-based analysis with that of the

reference value, both agree, showing an insignificant deviation of the spectrometric result of about -1.8 % relative from the gravimetric reference value. However, with the HITRAN-specified line strength uncertainty for the CO-P(1) line being in the range of 2-5 %, the spectroscopic and gravimetric results are in concordance. Our reproducibility is better than 1 %. The expanded uncertainty of a single measurement detailed in Appendix II is 4.6 % ($k = 2$) and compares well with the overall uncertainty of the regression-based CO amount fractions. This uncertainty figure however has to be improved in order to become competitive with existing gas standards. The uncertainty budget presented for our measurement result reveals that an improvement on the input parameters' side would have to be prioritized on a line strength value with reduced uncertainty. This will be the focus of upcoming work.

5.1.7 Acknowledgements

Parts of this work were financially supported by ERA-NET Plus, under the iMERA-Plus Project - Grant Agreement No. 217257, by the international graduate school of metrology, TU Braunschweig, and by the BMBF projects MEX07/004, and QUANSYS/QUANKAS, FKZ 13N8123. The authors acknowledge the continuous collaboration of Hans-Joachim Heine (BAM), Jorge Koelliker Delgado (CENAM), and the laser chemistry group of Prof. Dr. K.-H. Gericke (TU-Braunschweig).

5.1.8 References

1. J. Faist, F. Capasso, D.L. Sivco, C. Sirtori, A.L. Hutchinson, A.Y. Cho, Science 264, 553 (1994)
2. J. Wagner, C. Mann, M. Rattunde, G. Weimann, Appl. Phys. A 78, 505 (2004)
3. A. Evans, J.S. Yu, S. Slivken, M. Razeghi, Appl. Phys. Lett. 85, 2166 (2004)
4. T. Aellen, S. Blaser, M. Beck, D. Hofstetter, J. Faist, E. Gini, Appl. Phys. Lett. 83, 1929 (2003)
5. E. Normand, G. Duxbury, N. Langford, Opt. Commun. 197, 115 (2001)
6. C. Pflügl, M. Litzenberger, W. Schrenk, D. Pogany, E. Gornik, G. Strasser, Appl. Phys. Lett. 82, 1664 (2003)
7. T. Beyer, M. Braun, S. Hartwig, A. Lambrecht, J. Appl. Phys. 95, 4551 (2004)
8. R.F. Curl, F. Capasso, C. Gmachl, A.A. Kosterev, B. McManus, R. Lewicki, M. Pusharsky, G. Wysocki, F. Tittel, Chem. Phys. Lett. 487, 1 (2010)
9. G. Hancock, J.H. van Helden, R. Peverall, G.A.D. Ritchie, R.J. Walker, Appl. Phys. Lett. 94, 201110 (2009)
10. E. Normand, M. McCulloch, G. Duxbury, N. Langford, Opt. Lett. 28, 16 (2003)
11. A.A. Kosterev, R.F. Curl, F.K. Tittel, C. Gmachl, F. Capasso, D.L. Sivco, J.N. Baillargeon, A.L. Hutchinson, A.Y. Cho, Appl. Opt. 39, 4425 (2000)
12. I. Sydoryk, A. Lim, W. Jäger, J. Tulip, M.T. Parsons, Appl. Opt. 49, 945 (2010)
13. K. Namjou, S. Cai, E.A. Whittaker, Opt. Lett. 23, 219 (1998)
14. D.D. Nelson, J.H. Shorter, J.B. Mcmanus, M.S. Zahniser, Appl. Phys. B 75, 343 (2002)
15. M.T. McCulloch, E.L. Normand, N. Langford, G. Duxbury, J. Opt. Soc. Am. B 20, 1761 (2003)
16. T. Beyer, M. Braun, A. Lambrecht, J. Appl. Phys. 93, 3158 (2003)
17. B. Grouiez, B. Parvitte, L. Joly, D. Courtois, V. Zeninari, Appl. Phys. B 90, 177 (2008)
18. J. Manne, W. Jäger, J. Tulip, Appl. Phys. B 94, 337 (2009)
19. J. Manne, O. Sukhorukov, W. Jäger, J. Tulip, Appl. Opt. 45, 9230 (2006)
20. M.L. Silva, D.M. Sonnenfroh, D.I. Rosen, M.G. Allen, A. O'Keefe, Appl. Phys. B 81, 705 (2005)
21. S. Welzel, New enhanced sensitivity infrared laser spectroscopy techniques applied to reactive plasmas and trace gas detection, Dissertation, 2009, Ernst-Moritz-Arndt Universität Greifswald, http://ub-ed.ub.uni-greifswald.de/opus/volltexte/2009/723/
22. A.A. Kosterev, F.K. Tittel, R. Köhler, C. Gmachl, F. Capasso, D.L. Sivco, A.Y. Cho, S. Wehe, M.G. Allen, Appl. Opt. 41, 1169 (2002)
23. B.W.M. Moeskops, H. Naus, S.M. Cristescu, F.J.M. Harren, Appl. Phys. B 82, 649 (2006)
24. T. Fritsch, P. Hering, M. Mürtz, J. Breath Res. 1, 014002 (2007)
25. S.M. Cristescu, S.T. Persijn, S. Te Lintel Hekkert, F.J.M. Harren, Appl. Phys. B 92, 343 (2008)

26. V. Spagnolo, A.A. Kosterev, L. Dong, R. Lewicki, F.K. Tittel, Appl. Phys. B 100, 125 (2010)
27. M.R. McCurdy, Y. Bakhirkin, G. Wysocki, R. Lewicki, F.K. Tittel, J. Breath Res. 1, 014001 (2007)
28. E. Lanzinger, K. Jousten, M. Kühne, Vacuum 51, 47 (1998)
29. M.E. Webber, S. Kim, S.T. Sanders, D.S. Baer, R.K. Hanson, Y. Ikeda, Appl. Opt. 40, 821 (2001)
30. O. Werhahn, J. Koelliker Delgado, D. Schiel, Techn. Mess. 72, 396 (2005)
31. G. Padilla Viquez, J. Koelliker Delgado, O. Werhahn, K. Jousten, D. Schiel, IEEE Trans. Instr. Measur. J. 56, 529 (2007)
32. J. Koelliker Delgado, O. Werhahn, D. Schiel, IR-Spectrometric amount of CO_2 fraction determination in gas analysis applications, in: Anwendungen und Trends in der Optischen Analysenmesstechnik, VDI-Berichte 1959, p. 303, VDI-Verlag, Düsseldorf 2006, ISBN 3-18-091959-0
33. O. Werhahn, J.C. Petersen, *TILSAM* - draft A of a technical description, pdf-file, , http://www.euramet.org, EURAMET project no. 934, 2010
34. EUROMET-934, TILSAM - Traceable Infrared Laser Spectrometric Amount fraction Measurement, 2008, http://www.euramet.org, project no. 934
35. K. Wunderle, S. Wagner, I. Pasti, R. Pieruschka, U. Rascher, U. Schnurr, V. Ebert, Appl. Opt. 48, B172 (2009)
36. B.W.M. Moeskops, S.M. Cristescu, F.J.M. Harren, Opt. Lett. 31, 823 (2006)
37. S. Welzel, G. Lombardi, P.B. Davies, R. Engeln, D.C. Schram, J. Röpcke, J. Appl. Phys. 104, 093115 (2008)
38. S. Hunsmann, K. Wunderle, S. Wagner, U. Rascher, U. Schurr, V. Ebert, Appl. Phys. B 92, 393 (2008)
39. S. Wagner, B.T. Fisher, J.W. Fleming, V. Ebert, Proc. Comb. Inst. 32, 839 (2009)
40. P. Ortwein, W. Woiwode, S. Fleck, M. Eberhard, T. Kolb, S. Wagner, M. Gisi, V. Ebert, Exp. Fluids online first version, DOI 10.1007/s00348 (2010)
41. H. Teichert, T. Fernholz, V. Ebert, Appl. Opt. 42, 2043 (2003)
42. A.A. Kosterev, F. Tittel, K. Köhler, C. Gmachl, F. Capasso, D.L. Sivco, A.Y. Cho, Appl. Opt. 41, 573 (2002)
43. D. Weidmann, A.A. Kosterev, C. Roller, R.F. Curl, M.P. Fraser, F.K. Tittel, Appl. Opt. 43, 3329 (2004)
44. T. Laurila [ed.], 14th WMO/IAEA Meeting of Experts on Carbon Dioxide, Other Greenhouse Gases and Related Tracers Measurement Techniques, 2009, http://www.wmo.int/pages/prog/arep/gaw/gaw-reports.html
45. JCGM 100:2008, Evaluation of measurement data - Guide to the expression of uncertainty in measurement, GUM 1995 with minor corrections, ISO IEC Guide 98-3, 2008
46. L. Rothman et al., HITRAN2008, 2009, http://www.cfa.harvard.edu/HITRAN/, J. Quant. Spectrosc. Rad. Transf. 110, 533-572 (2009)

47. J. Henningsen, H. Simonsen, T. Møgelberg, E. Trudsø, J. Mol. Spectrosc. 193, 354 (1999)
48. G. Casa, R. Wehr, A. Castrillo, E. Fasci, L. Gianfrani, J. Chem. Phys. 130, 184306 (2009)
49. G. Casa, D.A. Parretta, A. Castrillo, R. Wehr, L. Gianfrani, J. Chem. Phys. 127, 084311 (2007)
50. J.T. Hodges, D. Lisak, Appl. Phys. B 85, 375 (2006)
51. J.T. Hodges, R. Ciurylo, Rev. Sci. Instrum. 76, 023112 (2005)
52. J.T. Hodges, H.P. Layer, W.W. Miller, G.E. Scace, Rev. Sci. Instrum. 75, 849 (2004)
53. L. RegaliaJarlot, V. Zeninari, B. Parvitte, A. Grossel, X. Thomas, D. P von der Heyden, Journal of Quantitative Spectroscopy & Radiative Transfer 101, 325 (2006)
54. G.J. Padilla Viquez, Investigation of TDLAS for its Application as Primary Standard for Partial Pressure Measurements, Dissertation, 2005, Technische Universität Berlin, http://opus.kobv.de/tuberlin/ source no. 1161
55. IPM, Fraunhofer Institut für Physikalische Messtechnik, Freiburg, Germany, http://www.ipm.fraunhofer.de
56. IAF, Fraunhofer Institut für Angewandte Festkörperforschung, Freiburg, Germany, http://www.iaf.fraunhofer.de
57. BAM, Bundesanstalt für Materialforschung und -prüfung, Berlin, Germany, http://www.bam.de
58. BAM, PRM certificate CO in N_2, 2000, BAM-G040, Fl.-Nr. 960554949-001122
59. G. Duxbury, N. Langford, M. McCulloch, S. Wright, Chemical Society Reviews 34, 921 (2005)
60. G. Duxbury, N. Langford, M. McCulloch, S. Wright, Mol. Phys. 105, 741 (2007)
61. E. Theocharous, J. Ishii, N.P. Fox, Appl. Opt. 43, 4182 (2004)
62. E. Theocharous, priv. communication (2010)
63. Origin 7.5 SR6, OriginLab Cooperation, Northampton, MA, USA 2006, http://www.OriginLab.com
64. Levenberg-Marquardt, Numerical Recipes, 2005, http://www.library.cornell.edu/nr/bookcpdf/c15-5.pdf
65. P. Robouch, N. Younes, P. Vermaercke, The "Naji Plot", a simple graphical tool for the evaluation of inter-laboratory comparisons, in: Data analysis of key comparisons, PTB-Bericht 10, p. 149, Physikalisch-Technische Bundesanstalt, Braunschweig 2003
66. D. Richter, W. Wöger, W. Hässelbarth eds., Data analysis of key comparisons, PTB-Bericht, Vol. PTB-IT-10, Physikalisch-Technische Bundesanstalt, Braunschweig 2003, 3-89701-933-3
67. ISO/IEC 17043, Conformity assessment — General requirements for proficiency testing, 2010, First edition, 2010-02-01
68. ISO 6143: 2001 Gas analysis - Comparison methods for determining and checking the composition of calibration gas mixtures, 2001
69. 2000/69/EC, Directive 2000/69/EC of the European Parliament and of the Council of 16 November 2000 relating to limit values for benzene and carbon monoxide in

ambient air, 2000, http://eur-lex.europa.eu/LexUriServ/LexUriServ.do?uri=OJ:L:2000:313:0012:0021:EN:PDF

70. GUM Workbench, 1.2 Win32, Metrodata GmbH, Grenzach-Wyhlen, Germany 1999, http://www.metrodata.de

5.1.9 Appendix II

In the following, an uncertainty budget [45] for a single measurement calculated by means of the GUM Workbench [70] is presented:

Model equation:

$$x_{\mathrm{CO}} = A_{\mathrm{line}} \cdot k_{\mathrm{B}} \cdot T \cdot 10^4 / (r_{\mathrm{iso}} \cdot S_T \cdot L \cdot p_{\mathrm{total}})$$

with:

$$r_{\mathrm{iso}} = x_{12\mathrm{CO}} / x_{12\mathrm{COHIT}},$$

$$S_T = S_0 \left(\frac{T_0}{T}\right)^j \exp\left\{-\mathrm{hc}\frac{\mathrm{E}}{k_{\mathrm{B}}}\left(\frac{1}{T}-\frac{1}{T_0}\right)\right\} \frac{\left[1-\exp\left\{-\mathrm{hc}\frac{v_0}{k_{\mathrm{B}}T}\right\}\right]}{\left[1-\exp\left\{-\mathrm{hc}\frac{v_0}{k_{\mathrm{B}}T_0}\right\}\right]},$$

$$A_{\mathrm{line}} = r_{\mathrm{sweep}} \cdot \Lambda$$

Quantity	Units	Definition
S_0	$cm^{-1}/(molecules \cdot cm^{-2})$	Line strength for norm temperature T_0 = 296 K
L	cm	Cell path length
k_B	J/K	Boltzmann constant
T	K	Temperature
P_{total}	hPa	Total gas pressure
r_{sweep}	cm^{-1}/SP	Chirp rate
Λ	SP	Area under the Voigt profile
E	cm^{-1}	Lower state energy
c	cm/s	Speed of light in vacuum
h	Js	Planck constant
T_0	K	Norm temperature

v_0	cm^{-1}	Line center position
x_{12CO}	1	Abundance of ^{12}CO in the sample
$x_{12COHIT}$	1	Conventional ^{12}CO abundance value given by HITRAN
r_{iso}	1	Deviation of isotopomeric abundance in the experiment from conventional value (HITRAN)
j	1	Exponent in the partition sum approximation given by (T/T_0)
A_{line}	cm^{-1}	Integrated absorbance line area
S_T	$cm^{-1}/(molecules \cdot cm^{-2})$	Line strength at temperature T
x_{CO}	µmol/mol	CO amount of substance fraction

Quant.	**Value**	**Standard uncertainty**	**Rel. uncertainty**	**Degrees of freedom**	**Sens. coefficient**	**Uncertainty contribution / mol/mol**	**Index**
S_0	9.072E-20	$1.81 \cdot 10^{-21}$	2.0 %	50	$-10 \cdot 10^{15}$	$-19 \cdot 10^{-6}$	77.3 %
L	82	0.2	0.25 %	50	$-11 \cdot 10^{-6}$	$-2.3 \cdot 10^{-6}$	1.1 %
k_B	$13.806505 \cdot 10^{-24}$	$24.0 \cdot 10^{-30}$	$1.7 \cdot 10^{-4}$ %	50	$67 \cdot 10^{18}$	$1.6 \cdot 10^{-9}$	0.0 %
T	296.09	0.2	0.07 %	50	$6.2 \cdot 10^{-6}$	$1.2 \cdot 10^{-6}$	0.3 %
P_{total}	326.70	0.2	0.06 %	50	$-2.8 \cdot 10^{-6}$	$-570 \cdot 10^{-9}$	0.1 %
r_{sweep}	$-1.72052 \cdot 10^{-3}$	$12.0 \cdot 10^{-6}$	0.7 %	50	0.54	$1.5 \cdot 10^{-6}$	9.4 %
Λ	31.964	0.213	0.7 %	50	$29 \cdot 10^{-6}$	$6.2 \cdot 10^{-6}$	8.6 %
E	3.845						
c	$29.9792458 \cdot 10^{-9}$						
h	$662.6069306 \cdot 10^{-36}$	$110 \cdot 10^{-42}$	$1.7 \cdot 10^{-5}$ %	50	$-9.2 \cdot 10^{24}$	$-1.1 \cdot 10^{-15}$	0.0 %
T_0	296						
v_0	2139.426100	$231 \cdot 10^{-6}$	$1.1 \cdot 10^{-5}$	infinity	0.0	0.0	0.0 %
x_{12CO}	0.98420	$4.00 \cdot 10^{-3}$	0.4 %	50	$-940 \cdot 10^{-6}$	$-3.8 \cdot 10^{-6}$	3.2 %
$x_{12COHIT}$	0.9842						

r_{iso}	1.00000	$4.06 \cdot 10^{-3}$	0.4 %				
j	1.000			infinity	$280 \cdot 10^{-9}$	$41 \cdot 10^{-9}$	0.0 %
A_{line}	0.054995	$376 \cdot 10^{-6}$	0.7 %				
x_{CO}	925.00	$21.1 \cdot 10^{-6}$		81			

The resulting CO amount fraction based on the uncertainty budget above reads 925 µmol·mol^{-1}. Its expanded uncertainty is ±42 µmol·mol^{-1}, $k = 2$, the relative figure reads 4.6 %. This uncertainty is expressed with a probability of 95 % that the value to be measured is covered by the resulting CO amount fraction result. The relative uncertainties of the input quantities except that of S_0 are less than 1 %. The standard uncertainty of S_0 is the lower limit of the range specified by HITRAN for the P(1) line [46]. The different input quantities reveal quite a large variation with respect to their specific impact (uncertainty contribution) on the resulting uncertainty of the CO amount fraction result. The main uncertainty source is the line strength S_0 reflected by its index of 77.3 %.

6 TDLAS, QCLAS and CRDS

Editorial note

In this chapter, a manuscript is presented that has been published in the Int. J. of Spectrosc. Volume 2011 (2011), doi:10.1155/2011/568913. The coauthorship is being held by J. Nwaboh, T. Desbois, D. Romanini, D. Schiel, and Olav Werhahn. The editorial note in the previous chapter holds for the numbering, the experimental and theoretical sections in this chapter.

Manuscript

The measurements in the last two chapters were carried out using the 0.82 m single pass gas cell shown in Figure 3.1. To improve the signal to noise ratio and to measure lower amount fractions of CO_2 and CO, the 21 m multipass gas cell was used for measurements presented in this manuscript. The measurements in the first and second parts were done using TDLAS and QCLAS, respectively. The last section of the manuscript was devoted to CRDS. With a ringdown time of 20 µs, corresponding to a path length of 6000 m, CO_2 amount fractions were measured to check for the CRD-spectrometer feasibility for absolute CO_2 amount fraction measurements based on the *TILSAM* method.

6.1 Molecular laser spectroscopy as a tool for gas analysis applications

Abstract

We have used the traceable infrared laser spectrometric amount fraction measurement (*TILSAM*) method to perform absolute concentration measurements of molecular species using three laser spectroscopic techniques. We report results performed by tunable diode laser absorption spectroscopy (TDLAS), quantum cascade laser absorption spectroscopy (QCLAS), and cavity ring down spectroscopy (CRDS), all based on the *TILSAM* methodology. The measured results of the different spectroscopic techniques are in agreement with respective gravimetric values, showing that the *TILSAM* method is feasible with all different techniques. We emphasize the data quality objectives given by traceability issues and uncertainty analyses.

6.1.1 Introduction

Throughout the last years many molecular laser spectroscopic techniques have been used to qualify and quantify different physical mechanisms taking place in atoms or molecules [1-7]. Molecular spectroscopy as performed by probing intra and inter molecular vibrational transitions and further underlying rotational sub-structure, has been used to study and

illuminate bond structures and formation of atomic and molecular agglomerates and clusters [8], [9].

These techniques are applied due to the absorption, emission or scattering of electromagnetic radiation by atoms or molecules. The choice of each of these physical phenomena, e.g. absorption, for molecular species quantification or qualification, depends on the intended application. Absorption spectroscopy, for instance, is employed to identify and quantify molecular species in gas analysis applications such as remote sensing, atmospheric monitoring, vehicle exhaust emissions or even exhaled breath gas tests [10-28]

In metrology, molecular absorption spectroscopy could be used to assign amount fractions[7] (concentrations) to species in gas mixtures of known molecular constituents. The determination of the amount fraction of a species without the use of calibrated reference gas mixtures, leads to the so-called "calibration-free" infrared spectrometry. Calibration-free means the amount of substance fraction of a species is measured in terms of the International System of Units (SI) derived unit $mol \cdot mol^{-1}$ without referencing to a standard or a measurement expressed in the same unit [29]. The desire to derive amount fraction results by means of spectroscopy that are directly traceable to the SI, triggered the idea of a traceable infrared laser spectrometric amount fraction measurement (*TILSAM*) method [29], [30].

In order to apply the *TILSAM* method, typically, a sufficiently resolved, spectrally isolated molecular ro-vibrational absorption line is preferable. Regarding the derivation of an amount fraction, the documentary description of *TILSAM* [29] describes the raw data processing, the modeling, the influence quantities, etc. based on tunable diode laser absorption spectroscopy (TDLAS) (see Chapter 4). However, other spectrometric techniques, such as, quantum cascade laser absorption spectroscopy (QCLAS) (see chapter 5), or cavity ring down spectroscopy (CRDS), can also be used to perform absolute amount fraction measurements based on *TILSAM*. The *TILSAM* method can be applied to perform laser spectrometric amount fraction measurements in metrological environments and in field applications [31], [32].

Figure 6.1 visualizes a simpe schematic (also see details in Figure 3.15) of the amount fraction determination due to the *TILSAM* method. Summarized to four steps, there are just the measurement process, the line area derivation, the incorporation of the input quantities, and the computation of the model equation to subsequently achieve a traceable amount fraction result. The uncertainty of the resulting amount fraction has to be reported according to the ISO GUM [33]. However, the determined amount fraction would be traceable if all input quantities were traceable to the SI units, which unfortunately, to the best of our knowledge, has been achieved very rarely. Although not new in its single steps, the *TILSAM* method aims to represent and document a combination of steps necessary to apply IR-spectrometry as an absolute method. There has been other groups and other termini dealing with this idea as discussed in chapter 1. From a metrology point of view, *TILSAM* promotes these ideas on some standardized basis, providing some descriptive framework and being as

[7] Note, for a clarification of different terms in use see e.g.: http://goldbook.iupac.org/A00296.html .

flexible as possible to different experimental implementations. Referring to Figure 6.1 and depending on the spectrometric technique applied, the measurements yield spectral absorbances or absorption coefficients as is the case for TDLAS/QCLAS and CRDS, respectively (see Figure 3.15). Then, line areas are determined either in units of cm^{-1} for TDLAS/QCLAS or cm^{-2} for CRDS by means of direct numerical integration or by means of fitting an appropriate line profile to the measured data. Crucial to *TILSAM* is the subsequent incorporation of the input quantities because, here, traceability of all parameters would be desired to maintain the quality issue of traceability to the final amount fraction result.

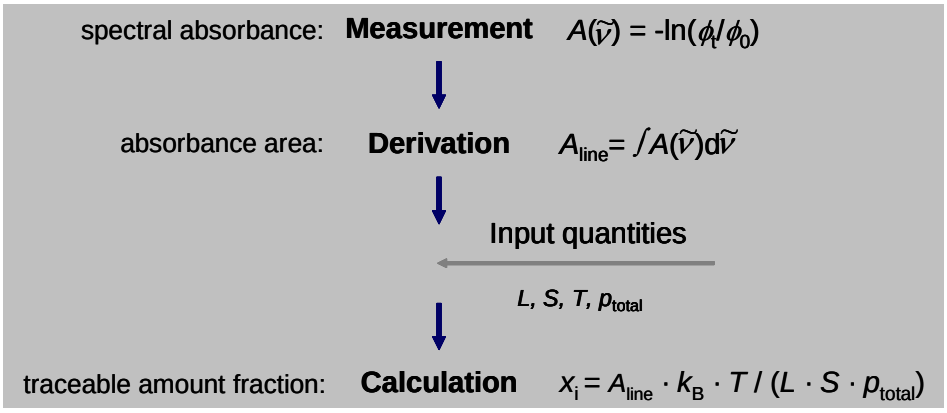

Figure 6.1: Process of the amount fraction determination according to *TILSAM* [21], schematic view for TDLAS/QCLAS.

Among the most indispensable input quantities there is the molecular line strength of the probed transition. Line strength values could be taken from data bases like HITRAN [34] and GEISA [35]. These data bases provide valuable information. Among them, there are some lines with incredibly small reported uncertainties, i.e. “error codes” [34], based on very sophisticated measurements. However, there is a larger number of lines as well, where the uncertainties, e.g. those of *S* are somewhat larger and more imprecise; uncertainty budgets in accordance with the ISO GUM [33] are generally not provided. This last point, also highlighted in the previous chapters, prevents any spectrometrically measured amount fraction based on HITRAN or GEISA from being traceable. As a consequence, a couple of studies have been undertaken to report line strength values and associated GUM compliant uncertainty figures [36], [37]. Recently in the EMRP call 2010 [38], there was a proposal to establish a new reference line data measurement program. The lack of reference data that are more precise than those typically provided by HITRAN and GEISA and which are equipped with quality flags in terms of GUM-compliant uncertainties had also been reported earlier [39]. As reported in [39], for instance, the accurate determination of the uncertainties of the spectrometric data is often suspect or even completely absent, suggesting the need for a precise quantification of the uncertainties associated with the reported spectrometric parameters in [34]. Despite of all above, it should been noted here, that HITRAN, GEISA and other line parameter sources provide absolutely valuable information to any spectroscopist, no matter whether in academic research environments or metrology community. The work

presented here takes advantage of the use of HITRAN's benificials, i.e. from line strength data on CO and CO_2 that are reliable within their specified error ranges.

Nevertheless, absolute amount fraction measurements sometimes meet other specific challenges depending on which spectroscopic technique is used. For instance, in intra-pulse mode QCLAS, an effect reported by [1] known as rapid passage is observed in the measured absorption signals of molecular species at low pressure. Rapid passage occurs when the laser frequency sweep through an absorption line is faster than the collisionally induced relaxation [1]. This results in an asymmetric or even inverted or oscillating absorption signal. Such molecular effects have to be investigated and considered for any absolute amount fraction measurement.

Also the temperature dependence of the line strength has to be considered. By convention in spectroscopy, line strength figures are reported at some conventional temperature as e.g. that of HITRAN as 296 K, S_0. Because of that, for measurements performed at any other temperature T, the line strength has to be transformed to S_T, e.g. applying a certain model that explicitly describes the temperature dependence of S. *TILSAM*, of course, does not require any specific model. However, we need to emphasize the importance of matching the line strength S_0 to the actual temperature T by means of any appropriate model, e.g. as being used in standard analysis.

Additionally there are isotopic abundance issues hidden in the line strength figure that have to be taken into account. Line strength values are typically reported for a certain abundance of the probed isotopologue. However, for a given mixture, generally the abundance of the probed isotopologue may differ from this norm-abundance. Therefore in principle, one would have to correct the line strength figure by substituting $S = S_T \cdot r_{\mathrm{iso}}$ where r_{iso} is the isotopic composition factor, given e.g. as $r_{\mathrm{iso}} = x_{12\mathrm{C16O}} / x_{12\mathrm{C16OHIT}}$, for a probed $^{12}C^{16}O$ excitation, where $x_{12\mathrm{C16O}}$ and $x_{12\mathrm{C16OHIT}}$ are the abundances of $^{12}C^{16}O$ in the sample and the conventional value given by HITRAN, respectively.

There has been a wide range of studies to measure trace species using laser spectroscopic techniques such as TDLAS, QCLAS, and CRDS [16], [26], [40-45]. However, with the most prominent exception of DOAS [46], most of them to the best of our knowledge were not referring to any documented standardized method for the spectroscopic measurements. The method of *TILSAM*, aiming at results that are directly traceable to the SI, and which were recently made online available [29], should be viewed as an attempt to make a first step towards standardization for gas analysis applications by means of laser spectroscopy.

In this paper**,** we focus on the use of the *TILSAM* method to perform absolute concentration measurements of molecular species using different laser spectroscopic techniques. We emphasize data quality objectives expressed by means of traceability and uncertainty issues. In section 2, we report CO_2 amount fraction results performed by TDLAS based on the *TILSAM* method. In section 3, similar results for CO performed with a quantum cascade laser operated in the intra-pulsed mode are reported and section 4 focuses on the application of the *TILSAM* method to CRDS.

6.1.2 Tunable diode laser absorption spectroscopy (TDLAS)

In this section, we report spectrometric CO_2 amount fraction measurements using TDLAS according to the *TILSAM* protocol [29]. The experimental setup is depicted Figure 6.2. The probed transition is the CO_2-R(12) line at 4987.31 cm^{-1} in the near infrared (NIR) combination band around 2 µm.

In absorption spectroscopy, the interaction of the gas species molecules at density n and the sensing radiation at wave number $\tilde{\nu}$ is modeled by the Beer-Lambert law

$$\Phi(\tilde{\nu}, L) = \Phi_0(\tilde{\nu}) \cdot \exp\{-S_T \cdot r_{\mathrm{iso}} \cdot \mathrm{g}(\tilde{\nu} - \tilde{\nu}_0) \cdot L \cdot n\} \tag{6.1}$$

with Φ_0 and Φ being the incident and transmitted radiant powers, respectively, of which the SI unit is W. The absorption is governed by the molecular transition line strength S_T at gas temperature T, that is in principle to be matched to the actual present isotopologue abundance by means of $r_{\mathrm{iso}} = x_{\mathrm{isoexp}} / x_{\mathrm{isoHIT}}$, the respective normalized absorption profile g centered at $\tilde{\nu}_0$, and the absorption path length L. The line strength

$$S_T = S_0 \left(\frac{Q_{T_0}}{Q_T} \right) \exp\left\{ -hc \frac{E}{k_{\mathrm{B}}} \left(\frac{1}{T} - \frac{1}{T_0} \right) \right\} \frac{\left[1 - \exp\left\{ -hc \frac{\tilde{\nu}_0}{k_{\mathrm{B}} T} \right\} \right]}{\left[1 - \exp\left\{ -hc \frac{\tilde{\nu}_0}{k_{\mathrm{B}} T_0} \right\} \right]} \tag{6.2}$$

is specific for the probed molecular transition. S_0 is the line strength at $T_0 = 296$ K, Q_{T_0}, and Q_T are the total internal partition functions of the molecule at temperature T_0 and T, respectively. The quantities, c, h, and k_{B} are the speed of light, the Planck and Boltzmann constants, respectively. E is the ground state energy of the probed transition and v_0 is its center wave number. For this work, we utilized the following expression for the line strength,

$$S_T = S_0 \left(\frac{T_0}{T} \right)^j \cdot \exp\left\{ -hc \frac{E}{k_{\mathrm{B}}} \left(\frac{1}{T} - \frac{1}{T_0} \right) \right\} \frac{\left[1 - \exp\left\{ -hc \frac{\tilde{\nu}_0}{k_{\mathrm{B}} T} \right\} \right]}{\left[1 - \exp\left\{ -hc \frac{\tilde{\nu}_0}{k_{\mathrm{B}} T_0} \right\} \right]}. \tag{6.3}$$

Eq. (3) is an approximation of Eq. (2) with the quantity (Q_{T_0}/Q_T) replaced by $(T_0/T)^j$, where j depends on the molecular structure of the species and the transition being probed.

Relying on the ideal gas law, the molecular density n of the absorbing species can be expressed in terms of its partial pressure p_{partial} of the absorbing molecules and the gas temperature. The partial pressure can be related to the total pressure p_{total} using the amount-of-substance fraction of the absorbing species, $x_{\mathrm{species}} = p_{\mathrm{partial}} / p_{\mathrm{total}}$. Measuring Φ and Φ_0 and

probing a certain molecular transition for a known path length, and measuring p_{total} and T, leads to the amount fraction of the species

$$x_{\text{species}} = -\ln\left(\frac{\Phi(\tilde{\nu})}{\Phi_0(\tilde{\nu})}\right)\frac{k_{\text{B}}\cdot T}{S_T\cdot r_{\text{iso}}\cdot \text{g}(\tilde{\nu}-\tilde{\nu}_0)\cdot L\cdot p_{\text{total}}} \tag{6.4}$$

Introducing the spectral absorbance $A(\tilde{\nu}) = -\ln(\Phi(\tilde{\nu})/\Phi_0(\tilde{\nu}))$, which in cases[8] can also be called extinction, and making use of the normalization of g, Eq. (6.4) may also be written in its integral form

$$x_{\text{species}} = \frac{k_{\text{B}}\cdot T}{S_T\cdot r_{\text{iso}}\cdot L\cdot p_{\text{total}}}\int_{-\infty}^{\infty} A(\tilde{\nu})\,\text{d}\tilde{\nu} = \frac{k_{\text{B}}\cdot T}{S_T\cdot r_{\text{iso}}\cdot L\cdot p_{\text{total}}}\cdot A_{\text{line}} \tag{6.5}$$

where A_{line} is the line area obtained by integration of the measured absorbance data over wave number. Direct absorption spectroscopy is described by the Beer-Lambert law, as expressed in Eq. (6.1). Using Eq. (6.5) to determine the amount fraction in a given gas mixture would deliver results that are SI-traceable if all input quantities were SI-traceable. An uncertainty budget for the measurement according to the ISO Guide to the expression of uncertainty in measurement (GUM) [33] can be evaluated with Eq. (6.5) as the model function.

For the following quantitative determinations the isotopic composition factor r_{iso} was always set to unity. This is due to the lack of a priori information on the actual isotopologue abundance present in the sample. However, this lack of information was to be transferred into to the uncertainty associated with the $r_{\text{iso}} = 1$ [47].

6.1.3 Quantitative amount fraction determination by TDLAS

Figure 6.2 depicts the TDL spectrometer. A distributed feedback (DFB) tunable diode laser (TDL) emitting at 2 µm was used to probe the desired CO_2 transition at 4987.31 cm^{-1}. A triangular-shaped laser current modulation was applied to sweep the diode laser wavelength across the R(12) line. After collimation, the TDL beam was split into a reference beam and a second sample beam transmitted through a 21 m multi-pass absorption cell. The reference beam was used for intensity normalization and for fixing the wavelength axis by means of a removable etalon. Both channels were terminated into extended indium-gallium-arsenide (XInGaAs) photo detectors. An A/D converter (ADLink-DG-9114) was used to digitize the electrical signals at 10 kS/s.

[8] See e.g. http://goldbook.iupac.org/A00028.html .

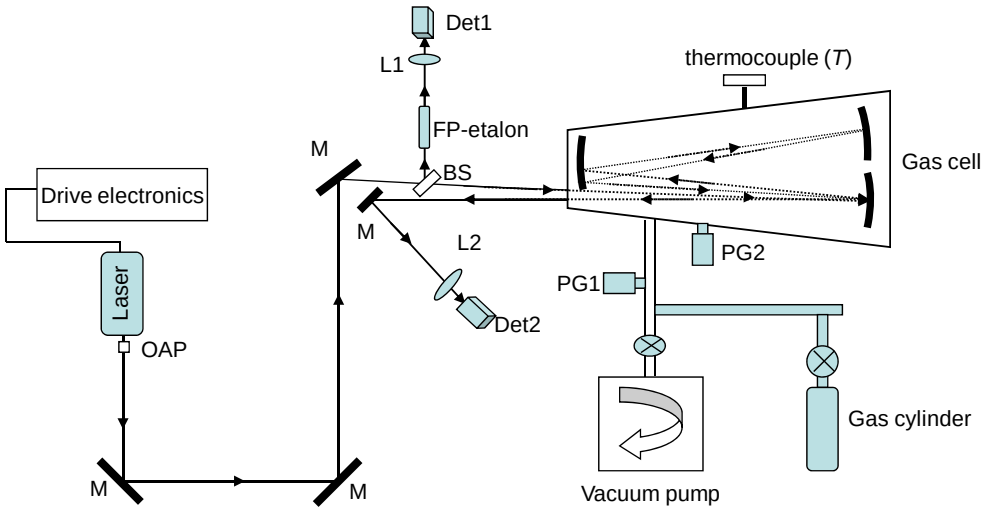

Figure 6.2: Schematic diagram of the setup used for species quantification in a two-channel regime. The multi-pass White-type absorption cell has a path length of L = 21 m. OAP: off-axis parabolic mirror, BS: beam splitter, M: mirror, Det: detector, PG: pressure gauge, L: lens.

A reference gas mixture of carbon dioxide in nitrogen, gravimetrically prepared with a nominal level of 11 mmol·mol^{-1} CO_2 was filled into the gas cell for analysis. Quantitative measurements were performed based on the *TILSAM* method [29] with p_{total} preset in the range of 10 to 43 hPa with the help of a gas sampling system equipped with a turbo molecular vacuum pump.

Figure 6.3a depicts the detector signals, representing a simultaneous two channel measurement scheme. Data has been measured in the time domain in units of sample points (SP). Figure 6.3b shows the signal of detector 1 when a Fabry Perot etalon with a free spectral range (FSR) of about 0.05 cm^{-1} is placed in the beam path. Figure 6.3d depicts the absorbance realized by means of the detector signals from the two channels. The residuals from the fitted R(12) line of CO_2 are shown in

Figure **6.3**e. The wave number axis was accomplished by means of the sweep rate $r_{sweep} = FSR_\nu/FSP_{SP}$. FSR_ν is the free spectral range of the etalon in wave numbers and FSR_{SP} is the experimental fringe separation measured in the time domain (SP) visible in

Figure **6.3**b. The sweep rate evaluated at the absorption peak position was used to realize the wave number axis.

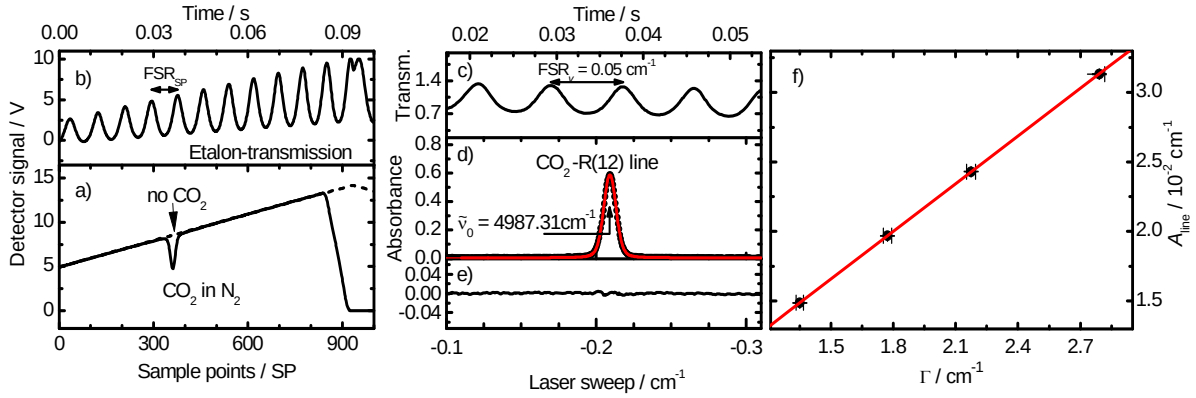

Figure 6.3: a) Data from the reference channel, without CO_2 absorption (dashed line) and the sample channel (full line) featuring CO_2 absorption, respectively. b) Etalon transmission signal seen by detector 1 with the etalon ($FSR_\nu \approx 0.05$ cm^{-1}) placed in the reference beam path. c) and d) Data transferred to the wave number domain. c) Etalon transmittance curve. d) Data of the lower panel of (a), converted to absorbance values (solid dots). A Voigt profile has been fitted to the data (full line) representing the CO_2-R(12) line at 4987.31 cm^{-1}. e) The residuals from the fitted line in (d). f) Generalized linear regression of A_{line} versus Γ.

In Figure 6.3f a plot of the derived line area A_{line} as a function of the experimental parameter $\Gamma = S_T \cdot L \cdot p_{total} / (k_B \cdot T)$ is shown. A variation in Γ is mostly related to a variation of the total gas pressure. From Eq.(4.3) the CO_2 amount fraction (x_{CO2}) can be identified as the slope of a generalized linear regression (GLR) of values of A_{line} as a function of Γ. A GLR is recommended by ISO 6143 [48] for purposes like that to account for uncertainties of both, the y- and the x-axis data. As also mentioned in ISO 6143, we applied the B_LEAST software to perform the GLR. B_LEAST is a software developed by Bundesanstalt für Materialforschung und –prüfung (BAM), that fits model functions, here i.e. a linear function, to experimental data by means of a generalised least square fit. The experimental data to be fitted must contain uncertainties in the x and y-axis. The uncertainties of both axes data are taken into account for the GLR by B_Least. The uncertainty of the line area in Figure 6.3f (vertical bars smaller than symbol size) is due to the uncertainty of the sweep rate r_{sweep} and that of the fitted line area [49]. The uncertainty of Γ is calculated from the uncertainties of the parameters, S_T, L, p_{total}, k_B and T. The line strength used for these measurements was taken from [36] as $1.255 \cdot 10^{-21}$ cm^{-1}/(molecule·cm^{-2}) with an expanded uncertainty of ±1.0 % relative. The CO_2 amount fraction resulting from the data in Figure 6.3f was evaluated to be (11.43±0.23) mmol·mol^{-1}. The uncertainty figure (±2.0 %, relative) is expressed as an expanded uncertainty. The deviation of the spectrometric x_{CO2} result from its gravimetric reference value of (11.38 ±0.16) mmol·mol^{-1} is 0.4 % relative, which is well covered by the uncertainty of 2.0 %.

6.1.4 Quantum cascade laser absorption spectroscopy (QCLAS)

In this section we report results on the spectroscopy of carbon monoxide (CO) by means of pulsed quantum cascade laser spectroscopy. A detailed discussion of our pulsed QCL spectroscopy can be found in [31] (chapter 5). The light source is a quantum cascade laser

(QCL) emitting around 4.6 µm where the fundamental band of CO is located. The experimental setup is the same as shown in Figure 6.2, except that the DFB diode laser discussed in section 6.2 was replaced by the QCL. Compared to the measurements published in [31] (section 5), for the present work, the 21 m multi-pass cell was used. This was to increase the absorption signal and the S/N ratio since lower amount fraction of 100 µmol·mol^{-1} was to be quantified. The probed transition is the CO-P(1) line at 2139.43 cm^{-1}. The two channels in Figure 6.2 were terminated into TE-cooled HgCdZnTe detectors (Vigo PDI-2TE-10.6) and the electrical signals were digitized at 5 GS/s by an 8 bit A/D-converter (Compuscope 85G).

The formalism of quantum cascade laser absorption spectroscopy (QCLAS) based on the Beer-Lambert law is the same as that of TDLAS (chapter 3 and 4). All QCL data shown in the present work were corrected for the detector nonlinearities as pointed out in [31] (also see chapter 5).

For the spectrometric QCL measurements of CO, a gravimetrically prepared multi-component gas mixture of CO, CO_2, and O_2 in N_2 with a nominal value of 100 µmol·mol^{-1} CO was filled into the 21 m gas cell for analysis**.**

Figure 6.4 shows typical data of the QCLAS similar to Figure 6.3. Although QCLAS is not covered by its documentary description the spectrometric measurements were performed according to the *TILSAM* method [29] with the total gas pressure p_{total} in the range of 100 to 300 hPa. Two methods for operating pulsed QCLs are known, the inter-pulse [50], [51] and the intra-pulse mode [52], [53]. A comparison of these two modes is published in [43], [54]. Since few years, also room temperature QCLs in continuous wave (cw) mode of operation have been used to perform laser spectroscopic measurements [55-57] . However, for the present work our QCL was operated in the intra-pulse mode.

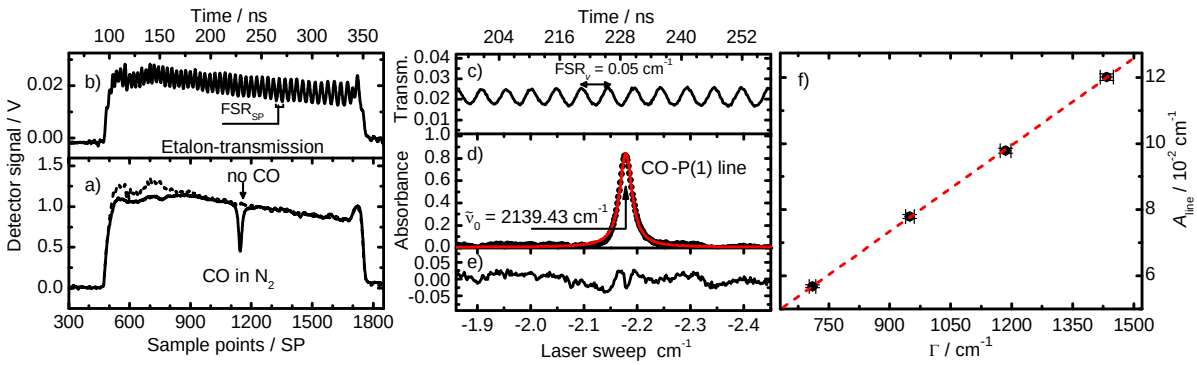

Figure 6.4: Intra-pulse chirp spectroscopy. a) Data from the reference channel, without CO absorption (dashed line) and the sample channel (full line) featuring CO absorption, respectively. b) Etalon transmission signal seen by detector 1 with the etalon (FSR$_\nu$ ≈ 0.05 cm^{-1}) placed in the reference beam path. c) and d) Data transferred to the wave number domain. c) Etalon transmittance curve. d) Data of a), converted to absorbance values. A Voigt profile has been fitted to the data (full line) representing the CO-P(1) line at 2139.43 cm^{-1}. e) The residuals from the fitted line in (d). QCL operating parameters: QCL substrate temperature 295 K, pulse length 255 ns, laser

voltage 10.5 V, repetition rate 2 kHz, QCL chip: Fraunhofer-IAF [9]. f) Generalized linear regression of A_{line} versus Γ.

The wave number axes in Figure 6.4c and d were realized in a similar manner as those in section 6.3. The CO amount fraction retrieved from the generalized linear regression performed by B_LEAST as shown in Figure 6.4f, was evaluated to be 87.3 µmol·mol^{-1}. The estimated uncertainty of this CO amount fraction result reads ±4.6 µmol·mol^{-1} (5.2 % relative). This uncertainty figure is comparably larger than those of the TDLAS result because of the uncertainty contribution originating from the line strength. The line strength of the P(1) line of CO at 2139.4261 cm^{-1} was taken from HITRAN [34]. Its uncertainty is in the 2 to 5 percentage range as specified by HITRAN. For this work we used the lower level of 2 % for the uncertainty evaluation, since the P(1) line is one of the most intense lines in this branch. However, as seen here, there is quite some room to improve the uncertainty figure of the spectrometric CO amount fraction to a significantly lower number, addressing the line strength contribution by first priority. The nominal CO amount fraction of the measured sample is specified as 100 µmol·mol^{-1}. A possible discrepancy between the spectrometrically derived amount faction of (87.3 ± 4.6) µmol·mol^{-1} and that of the nominal value could not be exactly quantified and further evaluated at the time this paper was prepared, because the sample was taken from an ongoing comparison for which exact reference values were not yet available. These QCL results were presented here, to demonstrate the application of the *TILSAM* method to intrapulse QCL spectrometry.

Line strength figures taken from HITRAN are not GUM-compliant, i.e. neither $S_{T=296K}$ nor S_T, as discussed in section 6.1. As a consequence, our spectrometrically measured CO amount fraction result is not yet traceable.

QCLAS faces a couple of challenges performing amount fraction measurements in the mid-infrared. Effects such as rapid passage [1] as introduced in section 6.1 and some possible nonlinearity of detectors are of concern [58]. The latter was accounted for in the presented amount fraction results by applying an appropriate correction [31] (see chapter 5). Rapid passage occurs when the laser frequency sweep through an absorption line is faster than the collisionally induced relaxation, resulting in an asymmetric or even inverted or oscillating absorption signal [1].

Rapid passage imprints can be present in QCLAS signals typically at low pressures [59]. Figure 6.5 displays results of a separate measurement at 5.1 hPa total gas pressure, performed with a gravimetrically prepared gas mixture with a nominal CO amount fraction of 1000 µmol·mol^{-1}, where rapid passage signals were observed. While increasing the pressure to 66.5 hPa, this effect was removed as visible in the inset of Figure 6.5. This is caused by the addition of collision partners to the absorbing medium, thus increasing the relaxation rate of the excited state molecules. Evidently, for any absolute amount fraction measurements, it is necessary to correct for such rapid passage effects or simply to eliminate them.

[9] IAF, Fraunhofer Institut für Angewandte Festkörperforschung, Freiburg, Germany, http://www.iaf.fraunhofer.de.

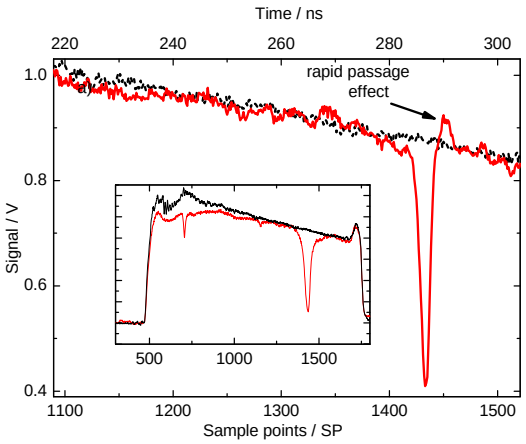

Figure 6.5: Rapid passage (RP) signal observed at 5.1 hPa. Inset: Pressure increased to 66.5 hPa, thus depleting the RP structure, i.e. no RP signal observable anymore.

6.1.5 Cavity ring down spectroscopy (CRDS)

In this section, we report CO_2 amount fraction measurements performed by CRDS referring to the *TILSAM* method. Different implementations of CRDS and related cavity-enhanced spectroscopy (CES) techniques can be found in [60], [61] as well as their underlying theory. A schematic diagram of the experimental setup is shown in Figure 6.6. The laser source is a DFB diode laser operating around 1.6 µm. We probed the CO_2-R(20) transition line at 6242.67 cm^{-1}.

In CRDS the absorption coefficient of a gas sample is measured by monitoring the temporal evolution of the intensity of light trapped inside an optical cavity consisting of highly reflective mirrors. The light is reflected typically thousands of times back and forth by the mirrors. After decoupling the incoming light beam from the cavity, the build-up of light intensity inside the cavity is stopped and the intensity will decay exponentially because of various linear loss mechanisms that are present (transmission of the mirrors, absorption by the gas sample, absorption by the mirrors, diffractive losses, and scattering). The time constant of the intensity decay is called ring-down time, and denoted by the symbol τ. A fast photo-detector monitors the intensity of the escaping light which is proportional to the intensity of light still inside the cavity. The detected signal, therefore, also exhibits an exponential decay function from which the ring-down time is obtained.

Light intensity leaking out of the cavity is given by

$$I(\tilde{\nu}) = I_0 \cdot \exp\left(\frac{-t}{\tau(\tilde{\nu})}\right) \tag{6.6}$$

where I_0 is the intensity of the light inside the cavity right after decoupling the incoming light from the cavity. If one assumes that the cell is filled homogenously with the gas sample over

its entire length, then the ring-down time is given by

$$\tau(\tilde{\nu}) = \frac{L}{c\left[|\ln R_{\text{eff}}(\tilde{\nu})| + k(\tilde{\nu}) \cdot L\right]} \tag{6.7}$$

where, L is the mirror separation and R_{eff} being the effective reflectivity of the mirrors including all other loss mechanisms except that of sample absorption. Note that as $R_{\text{eff}} \approx 1$, the term $|\ln R_{\text{eff}}|$ is frequently replaced by $(1\text{-}R_{\text{eff}})$. The quantity $k = S_T \cdot \mathrm{g} \cdot n$ is called the absorption coefficient. S_T is the line strength at temperature T, g the normalized line profile function and n the molecular density of the absorbing species, that might be expressed as $n = x_{\text{species}} \cdot p / (k_{\text{B}} \cdot \mathrm{T})$ as described in section 6.2. Thus, the ring-down time reads as

$$\tau(\tilde{\nu}) = \frac{L}{c\left[|\ln R_{\text{eff}}(\tilde{\nu})| + S_T \cdot r_{\text{iso}} \cdot \mathrm{g}(\tilde{\nu} - \tilde{\nu}_0) \cdot x_{\text{species}} \cdot \frac{p_{\text{total}}}{k_{\text{B}} \cdot T} \cdot L\right]} \tag{6.8}$$

where, x_{species} is the amount of substance fraction, p_{total} the total gas pressure, k_{B} the Boltzmann constant and T the gas temperature. The decay time obtained by measuring a non-absorbing gas sample or vacuum is called τ_0 and is given by

$$\tau_0(\tilde{\nu}) = \frac{L}{c\left[|\ln R_{\text{eff}}(\tilde{\nu})|\right]} \tag{6.9}$$

The absorption coefficient $k(\nu)$ is derived from the difference in the reciprocals of τ and τ_0,

$$k(\tilde{\nu}) = \frac{1}{c}\left(\frac{1}{\tau(\tilde{\nu})} - \frac{1}{\tau_0(\tilde{\nu})}\right) = S_T \cdot r_{\text{iso}} \cdot \mathrm{g}(\tilde{\nu} - \tilde{\nu}_0) \cdot x_{\text{species}} \cdot \frac{p_{\text{total}}}{k_{\text{B}} \cdot T} \tag{6.10}$$

By integrating both sides of Eqn.(6.10) and rearranging them, the amount fraction of a given species can be calculated as

$$x_{\text{species}} = A_{\text{line}} \cdot \frac{k_{\text{B}} \cdot T}{S_T \cdot r_{\text{iso}} \cdot p_{\text{total}}} \tag{6.11}$$

where, A_{line} is the line area calculated by integrating the absorption coefficient over wave number[10]. Eq. (6.11) is essentially the same expression as (6.5), where instead the path length L is included in the integral absorption coefficient A_{line}, allowing to obtain quantitative absorption measurements without measuring the path length. In CRDS the path length measurement is replaced by a time measurement. CRDS is restricted to the measurement of small absorptions. If absorption becomes much larger than empty cavity losses, virtually no intensity can build up in the cavity and the decay time will be correspondingly shorter. This

[10] Note: in CRDS A_{line} is given in units of cm^{-2} as compared to that of TDLAS and QCLAS given in units of cm^{-1}.

would lead to an unreliable determination of the τ as the decay trace consists then of a very limited amount of data points (determined by the sampling rate of the data acquisition system).

6.1.6 Quantitative CO_2 amount fraction detection by OF-CRDS

Details of the experimental setup of the optical feedback cavity-enhanced spectroscopy (OF-CES) shown in Figure 6.6 and the theoretical background can be found in [62]. The spectrometer is capable of performing optical feedback absorption spectroscopy (OF-CEAS) and optical feedback cavity ring-down spectroscopy (OF-CRDS). Here, we focus on OF-CRDS or simply cavity ring down as discussed in the previous subsection. Details on how to further benefit from the optical feedback performance and on the use of the different piezo-actuated mirrors displayed are a central focus of future work.

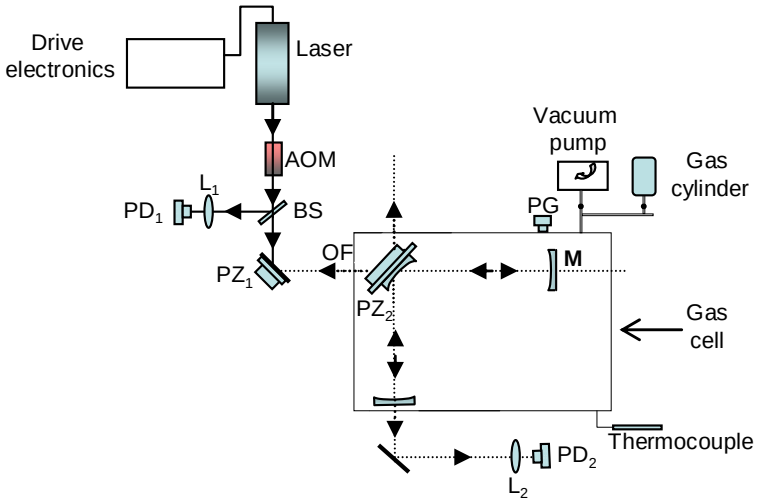

Figure 6.6: Schematic diagram of the experimental OF-CRDS setup. AOM: acousto optical modulator, PZ: piezo controlled mirrors, OF: optical feedback, PD: photodiode, M: mirror, PG: pressure gauge, BS: beam splitter, L: lens.

For quantitative detection of CO_2, the cavity was filled with a gravimetrically prepared gas mixture with a nominal value of 389 μmol·mol^{-1}. Carbon dioxide amount fractions were measured referring to the *TILSAM* method to demonstrate the feasibility of applying this method also to CRDS.

Figure 6.7a depicts typical raw data, each peak representing the built-up light intensity in a certain cavity mode. In Figure 6.7b, the absorption coefficient, derived from the measured ring-down times, is plotted as a function of wave number. The residuals from the fitted CO_2-R(20) line are depicted in Figure 6.7c. The wave number axis has been established by means of the known cavity FSR of 152 MHz between adjacent cavity modes displayed in part a) of Figure 6.7. From Eq. (6.11), the CO_2 amount fraction can be identified as the slope of a linear

regression of A_{line} (units: cm^{-2}) versus the experimental parameter $\Omega = S_T \cdot p_{total} / (k_B \cdot T)$ which is typically given in units of cm^{-2}. A variation in Ω is mostly related to a variation of the total gas pressure.

Figure 6.7d depicts the generalized linear regression (GLR) of the derived line area values versus Ω. The uncertainty of the line area is obtained from the line area fitting [49] and that of Ω is calculated from the uncertainties of the input parameters S_T, p_{total}, k_B, and T. The line strength of the probed R(20) line of CO_2 was taken from HITRAN. Its uncertainty is specified as being 2 to 5 %, relative.

The CO_2 amount fraction resulting from the generalized linear regression, performed by B_LEAST, was evaluated to be 384 $\mu mol \cdot mol^{-1}$ with an uncertainty of ±16 $\mu mol \cdot mol^{-1}$. The relative deviation of this spectrometric CO_2 amount fraction from its nominal value of 390 $\mu mol \cdot mol^{-1}$ was found to be -1.5 %, which is well covered by the uncertainty of ±16 $\mu mol \cdot mol^{-1}$ (±4.2 % relative) of the spectroscopic value. Being optimistic, the lower limit of 2 % of the line strength uncertainty was taken for this uncertainty analysis knowing that the amount fraction uncertainty were to be increased once the higher limit had to be used.

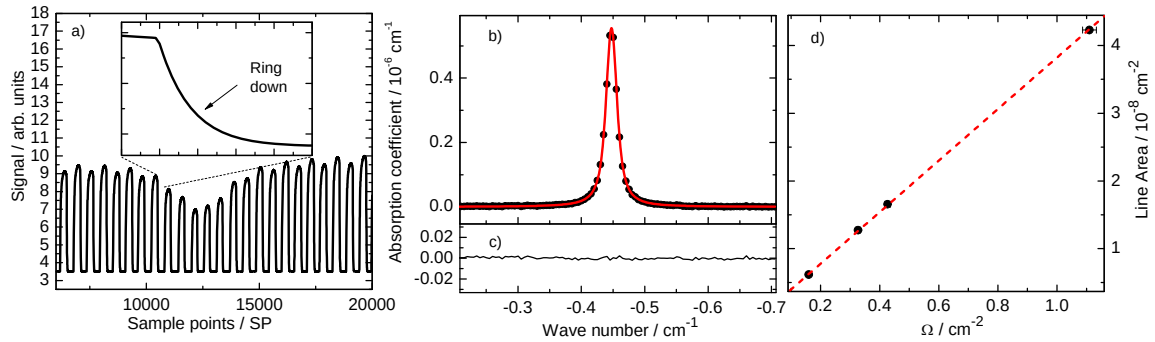

Figure 6.7: CRDS-based data retrieval: a) Typical signals from the OF-CES setup. Insert: A zoom in of a cavity mode depicting the ring down b) Derived absorption coefficients fitted by a Voigt profile (full line) representing the CO_2-R(20) line at 6242.6722 cm^{-1}. c) Residuals from the fitted line in (b). c) Linear regression of the determined line areas A_{line} versus the experimental parameter Ω.

6.1.7 Discussions

The resulting amount fractions derived by the different spectroscopic techniques are in good agreement with the respective reference values. The uncertainty evaluation is based on the method described by the ISO GUM [33].

The expanded uncertainties of the CO_2 amount fraction measured with TDLAS, and CRDS were found to be ±2.0 %, and 4.2 %, respectively, whereas the QCLAS uncertainty analysis delivered ±5.2 % for the CO quantification. The uncertainty figures of the QCLAS and CRDS quantification are comparably larger than that of the TDLAS result. This is because the

uncertainties of the line strength values used to evaluate the QCLAS and CRDS amount fraction results, were in the range 2 to 5 % relative, as specified by HITRAN. The *S* value and its relative expanded uncertainty of 1.0 %, used to evaluate the CO_2 amount fraction TDLAS result were taken from [36]. The standard uncertainties of the other input parameters, i.e. p_{total}, k_B, *T* and *L* were all in the sub percentage range. Comparing the 5.2 % uncertainty of the CO amount fraction, for instance, to the 7.5 %, requested by the data quality objectives set in EU directive 2000/69/EC [63] for CO field measurements, our presented results based on *TILSAM* would already be within this scope, although not yet validated for field measurements. However, one has to note that, if the line strength uncertainties used to derive QCLAS and CRDS amount fraction results presented in this paper were taken instead as the upper limit of 5 %, then the relative uncertainty of the spectrometric amount of substance fraction would have to be scaled accordingly larger. Since they are in accordance, our present results, however, does support the 2 % level.

A linear model developed from Eqn. (6.5) and (6.11) was used to evaluate the amount fractions of CO and CO_2 presented in this paper. The model does not predict any intercept. Therefore, as recommended in [29], the GLR were performed with a free intercept parameter. The resulting intercept parameters from the GLR is an additional measure of the quality of the measurements. The intercept parameter is either insignificant as predicted by the model or not. If the resulting intercept were significant, i.e. its uncertainty is smaller than its numerical value, the model does not describe the experimental conditions appropriately. Hence, the quality of the spectrometric amount fraction results presented here were judged by looking at the intercept parameters resulting from the respective generalized linear regressions. The intercept parameters of the TDLAS CO_2 amount fraction results calculated from the GLR was $(-5.8 \pm 5.8)\cdot10^{-4}$ cm^{-1} and that of the CRDS CO_2 amount fraction $(6.6 \pm 22.2)\cdot10^{-11}$ cm^{-2}, being both insignificant. A final answer could not be given at this stage for the instead significant intercept parameter of the QCLAS CO amount fraction of $(-5.2 \pm 2.6)\cdot10^{-3}$ cm^{-1}, since the measurements performed on a sample from an ongoing comparison between different institutes, for which exact reference values are not yet known. With this result there might be a further issue resulting from a “w” structure in the residuals in Figure 6.4e. This typical residual structure indicates that collisional narrowing effects the data which cannot be modeled appropriately by a Voigt-profile [64]. From the oscillatory nature of the residual “w” structure it can be expected that the line area is less affected [64]. However, this proofs already, that by means of the *TILSAM* recommended data retrieval strategy, some data quality flags are provided which indicates some hidden problems with a used setup, as it is apparently now the case with our 21-m-path length QCL setup.

All the measurements presented in this paper are based on the *TILSAM* method as discussed earlier. The online-available *TILSAM* documentary description [29] details the spectrometric measurement process, the raw data processing and the uncertainty assessment principles. Although, the *TILSAM* protocol in its present form considers only TDLAS, other techniques such as QCLAS and CRDS could be addressed by this documentary framework in a future edition as shown in this work, chapters 5 and 6 (also see Figure 3.15**).** The *TILSAM* method

has the potential of being used in the next generation of spectrometric reference methods in gas metrology. The method could also benefit other interesting fields of application, e.g. breath gas analysis, as is aimed at in an iMERA-plus project [65], or industrial process control [66]. The *TILSAM* method could also be used to trigger the development of similar documentary method descriptions for the measurement of molecular reference line data, such as e.g. those of line strengths, broadening coefficients and temperature dependencies, or those of molecular constants such as spin coupling constants, ground state energy, and rotational g factors. Or simply to support the development of process analyzers.

In contrary to measurements often performed by calibrated spectrometric systems, where the aim might be to eliminate systematic errors and study the Allan variance to provide the rms noise and the drift as a function of measurement time, our measurements performed using the *TILSAM* method are based on first principle measurements rather than relying on a comparison, since calibrated systems faces the challenges of recalibration especially when the analyte is changed. Therefore, the use of "absolute" methods for amount fraction measurements, such as the *TILSAM* method, could be more cost effective than calibrated methods. Further on, calibration requires the application of reference gas mixtures. Those have to be taken aboard the spectrometric instrument by means of suitable gas containers which is not always possible due to weight and size constraints premised by some applications.

However, for the time being the *TILSAM* method suffers from the unavailability of traceable line strength values and from comparably large associated uncertainties. Therefore, the line strength S_T is the limiting factor. Traceable line strength figures are rather rare throughout literature [39]. Nevertheless, in addition also other quantities like the optical path length L could often provide challenges if traceability is requested, e.g. if multi-pass absorptions cells were to be considered.

Regarding the line strength, currently, there are a few efforts being undertaken to improve the lack of traceable reference line data [36], [37], [65-67]. If line strength uncertainties used in this work were in the sub percentage range, then the relative uncertainty of the spectrometric amount of substance fraction would be rigorously smaller. Consequently, the applicability would be increased and the method more competitive to existing non-spectrometric techniques. In turn, with respect to the CO measurements reported above, there is still some way to go before the uncertainty figure assigned to the CO amount fraction would match, e.g., that of the data quality objective established by the WMO to be 0.5 % relative for the GAW programme [68]. Thus, with an uncertainty of the amount fraction result less than one percent, the spectrometric measurements based on *TILSAM* presented in this paper could be applicable to environmental measurements as well as to other interesting gas analysis applications.

6.1.8 Conclusions

We have demonstrated the feasibility of the *TILSAM* method using TDLAS, QCLAS and CRDS to perform absolute amount of substance fraction measurements. The spectrometric amount fraction results agree with their respective gravimetric reference values where available. The uncertainties of CO and CO_2 amount fractions evaluated by TDLAS, QCLAS and CRDS are ±2.0 %, ±5.2 %, and ±4.2 %, respectively. We project that, with a reduced uncertainty of the line strength value, absolute spectrometric measurements based on *TILSAM* could be applied to multiple gas analysis applications.

6.1.9 Acknowledgements

Parts of this work were financially supported by ERA-NET Plus, under the iMERA-plus Project - Grant Agreement No. 217257, by the international graduate school of metrology (IGSM), TU Braunschweig, and by the BMBF projects MEX07/004, and QUANSYS/QUANKAS, FKZ 13N8123. The authors acknowledge the continuous collaboration of Prof. Dr. Karl-Heinz Gericke (TU Braunschweig), Hans-Joachim Heine (BAM), and Jorge Koelliker Delgado (CENAM). Parts of this work were performed under the scientific collaboration agreement between PTB and LSP/Floralis (Université Joseph Fourier).

6.1.10 References

[1] G. Duxbury, N. Langford, M. McCulloch, and S. Wright, “Rapid passage induced population transfer and coherences in the 8 micron spectrum of nitrous oxide,” *Molecular Physics*, vol. 105, no. 5-7, pp. 741-754, 2007.

[2] W. Demtröder, *Laser spectroscopy - basic principles*, vol. 1. Berlin: Springer, 2008.

[3] K. McCann, M. Wagner, A. Guerra, P. Coronado, J. R. Villarreal, J. Choo, S. Kim, and J. Laane, “Spectroscopic investigations and potential energy surfaces of the ground and excited states of 1,3-benzodioxan,” *Journal of Chemical Physics*, vol. 131, pp. 044302, 2009.

[4] V. A. Kapitanov, A. M. Solodov, T. M. Petrova, and Y. N. Ponomarev, “Fourier Transform and Photoacoustic Absorption Spectra of Ethylene within 6035-6210 cm^{-1}: Comparative Measurements,” *International Journal of Spectroscopy*, 2010, doi: 10.1155/2010/203672.

[5] K. L. Plath, K. Takahashi, R. T. Skodje, and V. Vaida, “Fundamental and Overtone Vibrational Spectra of Gas-Phase Pyruvic Acid,” *The Journal of Physical Chemistry A*, vol. 113, pp. 7294-7303, 2009.

[6] M. Gharavi and S. Buckley, "Diode laser absorption spectroscopy measurement of linestrengths and pressure broadening coefficients of the methane $2\nu_3$ band at elevated temperatures," *Journal of Molecular Spectroscopy*, vol. 229, no. 1, pp. 78-88, 2005.

[7] X. Li, K. L. C. Hunt, F. Wang, M. Abel, and L. Frommhold, "Collision-Induced Infrared Absorption by Molecular Hydrogen Pairs at Thousands of Kelvin," *International Journal of Spectroscopy*, 2010, doi: 10.1155/2010/371201.

[8] F. Huisken, M. Kaloudis, M. Koch, and O. Werhahn, "Experimental study of the O-H ring vibration of the methanol trimer," *Journal of Chemical Physics*, vol. 105, pp. 8965-8968, 1996.

[9] F. Huisken, A. Ivanov, S. Krasnokutski, and O. Werhahn, "The O-H stretching vibrations of glycine trapped in rare gas matrice and helium clusters," *Journal of Chemical Physics*, vol. 111, pp. 2978-2984, 1999.

[10] J. Manne, O. Sukhorukov, W. Jäger, and J. Tulip, "Pulsed quantum cascade laser-based cavity ring-down spectroscopy for ammonia detection in breath," *Applied Optics*, vol. 45, no. 36, pp. 9230-9237, 2006.

[11] I. Ventrillard-Courtillot, T. Gonthiez, C. Clerici, and D. Romanini, "Multispecies breath analysis faster than a single respiratory cycle by optical-feedback cavity-enhanced absorption spectroscopy," *Journal of Biomedical Optics*, vol. 14, no. 6, pp. 064026, 2009.

[12] M. L. Silva, D. M. Sonnenfroh, D. I. Rosen, M. G. Allen, and A. O'Keefe, "Integrated cavity output spectroscopy measurements of nitric oxide levels in breath with a pulsed room-temperature quantum cascade laser," *Applied Physics B*, vol. 81, no. 5, pp. 705-710, 2005.

[13] G. Wysocki, A. A. Kosterev, and F. K. Tittel, "Spectroscopic trace-gas sensor with rapidly scanned wavelengths of a pulsed quantum cascade laser for in situ NO monitoring of industrial exhaust systems," *Applied Physics B*, vol. 80, pp. 617-625, 2005.

[14] G. Maisons, P. Gorrotxategi Carbajo, M. Carras, and D. Romanini, "Optical-feedback cavity-enhanced absorption spectroscopy with a quantum cascade laser," *Optics Letters*, vol. 35, no. 21, pp. 3607-3609, 2010.

[15] B. W. M. Moeskops, H. Naus, S. M. Cristescu, and F. J. M. Harren, "Quantum cascade laser-based carbon monoxide detection on a second time scale from human breath," *Applied Physics B*, vol. 82, pp. 649-654, 2006.

[16] G. Wysocki, M. McCurdy, S. So, D. Weidmann, C. Roller, R. Curl, and F. K. Tittel, "Pulsed quantum-cascade laser-based sensor for trace-gas detection of carbonyl sulfide," *Applied Optics*, vol. 43, pp. 6040-6046, 2004.

[17] S. Kassi, M. Chenevier, L. Gianfrani, A. Salhi, Y. Rouillard, A. Ouvrard, and D. Romanini, "Looking into the volcano with a Mid-IR DFB diode laser and Cavity Enhanced Absorption Spectroscopy," *Optics Express*, vol. 14, no. 23, pp. 11442, 2006.

[18] K. Wunderle, S. Wagner, I. Pasti, R. Pieruschka, U. Rascher, U. Schurr, and V. Ebert, "Distributed feedback diode laser spectrometer at 2.7 μm for sensitive, spatially resolved H2O vapor detection," *Applied Optics*, vol. 48, pp. B172-B182, 2009.

[19] M. R. McCurdy, Y. Bakhirkin, G. Wysocki, and F. K. Tittel, "Performance of an exhaled nitric oxide and carbon dioxide sensor using quantum cascade laser-based integrated cavity output spectroscopy," *Journal of Biomedical Optics*, vol. 12, pp. 034034-1, 2007.

[20] R. Q. Iannone, S. Kassi, H.-J. Jost, M. Chenevier, D. Romanini, H.A.J. Meijer, S. Dhaniyala, M. Snels, and E.R.T. Kerstel, "Development and airborne operation of a compact water isotope ratio infrared spectrometer," *Isotopes in Environmental and Health Studies*, vol. 45, pp. 303-320, 2009.

[21] V. Weldon, J. O'Gorman, P. Phelan, J. Hegarty, and T. Tanbun-Ek, "H_2S and CO_2 gas sensing using DFB laser diodes emitting at 1.57 μm," *Sensors and Actuator B*, vol. 29, pp. 101-107, 1995.

[22] M. Sowa, M. Mürtz and P. Hering, "Mid-infrared laser spectroscopy for online analysis of exhaled CO," *Journal of Breath Research*, vol. 4, pp. 047101, 2010.

[23] C. E. Miller, L. R. Brown, R. A. Toth, D. C. Benner, V. Malathy Devi, "Spectroscopic challenges for high accuracy retrievals of atmospheric CO_2 and the Orbiting Carbon Observatory (OCO) experiment," *Comptes Rendus Physique*, vol. 6, pp. 876-887, 2005.

[24] D. Crisp et al, "The Orbiting Carbon Observatory (OCO) Mission," *Advances in Space Research*, vol. 34, pp. 700-709, 2004.

[25] R. A. Toth, C. E. Miller, L. R. Brown, V. Malathy Devi, D. Chris Benner, "Line strengths of $^{16}O^{13}C^{16}O$, $^{16}O^{13}C^{18}O$, $^{16}O^{13}C^{17}O$ and $^{18}O^{13}C^{18}O$ between 2200 and 6820 cm^{-1}," *Journal of Molecular Spectroscopy*, vol. 251, pp. 64-89, 2008.

[26] E. R. Crosson et al., "Stable Isotope Ratios Using Cavity Ring-Down Spectroscopy: Determination of $^{13}C/^{12}C$ for Carbon Dioxide in Human Breath," *Analytical Chemistry,* Vol. 74, pp. 2003-2007, 2002.

[27] K. Heinrich, T. Fritsch, P. Hering, M. Mürtz, "Infrared laser-spectroscopic analysis of ^{14}NO and ^{15}NO in human breath," *Applied Physics B*, vol. 95, no. 2, pp. 281-286, 2009.

[28] A. Predoi-Cross, C. Hnatovsky, K. Strong, J. R. Drummond, D. Chris Benner**,** "Temperature dependence of self- and N_2-broadening and pressure-induced shifts in the 3←0 band of CO," *Journal of Molecular Structure*, vol. 695-696, pp. 269-286, 2004.

[29] O. Werhahn and J.C. Petersen (eds.), "TILSAM-protocol-V1_2010-09-29," 2010. Available from: http://www.euramet.org/fileadmin/docs/projects/934_METCHEM_Interim_Report.pdf.

[30] EUROMET-934, "TILSAM - Traceable Infrared Laser Spectrometric Amount fraction Measurement," 2008. Available from: http://www.euramet.org, project no. 934.

[31] J. A. Nwaboh, O. Werhahn, and D. Schiel, "Measurement of CO amount fractions using a pulsed quantum-cascade laser operated in the intrapulse mode," *Applied Physics B*, 2010, doi: 10.1007/s00340-010-4322-1.

[32] P. Ortwein, W. Woiwode, S. Fleck, M. Eberhard, T. Kolb, S. Wagner, M. Gisi, and V. Ebert, “Absolute diode laser-based in situ detection of HCl in gasification processes,” *Experiments on Fluids*, online first version, 2010, doi: 10.1007/s00348-010-0904-2.

[33] Joint Committee for Guides in Metrology (JCGM), "Evaluation of measurement data - Guide to the expression of uncertainty in measurement, GUM 1995 with minor corrections, ISO IEC Guide 98-3," *JCGM 100:2008,* 2008. Available from: http://www.bipm.org/en/publications/guides/gum.html.

[34] "HITRAN2008", 2009, L.S. Rothman et al., *Journal of Qauntitative Spectroscopy and Radiative Transfer*, vol. 110, pp. 533-572, 2009. Available from: http://www.cfa.harvard.edu/HITRAN/.

[35] N. Jacquinet-Husson et al., "The GEISA spectroscopic database: Current and future archive for Earth and planetary atmosphere studies," *Journal of Quantitative Spectroscopy and Radiative Transfer*, 2008, doi: 10.1016/j.jqsrt.2007.12.015.

[36] G. Padilla Viquez, J. Koelliker Delgado, O. Werhahn, K. Jousten, and D. Schiel, "Traceable CO_2-R(12) Line Intensity for Laser- Spectroscopy-based Gas Analysis near 2 µm," *IEEE Transactions on Instrumentation and Measurement,* vol. 56, no. 2, pp. 529-533, 2007**.**

[37] G. Casa, D. A. Parretta, A. Castrillo, R. Wehr, and L. Gianfrani, “Highly accurate determinations of CO_2 line strengths using intensity-stabilized diode laser absorption spectrometry,” *Journal of Chemical Physics*, vol. 127, pp. 084311, 2007.

[38] "EMRP Call 2010 Industry and Environment," 2010. Available from: http://www.emrponline.eu/call2010/srte.html

[39] L. S. Rothman, N. Jacquinet-Husson, C. Boulet, and A. M. Perrin, “History and future of the molecular spectroscopic databases,” *Comptes Rendus Physique*, vol. 6, pp. 897-907, 2005.

[40] C. Wang and P. Sahay, “Brearth Analysis Using Laser Spectroscopic Techniques: Breath Biomarkers, Spectral Fingerprints, and Detection Limits,” *Sensors*, vol. 9, pp. 8230-8262, 2009.

[41] S. Welzel, G. Lombardi, P. B. Davies, R. Engeln, D. C. Schram, and J. Röpcke, “Trace gas measurements using optically resonant cavities and quantum cascade lasers operating at room temperature,” *Journal of Applied Physics*, vol. 104, pp. 093115, 2008.

[42] T. Fritsch, P. Hering, and M. Mürtz, “Infrared laser spectroscopy for online recording of exhaled carbon monoxide - a progress report,” *Journal of Breath Research*, vol. 1, no. 1, pp. 014002, 2007.

[43] J. Manne, W. Jäger, and J. Tulip, “Sensitive detection of ammonia and ethylene with a pulsed quantum cascade laser using intra and interpulse spectroscopic techniques,” *Applied Physics B*, vol. 94, pp. 337-344, 2009.

[44] S. Crunaire, J. Tarmoul, C. Fittschen, B. Lemoine, and P. Coddeville, “Use of cw-CRDS for studying the atmospheric oxidation of acetic acid in a simulation chamber,” *Applied Physics B*, vol. 85, pp. 467-476, 2006.

[45] A. Foltynowicz, W. Ma, and O. Axner, "Characterization of fiber-laser-basedsub-Doppler NICE-OHMS for quantitative trace gas detection," *Optics Express*, vol. 16, no. 19, pp. 14689 - 14702, 2008.

[46] V. Rozanov and A. Rozanov, "Differential optical absorption spectroscopy (DOAS) and air mass factor concept for a multiply scattering vertically inhomogeneous medium: theoretical consideration," *Atmospheric Measurement Techniques*, vol. 3, 2010, pp. 751-780. DOAS tutorial vailable from: http://www.doas-bremen.de/doas_tutorial.htm.

[47] M. Berglund and Michael E. Wieser, "Isotopic compositions of elements 2009 (IUPAC Technical report)," *Pure Applied Chemistry*, vol. 83, no. 2, pp. 397-410, 2011.

[48] ISO 6143: 2001, "Gas analysis - Comparison methods for determining and checking the composition of calibration gas mixtures," *International Organization for Standardization*, Geneva, 2001.

[49] Origin 7.5 SR6, OriginLab Cooperation, Northampton, MA, USA, 2006. Available from: http://www.OriginLab.com.

[50] K. Namjou, S. Cai, and E. A. Whittaker, "Sensitive absorption spectroscopy with a room-temperature distributed-feedback quantum-cascade laser," *Optics Letters*, vol. 23, no. 3, pp. 219, 1998.

[51] D. D. Nelson, J. H. Shorter, J. B. Mcmanus, and M. S. Zahniser, "Sub-part-per-billion detection of nitric oxide in air using a thermoelectrically cooled mid-infrared quantum cascade laser spectrometer," *Applied Physics B*, vol. 75, pp. 343-350, 2002.

[52] E. Normand, M. McCulloch, G. Duxbury, and N. Langford, "Fast, real-time spectrometer based on a pulsed quantum-cascade laser," *Optics Letters*, vol. 28, no. 1, pp. 16-18, 2003.

[53] M. T. McCulloch, E. L. Normand, N. Langford, and G. Duxbury, "Highly sensitive detection of trace gases using the time-resolved frequency downchirp from pulsed quantum-cascade lasers," *Journal of the Optical Society of America B*, vol. 20, no. 8, pp. 1761-1768, 2003.

[54] B. Grouiez, B. Parvitte, L. Joly, D. Courtois, and V. Zeninari, "Comparison of a quantum cascade laser used in both cw and pulsed modes. Applications to the study of SO_2 lines around 9 μm," *Applied Physics B*, vol. 90, pp. 177-186, 2008.

[55] J. Wagner, C. Mann, M. Rattunde, and G. Weimann, "Infrared semiconductor lasers for sensing and diagnostics," *Applied Physics A*, vol. 78, pp. 505-512, 2004.

[56] A. Evans, J. S. Yu, S. Slivken, and M. Razeghi, "Continuous-wave operation of $\lambda \sim 4.8$ μm quantum-cascade lasers at room temperature," *Applied Physics Letters*, vol. 85, no. 12, pp. 2166-2168, 2004.

[57] T. Aellen, S. Blaser, M. Beck, D. Hofstetter, J. Faist, and E. Gini, "Continuous-wave distributed-feedback quantum-cascade lasers on a Peltier cooler," *Applied Physics Letters*, vol. 83, no. 10, pp. 1929-1931, 2003.

[58] E. Theocharous, J. Ishii, and N. P. Fox, "Absolute linearity measurements on HgCdTe detectors in the infrared region," *Applied Optics*, vol. 43, no. 21, pp. 4182-4188, 2004.

[59] S. Welzel, “New enhanced sensitivity infrared laser spectroscopy techniques applied to reactive plasmas and trace gas detection,” Dissertation, Ernst-Moritz-Arndt Universität Greifswald, 2009.

[60] G. Biel and R. Engeln, "Cavity ring-down spectroscopy: techniques and applications," Wiley, Chichester, 2009.

[61] R.D. v. Zee, "Cavity-enhanced spectroscopies," *Experimental methods in the physical sciences*. vol. 40, Academic Press, Amsterdam, 2002.

[62] J. Morville, S. Kassi, M. Chenevier, and D. Romanini, “Fast, low-noise, mode-by-mode, cavity-enhanced absorption spectroscopy by diode-laser self-locking,” *Applied Physics B*, vol. 80, pp. 1027-1038, 2005.

[63] Directive 2000/69/EC of the European Parliament and of the Council of 16 November 2000 relating to limit values for benzene and carbon monoxide in ambient air. 2000. Available from: http://eur-lex.europa.eu/LexUriServ/LexUriServ.do?uri=OJ:L:2000:313:0012:0021:EN:PDF.

[64] J. Henningsen and H. Simonsen, “The ($22^{0}1$-$00^{0}0$) band of CO_2 at 6348 cm^{-1}: linestrengths, broadening parameters, and pressure shifts,” *Journal of Molecular Spectroscopy*, vol. 203, pp. 16-27, 2000.

[65] "Breath analysis as a diagnostic tool for early disease detection," *Joint Research Projects funded under iMERA-plus, T2.J02,* 2010. Available from: http://www.euramet.org/index.php?id=1011.

[66] P. Ortwein, W. Woiwode, S. Wagner, M. Gisi, and V. Ebert, “Laser-based measurements of line strength, self and pressure-broadening coefficients of the $H^{35}Cl$ R(3) absorption line in the first overtone region for pressures up to 1 MPa,” *Applied Physics B*, vol. 100, pp. 341-347, 2010.

[67] D. Lisak, D. K. Havey, and J. T. Hodges, “Spectroscopic line parameters of water vapor for rotation-vibration transitions near 7180 cm^{-1},” *Physical Review A*, vol. 79, 052507, 2009.

[68] T. Laurila (ed.), "14th WMO/IAEA Meeting of Experts on Carbon Dioxide, other Greenhouse Gases and Related Tracer Measurement Techniques," GAW Report No. 186, 2009, World Meteorological Organization (WMO), Geneva. Available from: http://www.wmo.int/pages/prog/arep/gaw/gaw-reports.html.

7 CO quantification as aimed at in breath measurements

Editorial note

A manuscript submitted for publication in the Int. J. Spectrosc. (submission: 894841) is presented in this chapter. The coauthorship is being held by J. Nwaboh, S. Persijn, K. Heinrich, M. Sowa, P. Hering, O. Werhahn. Also, similar to the previous manuscripts, the numbering of the manuscript was changed from the original version to match that of this thesis.

Manuscript

This manuscript is focused on CO amount fraction quantifications aiming at breath measurements. The measurements presented have been carried out in three institutes. The measurements in sections 7.1.4 and 7.1.5 have been performed at VSL- Dutch Metrology Institute (Netherlands) and the Institut für Lasermedizin (ILM), Düsseldorf (Germany). All spectrometric CO amount fraction measurements have been performed based on the *TILSAM* method.

7.1 QCLAS and CRDS-based CO quantification as aimed at in breath

Abstract

Carbon monoxide (CO) in exhaled human breath is a biomarker for anaemias, oxidative stress and respiratory infections. Laser-spectrometric methods to derive absolute and traceable CO amount fractions in breath could be of advantage for early disease detection as well as for treatment monitoring. As proof-of-principle laboratory experiments, we employed direct absorption and cavity ring-down spectroscopy (CRDS) to measure the CO amount fraction in gravimetrically prepared gas mixtures. For these experiments intra-pulse and continuous wave (cw) quantum cascade laser absorption spectroscopy (QCLAS) spectrometers have been used, both operating at 4.6 µm. Additional experiments were carried out by means of cw CRDS performed in setups operated by a CO sideband laser and a QCL. Contrary to the QCLs the cw CO sideband laser was probing the P(25) line of the $^{13}C^{16}O$ isotopologue. The measurements were carried out in the framework of a joint research project titled “Breath analysis as a tool for early disease detection”. In this work, we emphasize metrological data quality objectives, i.e. traceability and uncertainty, which could serve as essential benefits to exhaled breath measurements. The spectrometric CO amount fraction results were evaluated and compared on a 100 µmol/mol CO level using the two QCLAS spectrometers, and the cw CO sideband laser CRDS setup. They agree with the respective nominal reference values. The

relative standard uncertainties of the pulsed and the cw QCLAS CO amount fraction results are ±4.8 and ±2.8 %, respectively, that from the CO sideband laser CRDS was ±2.7 %**.** Much higher sensitivities down to a 3 nmol/mol CO level were finally demonstrated and quantified by means of cw CRDS equipped with a QCL probing the R(12) $^{12}C^{16}O$ absorption to yield standard uncertainties that are exclusively limited by the available line strength figure quality, which is about ±2.5 %, given the 2 to 5 % error code range specified by HITRAN 2008.

7.1.1 Introduction

The last years exhibited the development of new laser sources such as quantum cascade lasers [1] operating in the mid infrared where the fundamental bands of most infrared active molecules are located. In breath analysis for instance, mid infrared light sources have been used to measure the amount fraction of biomarkers such as acetone or carbon monoxide (CO) found in exhaled human breath using different laser spectroscopic techniques with detection limits down to the $pmol \cdot mol^{-1}$ level [2].

Carbon monoxide, which we focus on in this work, is in air a pollutant resulting from the incomplete burning of carbon containing fuels. As a process product it can reach quite large concentration levels of several tens of $\mu mol \cdot mol^{-1}$, expressed as amount fractions. CO in breath on the other hand could be for healthy humans in the range of few $nmol \cdot mol^{-1}$ above atmospheric levels (typically 100 $nmol \cdot mol^{-1}$). Patients suffering from anaemias, oxidative stress and respiratory infections have been found with abnormal levels of carbon monoxide. Therefore, CO is discussed as being a biomarker for these diseases. However, because of the low sub $\mu mol \cdot mol^{-1}$ level of CO reported to be present in exhaled breath and because of the presence of several molecules at the same or even larger amount of substance fraction levels, a very selective and sensitive technique is required to measure the amount fraction of breath CO [2], [3]. Laser spectrometric techniques are seemly unique to perform such measurements because of their robustness from sample preparation to measurement, selectivity and sensitivity [2].

Laser spectroscopic techniques such as tunable diode laser absorption spectroscopy (TDLAS), quantum cascade laser absorption spectroscopy (QCLAS) and cavity ring-down spectroscopy (CRDS) applied to gas detection had been reported to be selective, sensitive, and have near real time and point of care capabilities [2].

Employing QCLAS and CRDS, which is the focus of this manuscript, to perform absolute amount fraction measurements of different molecular species had been reported by several groups [4-9]. Some scientists have reported CO amount fraction results based on QCLAS and CRDS [2], [10], [11]. What we found missing in most of the reports is information on metrological data qualifiers, i.e. traceability statements or uncertainty budgets and a methodological standardization attempt where performed measurements could be referred to.

In this work, we report laboratory-based amount fraction measurements of CO in gravimetrically prepared gas mixtures, as artificial breath samples, e.g. comprised of CO_2, O_2,

CH_4, and N_2 as matrix gas. We applied QCLAS operated with both, intra-pulse and continous wave (cw) QCLs, and cw CRDS operated by a QCL and a CO sideband laser setup, respectively. The measurements were performed in the framework set by an iMERA-Plus joint research project on "Breath analysis" [12]. The basic idea of the measurement method used was promoted in a previous EURAMET project and referred to as "traceable infrared laser spectrometric amount fraction measurement" (*TILSAM*) method [13]. Its application to spectroscopy techniques with potentials for breath analysis (BA) was projected in an extended BA-*TILSAM* descriptive document [12].

According to the *TILSAM* method, the aim of this paper was to rely on the quality of the input quantities such as the gas pressure (p), gas temperature (T) and the optical path length through the absorbing medium (L) to directly derive absolute CO amount fractions rather than to calibrate with reference gas mixtures. The uncertainties were estimated referring to the "Guide to the expression of uncertainty in measurement" (GUM) [14].

This manuscript is structured as follows. We briefly outline the background of QCLAS similar to what we reported in one of our earlier publications [9]. We then present the experimental setups, measurements and the results of pulsed-QCLAS, cw-QCLAS and CRDS in section 3, 4 and 5. The results from the three spectrometric techniques are compared and discussed in section 6. Some conclusions are presented in the last section.

7.1.2 Conceptual background

For absorption spectroscopy, the interaction of the gas molecules and the sensing radiation at wave number $\tilde{\nu}$ is modeled by the Beer-Lambert law

$$\Phi(\tilde{\nu}, L) = \Phi_0(\tilde{\nu}) \cdot \exp\{-S_T \cdot r_{\text{iso}} \cdot \text{g}(\tilde{\nu} - \tilde{\nu}_0) \cdot L \cdot n\} \tag{7.1}$$

with Φ_0 and Φ being the incident and transmitted radiant powers, respectively, of which the SI unit is W. The absorption is governed by the molecular transition line strength S_T at gas temperature T, the respective normalized absorption profile g centered at $\tilde{\nu}_0$, and the absorption path length L. The quantity r_{iso} is the isotopic composition factor, given e.g. as $r_{\text{iso}} = x_{12\text{C}16\text{O}} / x_{12\text{C}16\text{OHIT}}$, for a probed $^{12}C^{16}O$ excitation, where $x_{12\text{C}16\text{O}}$ and $x_{12\text{C}16\text{OHIT}}$ are the abundances of $^{12}C^{16}O$ in the sample and the conventional abundance value given by HITRAN [15], respectively. The line strength S_T is specific for the probed molecular transition. Relying on the ideal gas law, the molecular density n of the absorbing species can be expressed in terms of the partial pressure p_{partial} of the absorbing molecular species and the gas temperature. The partial pressure can be related to the total pressure p_{total} using the amount of substance fraction of the absorbing species, $x_{\text{species}} = p_{\text{partial}} / p_{\text{total}}$. Thus, Eqn. (7.1) becomes

$$\Phi(\tilde{\nu}, L) = \Phi_0(\tilde{\nu}) \cdot \exp\left(\frac{-S_T \cdot r_{\text{iso}} \cdot \text{g}(\tilde{\nu} - \tilde{\nu}_0) \cdot L \cdot x_{\text{species}} \cdot p_{\text{total}}}{k_B \cdot T} \right) \tag{7.2}$$

While probing a certain molecular transition measuring Φ and Φ_0 for a known path length, as well as p_{total} and T, leads to the amount of substance fraction of the species

$$x_{\text{species}} = -\ln\left(\frac{\Phi(\tilde{\nu})}{\Phi_0(\tilde{\nu})}\right)\cdot\frac{k_B\cdot T}{S_T\cdot r_{\text{iso}}\cdot \text{g}(\tilde{\nu}-\tilde{\nu}_0)\cdot L\cdot p_{\text{total}}} \tag{7.3}$$

Introducing the spectral absorbance $A(\tilde{\nu}) = -\ln(\Phi(\tilde{\nu})/\Phi_0(\tilde{\nu}))$, which in some cases[11] can also be called extinction, and making use of the normalization of g, Eqn. (7.2) can also be written in its integral form

$$x_{\text{species}} = \frac{k_{\text{B}}\cdot T}{S_T\cdot r_{\text{iso}}\cdot L\cdot p_{\text{total}}}\int_{-\infty}^{\infty} A(\tilde{\nu})d\tilde{\nu} = \frac{k_{\text{B}}\cdot T}{S_T\cdot r_{\text{iso}}\cdot L\cdot p_{\text{total}}}\cdot A_{\text{line}} \tag{7.4}$$

where A_{line} is the line area obtained by integration of the measured absorbance data over wave number. Direct absorption spectroscopy is described by the Beer-Lambert law, as expressed in Eqn. (7.2). All input quantities are SI-traceable. In turn, using Eqn. (7.4) to determine the amount of substance fraction, x_{species}, in a given gas mixture would deliver results that are SI-traceable. An uncertainty budget for the measurement according to the ISO Guide to the expression of uncertainty in measurement (GUM) [14] can be evaluated with Eqn. (7.4) as model function.

7.1.3 Intra-pulse QCLAS

Pulsed QCLs can be operated in inter and intra-pulse mode [11], [16-18]. A comparison of the two modes of operation is found in [19], [20]. Here, we focus on the intra-pulse mode operation of a QCL to perform absolute amount fraction measurements of CO. Measurements and results in this section are reported in a similar manner as in [9]. A single pass gas cell was used with an optical path length of 0.82 m [9].

Briefly, the intra-pulse chirp mode of operation utilizes the intrinsic temperature rise inside the active area of the QCL chip within each single pulse caused by the current driven through the chip [21]. Right from the beginning of each pulse the emission wavelength increases within several nanoseconds. Thus, the laser emission spans a certain pulse-length-dependent spectrum within a single pulse. The laser wavelength sweeps from the blue towards the red side of the spectrum. By setting the laser temperature and the laser voltage, chirp-onset wavelength and laser power can be tuned. The sweep width is then set by the pulse length. In principle the intra-pulse mode spectroscopy allows us to study the molecular spectrum of interest within one single laser pulse of a few nanoseconds, what could be important, e.g. in fast process studies.

Figure 7.1 depicts a schematic of the experimental QCLAS setup. The QCL (Fraunhofer-IAF) emitted at 4.6 µm and was operated with pulse length of 255 ns (2 kHZ repetition rate,

[11] see e.g. http://goldbook.iupac.org/A00028.html

substrate temperature 292 K). After collimation, the QCL beam was split into a reference beam and a second sample beam was directed through a 0.82 m stainless steel absorption cell. The reference beam was used for intensity normalization and for fixing the wavelength axis by means of a removable etalon. Both channels were terminated into TE-cooled HgCdZnTe detectors (Vigo PDI-2TE-10.6). The electrical signals were high speed digitized at 5 GS/s by an 8 bit A/D-converter (Compuscope 85G) to resolve the temporal evolution within single pulses.

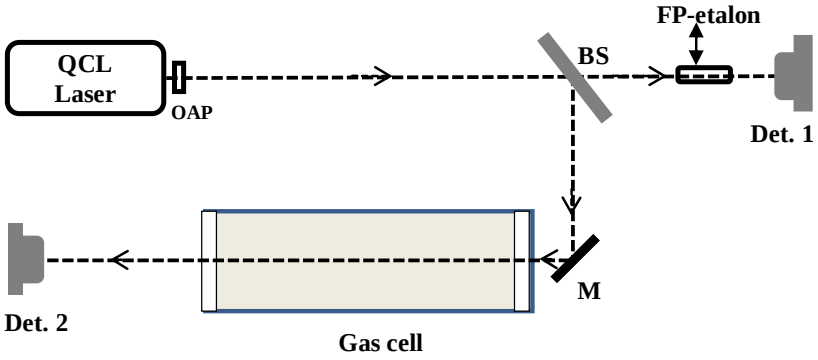

Figure 7.1: Schematic diagram of the setup used for species quantification in a two-channel regime. The gas cell has a path length of L = 0.82 m. OAP: off-axis parabolic mirror, BS: beam splitter, M: mirror, Det: detector. f) Generalized linear regression of A_{line} versus Γ.

For gas detection, the P(1) line of CO at 2139.4261 cm^{-1} [15] was selected. The choice of the P(1) line was based on practical criteria, since this line was easily accessible with the used QCL, first, and second, because this line has some intermediate line strength of $9.072 \cdot 10^{-20}$ $cm^{-1}/(molecule \cdot cm^{-2})$ [15] providing neither the ultimate limit in terms of sensitivity nor the smallest absorption feature. A carbon monoxide containing reference gas mixture of 5 % CO_2, 15 % O_2, and the rest N_2, gravimetrically prepared by the Instituto Portugues da Qualidade (IPQ) [22] with a nominal level of 100 µmol/mol CO was filled into the gas cell for analysis. The spectrometric measurements were performed at a total gas pressure of 407.1 hPa referring to [13]. Prior to the measurements, effects such as that of the "rapid passage" [23], a non constant chirp rate along the QCL pulse, the dependence of the instantaneous line width of the QCL on the chirp rate [24] and the non linearity of the TE-cooled HgCdZnTe detectors were checked and, if necessary, accounted for as pointed out in [9].

Figure 7.2a shows typical signals from the intra-pulse mode QCLAS setup. The mid-IR QCL radiation was transmitted through a removable etalon with a free spectral range (FSR) of about 0.05 cm^{-1} placed on the beam path to detector 1. As evidenced by 37 measured etalon fringes depicted in Figure 7.2b, the intra-pulse chirp for this condition was shown to be 1.85 cm^{-1}. Figure 7.2a represents the signal of the sample channel detector with CO absorption (solid line) and the reference channel detector (dashed line) with the etalon removed, respectively. One hundred QCL pulses were averaged and measured in the time domain in units of sample points (SP).

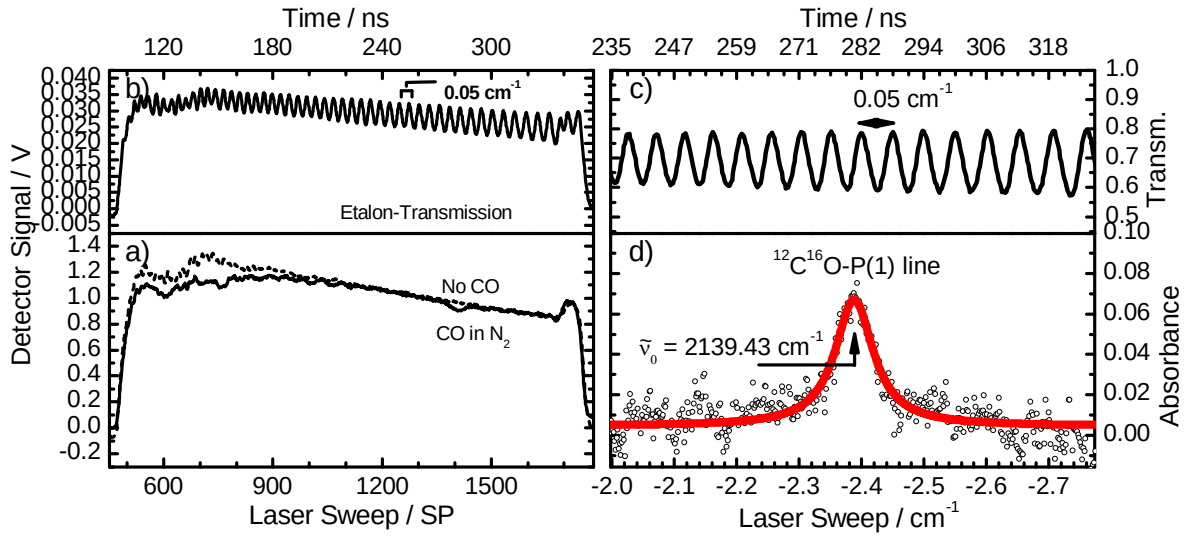

Figure 7.2: Intra-pulse chirp spectroscopy. a) Data from the reference channel, without CO absorption (dashed line) and the sample channel (full line) featuring CO absorption, respectively. b) Etalon transmission signal seen by detector 1 with the etalon ($FSR_\nu \approx 0.05$ cm^{-1}) placed in the reference beam path. c) Etalon transmittance curve. d) Data of a), converted to absorbance values (open circles). A Voigt profile has been fitted to the data (full line) representing the CO-P(1) line at 2139.4261 cm^{-1} [15].

The data in Figure 7.2a were converted to absorbances as depicted in Figure 7.2d using the detector signals of the two channels, representing a simultaneous two channel measurement scheme. The wave number axis in Figure 7.2d was accomplished by means of the chirp rate $r_{sweep} = FSR_\nu / FSR_{SP}$ [9]. FSR_ν is the known free spectral range of the etalon in wave numbers and FSR_{SP} is the experimental fringe separation measured in the time domain (SP) which is visible in panel c) of Figure 7.2. FSR_ν was determined by calculation, using the refractive index of the etalon material and its length; FSR_{SP} by fitting the measured etalon transmission spectrum with a multi-peak function.

Fitting a Voigt profile to the measured absorbance data in Figure 7.2d by means of a nonlinear least square fit [25] (Levenberg-Marquardt [26]) delivered the absorption peak area. The uncertainties in the absorption peak area from fitting ranged from 0.5 to 1 % relative.

Figure 7.3 depicts spectrometric CO amount fractions, derived directly using Eqn. (7.4), as a function of their sequence number. From them, the mean CO amount fraction was computed to be 93.7 µmol/mol. The expanded uncertainty of each measurement evaluated using the GUM workbench [27] is in the ±9 µmol/mol range. As presented in Figure 7.3, the directly retrieved CO amount fractions agree with the gravimetric reference value of (99.88 ± 0.68) µmol/mol certified by [22].

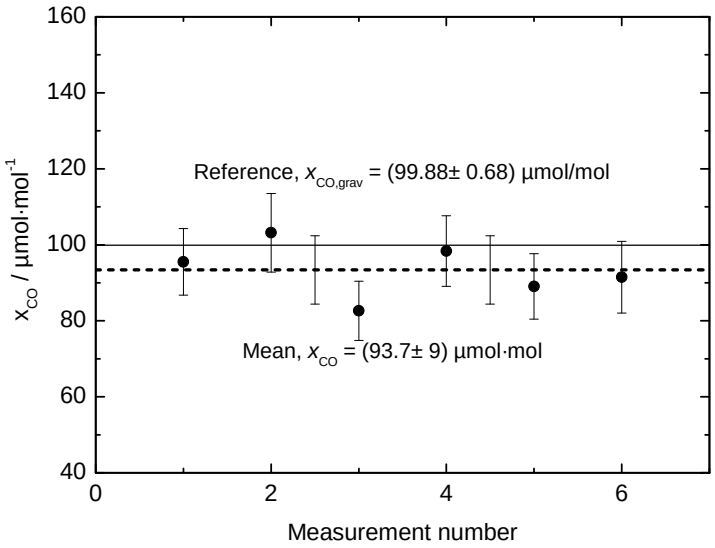

Figure 7.3: Spectrometrically derived CO amount fraction as a function of measurement number. The dashed line represents the resultant mean CO amount fraction, whereas the solid one represents the gravimetric reference value.

7.1.4 Cw QCLAS

The intra-pulse QCLAS measurements were performed with a path length of 82 cm. Because of the moderate line strength value of the probed P(1) line at 2139.43 cm^{-1} [15], we could only derive measurable absorbance values (Figure 7.2) at 407.1 hPa for the 100 µmol/mol CO gas mixture. However, for these conditions the signal to noise ratio of 3 is poor as seen in Figure 7.2d. Therefore, to enhance the sensitivity, we turned to a laser spectrometer comprising a continuous wave (cw) mode QCL (Hamamatsu). By means of the cw-QCL which was mounted in a high-heat load package, the R(12) line of CO at 2190.02 cm^{-1} **(**see Figure 7.4**)** was probed with a line strength about three times stronger than of the P(1) [15]. To slightly compensate for the larger line strength we used a single pass gas cell with reduced optical pass length of L = 46.1 cm to perform the spectrometric measurements.

The cw-QCL package was mounted on a water-cooled heat sink and an AR-coated aspheric lens (Lightpath) was used to collimate the highly diverging beam. The experimental set-up is shown in Figure 7.5. The temperature of the cw-QCL was kept constant using a Lightwave LDT-5545B temperature controller (long term stability of 0.01°C) and the laser current was regulated by a Lightwave LDX-3232 high compliance laser driver.

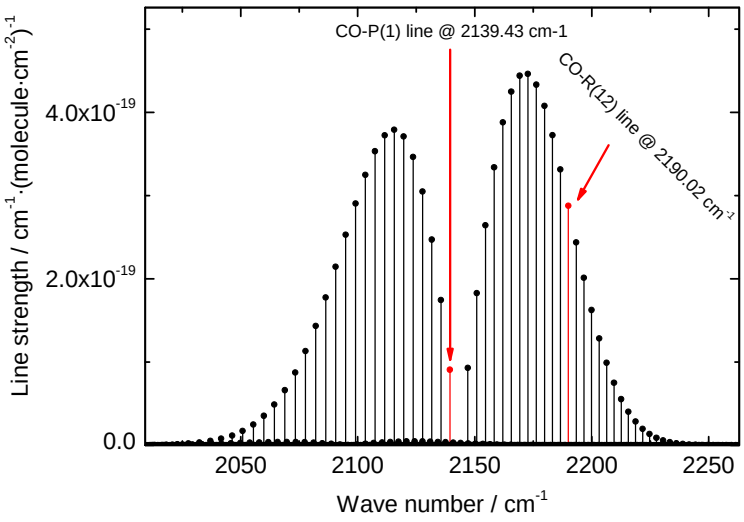

Figure 7.4: CO line strengths in the fundamental band [15].

Tuning of the laser wavelength was accomplished by applying a voltage ramp to the external modulation input of the laser driver.

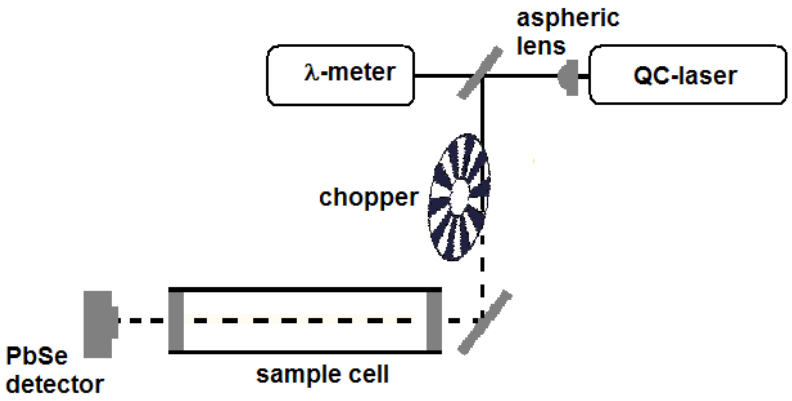

Figure 7.5: Experimental setup for the cw QCL measurements. An aspheric lens was used to collimate the highly divergent laser beam. The optical path length of the gas cell was 46.1 cm.

For the CO quantification, a similar gravimetrically prepared gas mixture prepared by IPQ [22] of nominal 100 µmol/mol CO, 150 mmol/mol O_2, 50 mmol/mol CO_2, and 3 µmol/mol CH_4 in N_2 balance was measured. The measurements were performed referring to the *TILSAM* method [13]. While probing the R(12) line, interferences from nearby lines of H_2O, CO_2, and CH_4, which were at least 10^4 times weaker, were negligible compared to the CO line strength of $S_0 = 2.876 \cdot 10^{-19}$ cm^{-1}/(molecule·cm^{-2}) [15].

To derive the absorbance from the measured detector signal, first a signal was measured with a non-absorbing gas (nitrogen) in the cell, after which, the gas mixture, subsequently filled into the gas cell, was measured. The absorbance was then evaluated using the ratio of these two signals.

Spectral data measured at atmospheric pressure are shown in Figure 7.6a. By comparing the measured absorbance to a simulation based on HITRAN [15], displayed in Figure 7.6b, a fairly good agreement is observed. A Lorentz function is fitted to the experimental data to derive the line area. The respective CO amount fraction result of $x_{CO} = 96.84$ µmol/mol calculated by means of Eqn. (7.4), using the derived line area and the HITRAN line strength figure (stated uncertainty of 2-5%) [15] is in good agreement with the nominal reference of 100 µmol/mol. The uncertainty of a single measurement is in the ± 5 µmol/mol range. The latter is pretty much limited by the availability of the line strength uncertainty.

Besides this quantitative agreement, the most striking feature of the experiments described in the last two sections is the much better raw data quality of the cw-QCLAS instrumentation. This is to some smaller extent due to the somewhat larger "absorption signal strength", i.e. peak absorbance of 0.18 and 0.07 for cw- and intra-pulse QCLAS, respectively, and to a much larger extent due to the much smaller noise level of our cw-QCL experiment.

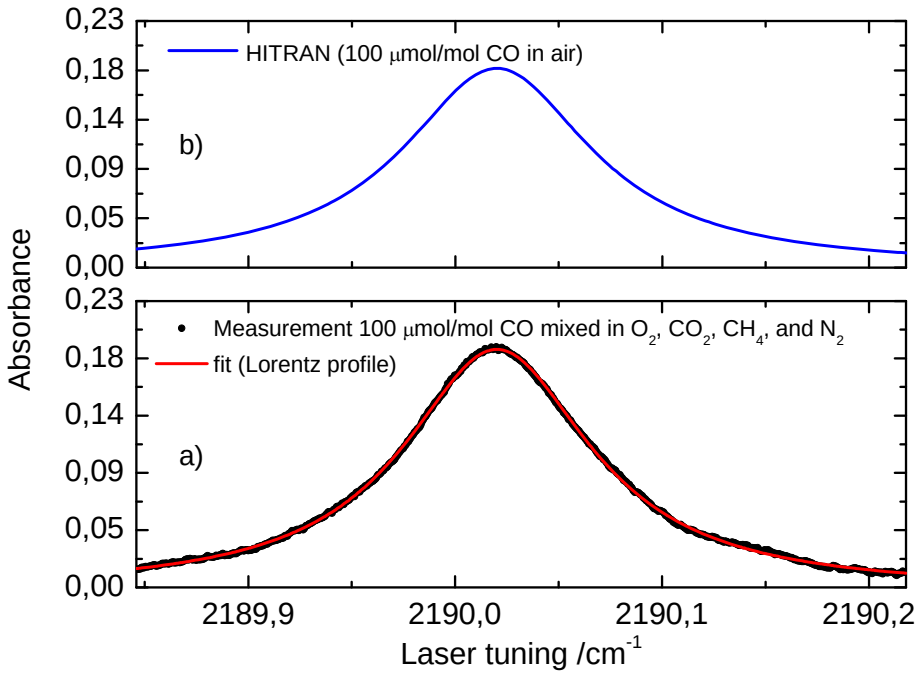

Figure 7.6: Lower panel a): CO R(12) line measured in a single pass absorption cell (46.1 cm) at a pressure of 1000 mbar. The measured absorbance is fitted using a Lorentz function to derive the line area. Upper panel b): HITRAN simulation [15].

7.1.5 Cavity ring-down spectroscopy (CRDS)

So far, the measurements above demonstrate the feasibility of pulsed and cw-QCLAS for absolute CO amount fraction quantification based on the *TILSAM* method on a 100 µmol/mol level of CO. However, to reach a sensitivity of 0.8 µmol·mol^{-1}, equivalent to the CO amount fraction in exhaled human breath, one has to enhance the sensitivity of the QCLAS instruments. This could have been done by increasing the absorption path length. However, we decided to change to another spectroscopy technique. Cavity ring-down spectroscopy has been proven to provide a very versatile tool in trace gas detection as well as in applications like breath analysis or process controlling [2], [28], [29]. First of all, we have compared QCLAS as demonstrated above with cw-CRDS on the 100 µmol/mol CO level. Then, we were applying QCL-based cw-CRDS to much lower amount fraction levels to demonstrate sensitivity and accuracy at relevant breath levels.

The theory of CRDS employed to the measurements shown in this section has been published in some very prominent studies [11], [30-33]. Briefly, there is not that much of a difference to the final equations presented in section 2 of this work. However, compared to Eqn. (7.4) (TDLAS and QCLAS), A_{line} in CRDS is given in units of cm^{-2} [4] and the path length L has to be omitted in Eq. (7.3) and (7.4) for CRDS.

Figure 7.7 depicts a schematic of a typical CRDS spectrometer. For the present study we have employed two different setups. The first one is referred to as the CALOS spectrometer based on a continuous wave CO sideband laser as was presented in [7], [33]. A high finesse cavity is used to confine the absorbing gas sample while continuously flowing through the cavity ring-down cell at constant and controlled flow rates of about 1000 cm^3/s.

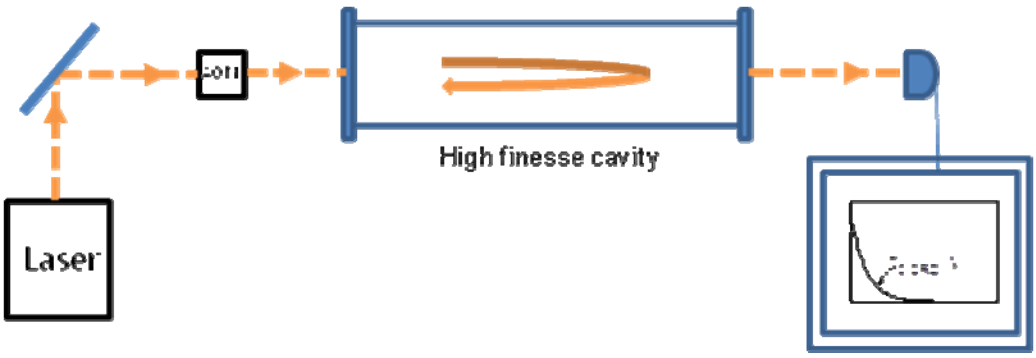

Figure 7.7: A schematic of a CRDS setup

For quantitative CRDS-based detection of CO, the CO sideband laser was tuned to probe the $^{13}C^{16}O$ P(25) line at 1994.7 cm^{-1} [15]. The measurements were also performed in accordance with [13]. Figure 7.8a shows cw CRDS data obtained by the CALOS setup from a single ring-down trace (a), where the ring-down time is fitted on, via processed absorption coefficient data of the probed line for a certain value of Ω (b), to the resultant regression-based retrieval [13] on a set of Ω values (c). Here, Ω summarizes the experimental parameters,

$\Omega = S_T \cdot p_{total} / (k_B \cdot T)$. The slope of the linear dependence A_{line} vs. Ω, derived by means of a generalized regression analysis is yielding the amount fraction result.

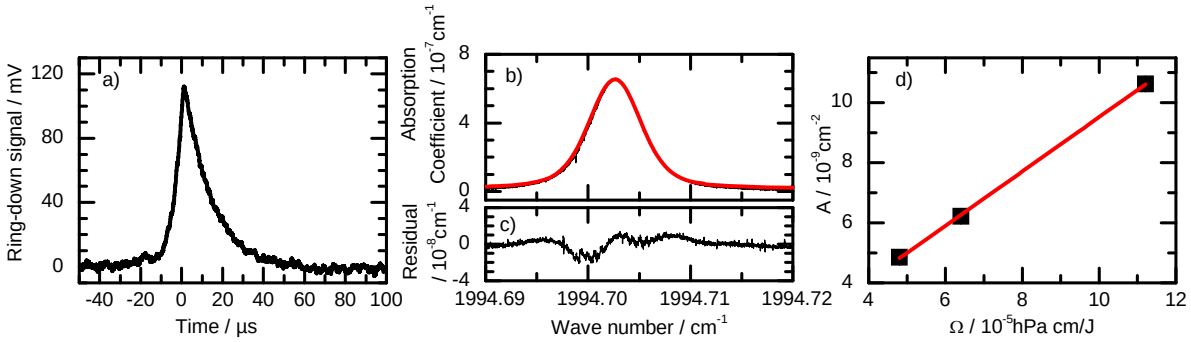

Figure 7.8: CRDS-based CO quantification: a) Typical signal from the CALOS setup. b) Derived absorption coefficients fitted by a Voigt profile (full line) representing the CO-P(25) line at 1994.7 cm^{-1}. c) Residuals from the fitted line in (b). c) Linear regression of the determined line areas A_{line} versus the experimental parameter $\Omega = S_T \cdot p_{total} / (k_B \cdot T)$.

The ring-down times, measured before and after the CO gas mixture was injected into the cavity, were used to derive the absorption coefficients at respective wave numbers. The measurements were performed at total gas pressures between 30 and 70 hPa and a gas temperature of 292 K. By fitting the absorption coefficient with a Voigt profile, the area of the absorption line A_{line} was determined. As evidenced by typical fingerprints in the residuals in Figure 7.8c, the Voigt profile does not completely describe the actual experimental line shape. This might be caused by some additional effects like the Dicke-narrowing which is not taken into account applying a Voigt profile. However, by means of a regression-based retrieval [9], depicted in Figure 7.8d, the determined CO amount fraction evaluated from these data was (90.1 ± 8.4) µmol·mol^{-1}. The reproducibility was estimated to be ±3 % based on the standard deviation of individual measurements. The direct retrieval yields a mean amount fraction of (97.7 ± 5.2) µmol·mol^{-1} as averaged on the different experimental runs. The 5.2 µmol/mol uncertainty figure derived for this direct retrieval is combined from the uncertainties of each individual result. Given the comparably larger uncertainty figure of the regression-based retrieval both results are agreeing with each other. Just to note, of course, the two retrievals are not independent, since they have been performed on the same identical data set. However, the regression-based result is based on a linear model whereas the direct retrieval is the mean of the different experimental runs. For the linear model approach a generalized linear regression has been performed by means of the BLeast software [34].

In order to go down to a few ppb of CO, a second, cw-QCL-based CRDS setup was used to perform low concentration CO measurements. Low CO amount fraction gas mixture standards were prepared dynamically by VSL by means of dilution of reference gas mixtures [35].

For the cw-QCL CRDS-based CO quantification we chose again the R(12) line at 2190 cm^{-1}. Measurements on mixtures of CO in nitrogen were complemented by data on mixtures of CO in hydrogen. The aim of these efforts was to demonstrate the quality and sensitivity of the CO quantification applied in this work down to breath-relevant amount fraction levels. Figure 7.9a depicts the two extremes of the CO-in-nitrogen-mixture data, spanning the range from 100 nmol/mol CO down to 10 nmol/mol. The lines were measured at (293.45 ±0.5) K and (1000.0 ±2.2) hPa, and subsequently, fitted by Lorentz profiles. The linearity of the applied quantification can be derived from Figure 7.9b where results on CO/N_2 and CO/H_2 mixtures are displayed, spanning the range from 200 nmol/mol down to 2.4 nmol/mol of CO.

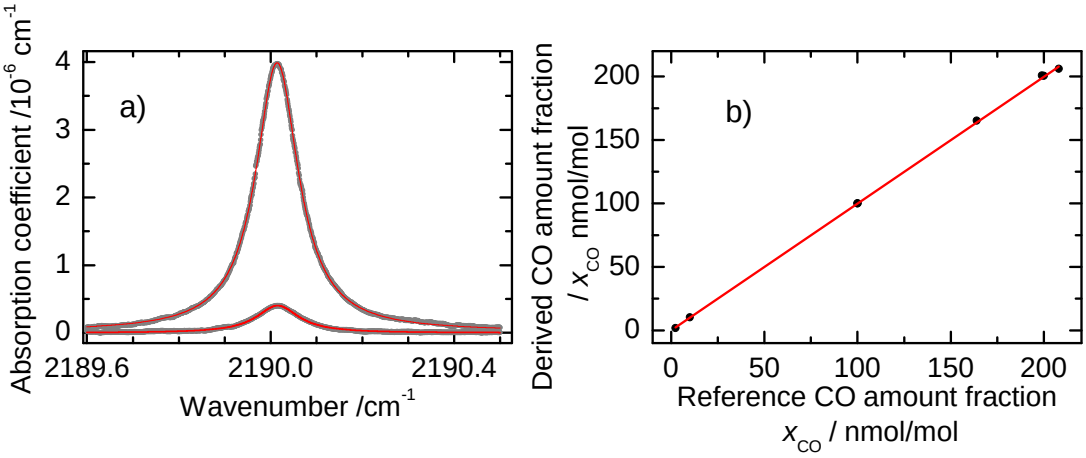

Figure 7.9: CO R(12) line measured with the cw-QCL CRDS setup on mixtures of 100 nmol/mol and 10 nmol/mol CO in nitrogen, respectively, at 1000 hPa total pressure. The straight lines are Lorentz profiles fitted to the experimental data (a). (b) Measured spectrometric amount fraction results compared to gravimetric reference values.

The reproducibility of the CO quantification achieved with cw-QCL CRDS was 0.6 % based on the derived standard deviation for the range of 200 nmol/mol to 10 nmol/mol CO.

7.1.6 Discussions

The spectrometric CO amount fraction results from three different spectrometers agree with the respective reference values at the 100 µmol/mol CO level. The relative standard uncertainties of these spectrometric CO amount fraction results are in the few percent range. Comparability was achieved among the direct absorption and the cavity ring-down results as summarized in Table 7.1 for direct retrievals. For each of the three results the value component of the degree of equivalence D calculated as the difference of the respective result and the gravimetric reference value is smaller than its uncertainty component $U(D)$.

Table 7.1: Carbon monoxide amount fraction results based on pulsed QCLAS, cw-QCLAS and CRDS (CALOS setup) compared to the gravimetric reference value; expanded uncertainties with $k = 2$.

	x_{CO} / µmol/mol	$U(x_{CO})$ / µmol/mol	$^{*}D$ / µmol/mol	$^{\#}U(D)$ / µmol/mol
grav. reference:	99.88	0.68	-	-
intra-pulse QCLAS	93.7	9.0	-6.18	9.03
cw-QCLAS	96.8	4.8	-3.08	4.85
CRDS (CALOS setup)	97.7	5.2	-2.18	5.24

$^{*}D = x_{CO}$ - $x_{CO,grv}$

$^{\#}U(D) = (U(x_{CO})^2 + U(x_{CO,grav}{}^2)^{1/2}$

Although direct absorption spectroscopy, as applied in the present study by means of intra-pulse and cw-QCLAS, could be improved in terms of sensitivity by increasing the optical path length, a much higher protential in breath analysis has to be attributed to the cavity ring-down spectroscopy for our purposes. This is demonstrated by the CALOS and the cw-QCL CRDS setups used in this work. However, to keep on going with direct absorption, it is clearly shown that based on the technology employed for this work, cw-QCLs are superior to pulsed systems in terms of noise and in turn on sensitivity for a given path length. With respect to the spectrometer's path length, one could argue that an increase would be possible, thus increasing our sensitivity towards that of our CRDS. In fact, we might have gained up to two orders of magnitude, since multi pass Herriott-type cells with path lengths of 100 or even 200 meters are available. Instead, the path length equivalent of CRDS systems is easily on the kilometers scale.

The ideas of the *TILSAM* method [13] were applied in this work to two different spectroscopic techniques. Its potential relevance to breath analysis is evidenced by the present study with respect to the achieved sensitivity down to a few ppb, shown for the cw-QCL CRDS setup. With this sensitivity, CO levels typically to be measured in applied breath analysis could be matched, while quality flags of the results as delivered by GUM [14] compliant uncertainty statements are still provided. The uncertainty for the cw-QCL CRDS is mostly limited by the availability of line strength data with uncertainties better than 5 %, as e.g. reported by HITRAN 2008 [15] on the probed R(12) of CO at 2190 cm^{-1}. At the 100 nmol/mol a reproducibility level of 0.5 %, relative, was achieved. The relative deviation of the spectrometric results from the gravimetric reference was determined to be in the range of 1 % to 0.3 % on the 200 to 10 nmol/mol level, what would totally be covered by a line strength uncertainty figure of 2 %.

With a documented method, such as e.g. that of *TILSAM*, spectrometric amount fraction results could be made comparable. Ensuring the comparability of measurement results is crucial e.g. in medical treatment or environmental measurements for decision making procedures. The comparability of measurement results is enssured if the results are traceable.

Traceability is also inline with the stated aims of the international quality assurance standard ISO EN 17025 [36].

7.1.7 Conclusions

The goals of the presented study were threefold, namely first, to demonstrate comparability of CO quantification by means of absolute laser spectroscopy referring to the *TILSAM* method. This goal was achieved at the 100 µmol/mol CO level for three different experimental techniques and setups used. The overall achieved level of comparability can be expressed by means of a maximum $D/x_{CO,grav}$ (s. Tab. 1) as to be within ±6 %. Second, to demonstrate CO quantification concepts based on metrological aspects such as uncertainty assessments, as it may provide impact to practical breath analysis. This was achieved best by means of the estimated uncertainty levels of the cw-QCL results at some few percent, mostly limited by the available line strength data. Finally, the third goal was to demonstrate CO quantification capabilities down to a few nmol/mol level as being relevant for the breath matrix.

7.1.8 Acknowledgements

Parts of this work were performed in an EURAMET joint research project and received funding from the European Union Seventh Framework Programme, ERA-NET Plus, under the iMERA-Plus Project – Grant Agreement No. 217257. J.A.N. acknowledges also the support from the Braunschweig International Graduate School of Metrology (http://www.igsm.tu-bs.de).

7.1.9 References

[1] J. Faist, F. Capasso, D. L. Sivco, C. Sirtori, A. L. Hutchinson, and A. Y. Cho, "Quantum cascade laser," *Science*, vol. 264, pp. 553-556, 1994.

[2] C. Wang and P. Sahay, "Breath Analysis Using Laser Spectroscopic Techniques: Breath Biomarkers, Spectral Fingerprints, and Detection Limits," *Sensors*, vol. 9, pp. 8230-8262, 2009.

[3] M. R. McCurdy, Y. Bakhirkin, G. Wysocki, R. Lewicki, and F. K. Tittel, "Recent advances of laser-spectroscopy-based techniques for applications in breath analysis," *Journal of Breath Research*., vol. 1, pp. 014001, 2007.

[4] J. A. Nwaboh, T. Desbois, D. Romanini, D. Schiel, and O. Werhahn "Molecular laser spectroscopy as a tool for gas analysis applications," *International Journal of Spectroscopy*, vol. 2011, doi:10.1155/2011/568913.

[5] J. Morville, S. Kassi, M. Chenevier, and D. Romanini, "Fast, low-noise, mode-by-mode, cavity-enhanced absorption spectroscopy by diode-laser self-locking," *Applied Physics B*, vol. 80, pp. 1027-1038, 2005.

[6] P. Ortwein, W. Woiwode, S: Fleck, M. Eberhard, T. Kolb, S. Wagner, M. Gisi, and V. Ebert, "Absolute diode laser-based in situ detection of HCl in gasification processes," *Experiments on Fluids*, Vol. 49. No. 4, pp. 961-968, 2010.

[7] K. Heinrich, T. Fritsch, P. Hering, M. Mürtz, "Infrared laser-spectroscopic analysis of ^{14}NO and ^{15}NO in human breath," *Applied Physics B*, vol. 95, pp. 281–286, 2009.

[8] K. Wunderle, S. Wagner, I. Pasti, R. Pieruschka, U. Rascher, U. Schurr, and V. Ebert, "Distributed feedback diode laser spectrometer at 2.7 μm for sensitive, spatially resolved H_2O vapor detection," *Applied Optics*, vol. 48, pp. B172-B182, 2009.

[9] J. A. Nwaboh, O. Werhahn, and D. Schiel, "Measurement of CO amount fractions using a pulsed quantum-cascade laser operated in the intrapulse mode," *Applied Physics B*, vol. 103, pp. 947–957, 2011.

[10] S. Wright, G. Duxbury, and N. Langford, "A compact quantum-cascade laser based spectrometer for monitoring the concentrations of methane and nitrous oxide in the troposphere," *Applied Physics B*, vol. 85, pp. 243-249, 2006.

[11] S. M. Cristescu, S. T. Persijn, S. te Lintel Hekkert, and F. J. M. Harren, "Laser-based systems for trace gas detection in life sciences," *Applied Physics B*, vol. 92, no. 3, pp. 343-349, 2008.

[12] EMRP, T2.J02–Breath Analysis, Joint Research Projects funded under iMERA-plus, 2010, http://www.euramet.org/index.php?id=imera-plus.

[13] O. Werhahn, J. C. Petersen (eds.), *TILSAM* technical protocol V1_2010-09-29. Available from: http://www.euramet.org/fileadmin/docs/projects/934_METCHEM_Interim_Report.pdf.

[14] JCGM 100:2008, Evaluation of measurement data - Guide to the expression of uncertainty in measurement, GUM 1995 with minor corrections, ISO IEC Guide 98-3, 2008. Available from: http://www.bipm.org/en/publications/guides/gum.html.

[15] HITRAN2008, http://www.cfa.harvard.edu/HITRAN/, L. Rothman et al., *Journal Quantitative Spectroscopy and Radiation Transfer*, Vol. 110, pp. 533-572, 2009.

[16] E. Normand, M. McCulloch, G. Duxbury, and N. Langford, "Fast, real-time spectrometer based on a pulsed quantum-cascade laser," *Optics Letters*, vol. 28, no. 1, pp. 16-18, 2003.

[17] M. T. McCulloch, E. L. Normand, N. Langford, G. Duxbury, and D. A. Newnham, "Highly sensitive detection of trace gases using the time-resolved frequency downchirp from pulsed quantum-cascade lasers," *Journal of the Optical Society of America B*, vol. 20, no. 8, pp. 1761-1768, 2003.

[18] T. Beyer, M. Braun, and A. Lambrecht, "Fast gas spectroscopy using pulsed quantum cascade lasers," *Journal of Applied Physics*, vol. 93, no. 6, pp. 3158-3160, 2003.

[19] B. Grouiez, B. Parvitte, L. Joly, D. Courtois, and V. Zeninari, "Comparison of a quantum cascade laser used in both cw and pulsed modes. Applications to the study of SO_2 lines around 9 μm," *Applied Physics B*, vol. 90, pp. 177-186, 2008.

[20] J. Manne, W. Jäger, and J. Tulip, "Sensitive detection of ammonia and ethylene with a pulsed quantum cascade laser using intra and interpulse spectroscopic techniques," *Applied Physics B*, vol. 94, pp. 337-344, 2009.

[21] C. Pflügl, M. Litzenberger, W. Schrenk, D. Pogany, E. Gornik, and G. Strasser, "Interferometric study of thermal dynamics in GaAs-based quantum-cascade lasers," *Applied Physics Letters*, vol. 82, no. 11, pp. 1664-1666, 2003.

[22] Instituto Portugues da qualidade (IPQ), http://www.ipq.pt/backhtmlfiles/ipq_mei.htm.

[23] G. Duxbury, N. Langford, M. McCulloch, and S. Wright, "Rapid passage induced population transfer and coherences in the 8 micron spectrum of nitrous oxide," *Molecular Physics*, vol. 105, no. 5-7, pp. 741-754, 2007.

[24] S. Welzel, "New enhanced sensitivity infrared laser spectroscopy techniques applied to reactive plasmas and trace gas detection," Dissertation, Ernst-Moritz-Arndt Universität Greifswald, 2009.

[25] Origin 7.5 SR6, OriginLab Cooperation, Northampton, MA, USA, 2006. Available from: http://www.OriginLab.com.
[26] Levenberg-Marquardt, Numerical Recipes, 2005, http://www.library.cornell.edu/nr/bookcpdf/c15-5.pdf.
[27] GUM Workbench Pro, Version 2.4.1.388, 1996 - 2010 Metrodata GmbH, Im Winkel 15-1, D-79576 Weil am Rhein, Germany, http://www.metrodata.de
[28] H. Teichert, T. Fernholz, and V. Ebert, "Simultaneous in situ measurement of CO, H_2O, and gas temperatures in a full-sized coal-fired power plant by near-infrared diode lasers," *Applied Optics*, vol. 42, no. 12, pp. 2043-2051, 2003.
[29] S.T. Persijn, F. Harren, and A. van der Veen, "Quantitative gas measurements using a versatile OPO-based cavity ring down spectrometer and the comparison with spectroscopic databases," *Applied Physics B*, vol. 100, pp. 383–390, 2010.
[30] R. D. van Zee and J. Patrick Looney, "*Cavity-enhanced spectroscopies*," in *Experimental Methods in the Physical Sciences*, vol. 40, Academic Press, Amsterdam, The Netherlands, 2002, ISBN 0-12-475987-4.
[31] P. Zalicki and R. N. Zare, "Cavity ring-down spectroscopy for quantitative absorption measurements," *Journal of Chemical Physics*, vol. 102, no. 7, pp. 2708-2716, 1995.
[32] J. Manne, O. Sukhorukov, W. Jäger, and J. Tulip, "Pulsed quantum cascade laser-based cavity ring-down spectroscopy for ammonia detection in breath," *Applied Optics*, vol. 45, pp. 9230-9237, 2006.
[33] D. Halmer, G. v Basum, P. Hering, and M. Mürtz, "Mid-infrared cavity leak-out spectroscopy for ultrasensitive detection of carbonyl sulfide," *Optics Letters*, vol. 30, pp. 2314-2316, 2005.
[34] BAM, Bundesanstalt für Materialforschung und -prüfung, Berlin, Germany, http://www.bam.de.
[35] VSL, Dutch Metrology Institute, Delft, The Netherlands, http://www.vsl.nl/
[36] ISO/IEC 17025:2005, General requirements for the competence of testing and calibration laboratories. Available from: http://www.iso.org/iso/catalogue_detail.htm?csnumber=39883.

8 Measurement of line strengths and broadening coefficients of CO_2

8.1 Introduction

In the last decades, advances in laser technology and spectroscopic methods have led to a tremendous improvement in the line strength and broadening coefficients measurements. Measured line data such as the line strength and broadening coefficients are used as input parameters for climate change and radiation transfer models in atmospheric science. The line strengths of CO_2, for instance, are used to quantify molecular species in gas analysis application such as environmental monitoring.

Carbon dioxide (CO_2) is a green house gas. Precise knowledge of its line data is impacting to breath analysis and environmental monitoring. Fourier transform infrared (FTIR) and laser absorption spectrometers have been widely used to carryout CO_2 line data measurements with most extensive studies done with FTIR spectrometers [1], [2]. However, FTIR spectrometers have lower resolution compared to laser spectrometers such as TDL-spectrometers as discussed in chapter 1.

Many spectroscopists have quantified CO_2 line data using different types of laser spectrometers [3-5]. The retrieved line data have been fed into data bases such as HITRAN [6] and GEISA [7]. These data bases provide valuable information of the line data of CO_2. However, up to now, the relative uncertainties of the majority of CO_2 line data are in the 2–5% range [6]. In some other cases the line data uncertainties are even larger than 10 %, undefined, or simply unreported. In addition, the application of metrological principles like the GUM [8] to spectrometric measurements was rarely reported [9] and the traceability of measured line data for CO_2 has been sparsely realized by spectroscopists [9]. As a consequence, also the *TILSAM* method suffers from the unavailability of traceable line strengths and compared to traditional gas analysis applications such as GC, large associated uncertainties. However, a report, dealing with a single line, has addressed some of these issues [4].

In this chapter, measurements of the line strengths, self and nitrogen broadening coefficients of the R(10)-R(14) lines of CO_2 in the ro-vibrational band around 2µm are presented. The measurements were done using TDLAS. The measured line strengths and broadening coefficients are compared to available literature data.

8.2 Measurement of line strengths of the R(10), R(12), R(14) line of CO_2 in the ro-vibrational band around 2 µm.

8.2.1 Theory, conceptual background

A brief background of line strengths and the expression to calculate the line strength S_T of a molecular transition at gas temperature T (Eqn. (2.9)) is presented in section 2. Eqn. (2.26) can be rewritten as,

$$A_{\text{line}} = S_T \cdot \frac{x_{\text{species}} \cdot r_{\text{iso}} \cdot p_{\text{total}} \cdot L}{k_B \cdot T} = S_T \cdot \chi \tag{7.1}$$

where, $\chi = x_{\text{species}} \cdot p_{\text{total}} \cdot r_{\text{iso}} \cdot L/(k_B \cdot T)$. The line strength ($S_T$) is identified as the slope of a linear relation of A_{line} versus χ.

8.2.2 Setup

The TDL-spectrometer similar in its implementation to that shown in Figure 3.1 was used to perform the line strength measurements presented in this chapter. The same diode laser type emitting at 2.004 µm was used for analysis. In order to perform spectrometric measurements, the wave length of the DFB diode laser was swept with a current ramp at a frequency of 138.9 Hz. Instead of the 0.82 m or 21 m gas cell in Figure 3.1, a 0.2 m gas cell utilized. The standard uncertainty of the path length of the gas cell was $2.9 \cdot 10^{-9}$ m. The path length of the gas cell and its uncertainty were certified by the department for coordinate measurements of the PTB. For signal detection, two photo diodes were employed. The signals from two photo diodes (a reference and a sample signal) were digitized by a 16 bits National Instrument DAC at a sampling rate of 1.2 MS/s.

8.2.3 Line strength quantification

To quantify the line strengths of the R(10), R(12) and R(14) lines of CO_2 at 4985.93 cm^{-1}, 4987.31 cm^{-1}, and 4988.65 cm^{-1}, respectively, pure CO_2 of quality 5.3 was injected into the 20 cm gas cell. The spectrometric measurements were performed varying the total pressure in the gas cell between 4 and 80 hPa. This pressure range was chosen, depending on the width of the spectral line, to minimize the influence of neighbouring CO_2 line on the probed transitions. The temperature tunability of the laser of 0.45 $cm^{-1}/°K$ was used to tune the emission wave length to reach the line of interest.

Figure 8.1 depicts absorbance data of the TDL-spectrometer for line strength quantification. The R(12) line of CO_2 at 4987.31 cm^{-1} was probed to derive the absorbance data. For the data in Figure 8.1 a signal to noise level of 250 was calculated. The wave number axis in Figure 8.1 was generated using the sweep rate (r_{sweep}) and center wave number of the R(12) transition of CO_2 of 4987.31 cm^{-1}. The value of the sweep rate was calculated in a similar manner as described in section 4.

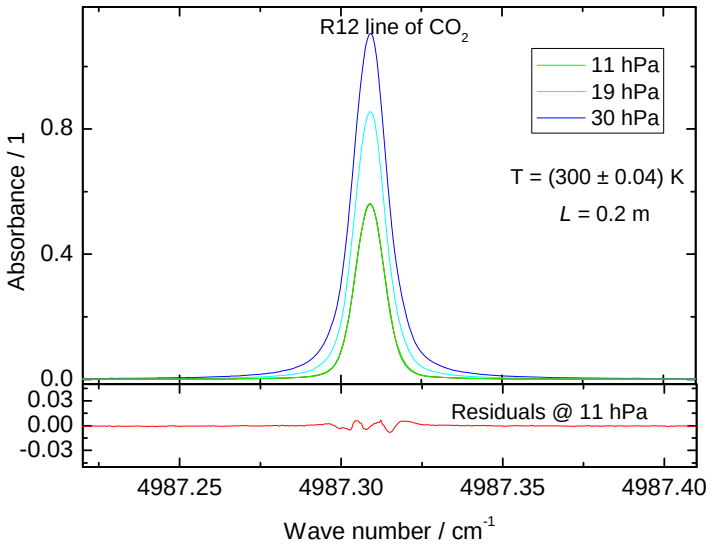

Figure 8.1: Upper panel: Measured R(12) line at different pressures as a function of wave number. Lower panel: Residuals from fitting a Voigt profile to the measured absorbance data at 11 hPa.

A Voigt profile was fitted to the absorbance data, by means of non-linear least square fit [10] (Levenberg-Marquardt), to derive the line area ($A_{\mathrm{line}(T)}$). The Gaussian width was kept fixed during each fitting process. The value of the Gaussian width was calculated using Eqn. (2.13). The residuals from the fit are shown on the bottom panel of Figure 8.1. The "w" structure visible on the residuals at 11 hPa, indicates the presence of collisional narrowing affecting the line shape which cannot be appropriately modeled by the Voigt profile. However, from the oscillatory structure it can be expected that collisional narrowing has a marginal influence on the line area that is less affected [11].

Using the linear model expressed by Eqn. (7.1), a "regression-based" line strength value for the R(12) line of CO_2 can be calculated. The regression-based line strength value is the slope of a linear relation between A_{line} and χ.

Line strength values in literature are typically reported at the temperature of $T_0 = 296$ K. This is to facilitate comparability and to conform to HITRAN convention. Hence, to derive the line strength at 296 K, all $A_{\mathrm{line}(T)}$ values were transferred from the measured gas temperature T to the reference temperature $T_0 = 296$ K using the model $A_{\mathrm{line}} = A_{\mathrm{line}(T)} \cdot (T_0/T)^{\mathrm{j}}$, where j€ℜ [6], [12]. In this work, j = 1.25 was used as explained in the following

Derivation of j

The approximation $A_{\mathrm{line}} = A_{line(T)} \cdot (T_0/T)^{\mathrm{j}}$ was derived from Eqn. (2.9), i.e.,

$$S_T = S_{T_0}\left(\frac{Q_{T_0}}{Q_T}\right)\exp\left\{-hc\frac{E_i''}{k_B}\left(\frac{1}{T}-\frac{1}{T_0}\right)\right\}\frac{\left[1-\exp\left\{-hc\frac{\tilde{\nu}_{0,i}}{k_B T}\right\}\right]}{\left[1-\exp\left\{-hc\frac{\tilde{\nu}_{0,i}}{k_B T_0}\right\}\right]} \tag{7.2}$$

which is also approximated by Eqn. (2.11),

$$S_T = S_{T_0}\left(\frac{T_0}{T}\right)^j\exp\left\{-hc\frac{E}{k_B}\left(\frac{1}{T}-\frac{1}{T_0}\right)\right\}\frac{\left[1-\exp\left\{-hc\frac{\tilde{\nu}_0}{k_B T}\right\}\right]}{\left[1-\exp\left\{-hc\frac{\tilde{\nu}_0}{k_B T_0}\right\}\right]} \tag{7.3}$$

From Eqn. (2.25) (expressing the Beer Lambert Law), the line area is directly proportional to the line strength. This implies that the line area can be approximated to $A_{\text{line}} = A_{\text{line}(T)}\cdot(T_0/T)^j$, (approximation based on Eqn. (7.3)). To derive a value of j, Eqn. (7.2) and (7.3) were compared while varying j. The values of Q_{T0} and Q_T were calculated using Eqn. (2.10).

Figure 8.2a shows plots of the line strength values of the R(12) line of CO_2 calculated using Eqn. (7.2) (open triangles) and Eqn. (7.3) (solid dots, stars and open circles) as a function of temperature T. As shown in Figure 8.2a, the line strength temperature dependent functions Eqn. (7.2) and (7.3), agree (open triangles and open circles) for j = 1.25. This is also visible in the values of the relative deviations (0.03 %), of the values of S_T calculated using Eqn. (7.3) from S_T evaluated using Eqn. (7.2), in the top panel of Figure 8.2a.

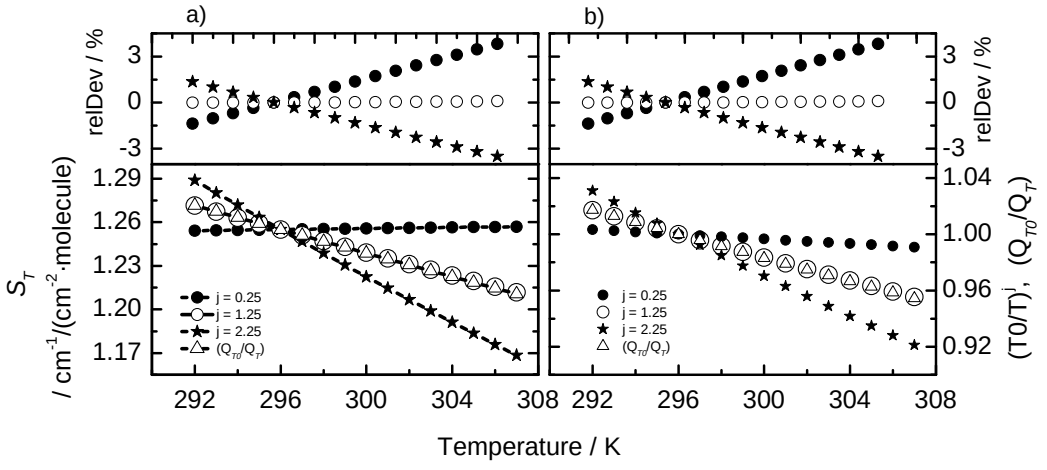

Figure 8.2: Plot of a) S_T and the relative deviation (relDev) of S_T calculated using Eqn. (7.3) from that calculated using Eqn. (7.2), and b) $(T_0/T)^j$ and (Q_{T0}/Q_T) as a function of temperature. The Line strengths of the R(12) transition of CO_2 calculated using Eqn. (7.2) are represented by open triangles and those

evaluated using Eqn. (7.3) for j = 0.25, 1.25, and 2.25 are represented by solid dots, open circles and stars, respectively.

Figure 8.2b shows the plot of the $(T_0/T)^j$ and (Q_{T0}/Q_T) that confirms the shape of the line strength temperature dependence curves in Figure 8.2a and further validate the value of j = 1.25. The spread of the values of j were assumed to have rectangular distribution with half widths equal to 0.25. The reason for chosing a half width of 0.25 for j was because a change in the j value of 0.25. i.e., j = 1 or 1.5, were to result to relative deviations of $(T_0/T)^j$ from (Q_{T0}/Q_T) in the subpercentage range compared to the 3 % (see Figure 8.2) for j = 0.25 or 2.25 (half width of j is 1) for the temperature range (working range) in Figure 8.2.

Figure 8.3 depicts a generalized linear regression (GLR) of values of $A_{line} = A_{line(T)} \cdot (T_0/T)^j$, j = 1.25, of the R(10), R(12) and R(14) transitions of CO_2 (see example spectra in Figure 8.1) as a function of the values of $\chi = x_{species} \cdot p_{total} \cdot r_{iso} \cdot L/(k_B \cdot T)$ used to derive the respective line strengths. The standard uncertainties of the line areas in Figure 8.3 (smaller than symbol signs) are in the ± 0.8 % range, relative. The line area uncertainties were derived by means of the GUM workbench [12] using $A_{line} = A_{line(T)} \cdot (T_0/T)^j$ as model equation. The standard uncertainties of the χ values (smaller than symbol signs) are in the ± 0.6 % range, relative. The values of χ and the associated uncertainties were calculated by the GUM workbench [12] (Appendix V), taking into account the uncertainty of p_{total}, L, k_B, r_{iso} and T whose uncertainty figures were all in the subpercentage range (Appendix V).

The GLR in Figure 8.3a, b and c yielded regression-based line strength values (S_{296K}) for the respective CO_2 transitions. The generalized linear regressions were performed by the B_Least software [13]. The expanded uncertainties of the regression-based line strength values of the R(10), R(12) and R(14) lines of CO_2 in Figure 8.3 are ±2.2, ±1.6 and ±2.0 relative, $k = 2$, respectively.

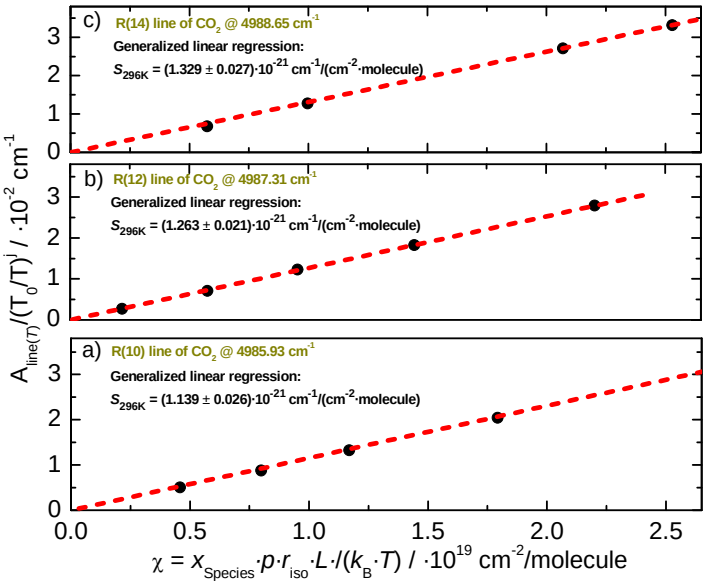

Figure 8.3: Plot of determined line area as a function $\chi = x_{species} \cdot p_{total} \cdot L/(k_B \cdot T)$ to derive a value for the line strength of the R(10), R(12) and R(14) lines of CO_2 at 4985.93 cm^{-1}, 4987.31 cm^{-1}, and 4988.65 cm^{-1}, respectively. The uncertainties in the line area values are in the ± 0.8 % range, relative, while those of the χ values are in the ± 0.6 % range, relative.

Alternatively, individual line strength (S_T) values (Eqn.(7.1)) calculated at each value of χ can be transferred to a line strength figures at T_0 (S_{T0}). Then, by averaging all values of S_{T0}, a directly retrieved line strength figure, given by the mean value, is calculated. Thus, for the data presented in Figure 8.3a, b and c, for the R(10), R(12) and R(14) transitions of CO_2, directly retrieved line strength values were calculated. The calculation of the directly retrieved line strength figures and respective uncertainties were computed by the GUM workbench. Uncertainty budgets, of the directly retrieved line strength value of the R(10) transition is shown in Appendix V.

Table 8.1 compares regression-based and directly retrieved line strength values of the R(10), R(12) and R(14) lines of CO_2.

Table 8.1: Regression-based (S_{reg}) and directly retrieved (S_{dir}) line strength figures for the R(10), R(12) and R(14) lines of CO_2. The uncertainty figures of the line strength values are all expanded uncertainties ($k = 2$).

Line	Line center / cm^{-1}	S_{reg} / 10^{-21} $cm^{-1}/(cm^{-2}\cdot mlecule)$	S_{dir} / 10^{-21} $cm^{-1}/(cm^{-2}\cdot mlecule)$	Normalized error $\lvert E_n \rvert$
R10	4985.93	1.139 ± 0.026	1.115 ± 0.012	0.8

R12	4987.31	1.263 ± 0.021	1.251 ± 0.017	0.4
R14	4988.65	1.329 ± 0.027	1.293 ± 0.014	0.9

The relative expanded uncertainties of the directly retrieved line strength figures of the R(10), R(12) and R(14) lines of CO_2 in Table 8.1 are ±1.0 % and ±1.2 %, and ±1.0 %, $k = 2$, respectively. The normalized error, all less than 1, in the last column in Table 7.1, indicate that the regression based and the directly retrieved line strength values agree with each other.

8.2.4 Discussions

Two data retrieval strategies have been used to derive the line strengths of the R(10), R(12) and R(14) transitions of CO_2. Although the S_{reg} values in Table 8.1 are larger than the S_{dir} values, the two values agree with each other. This is visible on the column holding the respective normalized error $|E_n|$ in Table 8.1.

Applying the linear model to values of $A_{line} = A_{line(T)} \cdot ((T_0/T)^j$ versus $\chi = x_{species} \cdot p_{total} \cdot r_{iso} \cdot L/(k_B \cdot T)$, whose slope is the line strength figure, some kind of systematic errors might be detected based on the value of the intercept. The linear model in Eqn. (7.1) does not predict any intercept value. Therefore, the intercept parameters resulting from the GLRs shown in Figure 8.3 are expected to be zero or insignificant. Hence, for instance, the intercept parameter given by the GLR in Figure 8.3b is $(-4.5 \pm 5.0) \cdot 10^{-5}$ cm^{-1}. Although not zero, the intercept parameter is insignificant, as its value is smaller than the uncertainty, indicating that the experimental conditions of the TDL-spectrometer used to perform the line strength measurement were appropriately described.

Regarding the derivation of the line strength figures presented above, the uncertainties of all the input quantities, such as the path length, the temperature and the pressure, were considered. The evaluation of the uncertainties of the measured line strength figures was done following metrological principles outlined in the GUM [8]. An uncertainty budget of the directly retrieved R(10) line strength figure is shown in Appendix V. Since the directly retrieved and the regression based line strength figures agree, Table 8.2 holds the measured line strength values (S_{dir}) at the reference temperature of 296 K for the R(10) to R(14) lines comparing them to corresponding values from literature.

The normalized errors in Table 8.2, calculated using the measured line strength results and the respective literature values, of the R(10), R(12) and R(14) line of CO_2 are less than one except that of the R(10) line strength of [14], thus, showing that these line strength values agree with each other. The disagreement of the line strengths of this work with those of [14] is mostly due to the extremely small uncertainties reported by [14]**.**

It should be noted here that, the line strength of the R(12) transition in this work of $(1.251 \pm 0.015) \cdot 10^{-21}$ $cm^{-1}/(cm^{-2} \cdot molecule)$ in the 2nd column of Table 8.2 agree perfectly with a previous value of $(1.255 \pm 0.0145) \cdot 10^{-21}$ $cm^{-1}/(cm^{-2} \cdot molecule)$ measured previously by PTB [4]

(on the last column of Table 8.2). Therefore, measured by a different sensor, the traceable line strength result for the R(12) in [4] is again confirmed.

Table 8.2: Measured line strengths (S x 10^{-21} ·cm^{-1}/(cm^{-2}·molecule)) values compared to HITRAN08 and previous studies. The quantities U_{rel} and $|E_n|$ are the relative uncertainties and the normalized errors, respectively.

Line	Wave number	S This work(S_{dir}) U_{rel} ±1.2 % range	S HITRAN08[a] U_{rel} ±1.9 % range	$\|E_n\|$ HITRAN08[a]	S Casa et al.[b] U_{rel} ±0.1 % range	$\|E_n\|$ Casa et al.[b]	S Thoth et al.[c] U_{rel} ±1.0 % range	$\|E_n\|$ Thoth et al.[c]	S Regalia et al.[d] U_{rel} ±3.2 % range	$\|E_n\|$ Regalia et al.[d]	S Padilla et al.[e] U_{rel} ±1.0 % range	$\|E_n\|$ Padilla et al.[e]
R10	4985.93	1.115 ± 0.012	1.127±0.021	0.5	1.1366±0.0012	1.7	1.119±0.008	0.3	-	-	-	-
R12	4987.31	1.251 ± 0.017	1.222±0.023	0.9	1.2344±0.0014	0.9	1.222±0.012	0.9	1.23±0.04	0.5	1.255±0.0145	0.2
R14	4988.65	1.293 ± 0.014	1.275±0.024	0.6	1.2889±0.0013	0.2	-	-	1.30±0.03	0.2	-	-

Note: Units: S - x 10^{-21} ·cm^{-1}/(cm^{-2}·molecule)), U_{rel} - %, Wave number – cm^{-1}

a –reference [6]
b-reference [14]
c-reference [15]
d-reference [16]
e-reference [4].

The relative uncertainties of S_{dir} presented in Table 8.2 are in the ±1.2 % range, $k = 2$. This relative expanded uncertainties of e.g. the R(10) line of CO_2, of ±1.0 % is an improvement to the uncertainty of $1 \leq u(S_{To}) < 2.0$ % given for these line by HITRAN [6]. The relative expanded uncertainty of the line strength results in this work, in the ±1.0 % range, might be similar to most of the respective uncertainties from literature in Table 8.2, except of those of [14]. However, the methods (not described here) of deriving the uncertainties were different. Note, the uncertainties of the measured line strengths of this work were calculated in accordance with the guidelines of the GUM [17]**.**

Regarding the uncertainty figures (quoted accuracies) of [14], they were calculated as 1-σ the standard error. Hence, a direct comparison with [14] would be to compare the standard uncertainty of the line strengths of this work, close to 0.5 % relative ($k = 1$), with the respective uncertainties of [14] in the range of 0.1 % relative. However, the uncertainties of the line strengths of this work are still large compared to those of [14]**.** Nevertheless, as noted above, compared to the calculation of the uncertainties of the line strengths of [14], the uncertainties of the line strengths in this work (see Appendix V**)** were calculated following the guidelines of the GUM [8] which are sparsely applied [9].

A novelty of this work was the fact that the traceability of all input parameters such as the path length, the temperature and pressure to the SI was addressed. Traceable line strength figures and the associated GUM compliant uncertainties are rarely reported. This concern has also been raised in a review [9]. Therefore, recently, increased effort have been started to improve this situation [18], although, line strengths data have been measured throughout recent years [4], [6], [14-16].

The metrological quality of line data has become indispensible as outlined in [18]. Relative uncertainties in the ±1 % range might be desirable in gas analysis application such as in environmental monitoring and breath analysis. The line strength value derived in this work can be used as input parameters to model spectroscopic measurements in gas metrology where traceability to the SI is a prerequisite. Carbon dioxide is a green house gas, therefore, the line strength results presented in this work could serve also as input parameters for codes used to model e.g. climate change.

Regarding the uncertainty of the line strength results of this work, a further improvement would be to reduce the uncertainty of the line area and that of r_{iso} (see Appendix V). The uncertainty of the line area is the most significant contribution to the final uncertainty of the line strength, the index values being the largest as presented in Appendix V, closely followed by the uncertainty of r_{iso} (due to $u(x_{12CO2})$).

The standard uncertainties of the line areas $u(A_{line})$ as mentioned above were in the range of ±0.8 % relative. The $u(A_{line})$ were based on the uncertainty of the line area fitting $u(A_{line(T)})$ [19] and the sweep rate $u(r_{sweep})$, $r_{sweep} = FSR/FSR_{SP}$ (see chapter 4). The $u(r_{sweep})$) in the range of ±0.7 % relative was the most significant source of uncertainty to $u(A_{line})$. The

uncertainty of the sweep rate was estimated in a similar manner as described in section 2, with the uncertainty of FSR_{SP} providing the larger contribution to the uncertainty of r_{sweep}. An improvement in the uncertainty of the sweep rate would be to reduce the uncertainty of FSR_{SP}, although, instability in the operation temperature of the laser might already be the limiting factor to reduce this uncertainty.

The uncertainty of $r_{iso} = x_{12C16O2} / x_{12C16O2HIT}$, where x_{12C16O} and $x_{12C16OHIT}$ are the abundances of $^{12}C^{16}O_2$ in the sample and the conventional value given by HITRAN, respectively, was significant (see Appendix V**)**. Generally, in spectroscopy, line strengths are given for a certain norm-abundance of the respective probed isotopologue. The abundance of the probed isotopologue in a sample may differ from this norm-abundance. Therefore, the quantity r_{iso} was introduced into the model equation. To account for the lack of knowledge of the abundance of the $^{12}C^{16}O_2$ in the 5.3 quality CO_2, r_{iso} was set to unity and its standard uncertainty was calculated to be ±0.8 % relative, $k = 1$. The standard uncertainty of r_{iso} was computed based on information of the isotopic composition of elements recently published in [20].

8.3 Measurement of the self and nitrogen broadening coefficients of CO_2

8.3.1 Quantification of the self broadening coefficients of the R(10), R(12), and R(14) transitions of CO_2 in the ro-vibrational band around 2 µm.

The experimental setup described in the previous section was also used to perform the measurements of the self and nitrogen broadening coefficients of the R(10) to R(14) transitions of CO_2 in the ro-vibrational band around 2 µm. The spectrometric measurements were performed by first injecting 4 hPa of CO_2 into the gas cell and subsequently increasing the total pressure in the gas cell (p_{total}), in steps, to about 100 hPa.

To calculate the self broadening coefficients of the three lines under investigation, Eqn. (2.16) was used, yielding,

$$\Delta\tilde{\nu}_L = 2 \cdot p_{CO2} \cdot \gamma_{CO2} \cdot \left(\frac{T_0}{T}\right)^n \tag{7.4}$$

In this work, n = 0.5 was used as discussed in section 2.3.3. Hence, from Eqn. (7.4), the slope value from a GLR of values of the Lorentzian width $\Delta\tilde{\nu}_L$ (FWHM) plotted as a function of the partial pressure of CO_2 (p_{CO2}) will result to the self broadening coefficient γ_{CO2} of CO_2.

The measured spectra used to derive the line strength values described in the previous section were used additionally to derive the respective CO_2 self broadening coefficients of the probed transitions. Figure 8.4 depicts a plot of the Lorentzian widths $\Delta\tilde{\nu}_L$ of the R(10), R(12) and the R(14) lines of CO_2 as a function of the partial pressure of CO_2 used to determine the individual self broadening coefficients. The partial pressures of CO_2 are multiplied by $(T_0/T)^n$. The partial pressure values of CO_2 were calculated using the amount fraction of the 5.3

quality CO_2 (x_{CO2} = 0.999993 mol·mol^{-1}) and the measured total pressure (p_{total}), i.e., p_{CO2} = 0.999993·p_{total}.

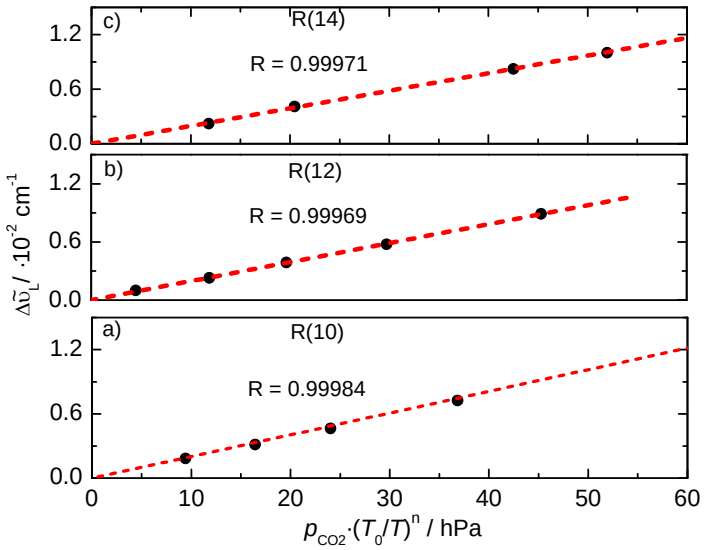

Figure 8.4: Plot of the derived Lorentzian line widths (FWHM) of the R(10), R(12) and R(14) transitions of CO_2 as a function of the partial pressure of CO_2.

Generalized linear regressions were applied to data presented in Figure 8.4. The slopes from the GLR, calculated by the B_Least software [21], yielded the respective self broadening coefficients of CO_2. For instance, the slope of the linear relation of the Lorentzian width of the R(12) line of CO_2 versus the partial pressure resulted to a value of γ_{CO2} for the R(12) line transition of 9.81·10^{-5} cm^{-1}/hPa, equivalent to 99.4·10^{-3} cm^{-1}/atm. Its expanded uncertainty is ±1.86·10^{-6} cm^{-1}/hPa, equivalent to about 1.9·10^{-3} cm^{-1}/atm, i.e., ±1.9 %, relative, k = 2. The R values shown in Figure 8.4 show a good agreement between the linear model and the measured data.

Table 8.3 summarizes measured self broadening coefficients of the R(10), R(12) and R(14) lines of CO_2. The expanded uncertainties of the self broadening coefficients of the R(10), R(12) and R(14) lines of CO_2 are ± 0.4 %, ± 1.9 % , ± 2.3 % relative, k = 2, respectively. The self broadening coefficients are compared to values from the HITRAN data base [6]. The deviation of the self broadening coefficients from the HITRAN values is in the large negative range (-0.6 % relative). This disagreement between the measured broadening coefficients and the values taken from the HITRAN data base [6] is also visible in the column holding the normalized errors ($|E_n|$). The values of the respective normalized errors are greater that one, thus, showing that measured self broadening coefficients do not agree with the values from the HITRAN data base [6].

The large negative deviation (-6 % relative) of the self broadening coefficients, in this work, from the values of [6] might be due to the composition of the used analyte (the 5.3 quality

CO_2). The abundance of $^{12}C^{16}O_2$ isotopologue in the 5.3 quality of CO_2 was unknown whereas that of HITRAN [6] was 0.9842.

Also, the value of the temperature dependent coefficient of n = 0.5 might have been the reason for the negative deviation of the measured self-broadening parameters from the values of HITRAN [6]. HITRAN in its current form does not contain temperature dependent coefficients for pure CO_2. Instead a temperature dependent coefficient of 0.7 for air is reported for the R(10), R(12) and R(14) transitions. If n = 0.7 was used, it were to correspond only to a change of about 0.3% in the self broadening coefficients. The 0.3 % change in the self broadening coefficients is already covered by the respective expanded uncertainties of the self broadening coefficients of the R(10), R(12) and R(14) transitions of CO_2 in the range of $0.4 \leq u(\gamma_{CO2}) \leq \pm$ 2.3 % relative, $k = 2$.

Thus, one could conclude here that the composition of the gas mixture might have been the reason for the negative deviation of the measured self broadening coefficients from the values taken from the HITRAN data base.

Table 8.3: Measured self broadening coefficients of CO_2 ($\gamma_{CO2MEAS}$) compared to values from the HITRAN data base (γ_{CO2HIT}) **[6]**.

Line	Wave number / cm^{-1}	$\gamma_{CO2MEAS}$ / $\cdot 10^{-3}$ cm^{-1}/atm	γ_{CO2HIT} / $\cdot 10^{-3}$ cm^{-1}/atm	$\lvert E_n \rvert$
R10	4985.93	104.8 ± 0.4	109.0 ± 2.1	1.9
R12	4987.31	99.4 ± 1.9	105.0 ± 2.0	2.0
R14	4988.65	96.9 ± 2.2	103.0 ± 2.0	2.1

8.3.2 Quantification of the nitrogen broadening parameters of the R(10), R(12), and R(14) transitions of CO_2 in the ro-vibrational band around 2 µm.

The N_2 broadening coefficients of the R(10), R(12) and R(14) lines of CO_2 were measured using the setup described in the previous subsection. To quantify the nitrogen broadening coefficients of these three lines, about 7 hPa of the 5.3 quality CO_2 was first injected into the 20 cm gas cell. Subsequently, nitrogen was added to the CO_2 in the gas cell to a total gas pressure of about 450 hPa. This was to keep the partial pressure of CO_2 as small as possible, thus reducing the effect of self broadening, while keeping that of the nitrogen high enough to increase its perturbation on CO_2. The spectrometric nitrogen broadening measurements were performed while stepping down the total gas pressure to about 20 hPa.

The nitrogen broadening coefficients (γ_{N2}) were calculated using Eqn. (2.16), leading to

$$\Delta\tilde{\nu}_L = 2\cdot p_{CO2}\cdot\gamma_{CO2}\cdot\left(\frac{T_0}{T}\right)^n + 2\cdot p_{N2}\cdot\gamma_{N2}\cdot\left(\frac{T_0}{T}\right)^n \tag{7.5}$$

The partial pressures p_{CO2} and p_{N2} were calculated using $p_{CO2} = x_{CO2}\cdot p_{total}$ and $p_{N2} = (1-x_{CO2})\cdot p_{total}$, assuming a pure binary mixture, respectively. The amount fraction of the analyte x_{CO2} was evaluated using Eqn. (2.26). The measured line strengths (see Table 8.2) were used for the calculation of x_{CO2}. Eqn. (7.5) can be rewritten as

$$\begin{aligned}\Delta\tilde{\nu}_L - 2\cdot p_{CO2}\cdot\gamma_{CO2}\cdot\left(\frac{T_0}{T}\right)^n &= 2\cdot p_{N2}\cdot\gamma_{N2}\cdot\left(\frac{T_0}{T}\right)^n \\ \Delta\tilde{\nu}_{LN2} &= 2\cdot p_{N2}\cdot\gamma_{N2}\cdot\left(\frac{T_0}{T}\right)^n\end{aligned} \tag{7.6}$$

where, $\Delta\tilde{\nu}_{LN2} = \Delta\tilde{\nu}_L - 2\cdot p_{CO2}\cdot\gamma_{CO2}\cdot(T_0/T)^n$. Since the self broadening coefficients (γ_{CO2}) of the three lines were already derived in the previous section, the slope from a GLR applied to the values of $\Delta\tilde{\nu}_{LN2}$ as a function of $p_{N2}\cdot(T_0/T)^n$, for all three lines, yielded the respective nitrogen broadening coefficients. Figure 8.5 shows these plots of the Lorentzian line widths $\Delta\tilde{\nu}_{LN2}$ of the R(10), R(12) and R(14) lines of CO_2 as a function of $p_{N2}\cdot(T_0/T)^n$. The uncertainties of the $\Delta\tilde{\nu}_{LN2}$ values were calculated by means of the GUM workbench software. The expression $p_{N2}\cdot(T_0/T)^n$ was used in GUM workbench files to calculate the uncertainties in the abscissa values in Figure 8.5.

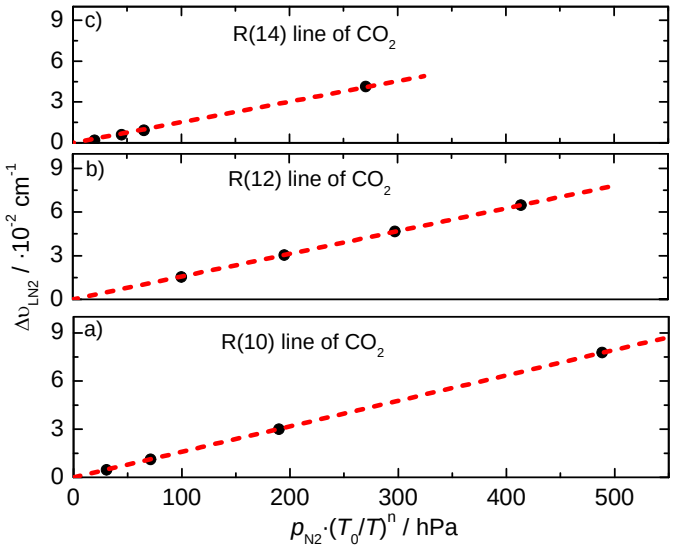

Figure 8.5: Plot of the derived Lorentzian widths as a function of $p_{N2}\cdot(T_0/T)^n$

Table 8.4 summarizes the N_2 broadening coefficient of the R(10), R(12) and R(14) lines of CO_2 resulting from the GLR depicted in Figure 8.5. The expanded uncertainties of the N_2

broadening coefficients of the R(10), R(12) and R(14) lines of CO_2 are ±1.5 %, ±2.1 % and ±2.6 % relative, $k = 2$, respectively. The γ_{N2} coefficients in Table 8.4 are compared to air broadening coefficients taken from the HITRAN data base [6]. Although, not a direct comparison, there is some agreement for the R(10) and R(12) transition of CO_2 shown by the values of the normalized errors $|E_n|$ being smaller than 1.

Table 8.4: N_2 broadening coefficients of CO_2 γ_{N2} compared to air broadening coefficients of CO_2 γ_{Air} values from **[6]**.

Line	Wave number / cm^{-1}	γ_{N2} / 10^{-3} cm^{-1}/atm	γ_{Air}[a] / 10^{-3} cm^{-1}/atm	$\lvert E_n \rvert$
R10	4985.93	80.8 ± 1.2	79.9±1.5	0.4
R12	4987.31	79.9 ± 1.7	78.0±1.5	0.8
R14	4988.65	79.5 ± 2.1	76.5±1.5	1.1

a-reference [6].

The air broadening coefficients of [6] were measured using a gas sample containing 21 % O_2 and 79 % nitrogen [6]. Therefore, a direct comparison with air broadening coefficients of [6] can be done by calculating the air broadening coefficients of three transitions in Table 8.4 using the respective O_2 and nitrogen broadening coefficients. However, since the O_2 broadening coefficients of the R(10), R(12) and R(14) transitions of CO_2 were not measured in this thesis, the comparison could not be made. Nevertheless, due to the fact the measured γ_{N2} (Table 8.4) are slightly higher than the γ_{air} of [6], one could conclude that the γ_{CO2N2} of the three CO_2 transitions are inline to a large extend.

8.4 Conclusions

A TDL-spectrometer was used to measure the line strength and broadening coefficients of CO_2 in the ro-vibrational band around 2 µm. The guidelines of the GUM were followed while deriving the line strength and collisional broadening coefficients of the R(10), R(12) and R(14) transitions of CO_2 at 4985.93 cm^{-1}, 4987.31 cm^{-1}, and 4988.65 cm^{-1}, respectively. The traceability of all input quantities, such as the pressure, the temperature and the path length of the gas cell, to the SI were addressed. The relative expanded uncertainties of the directly retrieved line strength figures are in ±1.2 % range, $k = 2$. All line strengths values, with GUM compliant uncertainty figures in a few percentage range, are in good agreement with respective values from literature. It is found that the uncertainties of the measured line strengths are limited to ±1.2 % by the standard uncertainties of the respective sweep rates of ±0.8 % relative. The nitrogen broadening coefficients, derived using measured self broadening coefficients, are in line with the values of HITRAN. The relative expanded uncertainties of the self and nitrogen broadening coefficients are in the ±2.3 % and ±2.6 % range, $k = 2$. The line data measured in this work can be used to model spectrometric

measurements in gas analysis applications such as breath analysis and environmental monitoring where the need for metrologically determined data is becoming more indispensible. The line data in this work can serve as input quantities for spectrometric measurements based on the *TILSAM* method to fulfil the criteria of a primary method.

9 Comparison measurements

The measurements presented in the previous chapters were done using the *TILSAM* method. In order to further prove the validity of the *TILSAM* method, comparison measurements were done by two laboratories**.** The two laboratories involved were named Lab.1 and Lab. 2 being the PTB.

Comparisons are organized as a tool to maintain or achieve international comparability of traceability. They are usually organized at a key or pilot level under the Consultative Committee for Amount of Substance – Metrology in Chemistry (CCQM) [22] or on a European level under the European Association of National Metrology Institutes (EURAMET) [23], respectively. So far, there has been no key comparison or pilot study in gas metrology in which laser spectroscopy has played a role.

There had been many key comparisons in the Gas Analysis Working Group (GAWG) of the CCQM that spectroscopy could compete [22]. Therefore, existing methods of laser spectroscopy have to prove their capabilities to gas metrology in order to play a role in the future. This goal of laser spectroscopic methods can be achieved by organizing comparisons.

The measurement campaign mentioned in the first paragraph of this chapter was carried out within the frame work of the EURAMET 934 project [24] on calibration-free infrared laser spectrometry. Actually, the *TILSAM* method is an outcome of the EURAMET 934 project. The effort in the campaign was to address spectroscopy as a primary method in gas metrology and to establish a comparable metrology basis on absolute amount fraction measuremements based on absolute infrared laser spectroscopy.

Due to the design of the comparison, spectrometric measurements had to be done using TDLAS. Gravimetric gas mixtures of CO_2 in nitrogen prepared by Lab. 3, with CO_2 amount fractions at the 300 µmol·mol^{-1} and 500 µmol·mol^{-1} level, were shipped to Lab. 1 and 2 for analysis. The spectrometric CO_2 amount fraction results were compared to the respective comparison reference value (CRV), which was based on the gravimetric preparation and its subsequent verification, and to those of the other participant.

Note, for this particular comparison, the participants agreed to utilize the same DFB diode laser type for analysis emitting at 2 µm. The R(12) line strength value of $(1.255 \pm 0.00725)\cdot10^{-21}$ cm^{-1}/(cm^{-2}·molecule) at 4987.31 cm^{-1} [4] was chosen in the evaluation process by both participants. The spectrometric amount fraction measurements were following strictly the *TILSAM* method protocol [25].

In the following subsections, spectrometric amount fraction measurements of PTB are presented. In the discussion section the spectrometric CO_2 amount fraction results evaluated at the PTB are compared to the CRVs and to the results from Lab.1.

9.1 Setup

The TDL-spectrometer used for the line strength measurements (chapter 8) was employed to carry out the spectrometic amount fraction measurements for the EURAMET 934 studycomparison [24]. The 0.2 m gas cell was replaced by the multipass gas cell presented in Figure 3.7 set to the the path length of (21.84 ± 0.11) m , whose determination was explained in section 3.1.1.3, for the measurements. The gas pressure was measured by a Baratron capacitance pressure gauge and the temperature with a Pt100-resistance device stuck on the absorption cell.

Carbon dioxide in the optical bench

The carbon dioxide level in the atmosphere is about 380 µmol·mol^{-1}. This means that, residual absorption of CO_2 in the optical bench was significant to the measurements of CO_2 at the 300 µmol·mol^{-1} and 500 µmol·mol^{-1} levels.

Figure 9.1 shows absorbance data, measured when there was no gas mixture in the gas cell (evacuated gas cell), exhibiting the residual CO_2 in the optical bench. A maximum absorbance of 0.008 was measured on the CO_2 content present in the optical bench.

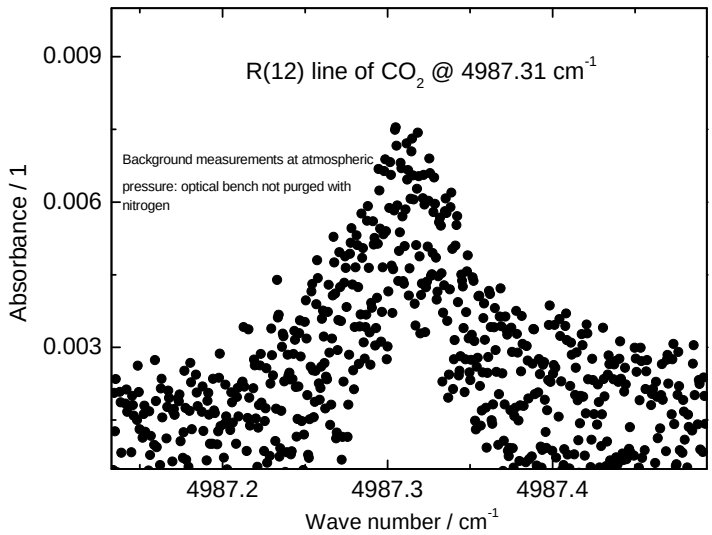

Figure 9.1: Residual CO_2: Plot of the absorbance as a funtion of wave number

In order to calculate the effect of the optical bench CO_2 to any measured spectra, a simulation was done. A simulation using 300 µmol·mol^{-1} CO_2 in nitrogen at a total pressure of 100 hPa and path length 21.84 m path yielded a maximum absorbance of 0.08. This is just about 10 times larger than the maximum absorbance of the CO_2 in the optical bench of 0.008. Therefore, the CO_2 in the optical bench had to be removed before the CO_2 content in the gas

mixture was measured. This concern was crucial in the CO_2 amount fraction measurements presented in this chapter.

In order to remove the CO_2 from the optical bench the TDL-spectrometer was continuously purged with nitrogen before and during measurements. Nevertheless, to be sure that the CO_2 in the optical bench was completely removed while the measurements were being carried out, background measurements done at the beginning and at the end of the measurements were compared (see section 3.3.1.1). These two measurements were also used to check for possible changes of the baseline due to possible fluctuations in the laser intensity. Although, not done here, if residual CO_2 in the optical bench were affecting the measured signals, a differential spectrum (absorbance) could have been derived. A differential spectrum is derived by subtracting the baseline spectrum (background) from measured spectrum with CO_2 present in the gas cell.

9.2 Results

In order to quantitate the CO_2 content in the 300 and 500 $\mu mol \cdot mol^{-1}$ gas mixtures, the measurement procedure described in section 3.3.1.1 was applied. The spectrometric measurements were done following the *TILSAM* method. The total pressure in the 21.84 m multipass gas cell was varied between 100 hPa and 900 hPa.

Figure 9.2a depicts typical absorbance data of the TDL-spectrometer. The data in Figure 9.2a was measued on the 300 $\mu mol \cdot mol^{-1}$ gas mixture. On the wings of the R(12) line of CO_2 in Figure 9.2a a second line (R(33e) at 4987.62 cm^{-1}) is visible that was perturbing the R(12) line. This line was only visible at total gas pressures higher than 500 hPa as shown in Figure 9.2a.

Fitting

Because of the R(33e) line of CO_2, the line area of the R(12) line was calculated by fitting a multi-line Voigt profile to the measured absorbance data. The voigt profile was fitted with the Gaussian widths fixed as calculated at the measured gas temperature for the two lines. On the other hand, if the R(33e) line of CO_2 was negleted, then the residuals from the fit at 500 hPa clearly show the presence to the R(33e) line at 4987.62 cm^{-1} as depicted in the bottom panel of Figure 9.2a.

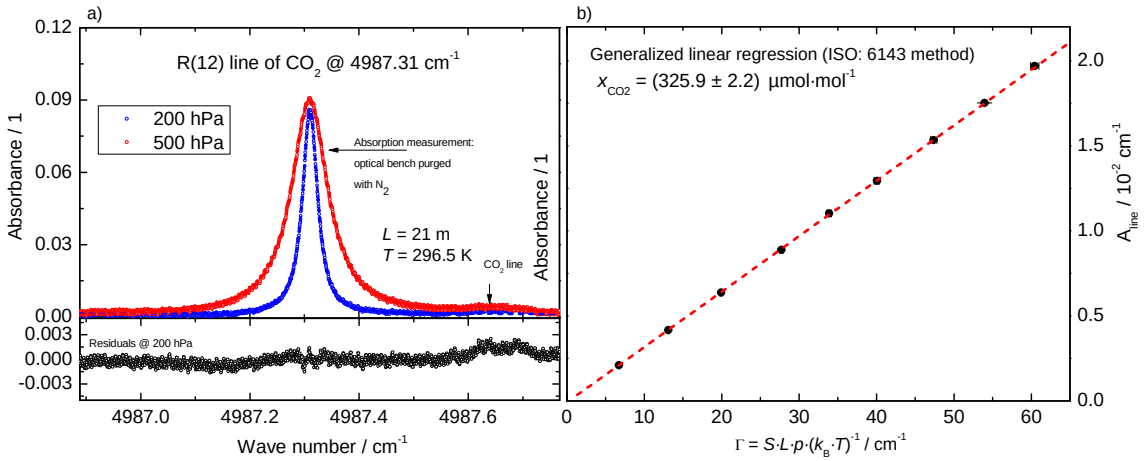

Figure 9.2: CO_2 at 300 µmol·mol^{-1}: a) Plot of derived absorbance data as a function of wave number. b) Plot of the line area as a function of Γ.

Derivation of CO_2 amount fractions at the 300 µmol·mol^{-1} level

Figure 9.2b shows a plot of the line area (A_{line}) of the R(12) line (example data are in Figure 9.2a) as a function of Γ used to derive a regression-based amount fraction result (see section 3.4.1) for the 300 µmol/mol gas mixture. A GLR has been applied to the values of A_{line} versus Γ. The GLR was performed by the B_Least software [21]. An amount fraction of (325.9 ± 2.2) µmol·mol^{-1} is derived from the data in Figure 9.2b.

By averaging individual amount fraction results at the different Γ values in Figure 9.2b, a directly retrieved amount fraction result of (321.6 ± 2.7) µmol·mol^{-1} was calculated. The standard uncertainty of 2.7 µmol·mol^{-1} (0.8 % relative) was evaluated using Eqn. (3.16). An uncertainty budget, holding the uncertainty of individual amount fraction results at different Γ values, for the directly retrieved amount fraction is shown in Appendix VI. The directly retrieved amount fraction result of (321.6 ± 4.3) µmol·mol^{-1} agrees with the regression-based amount fraction of (325.9 ± 2.2) µmol·mol^{-1}as corresponding to the normalized error (see section 3.4.1) of $|E_n| = 0.4$.

Derivation of CO_2 amount fractions at the 500 µmol·mol^{-1} level

The data pocessing procedure described above was also used to derive a spectrometric CO_2 amount fraction at the 500 µmol·mol^{-1} level. A multi-line Voigt profile was fitted to absorbance data in order to derive a value for the line area of the R(12) line. By means of a GLR, a regression-based CO_2 amount fraction of (449.7 ± 3.1) µmol·mol^{-1} was evaluated for the norminally 500 µmol·mol^{-1} gas mixture.

Similarly as for the 300 µmol·mol^{-1} gas mixture, a directly retrieved amount fraction of (447.1 ± 3.7) µmol·mol^{-1} was calculated for the 500 µmol·mol^{-1} gas mixture. Its standard

uncertainty of 3.7 mmol·mol^{-1} (0.8 % relative) was evaluated also using Eqn. (3.16). An uncertainty budget for the directly retrieved amount fraction result of (447.1 ± 3.7) µmol·mol^{-1} is shown in Appendix VI. The directly retrieved amount fraction result of (447.1 ± 3.7) µmol·mol^{-1} agrees with the regression-based amount fraction of (449.7 ± 3.1) µmol·mol^{-1} as confirmed by the normalized error of $|E_n| = 0.3$.

9.3 Comparison and discussions

The regression-based and the directly retrieved CO_2 amount fraction results agree with each other both at the 300 µmol·mol^{-1} and the 500 µmol·mol^{-1} level. The standard uncertainties of all the spectrometric results are in the range of ±0.8 % relative.

Table 9.1 holds the measured, directly retrieved and regression-based amount fraction results of Lab. 1 and 2, compared to the comparison reference values (CRVs). Of the four results reported at each amount fraction level, three are from Lab. 1. The uncertainties of all the directly retrieved and regression-based CO_2 amount fractions in Table 9.1 were calculated in the same manner, i.e., using Eqn. (3.16) and by means of a GLR applied to values of A_{line} plotted as a function of Γ, respectively. The CRVs were provided after the spectrometric CO_2 amount fraction results of Lab. 1 and 2 were reported. Most of the spectrometric CO_2 amount fraction results agree with the CRVs. The agreement in the spectrometric CO_2 amount fraction results is visible in the values of the normalized errors, $|E_n|_{Lab\text{-}CRV}$ in Table 9.1, which are less than unity.

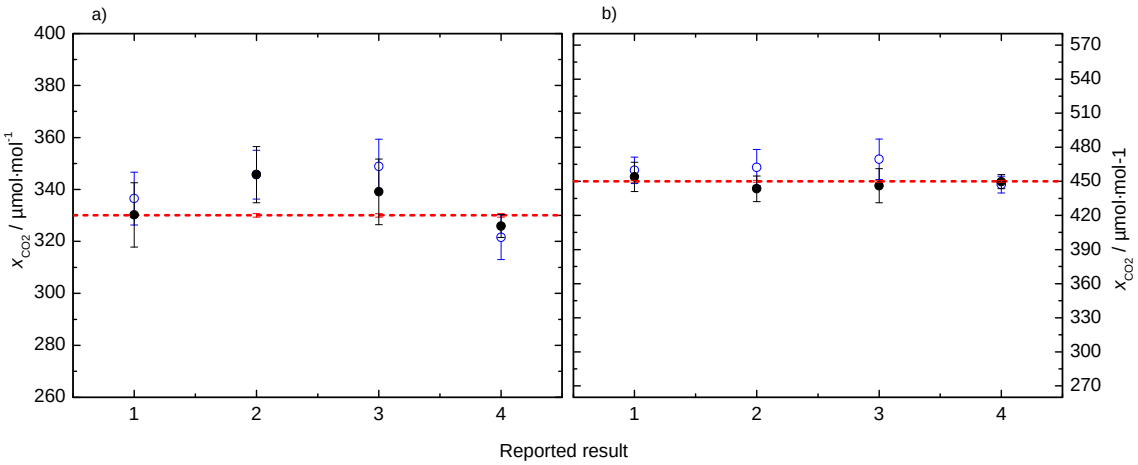

Figure 9.3: Directly retrieved (blue - open circles) and regression-based (black - solid dots) amount fraction results, a) at the 300 mmol·mol^{-1} level and b) at the 500 µmol·mol^{-1} level, as a function of result number. The uncertainties of all the results are expanded uncertainties, $k = 2$. The CRV is represented by the dashed line (red).

The comparability level of the reported results as expressed by the maximum relative deviations from the CRVs, at the 300 µmol·mol^{-1} and the 500 µmol·mol^{-1} level, are 5.7 % and 4.3 %, respectively. This is low compared to typical levels of comparability of gas standards of CO_2 in nitrogen (CCQM-K1.b and CCQM-K52) [22], being in the subpercentage range.

Nevertheless, looking at the results of the regresion-based CO_2 amount fractions at the 500 μmol·mol^{-1} level on Table 9.1, most of the values of the relative deviations are already in the subpercentage range. However, some further inprovements are needed.

To summarize the spectrometric results presented in Table 9.1, Figure 9.3 shows a plot of regression based (solid dots) and directly retrieved (open circles) CO_2 amount fraction results, at the 300 μmol·mol^{-1} and 500 μmol·mol^{-1} levels, as a function of the reported result number. The dashed lines in Figure 9.3 represent the CRVs. The associated uncertainties of the amount fraction results in Figure 9.3 are all expanded uncertainties ($k = 2$) calculated using the standard uncertainties of the results presented in Table 9.1. The uncertainty bars of the results in Figure 9.3 overlap with each other and with the CRVs except of the second result at the 300 μmol·mol^{-1} level, showing that the spectrometric CO_2 amount fraction results are in good agreement with the CRVs.

Note, all spectrometric measurements used to evaluate the amount fraction results in Table 9.1, were done based on the *TILSAM* method. The same type of laser was used to probe the R(12) line of CO_2 at 4987.31 cm^{-1}and a traceable line strength value of the R(12) line of $(1.255 \pm 0.00725)\cdot10^{-21}$ cm^{-1}/(cm^{-2}·molecule), used in the evaluation of the amount fraction results, was taken from [4].

The agreement of the CO_2 amount fraction results, from two laboratories, evaluated using traceable data, shows that the *TILSAM* method applied to the measurement of CO_2 in this thesis is valid. Although, interference by adjacent line might be a problem, when performing measurements based on the *TILSAM* method, these issue can easily be accounted for using appropriated fitting functions such as e.g., a multi-line Voigt profile used in this chapter.

Table 9.1: Comparison: Measured spectrometric amount fraction results compared to the comparison reference value (CRV) and to spectrometric amount fraction results from Lab. 1. The relative deviations (rD) are expressed in percentage (%).

			Spectrometric CO_2 amount fraction results at the 300 µmol·mol^{-1} level							
			Direct retrieval				Regression-based retrieval			
Reported result	CRV	u(CRV)	x_{CO2} / µmol·mol^{-1}		$\lvert E_n \rvert_{Lab\text{-}CRV}$	$rD_{Lab\text{-}CRV}$	x_{CO2} / µmol·mol^{-1}		$\lvert E_n \rvert_{Lab\text{-}CRV}$	$rD_{Lab\text{-}CRV}$
1	330.06	0.66	336.5	5.1	0.6	1.9	330.2	6.2	0.1	0.1
2	330.06	0.66	345.7	4.7	1.6	4.7	345.7	5.4	1.4	4.7
3	330.06	0.66	348.9	5.2	1.7	5.7	339.1	6.3	0.7	2.7
4	330.06	0.66	321.6	4.3	0.9	-2.5	325.9	2.2	0.9	-1.2

			Spectrometric CO_2 amount fraction results at the 500 µmol·mol^{-1} level							
			Direct retrieval				Regression-based retrieval			
Insitute	CRV	u(CRV)	x_{CO2} / µmol·mol^{-1}		$\lvert E_n \rvert_{Lab\text{-}CRV}$	$rD_{Lab\text{-}CRV}$	x_{CO2} / µmol·mol^{-1}		$\lvert E_n \rvert_{Lab\text{-}CRV}$	$rD_{Lab\text{-}CRV}$
1	450.00	0.9	459.7	5.8	0.8	2.1	453.9	6.4	0.3	0.8
2	450.00	0.9	462.2	7.9	0.7	2.7	443.5	5.6	0.5	-1.4
3	450.00	0.9	469.4	8.9	1.0	4.3	446.1	7.5	0.2	-0.8
4	450.00	0.9	447.1	3.7	0.3	-0.6	449.7	3.1	0.1	-0.1

9.4 Conclusions

By using the same diode laser type and probing the same CO_2 line, amount fraction measurements have been performed at CO_2 levels of 300 μmol·mol^{-1} and 500 μmol·mol^{-1} based on the *TILSAM* method. The spectrometric CO_2 amount fraction results, evaluated by two laboratories, using the same line strength figure are in good agreement with the comparison reference value. The agreement in the results proves that the *TILSAM* method is a valid method to perform absolute amount fraction measurements in e.g. breath analysis. Hence, the *TILSAM* method could be projected as a potential gas standard.

9.5 References of chapter 8 and 9

[1] R. A. Toth, L. R. Brown, C. E. Miller, V. M. Devi, and D. C. Benner, *JQSRT*, vol. 109, no. 6, pp. 906-921, (2008).

[2] R.A. Toth, L.R. Brown, C.E. Miller, V. Malathy Devi, and D.C. Benner, JQSRT 109, 906-921 (2008). Supplementedwith results of A. Predoi-Cross, A.R.W. McKellar, D. Chris Benner, V. Malathy Devi, R.R.Gamache, C.E. Miller, et al, *Can.J.Phys.* 87, 517-535 (2009).

[3] G. Casa, D. A. Parretta, A. Castrillo, R. Wehr, and L. Gianfrani, *J. Chem. Phys.*, vol. 127, p. 084311, (2007).

[4] G. J. Padilla-Viquez, J. Koelliker-Delgado, O. Werhahn, K. Jousten, and D. Schiel, *IEEE Trans. Instr. Measur. J.*, vol. 56, pp. 529-533 (2007).

[5] P. Ortwein, W. Woiwode, S. Wagner, M. Gisi, and V. Ebert, *Appl. Phys. B*, vol. 100, pp. 341-347, (2010).

[6] HITRAN2008, http://www.cfa.harvard.edu/HITRAN/, L. Rothman et al., *J. Quant. Spectrosc. Rad. Transf.* vol. 110, pp. 533 (2009).

[7] N. Jacquinet-Husson, N. A. Scott, A. Chédin, and e al., *J. Quant. Spectrosc. Rad. Trans.*, (2008), doi:10.1016/j.jqsrt.2007.12.015.

[8] ISO Guide 98-3, Guide to the Expression of Uncertainty in Measurement, 1. International Organization for Standardization, Geneva 2008, ISBN 9267101889.

[9] L. S. Rothman, N. Jacquinet-Husson, C. Boulet, and A. M. Perrin, *C. R. Physique*, vol. 6, pp. 897-907, (2005).

[10] Levenberg-Marquardt, Numerical Recipes, 2005, http://www.library.cornell.edu/nr/bookcpdf/c15-5.pdf

[11] J. Henningsen and H. Simonsen, *J. Molecular Spectroscopy*, vol. 203, pp. 16-27, (2000).

[12] GUM Workbench, 1.2 Win32, Metrodata GmbH, Grenzach-Wyhlen, Germany 1999, http://www.metrodata.de

[13] BAM, Bundesanstalt für Materialforschung und -prüfung, Berlin, Germany, http://www.bam.de

[14] G. Casa, R. Wehr, A. Castrillo, E. Fasci, and L. Gianfrani, *J. Chem. Phys.*, vol. 130, pp. 184306, (2009).

[15] R. A. Toth, L. R. Brown, C. E. Miller, V. Malathy Devi, and D. Chris Benner, *J. Mol. Spectrosc.*, vol. 239, pp. 221, (2006).

[16] Régalia-Jarlot, V. Zeninari, B. Parvitte, A. Grossel, X. Thomas, P. von der Heyden, and G. Durry, *J. Quant. Spectrosc. Radiat. Transf.*, vol. 101, pp. 325, (2006).

[17] "ISO Guide 98-3, Guide to the Expression of Uncertainty in Measurement, 1. International Organization for Standardization, Geneva 2008, ISBN 9267101889." .

[18] "EMRP Call 2010 Industry and Environment," 2010. Available from: http://www.emrponline.eu/call2010/srte.html

[19] Origin 7.5 SR6, OriginLab Cooperation, Northampton, MA, USA, 2006. Available from: http://www.OriginLab.com.
[20] M. E. Wieser and T. B. Coplen, *Pure Appl. Chem.*, vol. 83, no. 2, pp. 359-396, (2011).
[21] BAM, Bundesanstalt für Materialforschung und -prüfung, Berlin, Germany, http://www.bam.de
[22] Consultative Committee for Amount of Substance – Metrology in Chemistry (CCQM), available from: http://www.bipm.org/en/committees/cc/ccqm/.
[23] European Association of National Metrology Institutes (EURAMET), available from: http://www.euramet.org/.
[24] EUROMET-934 project, Available from: http://www.euramet.org
[25] O. Werhahn and J.C. Petersen (eds.), "TILSAM-protocol-V1_2010-09-29," 2010. Available from: http://www.euramet.org/fileadmin/docs/projects/934_METCHEM_Interim_Report.pdf.

10 Conclusions

Three laser spectrometers have been utilized to measure CO_2 and CO amount fractions. Using three laser spectroscopic techniques, i.e., TDLAS, QCLAS and CRDS, combined with an absolute method (*TILSAM*), the amount fractions of the target species have been quantified. An implementation of the GUM to infrared laser absorption spectroscopy has been derived. The feasibility of the respective spectrometric techniques for CO_2 and CO amount fraction measurements have been demonstrated.

The uncertainties of the different input quantities have been calculated by means of the GUM workbench to demonstrate software-assisted uncertainty assessment which could be beneficial to spectroscopists in gas analysis applications. It has been shown that the regression-based data retrieval strategy provides more reliable uncertainty figures than the direct retrieval strategy. For breath CO_2 and CO measurements, expanded uncertainties of 5 % were fit for purpose. Therefore, the GUM compliant uncertainties of the spectrometric CO_2 and CO amount fraction results, in the range of ±5.0 %, $k = 2$ and below, were already sufficient for breath analysis.

The capability of CO_2 amount fraction measurements, in the range of 20 to 60 mmol·mol^{-1} where the exhaled breath CO_2 amount fraction is found, performed by TDLAS, has been shown. It has been found that the relative expanded uncertainties of the spectrometric CO_2 amount fraction results derived using PTB-measured line strength values are in the range of ±2.0 %, $k = 2$. At the 50 mmol·mol^{-1} level (exhaled breath level) the relative expanded uncertainty of the spectrometric CO_2 amount fraction results is at ±1.4 %, $k = 2$. The repeatability of the CO_2 amount fraction results is in the ±0.9 % range, relative. It is concluded that with uncertainties being in the 1 % range, TDLAS has the potential to become a gas standard in gas metrology.

The practicability of absolute CO amount fraction measurements performed by QCLAS based on the *TILSAM* method was shown. Breath CO is in the 1-3 µmol·mol^{-1} range. Although, the spectrometric CO measurements were performed at 100 and 100 µmol·mol^{-1}, the resulting amount fractions are in agreement with the respective gravimetric reference values. The uncertainties of the spectrometric CO amount fractions derived for different Γ values are in the range of ±4.6 % relative, $k = 2$. The reproducibilties of the CO amount fraction results are in the ±1 % range. Due to the unavailability of a traceable line strength figure, the QCLAS CO amount fraction results are not traceable to the SI. By means of an uncertainty budget it has been concluded that to improve the uncertainty of the spectrometric CO amount fraction results, more effort has to be invested in the determination of traceable line strength figures with smaller uncertainties.

An OF-CES spectrometer has been proven to be feasible for performing absolute CO_2 amount fraction measurements referring to the *TILSAM* method. With HITRAN-based line strength values, the relative expanded uncertainty of the spectrometric CO_2 amount fractions were in the ±4.2 % range. The reproducibility of the amount fraction results is in the sub-percentage

level. Again, an improvement in the uncertainties of the CRDS CO_2 amount fraction results has to prioritize the determination of traceable line strength figures with reduced uncertainties.

Consequently, the *TILSAM* method suffers from the unavailability of traceable line data with reduced uncertainties. To support the *TILSAM* method for future measurements, traceable CO_2 line data have been measured with reduced uncertainties (in the ±1 % range, $k = 1$). These line strength values and broadening coefficients in the ro-vibrational band around 2 µm will fulfill the derivation of precise amount fraction results with reduced uncertainties and ensure the traceability of the results to the SI.

The *TILSAM* method has been validated in a measurement campaign. This method has the potential of being used in a next generation of spectrometric reference methods in gas metrology. It could benefit breath analysis, other gas analysis applications and support the development of process analyzers.

11 Appendices

11.1 Appendix III

Front panal- Labview software

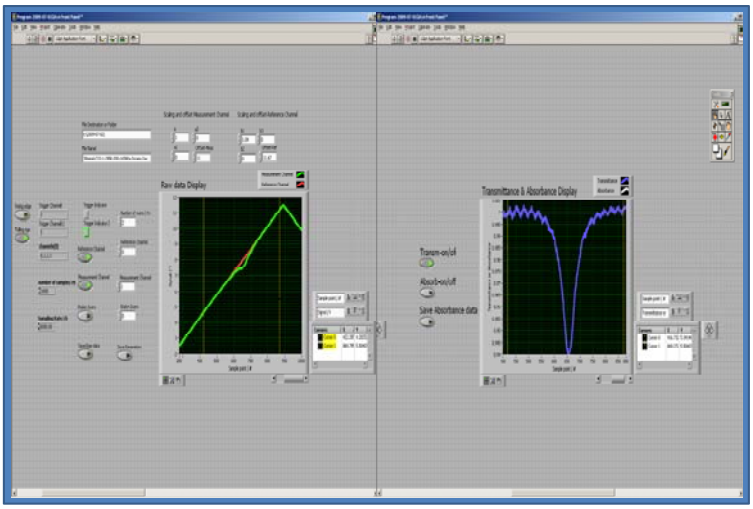

Right panel: Signals from the reference (red) and sample (green) channels as a function of the laser sweep in sample points. Left panel: Transmission spectrum. The transmission is derived by dividing the sample signal by the reference signal. By adjusting the different nobes on the front panel, an offset can be added to the measured signals. Scaling of the signals is also possible.

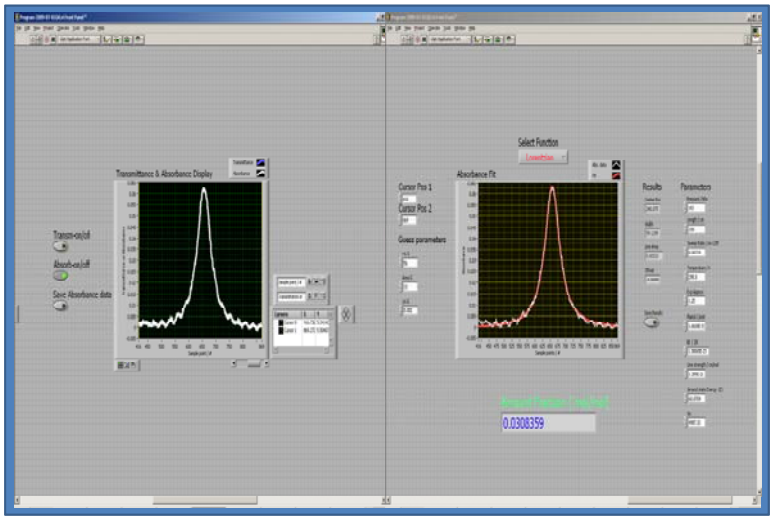

Right panel: Absorbance data as a function of the laser sweep in sample points. Left panel: A Voigt profile is fitted to the absorbance data in order to derive a value for the line area. The amount fraction of the analyte is calculated using the line area and the input parameters such as the pressure, the gas temperature, and the path length.

Schematic of the Labview program code

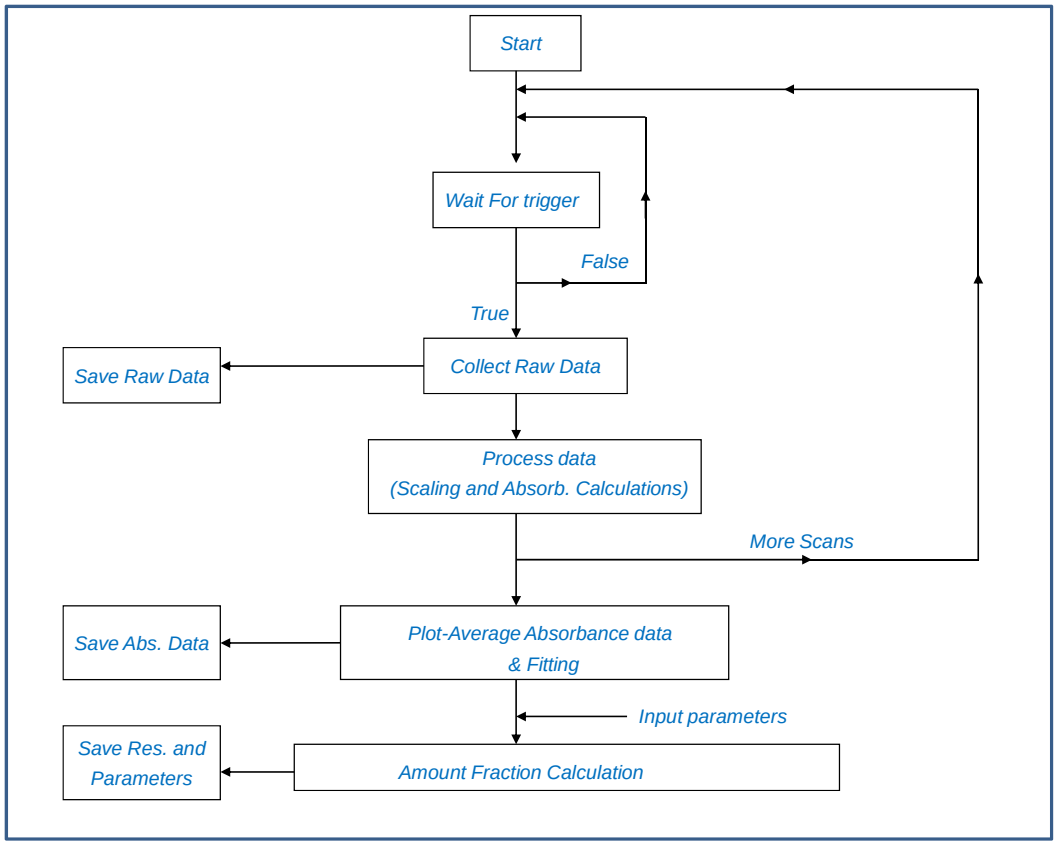

The program code holds information on data collection and processing. An amount fraction is calculated using input parameters such as the line strength of the probe transition, the gas temperature and pressure.

11.2 Appendix IV

Uncertainty budget of the gas pressure (p)

Pressure Measurements with the 1013 mbar Baratron gauge

Model Equation:

$p_{ind} = p_{reading} + dp_{resolution}$;

$b = -a_0 - a_1 * (p_{ind} - p_0)$;

$p = p_{ind} + b$

List of Quantities:

Quantity	Unit	Definition
$p_{reading}$	hPa	reading of the Baratron-controller display
$dp_{resolution}$	hPa	digital resolution of the display
p_{ind}	hPa	indicated pressure reading
a_0	hPa	zero order correction coefficient
a_1	hPa^{-2}	first order correction coefficient
p_0	hPa	reference pressure from calibration points eliminating correlation
b	hPa	Correction of the pressure reading due to the calibration
p	hPa	total gas pressure

$p_{reading}$: Constant
Value: 100 hPa

$dp_{resolution}$: Type B rectangular distribution
Value: 0 hPa
Halfwidth of Limits: 0.05 hPa

p_{ind}: Temporary
pressure reading: 0.1 hPa resolution of the digital reading of the 1013-Baratron gauge;

a_0: Type B normal distribution
Value: 6.61675772644963 hPa
Expanded Uncertainty: 0.00114154592639 hPa
Coverage Factor: 1

a_1: Type B normal distribution
Value: 0.03168405031453 hPa^{-2}
Expanded Uncertainty: $5.45864288411462 \cdot 10^{-6}$ hPa^{-2}
Coverage Factor: 1

p_0: Constant
Value: 229.06875000000002 hPa

b: Temporary

	Pressure Measurements with the 1013 mbar Baratron gauge	PTB

p: Result

Uncertainty Budget:

Quantity	Value	Standard Uncertainty	Degrees of Freedom	Sensitivity Coefficient	Uncertainty Contribution	Index
$p_{reading}$	100.0 hPa					
$dp_{resolution}$	0.0 hPa	0.0289 hPa	infinity	0.97	0.028 hPa	99.8 %
p_{ind}	100.0000 hPa	0.0289 hPa				
a_0	6.61676 hPa	$1.14 \cdot 10^{-3}$ hPa	50	-1.0	$-1.1 \cdot 10^{-3}$ hPa	0.2 %
a_1	0.03168405 hPa^{-2}	$5.46 \cdot 10^{-6}$ hPa^{-2}	50	130	$700 \cdot 10^{-6}$ hPa	0.1 %
p_0	229.06875 hPa					
b	-2.52734 hPa	$1.62 \cdot 10^{-3}$ hPa				
p	97.473 hPa	0.0280 hPa	infinity			

Result: Quantity: p
Value: 97.473 hPa
Expanded Uncertainty: ±0.056 hPa
Coverage Factor: 2.0
Coverage: t-table 95%

Date: 08/22/2011	File: p-Measurement_1013mbar-Gauge_2011-02-10	Page 2 of 2

Appendix V

Uncertainty budget: Directly retrieved Line strength of the R(10) line of CO_2 at 4985.93 cm^{-1}

	Line strength of CO_2	PTB

Line strength of CO_2

Line strength of the R(10) transition of CO_2 at 4985.93 cm^{-1}

Model Equation:

$r_{iso}=x_{12CO2}/x_{12CO2HITRAN}$;

$\chi_1=(x_{CO2}*p_1*L*r_{iso}/(k_B*T_1*100))$;

$S_{T1}=A_{line1}/\chi_1$;

$S_{T01}=(S_{T1}/((T_0/T_1)^j*\exp(-h*c*E/k_B*(1/T_1-1/T_0))*(1-\exp(-h*c*v_0/(k_B*T_1)))/(1-\exp(-h*c*v_0/(k_B*T_0)))))$;

List of Quantities:

Quantity	Unit	Definition
c	cm/s	speed of light in vacuum
T_0	K	Norm temperature
h	Js	Planck constant
E	cm^{-1}	Lower state energy
k_B	J/K/molecule	Boltzmann constant
v_0	cm^{-1}	line center
T_1	K	Measured temperature
χ_1	cm^{-2}·molecule	Chi
x_{CO2}	mol/mol	amount fraction
p_1	hPa	pressure
L	m	Length of gas cell
A_{line1}	cm^{-1}	Line area
j		Exponent from the partition sum approximation given by $(T/T_0)^j$
S_{T1}	$cm^{-1}/(cm^{-2}$·molecule)	line strength at measured temperature T_1
$x_{12CO2HITRAN}$		Conventional $12CO_2$ abundance value given by HITRAN
x_{12CO2}		Amount of 12C fraction of the CO2 in the sample
r_{iso}		Deviation of isotopomeric abundance in experiement from conventional value (HITRAN)
S_{T01}	$cm^{-1}/(cm^{-2}$·molecule)	line strength Line strength at norm temperature

c: Constant
Value: 29979245800 cm/s

Value 299 792 458 m s-1

From: CODATA Internationally recommended values of the Fundamental Physical constants, NIST(2000)

T_0: Constant
Value: 296 K

Norm temperature

conventional value (from Hitran) to report line strengths figures

Date: 08/23/2011	File: Sinlgle R10-CO2-linestrength-2011-07-08f.SMU	Page 1 of 6

Generated with GUM Workbench Pro Version 2.4.1.368

	Line strength of CO_2	PTB

h: Type B normal distribution
Value: $6.6260693 \cdot 10^{-34}$ Js
Expanded Uncertainty: $0.0000011 \cdot 10^{-34}$ Js
Coverage Factor: 1

Value 6.626 0693 x 10-34 J s

Standard uncertainty 0.000 0011 x 10-34 J s

Relative standard uncertainty 1.7 x 10-7

From: CODATA Internationally recommended values of the Fundamental Physical constants, NIST(2000)

E: Constant
Value: 42.9225 cm^{-1}

Ground state energy

k_B: Type B normal distribution
Value: $1.3806505 \cdot 10^{-23}$ J/K/molecule
Expanded Uncertainty: $0.0000024 \cdot 10^{-23}$ J/K/molecule
Coverage Factor: 1

Value 1.380 6505 x 10-23 J K-1

Standard uncertainty 0.000 0024 x 10-23 J K-1

Relative standard uncertainty 1.8 x 10-6

From: CODATA Internationally recommended values of the Fundamental Physical constants, NIST(2000)

ν_0: Type B normal distribution
Value: 4985.9322480000001 cm^{-1}
Expanded Uncertainty: 0.0002 cm^{-1}
Coverage Factor: 1

Center wave number (Hitran)

T_1: Type B normal distribution
Value: 299.38999999999999 K
Expanded Uncertainty: 0.5 K
Coverage Factor: 1

x_{CO2}: Constant
Value: 0.999993 mol/mol

p_1: Type B normal distribution
Value: 9.4801 hPa
Expanded Uncertainty: 0.028 hPa
Coverage Factor: 1

L: Type B normal distribution
Value: 0.2 m
Expanded Uncertainty: $2.5 \cdot 10^{-9}$ m
Coverage Factor: 1

A_{line1}: Type B normal distribution
Value: 0.00497688067222 cm^{-1}
Expanded Uncertainty: $2.64558966381688 \cdot 10^{-5}$ cm^{-1}
Coverage Factor: 1

Date: 09/27/2011	File: Sinlgle R10-CO2-linestrength-2011-07-08f.SMU	Page 2 of 6

Generated with GUM Workbench Pro Version 2.4.1.388

j: Type B rectangular distribution
Value: 1.25
Halfwidth of Limits: 0.25

$x_{12CO2HITRAN}$: Constant
Value: 0.984204

Conventional $12CO_2$ abundance value given by HITRAN

x_{12CO2}: Type B normal distribution
Value: 0.984204
Expanded Uncertainty: 0.0040
Coverage Factor: 1

Amount of 12C fraction of the CO_2 in the sample

Uncertainty Budgets:

χ_1: Chi

Quantity	Value	Standard Uncertainty	Distribution	Sensitivity Coefficient	Uncertainty Contribution	Index
k_B	$13.8065050 \cdot 10^{-24}$ J/K/molecule	$24.0 \cdot 10^{-30}$ J/K/molecule	normal	$-330 \cdot 10^{39}$	$-8.0 \cdot 10^{12}$ cm^{-2}·molecule	0.0 %
T_1	299.390 K	0.500 K	normal	$-15 \cdot 10^{15}$	$-7.7 \cdot 10^{15}$ cm^{-2}·molecule	10.0 %
x_{CO2}	0.999993 mol/mol					
p_1	9.4801 hPa	0.0280 hPa	normal	$480 \cdot 10^{15}$	$14 \cdot 10^{15}$ cm^{-2}·molecule	31.1 %
L	0.20000000000 m	$2.50 \cdot 10^{-9}$ m	normal	$23 \cdot 10^{18}$	$57 \cdot 10^{9}$ cm^{-2}·molecule	0.0 %
$x_{12CO2HITRAN}$	0.984204					
x_{12CO2}	0.98420	$4.00 \cdot 10^{-3}$	normal	$4.7 \cdot 10^{18}$	$19 \cdot 10^{15}$ cm^{-2}·molecule	58.9 %
χ_1	$4.5869 \cdot 10^{18}$ cm^{-2}·molecule	$24.3 \cdot 10^{15}$ cm^{-2}·molecule				

	Line strength of CO_2	PTB

S_{T1}: line strength at measured temperature T_1

Quantity	Value	Standard Uncertainty	Distribution	Sensitivity Coefficient	Uncertainty Contribution	Index
k_B	$13.8065050 \cdot 10^{-24}$ J/K/molecule	$24.0 \cdot 10^{-30}$ J/K/molecule	normal	79	$1.9 \cdot 10^{-27}$ $cm^{-1}/(cm^{-2} \cdot molecule)$	0.0 %
T_1	299.390 K	0.500 K	normal	$3.6 \cdot 10^{-24}$	$1.8 \cdot 10^{-24}$ $cm^{-1}/(cm^{-2} \cdot molecule)$	5.0 %
x_{CO2}	0.999993 mol/mol					
p_1	9.4801 hPa	0.0280 hPa	normal	$-110 \cdot 10^{-24}$	$-3.2 \cdot 10^{-24}$ $cm^{-1}/(cm^{-2} \cdot molecule)$	15.5 %
L	0.20000000000 m	$2.50 \cdot 10^{-9}$ m	normal	$-5.4 \cdot 10^{-21}$	$-14 \cdot 10^{-30}$ $cm^{-1}/(cm^{-2} \cdot molecule)$	0.0 %
A_{line1}	$4.9769 \cdot 10^{-3}$ cm^{-1}	$26.5 \cdot 10^{-6}$ cm^{-1}	normal	$220 \cdot 10^{-21}$	$5.8 \cdot 10^{-24}$ $cm^{-1}/(cm^{-2} \cdot molecule)$	50.2 %
$x_{12CO2HITRAN}$	0.984204					
x_{12CO2}	0.98420	$4.00 \cdot 10^{-3}$	normal	$-1.1 \cdot 10^{-21}$	$-4.4 \cdot 10^{-24}$ $cm^{-1}/(cm^{-2} \cdot molecule)$	29.3 %
S_{T1}	$1.08502 \cdot 10^{-21}$ $cm^{-1}/(cm^{-2} \cdot molecule)$	$8.14 \cdot 10^{-24}$ $cm^{-1}/(cm^{-2} \cdot molecule)$				

r_{iso}: Deviation of isotopomeric abundance in experiement from conventional value (HITRAN)

Quantity	Value	Standard Uncertainty	Distribution	Sensitivity Coefficient	Uncertainty Contribution	Index
$x_{12CO2HITRAN}$	0.984204					
x_{12CO2}	0.98420	$4.00 \cdot 10^{-3}$	normal	1.0	$4.1 \cdot 10^{-3}$	100.0 %
r_{iso}	1.00000	$4.06 \cdot 10^{-3}$				

deviation of isotopomeric abundance in experiement from conventional value (HITRAN)

	Line strength of CO_2	PTB

S_{T01}: line strength Line strength at norm temperature

Quantity	Value	Standard Uncertainty	Distribution	Sensitivity Coefficient	Uncertainty Contribution	Index
c	$29.9792458 \cdot 10^{9}$ cm/s					
T_0	296.0 K					
h	$662.606930 \cdot 10^{-36}$ Js	$110 \cdot 10^{-42}$ Js	normal	$-3.9 \cdot 10^{9}$	$-430 \cdot 10^{-33}$ $cm^{-1}/(cm^{-2} \cdot molecule)$	0.0 %
E	42.9225 cm^{-1}					
k_B	$13.8065050 \cdot 10^{-24}$ J/K/molecule	$24.0 \cdot 10^{-30}$ J/K/molecule	normal	80	$1.9 \cdot 10^{-27}$ $cm^{-1}/(cm^{-2} \cdot molecule)$	0.0 %
v_0	4985.932248 cm^{-1}	$200 \cdot 10^{-6}$ cm^{-1}	normal	$-47 \cdot 10^{-36}$	$-9.5 \cdot 10^{-39}$ $cm^{-1}/(cm^{-2} \cdot molecule)$	0.0 %
T_1	299.390 K	0.500 K	normal	$7.5 \cdot 10^{-24}$	$3.7 \cdot 10^{-24}$ $cm^{-1}/(cm^{-2} \cdot molecule)$	17.2 %
x_{CO2}	0.999993 mol/mol					
p_1	9.4801 hPa	0.0280 hPa	normal	$-120 \cdot 10^{-24}$	$-3.2 \cdot 10^{-24}$ $cm^{-1}/(cm^{-2} \cdot molecule)$	12.9 %
L	0.20000000000 m	$2.50 \cdot 10^{-9}$ m	normal	$-5.5 \cdot 10^{-21}$	$-14 \cdot 10^{-30}$ $cm^{-1}/(cm^{-2} \cdot molecule)$	0.0 %
A_{line1}	$4.9769 \cdot 10^{-3}$ cm^{-1}	$26.5 \cdot 10^{-6}$ cm^{-1}	normal	$220 \cdot 10^{-21}$	$5.8 \cdot 10^{-24}$ $cm^{-1}/(cm^{-2} \cdot molecule)$	41.6 %
j	1.250	0.144	rectangular	$13 \cdot 10^{-24}$	$1.8 \cdot 10^{-24}$ $cm^{-1}/(cm^{-2} \cdot molecule)$	4.0 %
$x_{12CO2HITRAN}$	0.984204					
x_{12CO2}	0.98420	$4.00 \cdot 10^{-3}$	normal	$-1.1 \cdot 10^{-21}$	$-4.5 \cdot 10^{-24}$ $cm^{-1}/(cm^{-2} \cdot molecule)$	24.3 %
S_{T01}	$1.09798 \cdot 10^{-21}$ $cm^{-1}/(cm^{-2} \cdot molecule)$	$9.04 \cdot 10^{-24}$ $cm^{-1}/(cm^{-2} \cdot molecule)$				

Date: 08/23/2011	File: Sinlgle R10-CO2-linestrength-2011-07-08f.SMU	Page 5 of 6

Generated with GUM Workbench Pro Version 2.4.1.388

	Line strength of CO_2	PTB

Results:

Quantity	Value	Expanded Uncertainty	Coverage factor	Coverage
χ_1	$4.587 \cdot 10^{18}$ $cm^{-2} \cdot molecule$	$49 \cdot 10^{15}$ $cm^{-2} \cdot molecule$	2.00	95% (normal)
S_{T1}	$1.085 \cdot 10^{-21}$ $cm^{-1}/(cm^{-2} \cdot molecule)$	1.5 % (relative)	2.00	95% (normal)
r_{Iso}	1.0000	0.81 % (relative)	2.00	95% (normal)
S_{T01}	$1.098 \cdot 10^{-21}$ $cm^{-1}/(cm^{-2} \cdot molecule)$	$18 \cdot 10^{-24}$ $cm^{-1}/(cm^{-2} \cdot molecule)$	2.00	95% (normal)

Date: 08/23/2011	File: Sinlgle R10-CO2-linestrength-2011-07-08f.SMU	Page 6 of 6

Generated with GUM Workbench Pro Version 2.4.1.388

Results:

Quantity	Value	Expanded Uncertainty	Coverage factor	Coverage
χ_1	$4.587 \cdot 10^{18}$ cm-2*molecule	$49 \cdot 10^{15}$ cm-2*molecule	2.00	95% (normal)
S_{T1}	$1.085 \cdot 10^{-21}$ cm-1/(cm-2*molecule)	1.5 % (relative)	2.00	95% (normal)
S_{T01}	$1.098 \cdot 10^{-21}$ cm-1/(cm-2*molecule)	1.6 % (relative)	2.00	95% (normal)
χ_2	$7.995 \cdot 10^{18}$ cm-2*molecule	0.94 % (relative)	2.00	95% (normal)
S_{T2}	$1.083 \cdot 10^{-21}$ cm-1/(cm-2*molecule)	1.4 % (relative)	2.00	95% (normal)
S_{T02}	$1.095 \cdot 10^{-21}$ cm-1/(cm-2*molecule)	1.6 % (relative)	2.00	95% (normal)
χ_3	$11.69 \cdot 10^{18}$ cm-2*molecule	0.91 % (relative)	2.00	95% (normal)
S_{T3}	$1.117 \cdot 10^{-21}$ cm-1/(cm-2*molecule)	1.4 % (relative)	2.00	95% (normal)
S_{T03}	$1.131 \cdot 10^{-21}$ cm-1/(cm-2*molecule)	1.5 % (relative)	2.00	95% (normal)
χ_4	$17.93 \cdot 10^{18}$ cm-2*molecule	0.89 % (relative)	2.00	95% (normal)
S_{T4}	$1.124 \cdot 10^{-21}$ cm-1/(cm-2*molecule)	1.4 % (relative)	2.00	95% (normal)
r_{Iso}	1.0000	0.81 % (relative)	2.00	95% (normal)
S_{T04}	$1.138 \cdot 10^{-21}$ cm-1/(cm-2*molecule)	1.5 % (relative)	2.00	95% (normal)
S_{296K}	$1.115 \cdot 10^{-21}$	1.1 % (relative)	2.00	95% (normal)

Uncertainty budget: Directly retrieved line strength of the R(12) line of CO_2 at 4987.31 cm^{-1}

TILSAM CO_2

Results:

Quantity	Value	Expanded Uncertainty	Coverage factor	Coverage
χ_1	$2.178 \cdot 10^{18}$ cm-2*molecule	1.5 % (relative)	2.00	95% (normal)
S_{T1}	$1.229 \cdot 10^{-21}$ cm-1/(cm-2*molecule)	2.8 % (relative)	2.00	95% (normal)
S_{T01}	$1.246 \cdot 10^{-21}$ cm-1/(cm-2*molecule)	2.9 % (relative)	2.00	95% (normal)
χ_2	$5.775 \cdot 10^{18}$ cm-2*molecule	1.0 % (relative)	2.00	95% (normal)
S_{T2}	$1.200 \cdot 10^{-21}$ cm-1/(cm-2*molecule)	2.6 % (relative)	2.00	95% (normal)
S_{T02}	$1.216 \cdot 10^{-21}$ cm-1/(cm-2*molecule)	2.6 % (relative)	2.00	95% (normal)
χ_3	$9.559 \cdot 10^{18}$ cm-2*molecule	0.92 % (relative)	2.00	95% (normal)
S_{T3}	$1.259 \cdot 10^{-21}$ cm-1/(cm-2*molecule)	2.5 % (relative)	2.00	95% (normal)
S_{T03}	$1.276 \cdot 10^{-21}$ cm-1/(cm-2*molecule)	2.6 % (relative)	2.00	95% (normal)
χ_4	$14.46 \cdot 10^{18}$ cm-2*molecule	0.90 % (relative)	2.00	95% (normal)
S_{T4}	$1.239 \cdot 10^{-21}$ cm-1/(cm-2*molecule)	2.5 % (relative)	2.00	95% (normal)
S_{T04}	$1.256 \cdot 10^{-21}$ cm-1/(cm-2*molecule)	2.6 % (relative)	2.00	95% (normal)
χ_5	$22.03 \cdot 10^{18}$ cm-2*molecule	0.89 % (relative)	2.00	95% (normal)
S_{T5}	$1.243 \cdot 10^{-21}$ cm-1/(cm-2*molecule)	2.5 % (relative)	2.00	95% (normal)
S_{T05}	$1.260 \cdot 10^{-21}$ cm-1/(cm-2*molecule)	2.6 % (relative)	2.00	95% (normal)
S_{296K}	$1.251 \cdot 10^{-21}$	1.4 % (relative)	2.00	95% (normal)

Date: 08/04/2011 | File: Mean R12-CO2-linestrength-2011-07-08f.SMU | Page 22 of 22

Generated with GUM Workbench Pro Version 2.4.1.388

Uncertainty budget: Directly retrieved line strength of the R(14) line of CO_2 at 4988.65 cm^{-1}

TILSAM CO_2

Results:

Quantity	Value	Expanded Uncertainty	Coverage factor	Coverage
χ_2	$9.967 \cdot 10^{18}$ $cm^{-2} \cdot molecule$	0.92 % (relative)	2.00	95% (normal)
S_{T2}	$1.264 \cdot 10^{-21}$ $cm^{-1}/(cm^{-2} \cdot molecule)$	1.3 % (relative)	2.00	95% (normal)
S_{T02}	$1.276 \cdot 10^{-21}$ $cm^{-1}/(cm^{-2} \cdot molecule)$	1.4 % (relative)	2.00	95% (normal)
χ_3	$20.70 \cdot 10^{18}$ $cm^{-2} \cdot molecule$	0.89 % (relative)	2.00	95% (normal)
S_{T3}	$1.288 \cdot 10^{-21}$ $cm^{-1}/(cm^{-2} \cdot molecule)$	1.3 % (relative)	2.00	95% (normal)
S_{T03}	$1.300 \cdot 10^{-21}$ $cm^{-1}/(cm^{-2} \cdot molecule)$	1.5 % (relative)	2.00	95% (normal)
χ_4	$25.30 \cdot 10^{18}$ $cm^{-2} \cdot molecule$	0.89 % (relative)	2.00	95% (normal)
S_{T4}	$1.292 \cdot 10^{-21}$ $cm^{-1}/(cm^{-2} \cdot molecule)$	1.3 % (relative)	2.00	95% (normal)
S_{T04}	$1.304 \cdot 10^{-21}$ $cm^{-1}/(cm^{-2} \cdot molecule)$	1.4 % (relative)	2.00	95% (normal)
S_{296K}	$1.293 \cdot 10^{-21}$	1.1 % (relative)	2.00	95% (normal)

Date: 08/04/2011 | File: Mean R14-CO2-linestrength-2011-07-08f.SMU | Page 14 of 14

Generated with GUM Workbench Pro Version 2.4.1.388

Appendix VI

Uncertainty budget, holding the uncertainties of individual amount fraction results at different Γ values, for CO_2 at the 300 µmol·mol^{-1}.

TILSAM CO_2

Results:

Quantity	Value	Expanded Uncertainty	Coverage factor	Coverage
S_{T1}	$1.252 \cdot 10^{-21}$ cm/molecule	1.0 % (relative)	2.00	95% (normal)
Γ_1	6.72 cm^{-1}	1.8 % (relative)	2.00	95% (normal)
x_{1CO2}	$313.4 \cdot 10^{-6}$ mol/mol	1.9 % (relative)	2.00	95% (normal)
S_{T2}	$1.253 \cdot 10^{-21}$ cm/molecule	1.0 % (relative)	2.00	95% (normal)
Γ_2	13.08 cm^{-1}	1.8 % (relative)	2.00	95% (normal)
x_{2CO2}	$318.0 \cdot 10^{-6}$ mol/mol	1.9 % (relative)	2.00	95% (normal)
S_{T3}	$1.253 \cdot 10^{-21}$ cm/molecule	1.0 % (relative)	2.00	95% (normal)
Γ_3	19.93 cm^{-1}	1.8 % (relative)	2.00	95% (normal)
x_{3CO2}	$319.5 \cdot 10^{-6}$ mol/mol	1.9 % (relative)	2.00	95% (normal)
S_{T4}	$1.253 \cdot 10^{-21}$ cm/molecule	1.0 % (relative)	2.00	95% (normal)
Γ_4	27.71 cm^{-1}	1.8 % (relative)	2.00	95% (normal)
x_{4CO2}	$320.7 \cdot 10^{-6}$ mol/mol	1.9 % (relative)	2.00	95% (normal)
S_{T5}	$1.253 \cdot 10^{-21}$ cm/molecule	1.0 % (relative)	2.00	95% (normal)
Γ_5	33.87 cm^{-1}	1.8 % (relative)	2.00	95% (normal)
x_{5CO2}	$325.7 \cdot 10^{-6}$ mol/mol	1.9 % (relative)	2.00	95% (normal)
S_{T6}	$1.253 \cdot 10^{-21}$ cm/molecule	1.0 % (relative)	2.00	95% (normal)
Γ_6	40.05 cm^{-1}	1.8 % (relative)	2.00	95% (normal)
x_{6CO2}	$323.1 \cdot 10^{-6}$ mol/mol	1.9 % (relative)	2.00	95% (normal)
S_{T7}	$1.253 \cdot 10^{-21}$ cm/molecule	1.0 % (relative)	2.00	95% (normal)
Γ_7	47.38 cm^{-1}	1.8 % (relative)	2.00	95% (normal)
x_{7CO2}	$323.8 \cdot 10^{-6}$ mol/mol	1.9 % (relative)	2.00	95% (normal)
S_{T8}	$1.253 \cdot 10^{-21}$ cm/molecule	1.0 % (relative)	2.00	95% (normal)
Γ_8	53.96 cm^{-1}	1.8 % (relative)	2.00	95% (normal)
x_{8CO2}	$324.7 \cdot 10^{-6}$ mol/mol	1.9 % (relative)	2.00	95% (normal)
S_{T9}	$1.253 \cdot 10^{-21}$ cm/molecule	1.0 % (relative)	2.00	95% (normal)
Γ_9	60.4 cm^{-1}	1.8 % (relative)	2.00	95% (normal)
x_{9CO2}	$325.9 \cdot 10^{-6}$ mol/mol	1.9 % (relative)	2.00	95% (normal)
x_{mean}	$321.6 \cdot 10^{-6}$	1.7 % (relative)	2.00	95% (normal)

Date: 05/17/2011 | File: TILSAM_Budget-NPL-300µmol-CO2-N2-2011-04-12_Total.SMU | Page 37 of 37

Generated with GUM Workbench Pro Version 2.4.1.388

Uncertainty budget, holding the uncertainties of individual amount fraction results at different Γ values, for CO_2 at the 500 μmol·mol^{-1}.

Results:

Quantity	Value	Expanded Uncertainty	Coverage factor	Coverage
S_{T1}	$1.256 \cdot 10^{-21}$ cm/molecule	1.0 % (relative)	2.00	95% (normal)
Γ_1	5.548 cm^{-1}	1.8 % (relative)	2.00	95% (normal)
x_{1CO2}	$442.5 \cdot 10^{-6}$ mol/mol	1.9 % (relative)	2.00	95% (normal)
S_{T2}	$1.256 \cdot 10^{-21}$ cm/molecule	1.0 % (relative)	2.00	95% (normal)
Γ_2	12.74 cm^{-1}	1.8 % (relative)	2.00	95% (normal)
x_{2CO2}	$444.3 \cdot 10^{-6}$ mol/mol	1.9 % (relative)	2.00	95% (normal)
S_{T3}	$1.256 \cdot 10^{-21}$ cm/molecule	1.0 % (relative)	2.00	95% (normal)
Γ_3	19.64 cm^{-1}	1.8 % (relative)	2.00	95% (normal)
x_{3CO2}	$444.4 \cdot 10^{-6}$ mol/mol	1.9 % (relative)	2.00	95% (normal)
S_{T4}	$1.256 \cdot 10^{-21}$ cm/molecule	1.0 % (relative)	2.00	95% (normal)
Γ_4	26.38 cm^{-1}	1.8 % (relative)	2.00	95% (normal)
x_{4CO2}	$446.1 \cdot 10^{-6}$ mol/mol	1.9 % (relative)	2.00	95% (normal)
S_{T5}	$1.256 \cdot 10^{-21}$ cm/molecule	1.0 % (relative)	2.00	95% (normal)
Γ_5	32.79 cm^{-1}	1.8 % (relative)	2.00	95% (normal)
x_{5CO2}	$448.4 \cdot 10^{-6}$ mol/mol	1.9 % (relative)	2.00	95% (normal)
S_{T6}	$1.256 \cdot 10^{-21}$ cm/molecule	1.0 % (relative)	2.00	95% (normal)
Γ_6	39.96 cm^{-1}	1.8 % (relative)	2.00	95% (normal)
x_{6CO2}	$451.2 \cdot 10^{-6}$ mol/mol	1.9 % (relative)	2.00	95% (normal)
S_{T7}	$1.256 \cdot 10^{-21}$ cm/molecule	1.0 % (relative)	2.00	95% (normal)
Γ_7	46.64 cm^{-1}	1.8 % (relative)	2.00	95% (normal)
x_{7CO2}	$451.9 \cdot 10^{-6}$ mol/mol	1.9 % (relative)	2.00	95% (normal)
S_{T8}	$1.256 \cdot 10^{-21}$ cm/molecule	1.0 % (relative)	2.00	95% (normal)
Γ_8	52.38 cm^{-1}	1.8 % (relative)	2.00	95% (normal)
x_{8CO2}	$448.1 \cdot 10^{-6}$ mol/mol	1.9 % (relative)	2.00	95% (normal)
x_{mean}	$447.1 \cdot 10^{-6}$	1.7 % (relative)	2.00	95% (normal)

Acknowledgements

I am grateful to my mentor, at the technische Universität Braunschweig, Prof. Dr. Karl-Heinz Gericke for his enlightening discussions and support during my studies.

To Prof. Dr. Peter J. Walla and Prof. Dr. Henning Menzel, I would like to express my gratitute for accepting to act as referees to my thesis.

Many thanks to Dr. rer. nat., Dir. u. Prof. Bernd Güttler, my mentor at the PTB, for the support, the encouragement during my studies, and reading through this work.

To Prof. Volker Ebert, I say thank you very much for the encouraging words and support.

I would like to thank Dr. Olav Werhahn, for his guidance thoughout my study period, support, and reading through this work. The detailed comments and insight were of great value to me. The enlightening discussions during our special coffee breaks were of great help. I cherish our many outings (swimming, play football with the kids, …., and the list continues…..). It was a great time working with Olav. There are many more to say. These words alone might not express the gratitude and respect I feel for all of those. I would say, thank you for all….

Special thanks to Dr. Detlef Schiel for reading through part of this work and for his support during my studies. The nice moments while visiting Eintracht Braunschweig football games will always remain fresh in mind.

I would like to thank the group members of departments 3.1 and 3.2 of the PTB. It was a great time working with such enormously great people.

I am grateful to the International Graduate School of Metrology (IGSM) TU-Braunschweig for the financial support during my first year of studies. I would like to say thank you to Prof. Meinhard Schilling for his enlightening discussions and advice. To Dr. Dezhen Li, I would say thank you for all…

Most importantly, I would like to thank my wife Mrs. Nwaboh Emeline, my kids Bradley and Patrila, for the continuous support and for keeping me cool althrough. Many thanks to my brother Augustine Nwaboh and to my parents, Mr. Nwaboh Victor and Mrs. Nwaboh Miriam, for their endless support…